Project UpWind

Contract No.:
019945 (SES6)

"Integrated Wind Turbine Design"

Final report Task 4.1

Deliverable D 4.1.5
(WP4: Offshore Foundations and Support Structures)

AUTHOR:	Tim Fischer
AFFILIATION:	Endowed Chair of Wind Energy (SWE), Universität Stuttgart
ADDRESS:	Allmandring 5B, 70569 Stuttgart, Germany
TEL.:	+49-711-68560338
EMAIL:	tim.fischer@ifb.uni-stuttgart.de
FURTHER AUTHORS:	Wybren de Vries (TU Delft)
REVIEWER:	Martin Kühn (Forwind), Po Wen Cheng (GE), Alan Wright (NREL) and Andrew Cordle (Garrad Hassan)
APPROVER:	Andreas Rettenmeier (SWE)

Document Information

DOCUMENT TYPE	Deliverable Report
DOCUMENT NAME:	Report
REVISION:	-
REV.DATE:	-
CLASSIFICATION:	General Public (R0)
STATUS:	S0 – Approved/Released

Acknowledgement

Disclaimer

STATUS, CONFIDENTIALITY AND ACCESSIBILITY								
Status				**Confidentiality**			**Accessibility**	
S0	Approved/Released	**X**	**R0**	General public	**X**		Private web site	
S1	Reviewed		**R1**	Restricted to project members			Public web site	**X**
S2	Pending for review		**R2**	Restricted to European. Commission			Paper copy	**X**
S3	Draft for comments		**R3**	Restricted to WP members + PL				
S4	Under preparation		**R4**	Restricted to Task members +WPL+PL				

PL: *Project leader*   **WPL:** *Work package leader*   **TL:** *Task leader*

Summary

The objectives within Task 4.1 of the UpWind Work Package 4 are to mitigate dynamic support structure loading and to compensate for site variability through integration of support structure and turbine design and the use of turbine control. Therefore the report focuses on the mitigation of aerodynamic and hydrodynamic loads on the total offshore wind turbine system, as through this an optimized and cost-effective design can be ensured. This can be achieved by integrating the design of the rotor-nacelle assembly (RNA) and support structure in the design process. Hence, the RNA is considered as an active component to mitigate the loads on the support structure.

The design process of the support structure of an offshore wind turbine is somewhat different compared to the one for offshore oil and gas structures. Due to the dynamic coupling of the RNA and support structure, the design process for an offshore wind turbine has to be done in an integrated manner. Such an integrated design process is described in this report. As support structures and foundations are major cost items for large offshore wind turbines, especially in deeper water, the optimisation of these components through integrated design is a powerful means of reducing cost. The approach taken here is to include load mitigation concepts already in the design phase for offshore support structures. This includes a consideration of design solutions that lead to lower loads as for example by minimizing hydrodynamic sensitivity by using small water-piercing members. But also the use of operational and dynamic controls can be effective in order to mitigate both aerodynamic and hydrodynamic loads and to compensate variations and uncertainties of site conditions within the wind farm.

Favourable use of control systems, structural tuning and the selection of structures which are relatively insensitive to site conditions may increase the range of applicability for certain support structure types and may allow a single design of support structure to be used over a wide range of site conditions. For current offshore wind farms, monopiles are by far the most popular support structure type. However, for deeper water and/or larger turbines, the fatigue loading becomes critical and the monopile dimensions can exceed the current economical feasibility. Therefore the work in this report focuses on an integrated optimization process for a 5 MW offshore wind turbine design on a monopile. The chosen site with 25 m water depth is considered to be challenging for such a large and heavy turbine type. The approach presented in this report is to integrate an optimization for load mitigation in the design process of offshore support structures. Depending on the turbine- and site-specific loading, an appropriate control strategy of the RNA shall be adapted in the design process of the support structure and shall result in an optimized overall performance. Here different control options are possible depending on the given critical loading situation.

In general, the study showed that offshore-specific controls can be effective in reducing hydrodynamic-induced loading, and here shown for monopile support structures. Here the degree of mitigation is very much dependent on the importance of hydrodynamic loading with respect to the overall fatigue loads. But the reference study has shown that a fine-tuned controller can provide sufficient damping to the system in order to reduce hydrodynamically induced vibrations without significantly increasing the loading on other components. In the given example the load reduction was used to optimize the structure in terms material savings. But the application of such control concepts could also extend the application range for monopiles to deeper sites, as this concept will probably still be competitive against other more complex structures, such as jackets or tripods.

Table of Contents

1. Introduction

1.1 The UpWind project

The offshore wind energy industry is turning out ever larger numbers of offshore wind turbines every year. Although significant progress has been made in making offshore wind energy more cost-effective, further cost reductions must be achieved to compete on equal terms with other sources of energy, such as gas and coal powered energy and land based wind energy. One way to achieve this is to turn to economies of scale, both in numbers and in terms of power output of turbines. To facilitate this development the EU funded research project was initiated in 2006. UpWind looks towards wind power of tomorrow; towards the design of very large turbines (8 to 10MW) standing in wind farms of several hundred MW, both on- and offshore.

The project brings together participants from universities, knowledge institutes and the industry from across Europe. Topics of research are gathered in work packages for example focussing on aerodynamics and aeroelastics, rotor structure and materials, control systems and electrical grids. One topic specifically geared towards the offshore development is the development of offshore support structures to enable the offshore application of large turbines in deep water sites.

1.2 Work Package 4: Offshore Support Structures and Foundations

The primary objective of the offshore support structure work package (WP4) is to develop innovative, cost-efficient wind turbine support structures to enable the large-scale implementation of offshore wind farms, for sites across the EU.

To achieve this objective, the work package focuses on the development of support structure concepts suitable for large turbines and for deep water which are insensitive to site conditions. Further focus lies on the assessment and enhancement of the design methods and the application of integrated design approaches to benefit from the integrated design of turbines and monopile support structures. The work package is divided into three tasks to execute the research for these subjects:

- Task 4.1: Integration of support structure and turbine design for monopile structures
- Task 4.2: Support structure concepts for deep-water sites
- Task 4.3: Enhancements of design methods and standards for floating support structures

To this end three main types of support structure concepts are addressed: monopile structures, braced structures and very soft and floating structures. The level of detail in the research reflects the state of current knowledge. The work package aims at making the "next step" in the development of these main concepts:

- For monopile structures focus will be on structural optimisation and pushing the boundaries of the range of application by integrated design.
- For braced support structures the focus is on structural development and making such structures suitable for large scale application.
- For very soft and floating structures the focus is on concept development and on the development of tools to assess these structure types

This report is part of a set of reports which together make up the final reporting of Work package 4. The work done in each task is documented in a separate final report. One encompassing

report summarises the findings of the WP in an executive summary. The interrelation of the four reports is show in Figure 1.1.
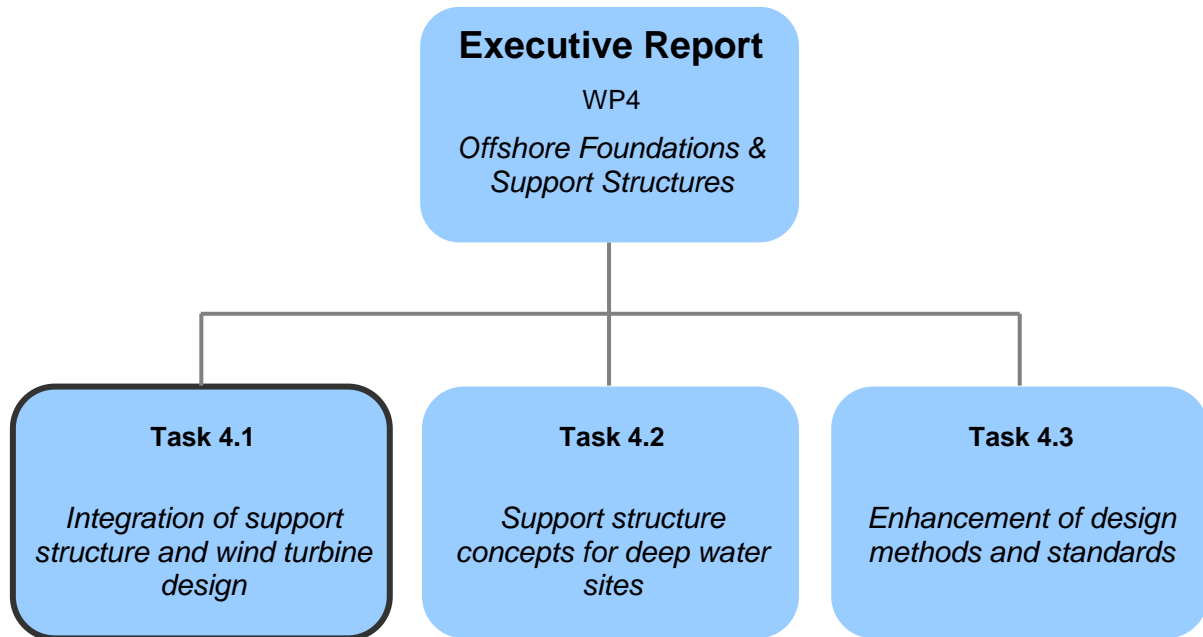
Figure 1.1: Context of reports in WP4

1.3   Task 4.1: Integration of support structure and wind turbine design

The primary objective of WP 4 "Offshore Foundations and Support Structures" of the Integrated Project UpWind is to develop innovative, cost-efficient wind turbine support structures to enable the large-scale implementation of offshore wind farms across the EU. Within Task 4.1 this is achieved by seeking solutions which integrate the designs of the foundation, support structure and turbine machinery in order to optimise the structure as a whole. The goals are to mitigate dynamic loading and to compensate for site variability through integration of support structure and turbine design and especially through the use of smart turbine control.

The design process of the support structure of an offshore wind turbine is somewhat different compared to the one for offshore oil and gas structures. Due to the dynamic coupling of the rotor-nacelle-assembly (RNA) and support structure, the design process for an offshore wind turbine has to be done in an integrated manner.

Nevertheless, in design practice a sequential design approach between turbine manufacturers and experts from the field of offshore technology is still quite popular due to different technical and commercial reasons. Nowadays, the rotor-nacelle-assembly is provided by a manufacturer chosen for supplying the project. The RNA offers only a very limited number of project-specific properties such as adapting the SCADA or control parameters. In general, the suitability of the RNA design is checked at the beginning of the design process of the offshore wind farm on the basis of preliminary site data. Towards the end of the design process and during project certification the suitability of the RNA design is again assessed based on the actual project design data. Therefore the main emphasis within the structural design process concentrates on the support structure design, as this has to be site-specific.

As support structures and foundations are major cost items for large offshore wind turbines, especially in deeper water, the optimisation of these components through integrated design is a powerful means of reducing cost. The approach taken here is to include load mitigation concepts already in the design phase for offshore support structures. This includes a consideration of design solutions that lead to lower loads as for example by minimizing hydrodynamic sensitivity by using small water-piercing members. But also the use of operational and dynamic controls can be effective in mitigating both aerodynamic and hydrodynamic loads and in compensating for deviations and uncertainties in site conditions within wind farm clusters.

Favourable use of control systems, structural tuning and the selection of structures which are relatively insensitive to site conditions may increase the range of applicability for certain support structure types and may allow a single design of support structure to be used over a wide range of site conditions. For current offshore wind farms, monopiles are by far the most popular support structure type. However, for deeper water and/or larger turbines, the fatigue loading becomes critical and the monopile dimensions can exceed the current economical feasibility. Therefore the work in Task 4.1 focuses on an integrated optimization process for a 5 MW offshore wind turbine design on a monopile. The chosen site with 25 m water depth is considered to be challenging for such a large and heavy turbine type. The approach presented in this report is to integrate an optimization for load mitigation in the design process of offshore support structures. Depending on the turbine- and site-specific loading, an appropriate control strategy of the RNA shall already be adapted in the design process of the support structure and shall result in an optimized overall performance. Here different control options are possible depending on the given critical loading situation.

1.4   Report structure and context

The report is structured in nine Chapters. After this introduction the second Chapter gives an overview about sources of loading and damping in the scope of offshore wind turbines. In the third Chapter prospects and requirements of load mitigation are given together with a discussion on the control requirements of particular offshore support structure types. In this Chapter there is a definition of three particular levels of load mitigation – namely a consideration at the design level, the operational control and finally dynamic control level. These three levels together with some exemplary concepts are described in Chapters 4 to 6. Chapter 7 then introduces the core of the work of Task 4.1, the integrated design process by including load mitigation concepts in the offshore support structure design. In order to demonstrate the effectiveness of this approach, in Chapter 8 a demonstration for a given turbine and support structure (5 MW turbine design on a monopile) at a 25 m deep offshore location in the Dutch North Sea is given. The report concludes with Chapter 9

2. Dynamics of offshore wind turbines

This report is mainly concerned with loads on offshore support structures. Therefore this Chapter aims to give an introduction to the topic of offshore wind turbine loading, in particular to those loads acting upon offshore support structures. Here, sources of loading and damping will be introduced to provide a basis for the load mitigation concepts discussed later on.

2.1 Sources of loading

Through the erection of wind turbines at sea, new problems arise in comparison to onshore locations. These are caused by additional loads from the sea environment and specific design features. Figure 2.1 illustrates various impacts on an offshore wind turbine. The Figure shows that the turbine has to withstand many different influences, which results in challenging requirements in the turbine design.
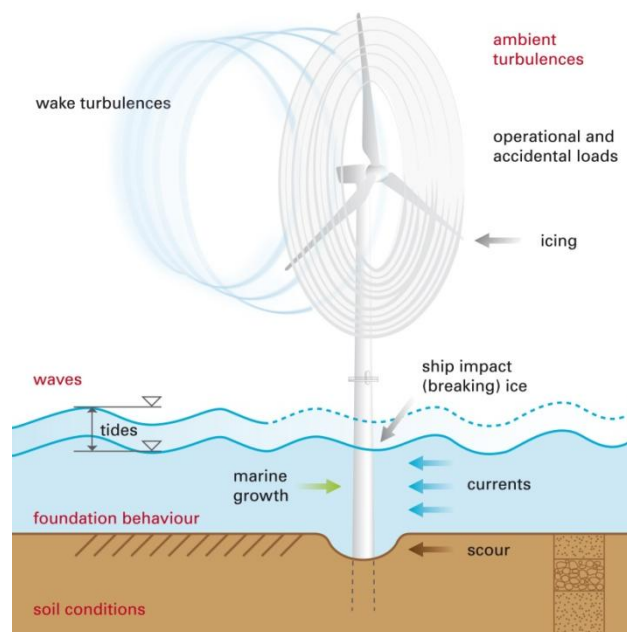
Figure 2.1: Environmental impacts on offshore wind turbines

Offshore wind turbines are exposed to many different loads, which are primary coming from:

- Aerodynamic loads
- Inertia loads
- Hydrodynamic loads
- Ice loads (not considered here, but can be important for certain locations)
- Ship impacts loads (not considered here, but also important for certain investigations)

In general, loads can be sorted according their variation in time and their origin. Table 2.1 gives an exemplary overview of some load types. In the following Section, a brief introduction to these loading effects on offshore wind turbines is given.

Table 2.1: Classification of exemplary excitation loads

Load types		Steady	Periodic	Random	Transient
	Operational	Tower and nacelle gravity loads Rotational loads	Loads from mass imbalance Tower shadow Blade gravity		Stopping and breaking events Yawing Grid failure Pitching
	Aero-dynamic	Mean wind speed	Skewed inflow Aerodynamic imbalance	Turbulence	Gusts Directional changes
	Hydro-dynamic	Currents		Sea states Sea ice	Extreme waves Breaking waves Breaking ice

2.1.1 Aerodynamic loading

Aerodynamic loading on an offshore wind turbine results from the interaction of the rotor and parts of the tower with the turbulent wind field. The loading experienced within an offshore environment is considerably lower than within an onshore environement. This is due to free flow conditions along with lower ground roughness. This advantages of reduced dynamic loading is partly undone by higher mean wind speeds.

In general, the aerodynamic loading can be characterised by the following aspects:

- Vertical wind profile
- Mean wind speed distribution
- Turbulence effects

As for offshore conditions the ground roughness is low and only slightly increased in the event of severe sea states with high waves, the wind profiles are generally very steep compared to onshore sites. At a specific height, the wind speed can be described by using an exponential wind speed law, which is defined as

$$V(z) = V(z_0) \cdot \frac{z}{z_0}^{\alpha}$$

(2.1)

where current standards [1] recommend a wind shear exponent of α=0.14 for offshore applications.
Due to the steep profiles, the hub heights are typically lower at offshore sites and defined by the clearance limit to the service platform rather than by the gain in energy yield as it holds for onshore designs. Additionally, the steep wind profiles reduce periodic load effects on the

turbines, as the differences in mean wind speed between the upwards and downwards moving blades are low.

The wind speed distribution differs on- and offshore as well. It is typically described by a Weibull distribution with

$$f_w(V) = \frac{k}{A} \cdot \left(\frac{V}{A}\right)^{k-1} \cdot \exp\left(-\left(\frac{V}{A}\right)^k\right)$$

(2.2)

For offshore sites the scale parameter *A* tends to higher values and thus higher probabilities of higher wind speeds. Furthermore the shape of the distribution is defined by the parameter *k* and here larger values tend to more pronounced shapes.
These differences in the wind speed distributions result in a higher power output and higher mean wind load level. For the prediction of energy yield of a wind turbine, long-term variations of the wind speed are significant, where in contrast for loads the short-term fluctuations are more relevant. Here the stochastic effects in the wind speed, namely the turbulence, and transient events like gusts are main contributors to fatigue and extreme loading.

Turbulence is the momentary deviation from the mean wind speed. The extent of turbulence depends on several meteorological and geographical conditions like the atmospheric layering or the terrain. A measure for turbulence is the so called turbulence intensity *I*, which is defined as the ratio between of the standard deviation of the wind speed and the mean wind speed

$$I = \frac{\sigma_1}{V_{hub}}$$

(2.3)

The turbulence intensity is correlated with the surface roughness of a turbine site and decreases with the height, as the influence of the surface decreases as well with the height.

A further factor is that the turbulence intensity decreases with increasing wind speed. But this assumption is not directly valid for offshore locations, as through the nature of the ocean surface it is correlated with the wind conditions. Here the waves and therefore also the surface roughness is connected with the existent wind speeds and duration of the wind impact. Depending on the duration, a sea state can be fully or not fully developed. For higher wind speeds the effects of the wind-wave-correlation lead to a slightlincrease in turbulence caused by the increase in surface roughness.

Another aspect for fluctuating wind speeds is the turbulence induced in wake conditions in a wind farm. Especially in dense wind park layouts wake effects play an important role. In a wind farm, a turbine experiences a superimposed turbulent wind coming from the ambient and the wake turbulence. Again, as offshore the ground roughness and thus also the ambient turbulence is lower than onshore, the mixture of ambient and wake-induced turbulence is less and therefore the wake fields remain longer in the atmosphere. This results in a higher loading from wake effects at offshore sites than compared to onshore sites at a fixed turbine distance. Here especially the partial wake operations can be critical. As the swept area of a turbine is only partly affected by a wake the load fluctuations are higher.

In general, with respect to fatigue, ambient and wake-induced turbulence have a crucial influence. Through the permanently fluctuating wind speeds and loads, the number of load cycles is extremely large, which plays a major role in the operational stability.
In terms of extremes, the effect of turbulence is not that important. Here the occurrence of certain transients is crucial. Offshore, the probability of extreme wind speeds, like gusts or wind

directional changes, is more significant than for most of the onshore sites. The result is that offshore wind turbines are generally defined for more severe wind classes according to standards [1].

2.1.2 Hydrodynamic loading

Hydrodynamic loads are caused by the interaction of the water flow with a structure when passing. The main loadings are generated by waves and currents, but can also come from other sources like sea level variations due to tides or swell. The most important loading source is waves.

A wave can be classified by its source of generation, the wave formula, the wave form and certain effects depending on the water depth. Most waves are wind-induced. The fetch limits, i.e. the distance that a sea state is travelling over the sea before reaching the site, results in under developed sea states with lower energy content and smaller significant wave heights than far offshore [2]. Therefore the developed sea state is strongly dependent on the distance to the shore. Another parameter is the actual water depth. The generation of high waves is here limited by the water depth when travelling from the open sea to the shore, as they will break at a certain stage. Here the topography of the sea bed will increase the waves steepness until they break. Such events can have a significant contribution to the loading of offshore wind turbines, as breaking waves release a high amount of energy.

Sea states are typically defined by a wave spectra. In offshore engineering, the Pierson-Moskowitz spectrum [3] and JONSWAP spectrum [4] are commonly used in practise. The two spectra differ in their definition of fetch and duration. The Pierson-Moskowitz spectrum assumes a fully developed sea state with an unlimited fetch and duration. It is defined by

$$S_{PM}(f) = \frac{5}{16} \cdot \frac{H_S^2 \cdot f_p^4}{f^5} \cdot e^{-\frac{5}{4}\left(\frac{f_p}{f}\right)^4}$$

(2.4)

with the frequency component *f* and the spectral peak frequency f_p

$$f_p = \frac{1}{T_p}$$

(2.5)

For developing sea state with limited fetch and duration, the JONSWAP spectrum is used, which is defined by

$$S_{JWP}(f) = F_N \cdot S_{PM}(f) \cdot \gamma^{\exp\left(\frac{-(f-f_p)^2}{2 \cdot \sigma^2 \cdot f_p^2}\right)}$$

(2.6)

with

$$F_N = \left(5 \cdot \left(0.065 \cdot \gamma^{0.803} + 0.135\right)\right)^{-1}$$

(2.7)

$$\sigma = \begin{cases} \sigma_a & \text{for} & f \le f_p) \\ \sigma_b & \text{for} & f > f_p) \end{cases}$$

(2.8)

In general, for fatigue load calculations a fully developed sea state is assumed, where for extremes a non-developed sea state is more realistic.

In addition to fatigue loading caused by waves, extreme sea states have to be considered. In current standards, extreme waves are analysed as single design waves with different associated wave periods and directions in conjunction with a non-linear wave theory [5]. But stochastic effects of severe sea states have to be taken into account as well. In general, extreme waves with reoccurrence periods of 50 years are analysed for an offshore site [1].

For the calculation of wave forces, the Morison equation is commonly used [6]. The equation is defined by

$$dF = C_m \cdot \rho_w \cdot \frac{\pi}{4} \cdot D^2 \cdot \ddot{u}_w - (C_m - 1) \cdot \rho_w \cdot \frac{\pi}{4} \cdot D^2 \cdot \ddot{u} + C_d \cdot \rho_w \frac{D}{2} \cdot |\dot{u}_w - \dot{u}| \cdot (\dot{u}_w - \dot{u})$$

(2.9)

The first term of the equation is the inertia contribution, which depends on the water density ρ_W, the inertia coefficient C_m, the cylinder diameter D and the water acceleration $\ddot{u}_W$. Beside this first mathematical term a second inertia contribution – the water added mass force – can be expressed, which depends again on the geometry, the density, the inertia coefficient and structural acceleration $\ddot{u}$. This expression could also be written on the other side. As it depends on the structural movement it increases or decreases the forces experienced by the structure.
The third and last term in the Morison equation is the drag force part, which depends on the structure diameter and the drag coefficient C_d. As the drag force generates hydrodynamic damping, the relative particle velocity is important, which results from the water velocity $\acute{u}_W$ and the structure velocity $\acute{u}$.

The Morison equation is only applicable for slender piles with a diameter smaller than approximately 0.2 times the wave length. For larger structures like gravity based ones but also for monopiles with very large diameters, the wave field is significantly influenced and the equation becomes invalid. Here either a diffraction theory is used based on potential flow theories [7] or a correction term such as the MacCamy-Fuchs correction [8] needs to be added.

In terms of order of magnitude, the hydrodynamic forces found from the Morison equation have generally a much smaller impact on the tower deflection than the rotor thrust reaction to the wind loads. This results mainly from the reduced area on the sub-structure where the waves interact with the turbine in comparison to the overall length of the tower and the larger lever arm of the rotor thrust. Only for high water depth or large wave heights the hydrodynamic forces become important, as the lever arm of the hydrodynamic force is increased.

Besides wave loading, sea currents and water level variations also contribute to the total hydrodynamic loading on support structures.

The mean sea level is continuously varying in time due to tides or storm surges. Due to the water level, the contact surface of the hydrodynamic forces varies and thus the load level. The influence of this tidal effect is particularly important for shallow water sites, where due to the decreasing water level the probability of breaking waves might be increased. But also for extreme load calculations, the sea level can have a significant influence and has to be carefully taken into account.

Another effect of such tides is tidal currents. Currents play an smaller role in the load of offshore wind turbines. They can be generated by tides but also from river outflows, differences in temperature or salinity and storm surges. Basically three different currents can be identified – surface currents resulting from waves and wind, sub-surface currents from tides and near shore currents due to surfing. Current adds an additional velocity component to the water particles, hence it increases the drag. Currents are commonly not contributing with significant loadings on bottom-mounted support structures in terms of fatigue loads. Only for a few sites, for example close to river outflows, they can play a role. However, in extreme calculations they have to be taken into account particularly due to the soil erosion of the sea bed.

2.1.3   Correlation of wind and waves

Loads on an offshore wind turbine are introduced from stochastic processes, namely wind and waves which are rapidly changing in their characteristics and especially directions. Both are random processes in time and in space. Because of their low correlation at the short time scale, it means they are independent and so often do not coincide in direction. Therefore, loads generated from wind and waves often act from distinct directions.

difference between wind an wave direction [deg]
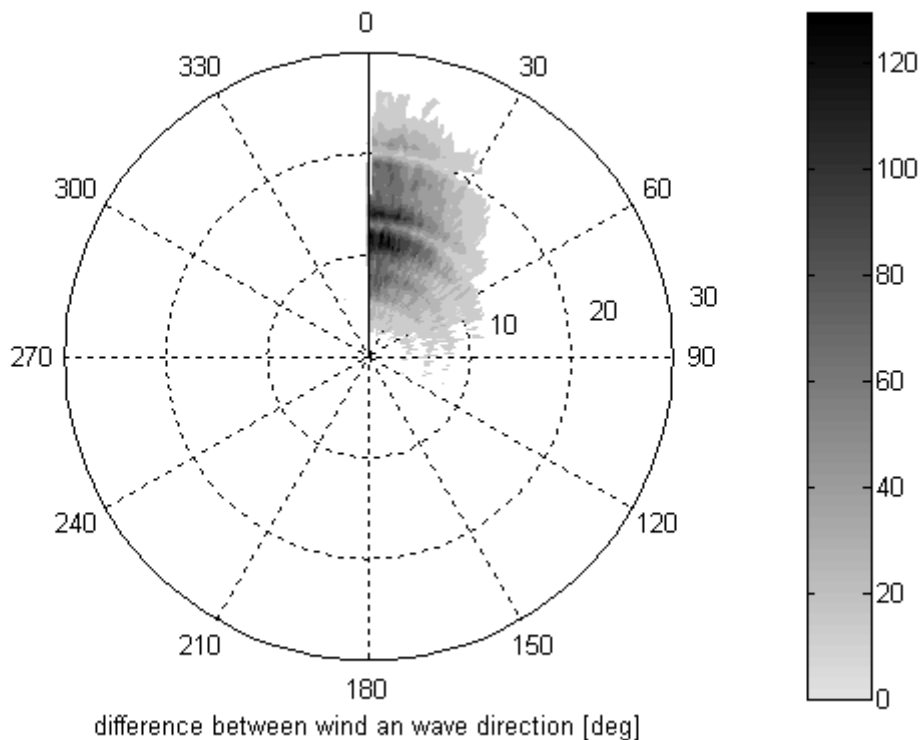
Figure 2.2: Absolute value of the misalignment between wind and waves as function of wind speed (shown from 0 – 30 m/s) and wind speed probability (colour scale)

In Figure 2.2, wind-wave-misalignments are shown as absolute values for an exemplary site in the Dutch North Sea (see site description in Sub-Section 8.1.1). Moreover, the Figure illustrates for each misalignment the corresponding wind speed probability, here shown as occurrence related to the total number of measurements. It can be seen that small misalignments appear at all wind speeds and large misalignments appear at lower wind speeds. The reason is that wind-wave-correlation at high wind speeds is often combined with fully developed sea states and

weather regimes. A consequence of this phenomenon is that for large misalignments the wave peak periods are closer to the first support structure eigenfrequency, resulting in higher dynamic amplification. Furthermore, as turbines are getting larger, they tend to have lower first eigenfrequencies, i.e. introducing an even closer gap between the wave frequencies and the support structure eigenfrequencies [9]. In addition to the tendency of having dynamically more critical wave periods associated to misaligned waves, the higher loading due to misalignments is also affected by damping. In general, in comparison to the fore-aft modes the side-to-side modes are less damped than the fore-aft ones as nearly no aerodynamic damping exists and general the hydrodynamic and soil damping is low compared to the aerodynamic damping [9].

Table 2.2: Comparison of DEL for different kinds of directional scattering

	No Misalignment	180° directional scatter	360° directional scatter
M_x	23.9 MNm	64.1 MNm	66.4 MNm
M_y	132.1 MNm	92.6 MNm	91.9 MNm

The effect of wind-wave-misalignment on fatigue loads of a reference design with a 5 MW turbine in 25 m deep water (see Appendix A) is illustrated in Table 2.2. The fatigue loads are shown as damage equivalent loads (DEL) for a reference cycle number of N=2E07, a lifetime of 20 years and am inverse S-N-slope of m=4 for the steel components. In the fatigue runs all power production and idling load cases according to current guidelines [10] with wind always acting from North are taken into account. A technical availability of 100 % has been applied for the fatigue analysis. It can be seen that the side-to-side loading (M_x) increases and the fore-aft loading (M_y) decreases in cases of using all misalignments for the load simulations. The side-to-side damage equivalent moment is increased by a factor of 3 and the fore-aft reduced, respectively. This leads for the combined case to a 33 % higher moment under misaligned conditions.

Furthermore, wind-wave-misalignment may significantly influence the design loads as shown in Figure 2.3 as well as in Table 2.2. Here in the Figure the wind-wave-directional scatter is once used in a limited way for just 180 degrees and once for the full set of 360 degrees. The values shown are non-lifetime weighted DEL assuming one misalignment occurring for the full lifetime in order to see relative effects between the different directions. In all simulations the wind direction is coming from North (0 degree) and waves are iterated according to the absolute differences in the directional scatter between wind and waves.
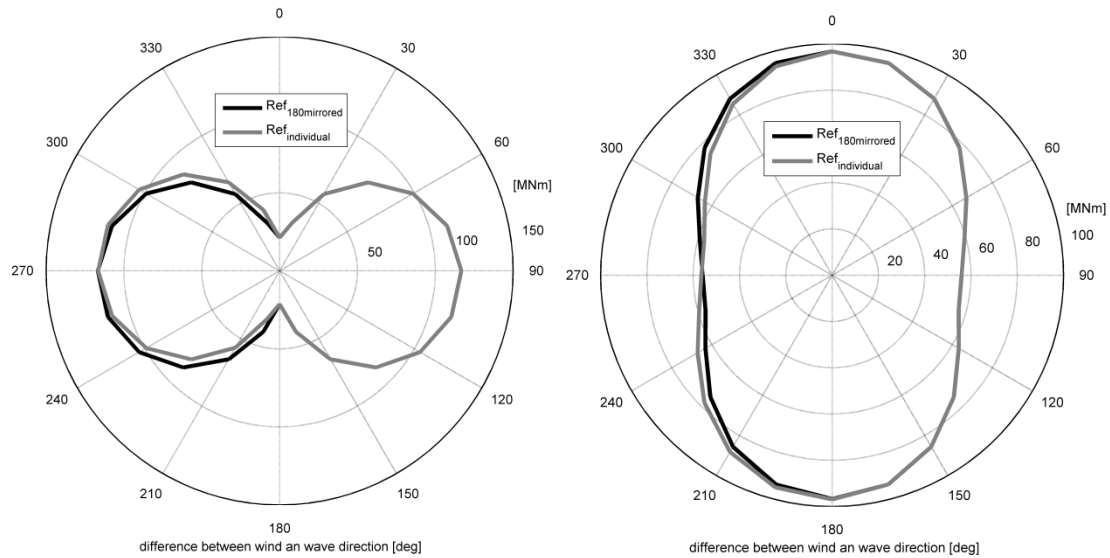
Figure 2.3: Polar distribution of non-lifetime weighted DEL for the support structure side-to-side (M_x) and fore-aft (M_y) bending moment at mud line taking different wind-wave-misalignment into account

The Figure shows the enormous increase in side-to-side (M_x) support structure loading, here expressed as moment at mud line, in cases of misalignment by keeping relative smaller change of fore-aft moment (M_y). This shows that for sites with large misalignments, the side-to-side loading becomes a design driver. Moreover, the polar distribution shows the kind of effects that are not considered if just half of the directional scatter (360 degrees mirrored to 180 degrees) is simulated. In some cases the side-to-side and fore-aft moment is under- or overestimated. In total, the lifetime damage is underestimated by about 6 % for the side-to-side moment (M_x) and slightly overestimated with 5 % for the fore-aft moment (M_y) if the waves are just used in a mirrored way in order to reduce the amount of simulations.

2.1.4 Loading influence by turbine availability

The technical availability of wind turbines is defined as the ability to operate when the wind speed is higher than the wind turbine's cut-in wind speed and lower than its cut-out wind speed. For modern onshore wind farms the availability is typically higher than 96 %. Offshore wind farms might have significantly lower availabilities, especially for the first two years of operation. The availability is closely related to turbine reliability and accessibility for maintenance and repair works. The aspect of availability is even more important for offshore projects. Here, a higher availability can lead, beside the comprehensible increase of revenue, to lower support structure fatigue damages for deep-water offshore sites. This is due the fact that the impact of aerodynamic damping during operation is enormous and acts as a damping device for the high hydrodynamic loading.

Aerodynamic damping is the dominant damping component during operation. The responses on both the aerodynamic and hydrodynamic excitations are reduced by this damping source mainly for flapwise blade and the nacelle fore-aft motion. A description of the effects of aerodynamic damping is given in the following Section.

For monopile support structures, fatigue loading is driving the design in most cases. Here, the overturning bending moment at mudline is critical. The fatigue loading at the support structure is always a combination of an aerodynamic and a hydrodynamic loading component. However,

depending on the site, the type of turbine and the support structure, the main fatigue contribution can result from the aerodynamic or the hydrodynamic loading.

The tower top mass and hub height of the turbine are the two key parameters that determine the natural frequency of the support structure. In general, it can be said that the softer the support structures the higher the loading effect from the waves. Of course this does not account for compliant structures with eigenfrequencies below the wave spectrum. Furthermore the turbine defines through its rotor design the aerodynamic loading. However, a large rotor forces higher vibrational amplitudes to the entire structure and thus larger aerodynamic damping, if there are no aerodynamic instability issues.

 The support structure influences the fatigue loading over its water-piercing members and again the dynamics. A monopile with a large diameter is expected to experience a much higher hydrodynamic loading than a structure with a smaller diameter or a jacket with many small braces and legs. Effects like marine growth or corrosion can also enlarge the load contributions from the hydrodynamics.

Finally the actual offshore site defines how much fatigue load contribution is present. A shallow water location has generally a lower hydrodynamic fatigue load contribution than a deep-water location. Of course, this can rapidly change in cases of breaking waves. Furthermore, the conditions of the soil can affect the eigenfrequency of the structure and consequently the structural sensitivity against waves.
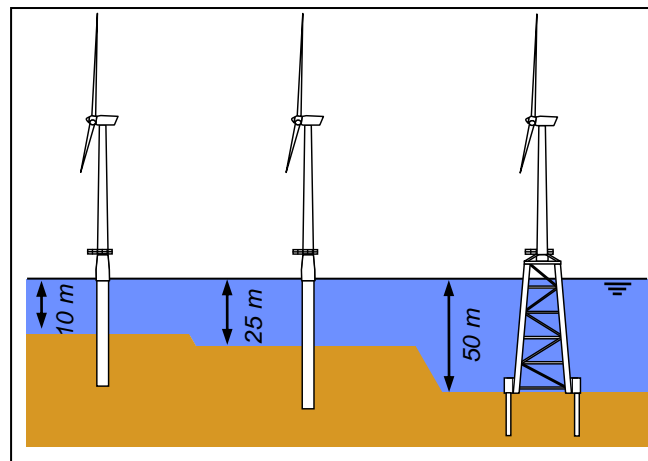
Figure 2.4: Support structure design concepts for availability study

At larger water depths and for softer support structure types, the amount of hydrodynamic loading can be higher than the loading from the aerodynamics, which leads to the importance of availability. If for such a case the turbine is not operating and is in an idling or parked mode, there is only a negligible amount of aerodynamic damping available. Thus, there is a high amount of hydrodynamic excitation without the benefit of the aerodynamic damping on the structure. This can cause significant increases in the overall damage and can limit the lifetime of the support structure of the offshore wind turbine. However, for the opposite case with a site with a very low hydrodynamic load contribution, a reduction in availability would lead to a reduction in overall loading.
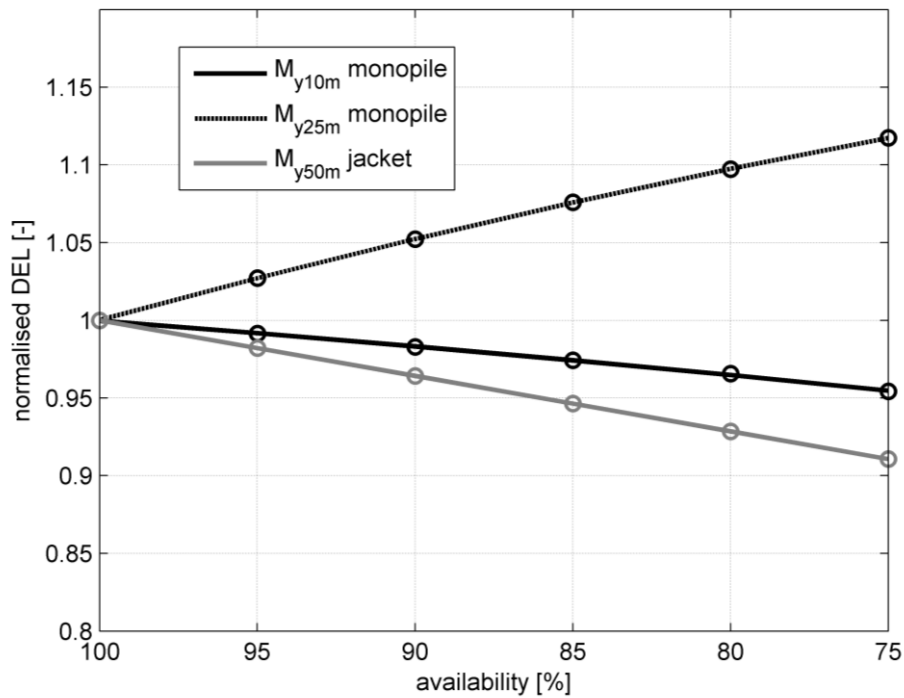
Figure 2.5: Relative change in lifetime fatigue loading for different support structure designs, offshore sites and availabilities

To illustrate these phenomena, a case study is performed. As shown in Figure 2.4, a 5 MW turbine is placed on three different kinds of support structure types and offshore sites - a shallow water location in 10 m with a rather slender monopile, an intermediate location in 25 m water depths together with a massive monopile and finally a deep water site with 50 m depths and a 4-leg jacket (all structure descriptions in Appendix A). For all cases the same turbine type and wind conditions are assumed. Only the wave conditions are chosen as site-specific. The compared loads are DEL of the monopile bending moment and the axial force in a leg of the jacket. All considerations are related to mudline.

In Figure 2.5 the normalized lifetime damage equivalent loads (DEL) for the overturning moment at mudline are shown for different availabilities. For the shallow water location with the slender monopile, the overall fatigue loading is driven by the aerodynamics. This can be seen in the change in DEL. For lower production times the overall load contribution goes down.
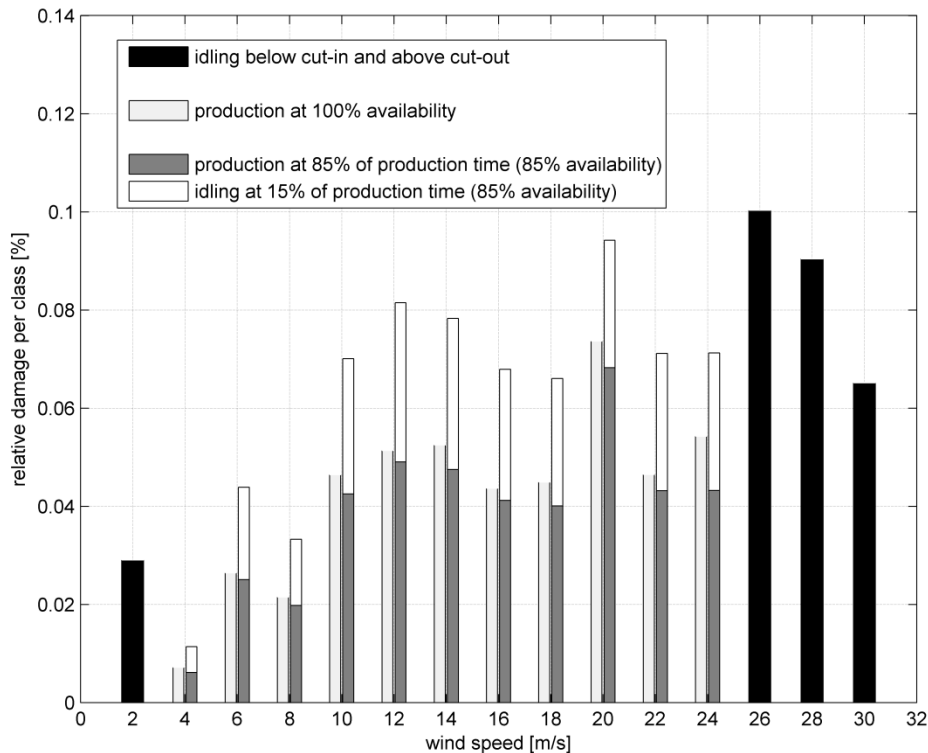
Figure 2.6: Distribution of damage on wind speed classes for different availabilities (total damage for 85 % availability normalized to one) for a 5 MW turbine design on a monopile in 25 m water depth

A similar effect can be seen for the jacket. Here, the jacket is reducing the amount of hydrodynamic loading due to its small water-piercing members. Therefore, as for the slender monopile, the aerodynamics are driving the fatigue loads and go down for lower availabilities respectively. Finally for the monopile in the intermediate depths of 25 m, the effect is contrary. Here the waves are the main contributors to the fatigue damage of the structure. In cases of low availability, the loading increases. An availability of for example 85 % leads to an 8 % higher damage. This is illustrated in more detail in Figure 2.6. It shows the effect of a full (100 %) and a reduced (here 85 %) availability case for the 25 m site. In the reduced one the fatigue damage, here expressed as relative damage per wind speed class, is increased and the extra loading in cases of non-availability (here shown as a 15 % idling mode). For some wind speed classes this almost increases the loading by 50 %. This leads to the conclusion that availability and the associated effect of aerodynamic damping can be seen as design driving in some cases.

2.1.5   Other load influencing parameters

In addition to the already mentioned effects on loads for offshore wind turbines, there are several others to be considered. Here effects like marine growth, corrosion, scour and sea ice will be mentioned.

Marine growth comes from fouling and settlement of sea dwellers on a structure and it generates extra mass. The thickness can be up to 100 to 300 mm depending on the site and occurs at the splash zone down to the sea bed. Due to the increased thickness of the piles, the induced hydrodynamic loadings are increasing, as the diameter of the pile is affecting the inertia and drag loads (see equation 2.9). Additionally, the higher surface roughness increases the hydrodynamic drag coefficient. These higher loadings can have a considerable impact on fatigue and extreme loads of support structures.

Corrosion is another important effect to be considered in the design of support structures. It deteriorates material by removing its thickness. This then affects load carrying abilities of a structure, as the structure's eigenfrequencies will be reduced by the lower thickness.

Another influence on the structure's stability is scour. Strong tides or other currents increase locally the flow at sea bed due to the disturbance in the flow caused by the presence of a foundation. This effect can cause sediments to be transported from the sea bed around the pile and deposited further downstream. The result is a scour hole around the foundation, which will increase the actual length of the pile and lower the structure's eigenfrequencies and can have negative effects on stability and loads.
Several solutions are suggested such as to include possible scour holes already in the design process by applying sufficient pile penetrations. Furthermore, scour protection like rock dumping around the foundation can be a solution.

Finally in offshore conditions pack ice or floating ice blocks on the sea surface cause additional static and dynamic forces to the support structure. The effects of sea ice occur as mechanical shocks and increased vibrations that may result in additional operational loads that are high if pushed by wind and waves against the structure. The ice formation depends on the salinity and the climate. In the Baltic Sea there is a high probability of sea ice while in the North Sea and Atlantics the probability is very low.

2.2 Sources of damping

Offshore support structures are stressed by several loads, especially if the excitation loads have frequencies that are close to the structure's eigenfrequencies. Excitations on a dynamic system can be mitigated by damping. In general, the role of damping is to remove energy from a system by energy dissipation. This can be done internally and externally.
An externally introduced damping effect is caused by external forces affecting the dynamic system. Here examples are effects like aerodynamic or hydrodynamic damping. Internal damping is related to the energy dissipation in the materials and is mainly introduced by material damping through internal friction. But also in soil dynamics the material damping enables energy dissipation by grain boundaries and micro-structure defects.

Damping can be measured in different ways and accordingly there are different damping constants available. Form time-domain measurements the logarithmic decrement can be determined from two adjacent peaks of a decay curve. The resulting logarithmic decrement δ can be defined by

$$\delta = \frac{1}{n} \ln\left(\frac{y_1}{y_{n+1}}\right)$$

(2.10)

The damping ratio ζ is related to the logarithmic decrement through

$$\zeta = \frac{1}{\sqrt{1+\left(\dfrac{2\cdot\pi}{\delta}\right)^2}}$$

(2.11)

The amount of damping in a dynamic system, such as an offshore wind turbine, is difficult to determine. There are different damping factors contributing to the total damping of the system, which are:

- Aerodynamic damping
- Hydrodynamic damping
- Structural damping
- Soil damping

The single contributions of the different damping factors depend very much on the turbine type, offshore site, materials and soil conditions. Previous studies by DONG Energy have shown that a total damping of approximately 12 % of the logarithmic damping is possible for a typical 3.6 MW offshore design [9]. To determine these values, a turbine in the offshore wind farm Burbo Banks [11] was stopped several times with an emergency stop to generate a decay curve in nearly undisturbed operational conditions. The found values in total damping are shown in Figure 2.7. They range between 10 to 20 % with a mean of approximately 12 % [9].
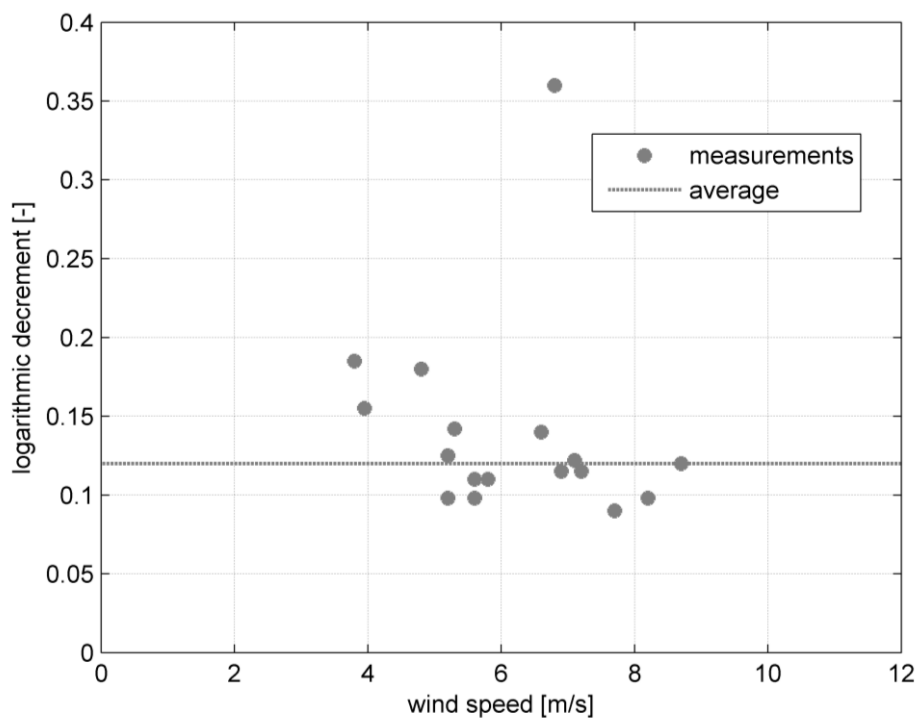
Figure 2.7: Estimated logarithmic decrements from Burbo Banks [9]

The study by DONG Energy also tried to determine the different damping contributions from aerodynamic, hydrodynamic, structural and soil damping. Due to the fact that the studied turbine had a tower damper included with an unknown damping factor, a final distinction was difficult. Further results of this study can be found in [12].

In the following the main damping contributions are again explained in more detail, especially in their context to offshore support structures.

2.2.1 Aerodynamic damping

Aerodynamic damping is one of the main damping sources of wind turbines and is mainly caused by oscillations of the tower top. The damping of the flapwise blade and tower fore-aft movement are the most affected modes, where the damping effects for other modes are considerably small. The effects causing aerodynamic damping are well described by different authors [5], [13]. Therefore, only the most important aspects are summarized here.

Support structures of offshore wind turbines show a significant dynamic behaviour in terms of vibrations due to the excitation from both aerodynamic and hydrodynamic forces. The RNA located at the top of the tower therefore experiences deflections and velocities ΔV in fore-aft direction (and to a lesser extent in side-to-side or lateral direction) that are superimposed to the wind conditions in the rotor plane. Due to the RNA movement in fore-aft direction the rotor experiences certain changes in the relative wind speeds. The relative wind speed V_{rel} experienced by the rotor is:

- $V_{rel} = V_2 + \Delta V$ if RNA moves upwind
- $V_{rel} = V_2 - \Delta V$ if RNA moves downwind

These changes in the relative wind speeds cause changes in the aerodynamic conditions on the rotor blades.

Figure 2.8: Tower top deflections and velocities for one period of a harmonic vibration

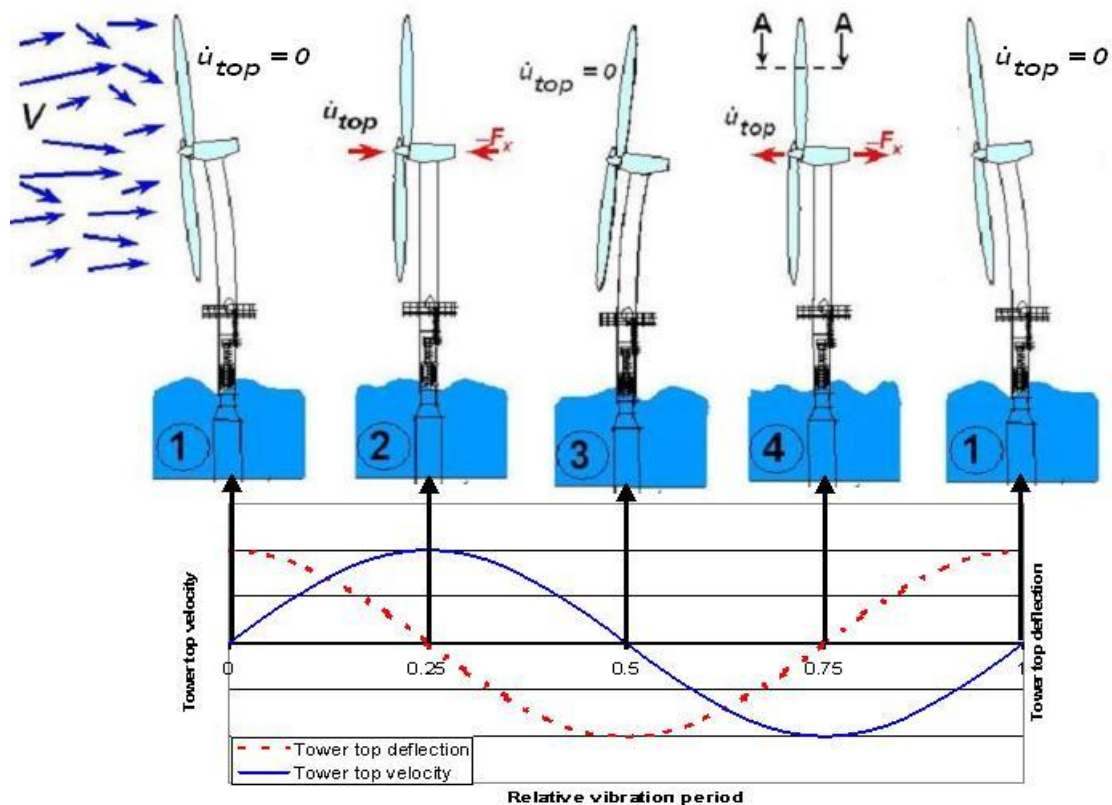Figure 2.8 shows the deflections and velocities of the RNA during one vibration period. For convenience a harmonic vibration of the tower top is assumed. Furthermore, no wind speed variations in space or time are considered [5]

Starting in state 1 the RNA experiences the maximum upwind deflection, but a zero velocity ΔV induced by the support structures fore-aft movement. Figure 2.9 shows the instantaneous aerodynamic inflow conditions and forces in that state for a particular rotor blade section (compare A-A in Figure 2.8).

β - inflow angle
α_d - deployment angle
θ - pitch angle
α - angle of attack
dF_l - lift force
dF_d - drag force
dF_t - thrust force
dF_c - circumferencal force
Ω - angular velocity (rotor)
r   - distance from rotor axis
V_1 - undistributed wind speed
V_2 - wind speed in rotor plane
C   - resulting inflow
a   - axial induction

$$V_2 = V_1(1-a)$$
$$\beta = \theta + \alpha_d + \alpha$$
$$dF_t = dF_l \cos\beta + dF_d \sin\beta$$
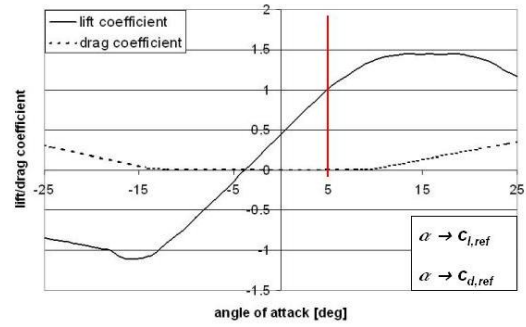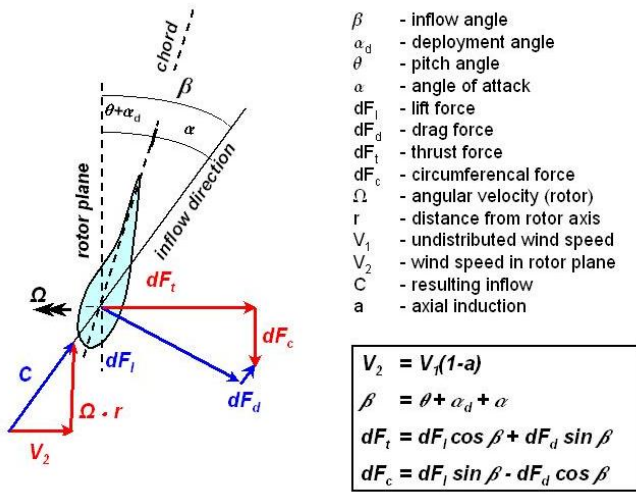$$dF_c = dF_l \sin\beta - dF_d \cos\beta$$

Figure 2.9: Aerodynamic conditions at the reference blade section in state 1 (left) and resulting angle of attack and aerodynamic coefficients (right) [5]

The inflow c results from the (constant) rotor speed and the relative wind speed in the rotor plane only, with the inflow angle depending on the magnitudes of both. Adding the deployment angle (together with the sectional blade twist angle) and the instantaneous pitch angle, both measured from the rotor plane, gives the direction of the chord. The actual angle of attack of the inflow c is the difference of the inflow angle and both, the deployment angle and the pitch angle. Both, the lift and the drag coefficient can be derived from the corresponding airfoil tables on basis of the angle of attack and used for calculation of the sectional lift and drag force. The lift force and the drag force shows components in direction of the rotor plane (circumferential or tangential force) and perpendicular to the rotor plane (thrust force). It can be seen from the exemplary diagram in Figure 2.9 that for the exemplary angle of attack the drag coefficient is much smaller than the lift coefficient. This is typical for modern variable speed, pitch-regulated turbines over a wide range of operational conditions. For convenience the portion of the drag force will be neglected here.

In state 2 the tower top shows no displacement relative to the mean configuration while the velocity in downwind direction is at the maximum. Since the RNA moves relative to the wind field the rotor experiences a lower wind speed. This relative wind speed results from the superposition of the wind speed V_2 and the speed of the RNA. The relative wind speed therefore is $V_{rel} = V_2 - \Delta V$. Assuming that the rotational speed is the

Figure 2.10: Aerodynamic condition at the reference blade section in state 2 (upper) and resulting angle of attack and aerodynamic coefficients (lower) [5]

same as in state 1, changes in geometry of the inflow occur. On the one hand the resulting inflow shows a lower magnitude which is negligible over a wide range of operational conditions, especially in the outer part of the rotor blades. On the other hand the inflow angle is decreased resulting in a decreased angle of attack. Decreasing the angle of attack results in changes of the aerodynamic coefficients as shown in Figure 2.10. In normal operation conditions a decreased angle of attack correlates with decreased lift coefficients and therefore with decreased lift forces. The decreased inflow angle tends to increase the sectional thrust force as a portion of the lift force, but the influence of the decreased sectional lift force is generally larger due to relatively small inflow angles. Of course this is only valid for the outer part of the blades, but the influence from the inner parts of the blades is much smaller due to the much smaller inflow velocity c. This reduction of the total thrust force F_t can be considered as an additional force superimposed to the reference thrust force (from state 1) acting against the direction of the tower top movement and therefore having a damping effect.

It should also be noted that the circumferential (= tangential) force dF_c decreases due to the change in the lift coefficient resulting in a lower overall torque and therefore in a lower power output.

In state 3 the RNA shows the maximum downwind deflection but a zero velocity from the support structure movement. The instantaneous aerodynamic inflow conditions and forces correspond to those given in state 1 as shown in Figure 2.9. Differences in the deformed configurations of state 1 and state 3 due to the different orientation of the rotor plane with respect to the undeflected rotor plane are neglected.

In state 4 the tower top shows no displacement relative to the undeflected configuration while the velocity $\varDelta V$ against the wind direction is at the maximum. Again, the wind speed experienced by the rotor is changed due to the tower top movement and the relative wind speed results from the superposition of the wind speed V_2 and the speed of the RNA $\varDelta V$. The relative wind speed therefore is $V_{rel} = V_2 + \varDelta V$ increasing the inflow angle and the angle of attack as shown in Figure 2.11. By the increased angle of attack the corresponding lift coefficient also increases resulting in a larger sectional lift force. Although the increased inflow angle β tends to lower the sectional thrust force, which is a portion of the sectional lift force, the resulting sectional thrust force increases since the influence of the increased lift coefficient is generally larger due to relatively small inflow angles (compare state 2). This leads to an increase in the total thrust force F_t which can be considered as an additional force superimposed to the mean thrust force (from state 1 or 3). The additional force is acting against the direction of the tower top movement and therefore has a damping effect.
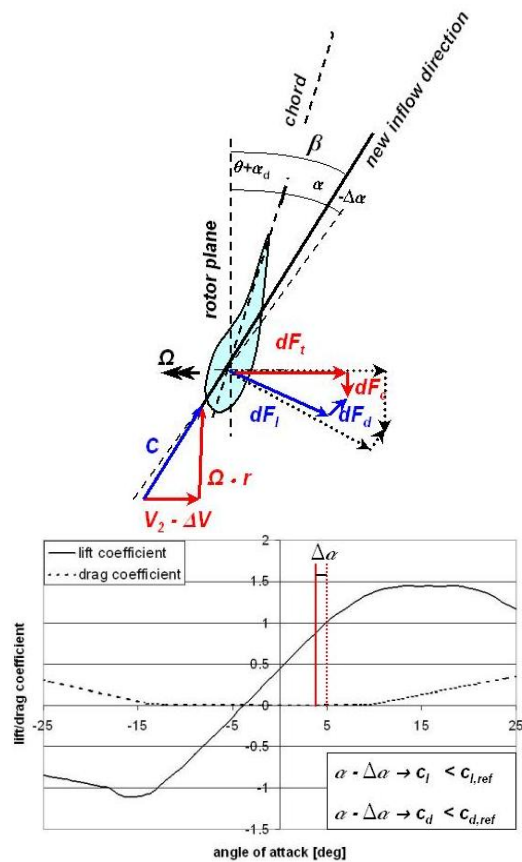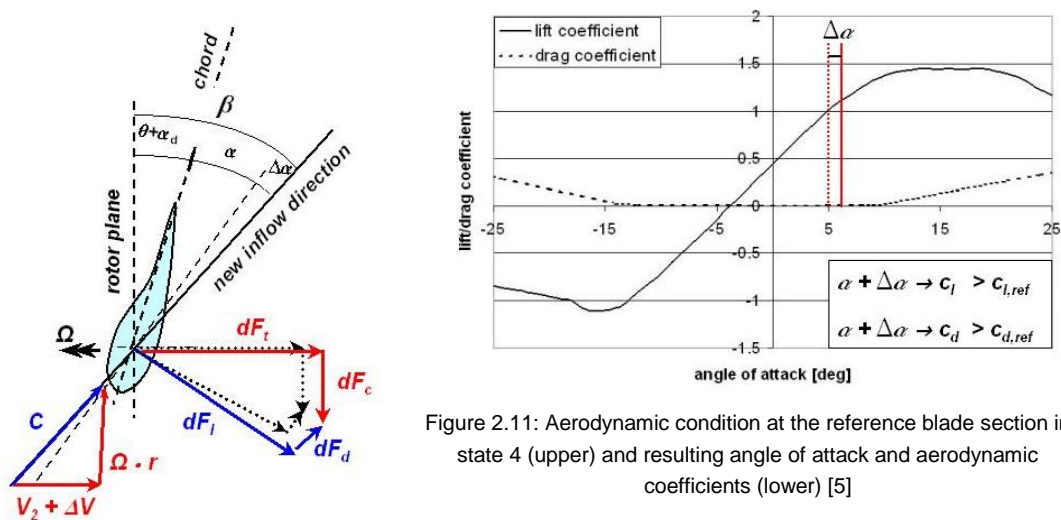

Figure 2.11: Aerodynamic condition at the reference blade section in state 4 (upper) and resulting angle of attack and aerodynamic coefficients (lower) [5]

A direct correlation between the angle of attack and the aerodynamic damping can be seen. Kaiser [14] found that especially when stalling occurs, the damping effect tends to decrease enormously, even into negative damping. Thus, the aerodynamic damping phenomenon has to be coupled with the attachment conditions of the flow at the airfoil. Even pitch regulated turbines, which operate in attached flow regimes through active pitching, might experience this effect at partial stall conditions. Here, the turbine can come into short stall states right before rated power and thus before pitching starts. But still, an increase of aerodynamic damping after rated power can be achieved, through which the pitch control system becomes a powerful tool for damping control.

2.2.2   Hydrodynamic damping

For offshore support structures, internal water in the piles but also the surrounding water affect fluid loading on the structure. Here hydrodynamic damping occurs as a moving body, such as a pile, is generating waves in the surrounding water. This wave radiation is directly proportional to the velocity. Also the dissipation due to drag will contribute to hydrodynamic damping, which depends on the square of the relative velocity. Still, the contribution of hydrodynamic damping, for example compared to the aerodynamic one, is low. An important parameter is the stiffness of the submerged part of the support structure compared to the upper part above the transition piece. Due to this stiffness the structural deflections are small and thus the relative velocities as well. This results in small damping contributions from energy dissipation due to drag.

2.2.3   Structural damping

Besides aerodynamic damping the structural damping is the most important damping source for an offshore wind turbine. A number of influences contribute to the total structural damping in any structure, such as different temperature, eigenfrequencies and stress levels. Structural damping can be divided into internal and added damping. An internal damping is the naturally included damping of a structure, where added damping is achieved by added systems like clamped masses or viscous dampers.

For offshore support structures, the internal material damping is present as well as damping at structural joints. Material damping occurs as absorption of vibrations by internal friction. The result of the energy dissipation is heat [12]. Internal damping of material results in an elliptical hysteresis cycle [15]. Here the area of the hysteresis curvature is proportional to the dissipating energy. The amount of energy dissipated by internal material damping depends on the structure's material and is quantified by the loss factor [16].

Still, the effect of internal material damping is considerably low and most structural damping occurs in the joints. Internal material damping is relatively small, as most of the damping which occurs in real structures originates from structural joints. The energy dissipation in structures is a complex process which arises largely from interface pressure such as at flanges of two tower sections. In cases of joint clamping with low pressure, sliding on a macro scale occurs. Especially for joints with high clamping pressure, where mutual embedding of the surface takes place, energy dissipation is high. Damping in structural joints, depending on the clamping pressure, results in heat or plastic deformation [16].

A certain amount of damping occurs in the grout material, a material used in the joint to connect pile and transition piece. The concrete in the grout causes in general more damping than steel materials. But also other secondary structural elements, such as jointed platforms, cables or elevators increase the overall structural damping in the support structure.

2.2.4 Soil damping

For offshore wind turbines, the displacement of the pile causes cyclic motions in the surrounding soil, which is affecting the soil damping behaviour. In general, soil damping is influenced by wave radiation, material damping and due to pore pressure dissipation.

Damping due to wave radiation occurs as the pile generally vibrates in the soil. This effect can typically be neglected for frequencies below 1 Hz [12]. For most of the bottom-mounted support structures, the first eigenfrequency in the soft-stiff design region is between 0.2 and 0.8 Hz depending on the turbine type. In such frequency ranges the damping contribution from wave radiation is negligible.

For the case of material damping in the soil, a hysteresis occurs due to the deformation of the ground. The contribution from hysteresis soil damping is significant and is said to contribute to the total damping with up to 2 to 3 % logarithmic decrement [12]. Of course the size of the pile and the type of soil plays an important role.

Soil damping due to pore pressure dissipation is affecting both, the energy dissipation itself and the lateral stiffness of piles. The role of energy dissipation, however, is marginal compared to other damping mechanisms acting on offshore wind turbines. When determining damping due to pore pressure dissipation, the magnitude of the permeability has to be measured accurately, as this soil property affects the energy dissipation most significantly [12].

3. Requirements and levels of load mitigation

In this Chapter, requirements for load mitigation are defined. This includes a definition of design ranges for offshore support structures and their dynamic behaviour. Based on these requirements, three different levels of load mitigation are introduced, which shall be further elaborated later on.

3.1 Design ranges for offshore support structures

In the design of offshore support structures, the first eigenfrequency of the structure is an important factor to consider as it describes the dynamic behaviour of the offshore wind turbine. As for every dynamic system, if an excitation frequency gets close to this structural eigenfrequency, resonance occurs and the resulting response will be larger than in the quasi-static case. This leads to higher stresses in the support structure and, more importantly, to higher stress ranges, which is an unfavourable situation with respect to the fatigue life of the offshore wind turbine. Therefore it is important to ensure that the excitation frequencies with high energy levels do not coincide with the eigenfrequency of the support structure.

In the offshore environment, wind turbines are excited by wind and waves. Here for wave-induced fatigue loading sea states with a high frequency of occurrence have the largest impact. These sea states are generally characterized by relatively short waves with significant wave heights of H_s around 1 m to 1.5 m and a zero-crossing period of T_z around 4 s to 5 s [17]. The excitations from the wind are in general connected to rotational frequency effects of the rotor. Due to the rotation of the rotor, aerodynamic loads are concentrated around the rotor frequency and multiples of the blade passing frequencies. Rotational-sampling effects like the *1P* frequency are generated due to mass imbalances in the blades or *3P* frequency effects generated due to tower shadow effects.

Thus, the ratio between the rotor speed, or more precisely the rotor speed range, and the fundamental eigenfrequency f_0 of the support structure is an important design driver for the support structure design since resonance frequencies must be avoided.
In general, three design solutions exist depending on the ratio between the fundamental eigenfrequency f_0 and either the rotor frequency *1P* or the blade passing frequency *3P*:

- soft-soft, i.e. $f_0 < 1P$
- soft-stiff, i.e. $1P < f_0 < 3P$
- stiff-stiff, i.e. $3P < f_0$

In practice, soft-stiff designs are most common. Sometimes soft-soft designs are used for tall towers, but the impact of the wave energy can become critical in several cases. Stiff-stiff designs are rare, as the necessary material for achieving such stiff structures imposes high costs.

Offshore wind turbines nowadays operate with variable rotor speed, hence the frequency ranges depends on the rotational speed. This enables further design ranges:

- Very soft, hardly realizable due to strength requirements and exposure to excessive dynamic wave excitation (unless a compliant design with an eigenfrequency below the significant wave excitation is chosen)

- Soft-soft design in the resonance range of the rotor speed requires an exclusion window for stationary operation of the rotor speed, soft-soft designs are subject to quite significant wave excitation

- Classical soft-stiff design range, proven to be suffering from significant wave excitation

- Blade resonance range with excessive excitation from cyclic aerodynamic loading, design impossible without a large exclusion window of the rotor speed

- Stiff-stiff, design is considered uneconomical due to the high consumption of material required for the stiffness

Figure 3.1 illustrates these options applied for the Upwind 5 MW reference turbine (see Appendix A).

At state of the art offshore wind farms, mostly the second and third design ranges shown in Figure 3.1 are found. The reason is that most of the structures are supported by monopiles. For such structures it is difficult to achieve the stiff-stiff region due to economical constraints. The very soft region is critical due to high wave loading. Therefore most of the structures are placed into the soft-stiff region, where the structures are out of any rotational-dependent resonance, economic in material consumption and where the wave impacts are lower. For future larger turbine types with 5 MW rated power and larger water depths, monopile structures in the soft-stiff design region are difficult to design, as certain limits in pile diameter and wall thicknesses are reached. Therefore the soft-soft design region, in the *1P* rotor frequency range, could be an option. To avoid resonances, different operational control concepts like a rotational speed window can be used as described later in Chapter 4.
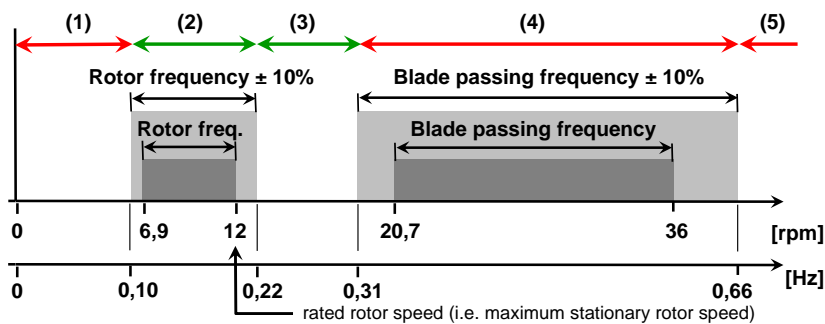
Figure 3.1: Design ranges for the fundamental eigenfrequency of the support structure of a variable-speed wind turbine at the example of the Upwind 5 MW design

3.2 Critical load effects for certain support structure types

Depending on the type of the support structure, different loading events can be critical. An important difference can be found for bottom-mounted and floating structures, but also for single-piled and braced ones. The Section below deals with steel-type structures only and will point out certain aspects of some exemplary structures.

For state of the art offshore wind farms, monopiles are by far the most widely used support structure types. Monopiles consist of a single tubular pipe that transfers the loads mainly laterally into the sea bed. This layout makes the structure relatively sensitive to the uncertainties of the soil conditions. On the other hand, monopiles might be applied in a range from soft to relatively stiff soil conditions. However, monopiles are not the best suited concept for very soft or very stiff soil conditions or when boulders occur in the sea bed. In the presence of bedrock, drilled and subsequently grouted monopiles can be applied, or a combination of drill and drive.

The bending stiffness of monopiles is relatively low leading to a low fundamental eigenfrequency which tends to be in the vicinity of the *1P* excitation at rated rotor speed. Large tower top masses therefore have an unfavourable effect on the modal properties at least for soft-stiff configurations. Due to relatively large modal displacements in the submerged part and therefore large associated hydrodynamic participation factors, monopile support structures of offshore wind turbines are inherently sensitive to dynamic wave excitation. Furthermore, the single, large diameter tubular tower attracts much higher wave forces than typical space frame structures composed of small diameter members such as jackets. Both dynamic amplification and large exciting forces affect monopile structures in a cumulative, unfavourable manner.

Monopiles are typically designed in the soft-stiff design region. Designing monopiles with a soft-soft characteristic attracts larger wave excitation, but can still be cost-efficient when an overly heavy structure is avoided as these employ large amounts of material solely for driving the first structural eigenfrequency out of the resonance range. The more common soft-stiff monopile designs require higher structural and dynamic stiffness, which might be achieved by an increase in diameter and less efficiently by reinforcing wall thickness. However, large diameters introduce drawbacks such as larger wave loads, installation requirements of larger driving equipment and lower buckling resistance of monopiles.

For deeper water, but also heavier turbines, braced support structure types are becoming interesting. Here jackets and tripods are possible contenders.

Similar to monopiles, tripods consist of a large-diameter central tubular pipe. However, in contrast to monopiles an additional framework of three braces is connected to the central tube providing additional stiffness to the lower part of the support structure. Furthermore, not the central tube, but the braces are connected to the foundation which can be designed in different configurations, i.e. piles, gravity bases and suction buckets. The braces of the framework reduce the bending moment loading of the lower part of the central tube. Assuming similar configurations of the RNA and environmental conditions, typical eigenfrequencies of tripods will vary between those of monopiles and jackets.

While the lower submerged part of tripods consists of relatively slender members, similar to jackets, the upper part above the main joint close to the sea surface consists of a central tube showing characteristics similar to monopiles. The overall bending stiffness is larger compared to monopiles resulting in higher eigenfrequencies, which are not as high as for jackets. Therefore, hydrodynamic excitation is less severe than for monopiles. However, the large-diameter structure in the range of the sea surface elevation attracts large wave forces similar to monopiles.

Loads are transferred mainly axially through the braces to the seabed, while the load transferred to the seabed depends on the actual type of the foundation.

Installation may require special equipment, for example for driving or drilling and working under water. The joints must be manufactured carefully because welded connections attract stress concentration and tend to be the weak link regarding fatigue failures. Access to the structure from sea is very difficult when there are main joints located close to or above mean water surface levels. An alternative are casted joints.

In contrast to tripods, jackets are composed of small-diameter members and might be designed with different types of foundations similar to the tripods. This concept is more flexible in relation to different site conditions and therefore increases the range of application due to the fact that geometrical variations of the sub-structure part can be done relatively simply without altering the structural stiffness and the wave loading too much. Due to small-diameter members, jackets are very transparent hydrodynamically and therefore attract lower wave forces. Furthermore, the braced layout of jackets provides large structural bending stiffness and a favourable mass-to-stiffness ratio resulting in relatively high bending eigenfrequencies and therefore reduced hydrodynamic excitation compared to monopiles. However, because of the braced layout there is reduced torsional stiffness, which can potentially lead to dynamic problems.

As a result of the large structural bending stiffness jackets are designed either soft-stiff or stiff-stiff. Especially for soft-stiff designs an exclusion range for the rotor speed in the lower partial load range might be required in order to avoid a resonance with the blade passing frequency.
Loads are transferred mainly as tension/compression of the members while the load transferred to the seabed depends on the actual type of foundation.
Recent findings suggest that jackets could offer relatively cost-efficient support structures for deep-water locations, even if there are also some design challenges for this type of structure. Boat access to a lattice structure is difficult due to the braced layout and the larger number of joints. The tubular joints themselves are prone to stress concentrations and sensitive to high cycle fatigue through aerodynamic tower top loading. Furthermore, the welding of tubular joints is labour and cost extensive.

In addition to bottom-mounted support structures, floating structures will enter the market in the future. Such floating wind turbines will impose many new design challenges. Currently, tension leg platform (TLP) concepts are considered the most economic solution because the rigid body modes of the floater are limited to horizontal translation (surge and sway) and rotation around the vertical axis (yaw). Spar buoy floater, if ever viable, would require a dynamic damping of the three angular rigid body modes (roll, pitch and yaw). Control of the axial thrust by low frequent collective pitch variation and control of lateral thrust and yaw moment by cyclic pitch will be one of the main design needs for such structures in order to achieve stability and reliability.

3.3   Requirements for load mitigation

The objectives of this work are to mitigate dynamic loading on support structures and to compensate for site variability through integration of the support structure and the turbine design with means of turbine control. The work focuses on the mitigation of aerodynamic and hydrodynamic loads on the total offshore wind turbine system in order to allow a cost-effective design. This can be achieved by integrating the design of the rotor-nacelle assembly (RNA) and support structure in the design process. Hence, the RNA is considered as an active component to mitigate the loads on the support structure. Simultaneously high energy yield of the wind turbine should be facilitated and any significant increase in loading of the RNA through aero-elastic response, controller action or hydrodynamically induced dynamic response should be avoided.

Different means exists to achieve this overall objective including:

- Reduction of the wave induced dynamic response and associated fatigue of the support structure caused by vibrations of the RNA mainly at the fundamental fore-aft and lateral eigenmode.

- Optimisation of the ratio of the aerodynamic and hydrodynamic load contribution with the goal of a reduction of the total loading of certain unfavourable load cases.

- Reduce the sensitivity of designs to the site conditions in a wind farm by applying operational and dynamic control.

The implementation of a control concept for load mitigation at the support structure imposes a number of general requirements to other components and the wind turbine system, which have to be fulfilled. Examples are:

- Possible additional loading of other components of the RNA especially pitch drives, blades and sensitive drive train components like the gear box should be minimised, together with reducing possible negative impacts on the reliability of the machine.

- Extra controller action can reduce the energy yield of the offshore wind turbine by operating outside the aerodynamic optimum and increased energy consumption of the actuators. As a rule of thumb at least 4 to 5 % cost reduction in the total support structure costs (material, manufacturing and installation) is required for compensation of each percentage loss in energy yield, assuming a 20 to 25 % proportion of support structure cost relative to the cost of the energy.

- New control concepts require innovative control algorithms as well as robust load feedback sensors for structural response and possibly also for environmental conditions like wind and wave.

Based on the requirements for load mitigation and the consideration of requirements for additional loading on other system mentioned above, different levels of load mitigation are defined. These levels provide different possibilities to achieve a more cost-effective support structure designs.

3.4   Levels of load mitigation

For load mitigation of the support structure, different concepts are possible and can be distinguished at three different levels according to the time scale involved. These levels can be identified as the design, operational control and dynamic control shown in Figure 3.2.
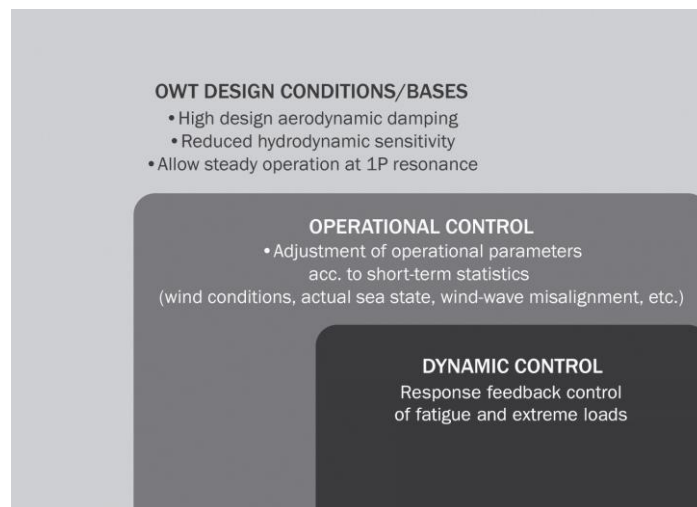
Figure 3.2: Levels of load mitigation

On the design level, the objective is to include load mitigating aspects already in the design of the offshore turbine itself or the wind farm layout. The design considerations can involve the type of turbine and support structure or shape of the farm. The design concept aims to enhance the important damping effects like aerodynamic damping, but also in reducing excitations from hydrodynamics with the aid of hydrodynamic-transparent support structure designs. Further design criteria could involve steady operations in low resonance frequencies with low energy contents like the *1P* frequency, which can be achieved with specific operational or dynamic control mechanisms.

The next level of load mitigation concepts is concerned with the operational control and especially the adjustment of the operational parameters to match the statistical properties of the actual met-ocean parameters for example wind conditions, sea states or wind-wave misalignment averaged over a period of 10 minutes to one hour with the aid of load response measurements. A major difference to the latter discussed dynamic control is that only the statistics of the load response are measured and evaluated for control purposes. Such a procedure is much easier, does not need real time operations and avoids possible counteractions with the safety critical control system and safety system implemented in the programmable logic control (PLC) system of the turbine.

In the final level different advanced dynamic control systems are available to damp the loads on an offshore wind turbine actively. Dynamic control includes adapted control loops, where certain system properties are changed actively in order to mitigate certain loads, in this case the loads at the support structure. Several dynamic control concepts are readily available in the industry, but not all of them are used for offshore wind farms. Depending on the site, turbine and support structure type certain onshore-tested control concepts can work much more effectively offshore.
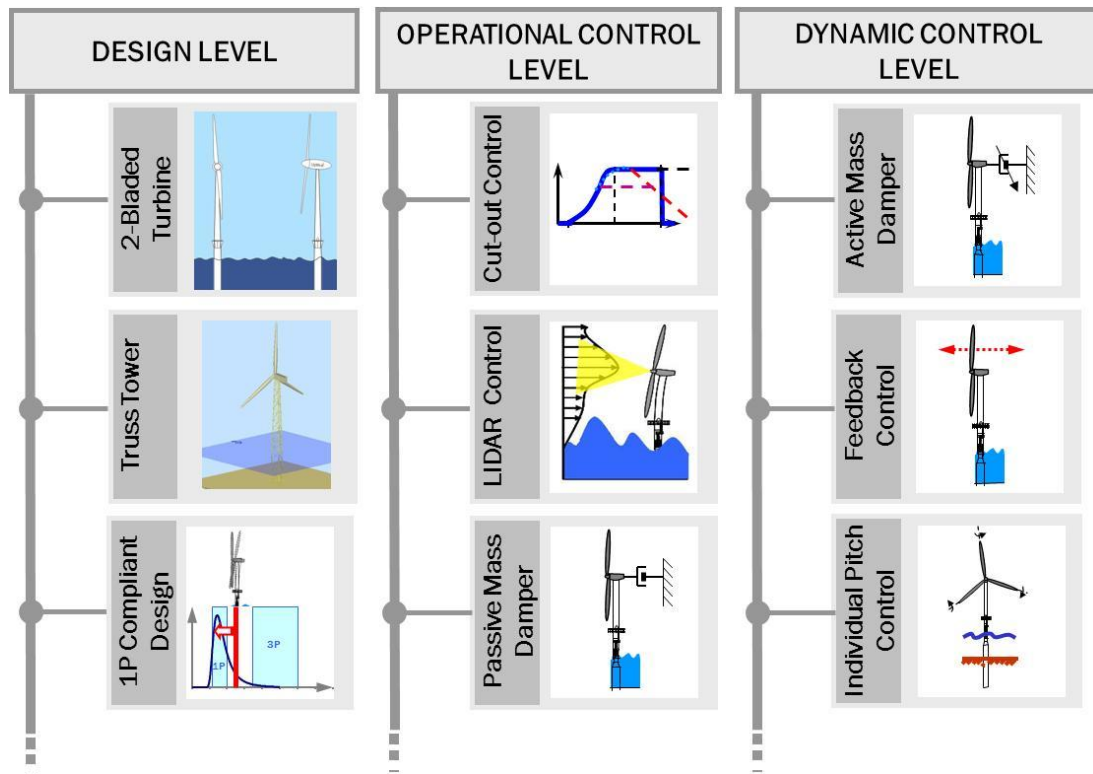
Figure 3.3: Levels and possible implementation of load mitigation

For support structure load mitigation, different concepts were studied and distinguished at the three above mentioned levels of load mitigation. The goal is to identify a suitable selection of options to finally obtain an optimised offshore wind turbine design. In Figure 3.3, the three levels of load mitigation are listed again along with some examples for implementations. These and further examples are discussed in the next three Chapters according to their prospects in load mitigation.

4.   Load mitigation concept analysis at design level

In the following Chapter, several concepts for load mitigation in the design level are introduced. These concepts range from specific turbine and support structure designs to the design of whole wind farm clusters. The shown concepts just give an overview of possible options and could be extended.

4.1   Two-bladed concept

For current offshore turbine types, usually three-bladed designs are used, as the concept has proven to have the best dynamic properties due to its symmetric layout. For future large turbine concepts, the blades are getting much larger and therefore play a major role in terms of mass and costs. Besides, installation and maintenance of these wind farms are a factor in the cost-effective design of offshore projects. Therefore a two-bladed offshore-specific turbine design can be one design solution of the future, as the reduction of the number of blades lowers the costs for maintenance and holds a significant potential to be more cost effective in the production process. Two-bladed offshore turbines are also easier and faster to erect, which offers a considerable cost reduction to the expensive offshore installations.
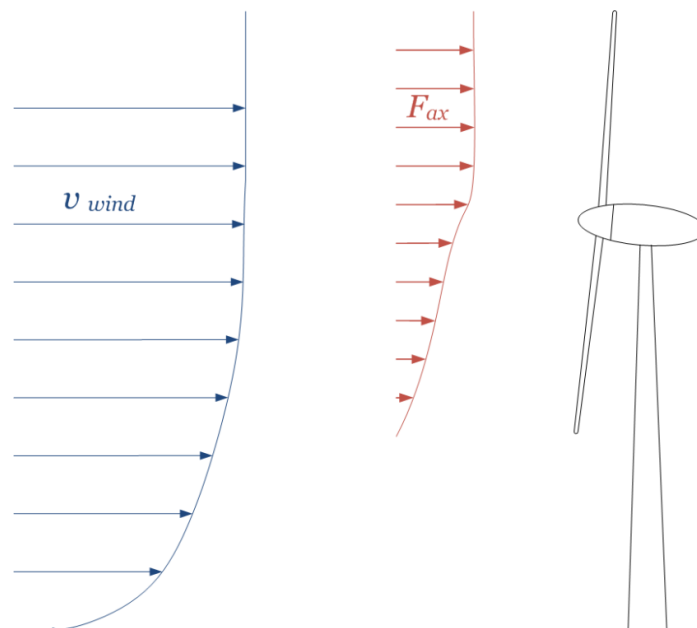
Figure 4.1: qualitative graph of wind shear [18]

In the past, several prototypes of large two-bladed turbines were built [19]. Even if some of them reached a commercial state, they never have been applied in large scales because of the lack in reliability and their application for onshore purposes mainly due to their visual impacts.
With modern wind turbines reaching the size of the early prototypes and costs for the blades taking a large part of the overall costs, two-bladed designs are becoming attractive for wind turbine manufacturers again [18].

Two-bladed wind turbines have a number of advantages over turbines with more blades, but also some great drawbacks, which have to be faced when designing a wind turbine with two blades.

One of the most obvious advantages is that one blade is saved compared to three-bladed designs. This leads to lower costs in production but also in maintenance. If for maintenance a helicopter is used, a two-bladed design offers much safer personal lifting options, as the rotor can be parked in a horizontal position and thus does not create potential collision situations with the helicopter.

Furthermore, two-bladed designs are faster to install offshore. For a two-bladed concept, the rotor can be assembled on the ground and lifted in one lift onto the nacelle using only one crane [20]. This reduces the needed crane capabilities and the storing capacity requirements on the installation vessel. Additionally, the installation time is shorter, which is an important factor offshore, as installations are restricted due to weather conditions and crane rental costs.

Finally, the structural stability can be increased if a continuous beam containing both blades is designed and the chord length of the blade is increased. This is done, if the rotating speed is not altered compared to the three-bladed designs, in order to obtain the same rotor solidity [18].
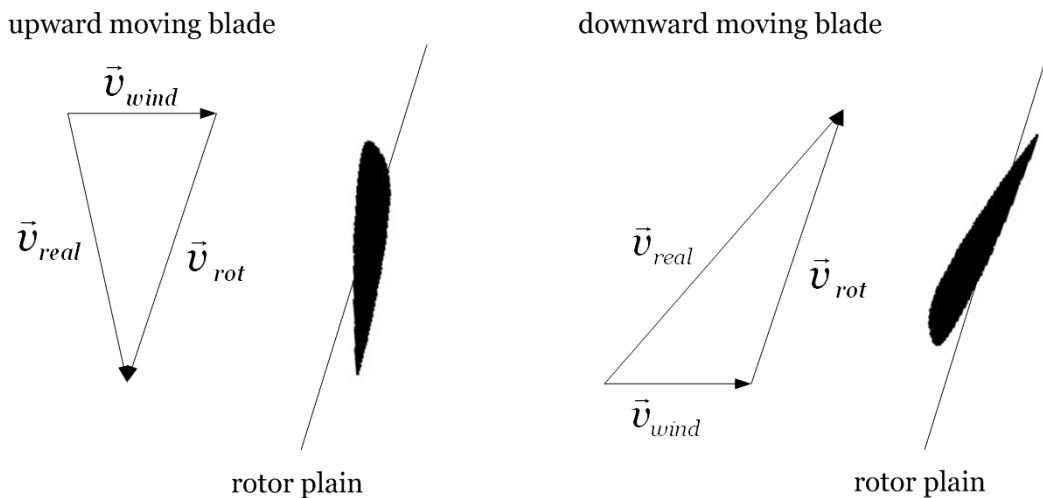

Figure 4.2: Approaching airflow left and right blade [18]

But there are also still several disadvantages for two-bladed concepts, especially due to its difference in the rotational moment of inertia compared to three-bladed concepts. Even if such effects are also present for three-bladed concepts, the effects are stronger for two-bladed designs. Because of wind, the non-circular rotor-layout strains the drive-train periodically every time the rotor passes the vertical position. In such an event, the blade pointing upwards experiences a stronger load than the lower blade. Additionally, the lower blade passes the tower shadow, where the wind speed is reduced and the turbulence higher. This results in an axial load, which is a combination of the tower shadow and wind shear load effect. For a three-bladed design the effect is more balanced out due to its circular layout and thus the loads are more equally distributed. Figure 4.1 illustrates schematically the effect of this axial force on a two-bladed design operating in the vertical rotor position.

Another load effect on the two-bladed rotor is caused by the tilt angle. While moving through the horizontal position, the two blades experience uneven loading. Here one blade is moving slightly forward while the other one moves back. The result is a difference of actual wind speed on the blades. As shown in Figure 4.2, the downwind moving blade is experiencing a stronger load than the upwind moving one. Here the blade experiences a wind speed v_{real}, which is larger than the incoming wind speed v_{wind}. Due to the rotational speed, a tangential component v_{rot} is added to the mean wind speed vector.

A similar effect is caused by yaw misalignment. As shown in Figure 4.3, this effect is strongest when passing through the vertical position. Depending on the direction of the misalignment, the upper or the lower blade is moving slightly towards the wind, while the other one moves away.

Especially for stall regulated turbines this effect has to be considered. In some cases the blade can stall in one azimuthal position which creates highly uneven loads through cyclic stall.

Additionally, the non-circular layout also causes an alternating inertia around the vertical yaw axis. It is maximal in the horizontal position and becomes minimal in the vertical position. This needs to be considered when designing the yaw actuator. Varying inertias make a stronger and more robust yaw drive necessary than in three-bladed turbines.

As already stated in the beginning, the experiences gained in the latest developments can eliminate the above mentioned disadvantages for two-bladed designs and enable them to be a competitive concept for coming offshore projects.

Load phenomena that depend on the rotational speed, like wind shear, tower shadow or the impact of a tilted rotor, can be mitigated by using individual pitch control. Especially for these azimuth dependent loadings, the design of a controller can be implemented without any problems. Bossanyi has shown in [21] that these effects can be limited by introducing an individual pitch controller.
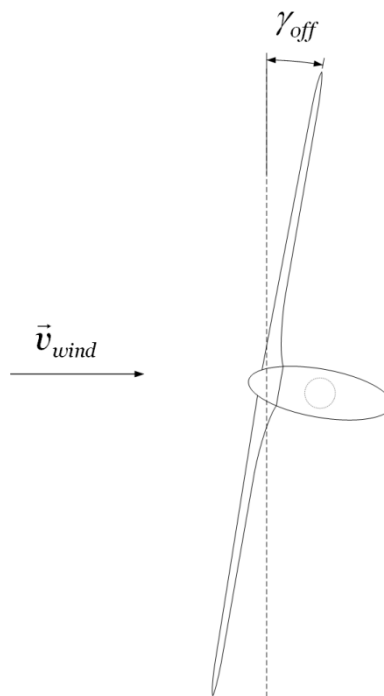
Figure 4.3: Top view of turbine - yaw misalignment [18]

Another option is to change the turbine layout into a downwind design. This has particular advantages for the large blades of future offshore wind turbines, as in downwind concepts there is a lower risk of the blades touching the tower in extreme operation. This leaves a larger margin for lighter designs of the rotor blades and the tower. Another advantage of a downwind concept is related to the yaw drive. A turbine with a downwind layout always passively orients towards the optimal position and usually does not need an active yaw control [22]. However, an active yaw drive might still be necessary for some operations like to untwist cables. As the high currents from the generator in the megawatt class cannot be transported over the slip rings but have to be ducted through cables [23], an active yaw mechanism is necessary to be able to untwist the cables.

Still, there are also some drawbacks of downwind configurations. The tower has a greater influence on downwind turbines than for upwind designs. This results in cyclical loads that influence the blades and the drive train. Higher loads make it necessary to increase the

structural stability of the drive train components which in turn compensate the mass advantages that are gained in the blade. To reduce the influence of the tower on the aerodynamics in downwind concepts, a truss tower is an alternative to a tubular tower design, as described in Section 4.2. Besides, individual pitch control can again be used to mitigate the effect of operating in the tower shadow.

In conclusion, the design of a two-bladed, offshore-specific turbine can be one of the solutions for coming offshore wind farms. Especially by using concepts like individual pitch, downwind configurations or truss-type support structures, most of the disadvantages compared to three-bladed designs can be mitigated enabling the two-bladed concepts to be a competitive solution.

4.2   Truss-tower configuration

As described in Chapter 2, the reduction of hydrodynamic sensitivity is one option to reduce loading on offshore support structures. Therefore jackets can be a solution, as they have small water-piercing members and they are hydrodynamically transparent for the wave field and less prone to direct wave loading. In addition, hydrodynamic excitation is significantly reduced since jackets have a much higher structural stiffness than for example monopiles. But the common type of jacket support structures with a tubular tower on top requires a massive and complex transition piece which is costly to design.

Therefore an option could be to use the braced-type structure continuously up to the tower top in order to save material. Such truss towers are well-known from offshore oil and gas platforms but also for some rare onshore projects. These full truss towers have a number of advantages, but also some drawbacks.

An obvious advantage is the amount of steel needed for the structure, which is much less than for jackets with tubular towers or even monopile configurations. The reason is that the structure is defining its stiffness mainly by the distance of the bottom legs, thus moment of inertia, rather than by wall thickness and diameter as for structures like monopiles. Especially for future offshore projects with a large and heavy RNA, a truss-type support structure can support such high tower top loads better than a tubular one. These large turbine types will also have lower rotor speeds, which might enable together with the high stiffness of the truss tower the design of support structures beyond the *3P* rotational speed range, namely the stiff-stiff design region according to Chapter 2.
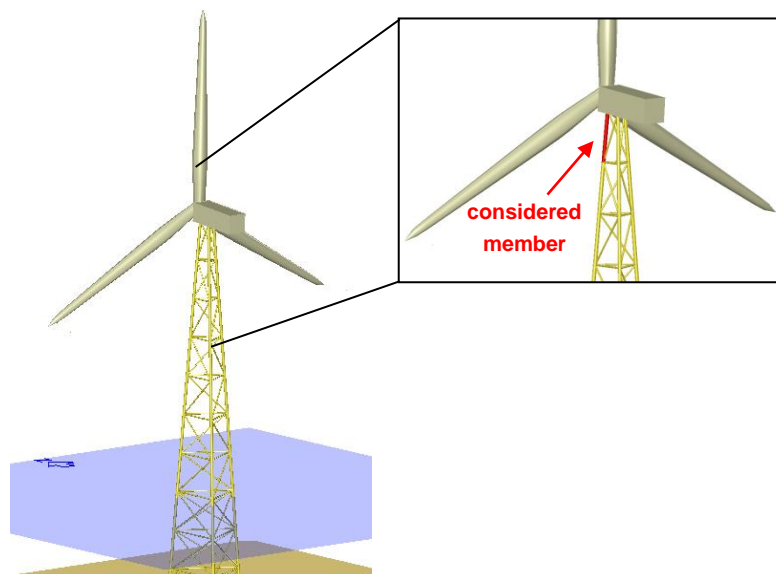

Figure 4.4: Truss-tower design

Another fact is that the dynamically critical and costly transition piece, as for jacket-tubular tower configurations, can be saved for truss-type support structures. Therefore the transition piece is moved to the connection between truss tower top and nacelle, which can also be difficult to design but in general lighter due to the lower bending moments from the aerodynamic loading from the rotor. Besides, the truss tower offers a geometrical flexibility. They can be designed as three leg towers but also as four leg solution. They can have different types of bracings, for example x-braces or z-braces.

The complex structure of a truss tower also imposes much higher cost for manufacturing and maintenance, as the number of welds is increased significantly as well as the amount of joints to maintain and to secure against corrosion. The transparent tower cannot be used anymore for storage of power electronics or spare parts like heavy converters, as done for some offshore turbines in order to reduce the mass of the nacelle.

Beside all the disadvantages in fabrication and maintenance, truss towers experience also different loading phenomena compared to designs with tubular towers. In general, the tubular joints with their stress concentrations are sensitive to high cycle fatigue introduced by the aerodynamic tower top loading and the reduced torsional stiffness. This can potentially lead to dynamic problems. At the bottom of the structure (close to seabed) the bending or buckling of the elements is critical and closer to the tower top (close to the nacelle) the torsional modes are also critical. The torsion at the tower top is induced by unbalanced loadings on the rotor from wind shear or skewed inflow. This also includes a much higher sensitivity to certain extreme events such as extreme directional changes. Therefore truss towers would benefit from particular aerodynamic load mitigation concepts like individual pitch control in order to reduce the torsional response.
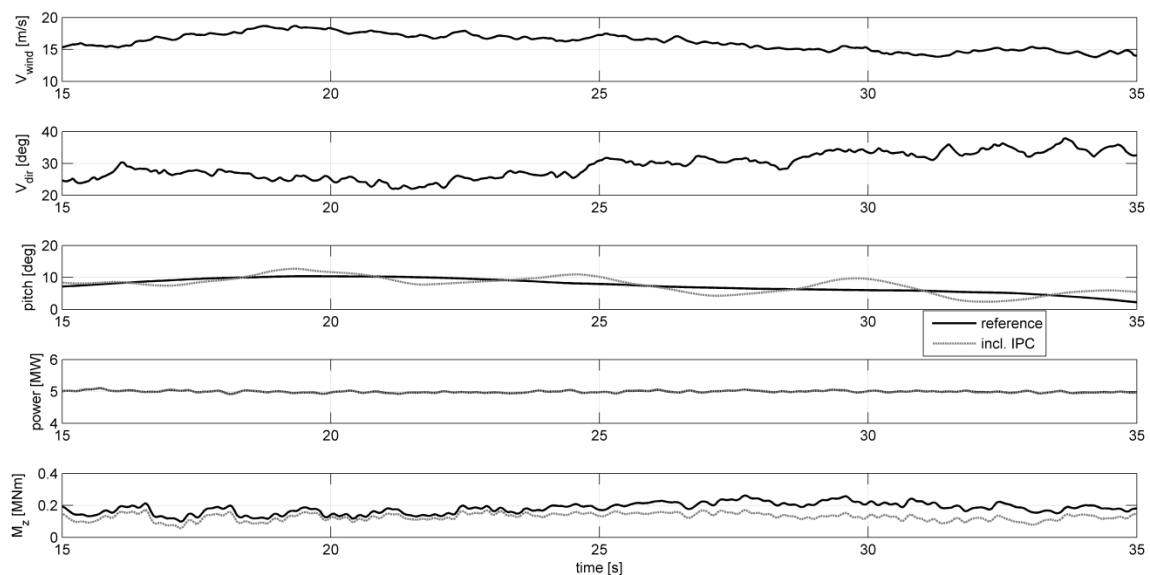
Figure 4.5: Torsional loading at truss-tower top with and without IPC

Figure 4.4 illustrates an exemplary truss tower design for a 5 MW reference turbine (see Appendix A). In the here shown case the support structure consists of a 3-leg truss tower and a z-type bracing (see Appendix A and [24]). As stated before, for such structures the torsional loading at the tower top can become a critical design driver. However, an industry-standard individual pitch controller without additional tuning for the tower loading can mitigate these loads already. As an example an advanced power controller designed for the UpWind project [25] is applied. The controller includes *1P* individual pitch control to reduce asymmetric rotor loads, and here especially *1P* loads on rotating components and lower frequency loads on non-rotating

components. Moreover, the controller has additionally the capability of *2P* individual pitch control in order to reduce *3P* loads on non-rotating components.

In Figure 4.5, a detail of a time-series for the discussed support structure is shown. In this case, high variations of wind speed, direction and shear are included, which can be seen in the upper plots in Figure 4.5 for wind speed and direction. These effects will introduce high torsional loading on the structure. The introduction of the IPC can be seen on the three lower plots in Figure 4.5. It shows that an additional pitch angle variation is introduced, here illustrated for the pitch angle of blade 1, and how the power output is still kept rather constant. Finally the plot shows the torsional moment at the truss-tower, and here for a member at the upper part close to the nacelle as shown in Figure 4.4. The curvature identifies a much lower torsional moment. The damping effect can possibly even be reduced if the controller will be tuned for the tower loads in particular. However, the example shows how an IPC can already be used for load mitigation.

In conclusion, the usage of truss towers for offshore wind turbines still has some major drawbacks like much higher costs for fabrication and maintenance, which must be weighted up against the advantage of saving material compared to the solutions with tubular towers. The critical loadings for truss towers can be mitigated by using control concepts like the individual pitch control. In a combination with an offshore-specific turbine concept, such as two-bladed machines, these structures can become a competitive solution for future projects. Especially their high stiffness might enable stiff-stiff design solutions beyond the critical turbine operation ranges with reduced wave loads.

4.3   Site sensitive design

Offshore wind farm designs nowadays follow an established procedure. In a pre-defined group of structures the worst possible conditions are assumed as to water depth, soil condition, marine growth and turbine weight and are then taken as design drivers for all structures in the group as shown in Figure 4.6. In that Figure the turbine is placed at the deepest location with the lowest soil stiffness. This results in conservative designs of all the structures with better soil conditions. Because of this, in 2007 a Danish engineering consultant, Rambøll, presented a different concept where individual designs for each location are done [26]. This implies, for example, that the actual water depths and soil conditions for each installation site are determined and taken into account. But still, the uncertainties and costs are high as there has to be accurate soil and water depth measurements for each site and individual fabrications and adjustable installation logistics are needed.
For some monopile designs in larger water depths with poor soil conditions and/or larger turbines the support structure design might not be driven by the wind and wave loads but mainly driven by the requirement of sufficient dynamic stiffness in order to achieve a fundamental eigenfrequency at least 10 % higher than the rated rotational frequency of the machine (*1P*).

Due to the inherent uncertainties in water depth, soil properties and structural parameters an additional safety margin on top of the 10 % is applied during design. Especially for larger and heavier turbines, monopile supported structures tend to have lower eigenfrequencies and thus are getting closer to the *1P* frequency range. In such cases, the structural stiffness is mainly increased to match the limitations in frequency ranges rather than critical loadings. This will jeopardize the economics of monopile support structures.

This design philosophy is in a lot of cases debatable, as in many situations the *1P* excitation, mainly caused by structural or aerodynamic imbalance, is relatively low and only a certain number of machines in the fleet suffer a larger excitation due to poor balancing during manufacturing and commissioning or due to aging effects. Considering the overall benefits for the whole offshore wind turbine one may invest in a *1P* vibration control system including either

dynamic balancing or an active or passive damping system in order to facilitate safe operation of the machine in the *1P* resonance. Given the aforementioned uncertainty in the actual fundamental eigenfrequency only a fraction of the wind turbines in a large offshore wind farm will actually struggle with a really pronounced *1P* resonance and will require maximum employment of the vibration control system while softer, lighter and more cost-effective monopile structures could be employed for many turbines.

- soft soil (varying soft clay and sand profiles)
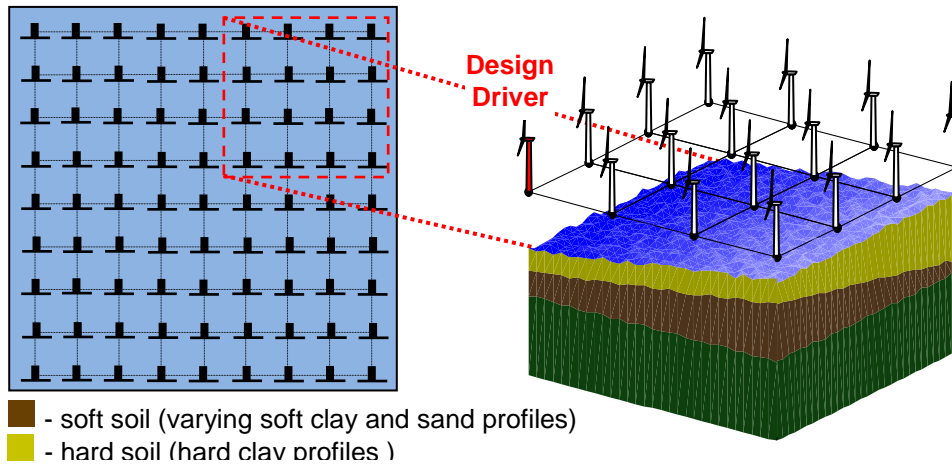- hard soil (hard clay profiles)

Figure 4.6: Illustration of grouped design for an offshore wind farm

The mentioned vibration control system for the compensation of such variable site conditions and the connected *1P* resonance effects can be done in different ways. A straight forward solution is the implementation of a rotational speed-window, as further explained in Section 5.1, which will avoid the critical resonance frequency during operations. Of course, such an application is only possible if the resonance is occurring in the variable rotor speed region of turbine operations. In the worst case, the resonance coincides with the rated rotor speed. For such cases a more sophisticated vibration control system is necessary. A solution can be to operate the turbine with up to 10 % increase of the rotational speed value by lowering the corresponding torque [27]. This will lead to higher tip-speeds, which is generally not an issue offshore. Additionally, the approach will increase the loading on the RNA, especially the blades. However, this can still be acceptable from a wind farm perspective, if this affects few turbines and the overall support structure costs are reduced.

Besides changing the operational characteristics of the turbine, another solution could be the implementation of a structural damper device, such as a semi-active concept as described in Section 6.5. Due to its semi-activity, the damper can be tuned for different vibrational conditions, which can be for example the resonance at *1P*. With such device, varying site conditions and critical operational frequency ranges can be taken care of during the design process.

As conclusion, it might be more cost-effective to design a larger group of support structures by not taking the worst site and turbine conditions into account for the design-group, but an intermediate or even the best conditions. If in such cases loading is not driving for the softest structures but exclusion ranges of certain rotational dependent turbine frequencies are being used, there are a range of concepts available. By using different operational control or even dynamic control concepts, an overall trade-off for the whole offshore wind farm can be achieved.

4.4 Park configuration

In addition to the concepts in this report concerning specific turbine or support structure designs to achieve reduced loadings and a more cost-effective solution, the layout of an offshore wind farm can also have significant effects on the loads and costs. There are three major effects on the wind farm layout costs, two of which are also directly connected to turbine loading. These are:

- Electrical infrastructure (cost-related)
- Local bathymetry and soil conditions (load- and cost-related)
- Wake effects (load- and cost-related)

The electrical infrastructure is affecting costs only, but not the turbine loading. Here depending on the distances in-between the turbines and the main transformer station, the costs are well defined. The optimization of the wind farm layout depends largely on the costs and losses of the electrical transmission balanced against the aerodynamic losses caused by wakes and costs due to site-specific support structure designs depending on the local bathymetry. In general, the turbine distances shall be as small as possible for an optimized cabling cost and as large as possible for optimized power outputs.

In addition, the turbines cannot be erected at any location, as local bathymetries and soil conditions can also affect the design significantly. Here the optimization target is to select as shallow as possible the locations for the wind turbines together with adequate soil conditions. These preferred locations enable cost effective designs of the support structures because of lower loads and weight reduction.

A major parameter in terms of load mitigation for optimal wind farm designs is the impact of turbine wakes. As the wind turbine extracts energy from the wind, it creates a wind speed deficit behind that meanders in time and space due to the ambient turbulence (major wake load effect) and the wake vortex also leads to an increased turbulence (minor wake load contribution). Finally, those wake effects result in higher fatigue loading on downstream rotors. Here the number of turbines and their power ratings, but also the layout and spacing is defining the strength of the wake effects. But the wake effects also have a significant impact on the energy yield. Generally speaking, an increased installed capacity for a fixed space leads to decreased power efficiency [28].

However, a reduced power efficiency is not necessarily connected to the trends in additional loading. In the European TOPFARM project, studies for an exemplary 5 MW turbine model [29] have shown that a spacing of 3 to 10 rotor diameters can lead to an effective increase of the ambient turbulence of up to 25 to 14 % respectively [30]. The resulting blade fatigue loads are increased between 60 and 5 % compared to the turbine loading in free-flow conditions for a specific spacing between 7 and 10 rotor diameters, with the increase depending on wind speed and ambient turbulence [31]. But the loading is additionally very much dependent on the kind of wake effect. A downstream turbine can be in full wake or only be affected for half or another percentage of its rotor area by the upstream turbine. In full wake conditions, the loading is of course increased by the increased turbulence intensities, but in half wake conditions the rotor additionally experiences a much more unbalanced loading. This effect is worse for conditions where the outer part around the blade tip is the only affected section of the downstream rotor. For the power output a different trend is known. In full wake conditions the losses are highest, where for half wake or any other part wake conditions the losses are decreasing. Thus, the optimized conditions for power output and loading differ.
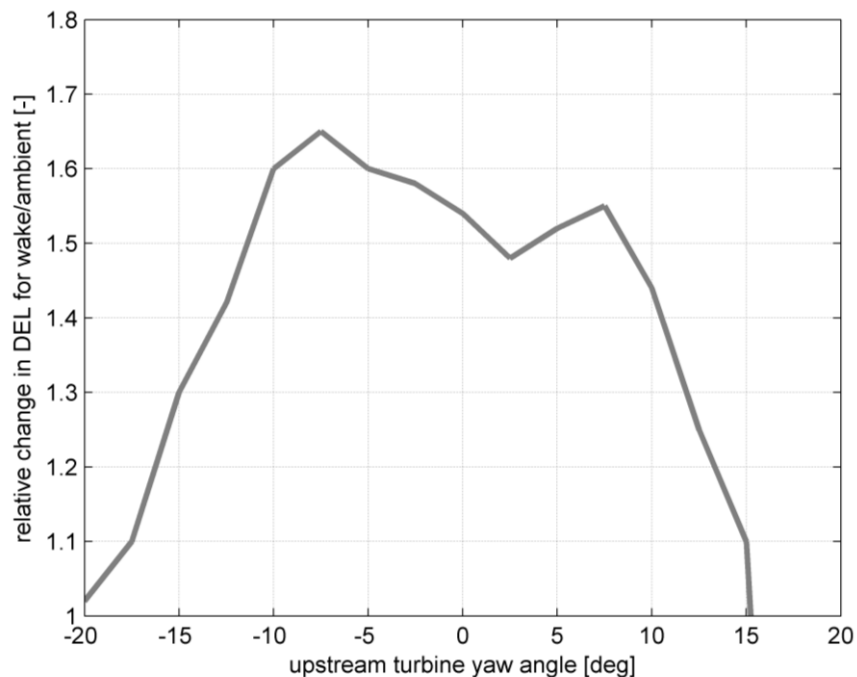
Figure 4.7: Normalized tower base overturning moment vs. upstream turbine yaw angle [30]

Figure 4.7 shows an example from the European TOPFARM project for wake condition at a turbine distance of *6D* and the effect on the tower base overturning damage equivalent fatigue load for an SN exponent of 4 as relative change in loading compared to the free-flow conditions. The plot illustrates that for full wake conditions, here at an x-axis value of 0 degrees which corresponds to parallel rotors for the upstream and downstream turbine, the loading is increased by a factor of 1.5 If the upstream turbine is yawing and thus the downwind turbine experiences only a partly wake, the loading increases. The curve reaches its maximum with a factor of 1.65 for conditions where the wind direction that contains the wake is at approximately -8 degrees, which corresponds in this example to the conditions where the center of the meandering wake is at the blade tip. This clearly indicates the importance of wake effects.

In conclusion it can be stated that for an optimized wind farm layout, several parameters have to be taken into account. For an optimal layout in terms of loading, the selected sites and the shape of the wind farm have the major impact. In order to reduce wake-induced loadings, the wind farm layout target has to be to obtain as few as possible wake situations or at least highest possible turbine spacings in the prevailing wind directions. However, for a final cost-effective design solution, the cost of energy is leading the decisions and here aspects like the electrical infrastructure play another important role [32].

4.5   Robust design

Within this work, the main emphasis is on advanced turbine design and control concepts in order to achieve a cost-effective offshore wind turbine design. In order to complete the conceptual evaluations, an opposite concept has also to be discussed. This concept excludes all advanced systems and reduces the amount of components in the turbine. Therefore this concept is called robust design. Due to the lower amount of components, less failure shall occur or the investment costs shall be lower as well as costs for operations and maintenance. These aspects are defined as design according to RAMS – **R**eliability, **A**vailability, **M**aintainability and **S**erviceability [33], where each of the four criteria shall be maximized. Several pre-studies have

shown that such robust concepts can achieved up to 40 % lower failure rates, 20 % lower operational and control costs and up to 3 % higher availabilities [33]. This leads in conclusion to lower levelized production costs, which are a measure of costs of a turbine per produced energy yield.

In the past, passive stall-regulated and fixed rotor speed with 2 blades and a direct drive transmission concept were often promoted as robust designs [34], as for such stall-regulated turbines there is no need for pitch actuators or bearings at the rigidly mounted blades. But one of the main disadvantages about stall-regulated and fixed-speed turbines is their non-optimal power output and the variable loads, which are very sensitive for blades. Furthermore, this concept does not fulfil the increasing grid compatibility requirements due to a growing part of decentralized offshore wind power production in the future.

The solution for such a future robust stall-regulated concept can be achieved by using a variable-speed electric system and controlling generator torque such that the power output is kept stable beyond rated wind speed. This concept still includes on the one hand all the advantages of a robust design with its rigidly mounted blades and fewer components for bearings and pitch actuators and on the other hand it provides a stable power curve and better controlled loadings. Additionally, due to its variable-speed characteristics provided by a controlled torque from the direct drive generator, the power losses before rated wind speed can be reduced. This is because of longer operations in the region of the optimal tip speed ratio.

In comparison to all further discussed advanced turbine concepts in this report, the here briefly described robust design can be solution for coming offshore wind farms without recurring to any advanced operational and dynamic control systems. Especially for offshore wind farms far away from shore, such a system design for maximized RAMS can be a competitive solution.

5. Load mitigation concept analysis at operational control level

In the following Chapter, several concepts for load mitigation in the operational control level are introduced. These concepts include already available turbine operations in order to reduce overall loading. The shown concepts just give an overview of possible options and could be extended.

5.1 Rotational speed window

As explained in Chapter 2, the design ranges for support structures are important from a dynamic point of view. In general, most bottom-mounted support structure concepts are designed for the soft-stiff design region, which is between the *1P* and *3P* of the rotor speed range. An example of such a design is shown in Figure 5.1, where a support structure is designed for a first eigenfrequency of 0.22 Hz (here named as *old* design). In many cases the support structure's eigenfrequency does not coincide with the prediction as illustrated in Figure 5.1 as *new* design. This can happen due to changes in the foundation properties, such as scour holes, or simply due to errors in the soil measurements performed prior to the support structure erection, on which the design was based. This means first of all that the design moves into the high energy range of the wave spectrum, as illustrated in Figure 5.1 for a typical wave spectrum. This will cause higher excitation from the hydrodynamics. But beside that, the eigenfrequency falls within the *1P* rotational speed range, which means that at some operational points the rotor will operate at the same frequency as the first eigenfrequency of the support structure. The result is that the support structure can vibrate at an unacceptable level and the loading in the structure will increase.
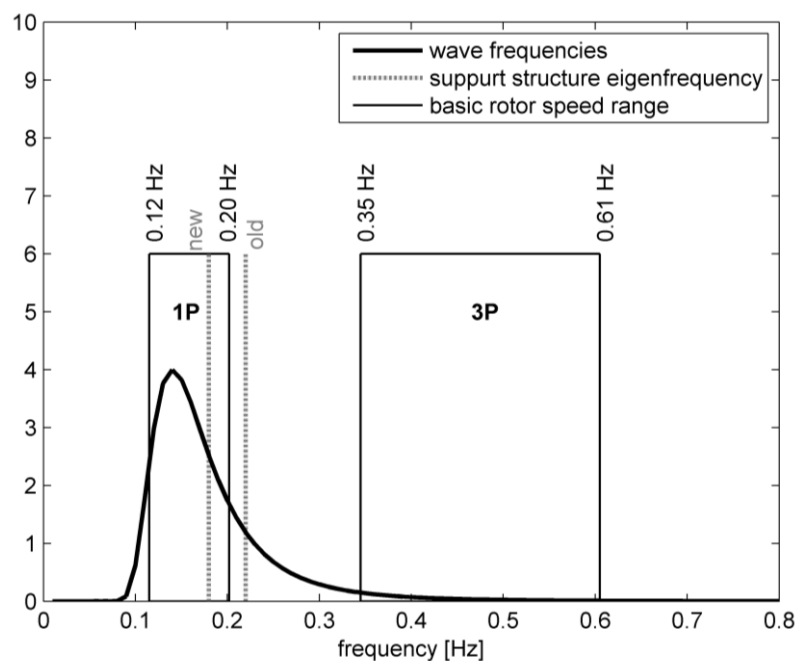

Figure 5.1: Frequency ranges for different support structure designs

Such a resonance can also be shown using a Campbell diagram, see Figure 5.2. The Figure shows that for the first design (here named as *old* design) the first support structure

eigenfrequency was well distanced to important rotational frequencies, such as *1P*, *3P*, *6P* or *9P*. But for the new case (here named as *new* design), where the eigenfrequency of the support structure decreased from 0.22 Hz to 0.17 Hz, as an example, at the rotor speed of 10 rpm resonance would occur. In Figure 5.3, the effect is shown for the fore-aft bending moment of the support structure at the mudline in the frequency. It can be seen that in the case of a resonance at 0.167 Hz, the loading is increased clearly at the frequencies of *1P*, *3P* and *6P*.

An operational control solution for such a resonance case in the variable speed region is the concept of a rotational speed window. Figure 5.4 illustrates the generator speed versus generator torque curve of an exemplary 5 MW turbine design (see Appendix A), which is a variable-speed and pitch-controlled design.
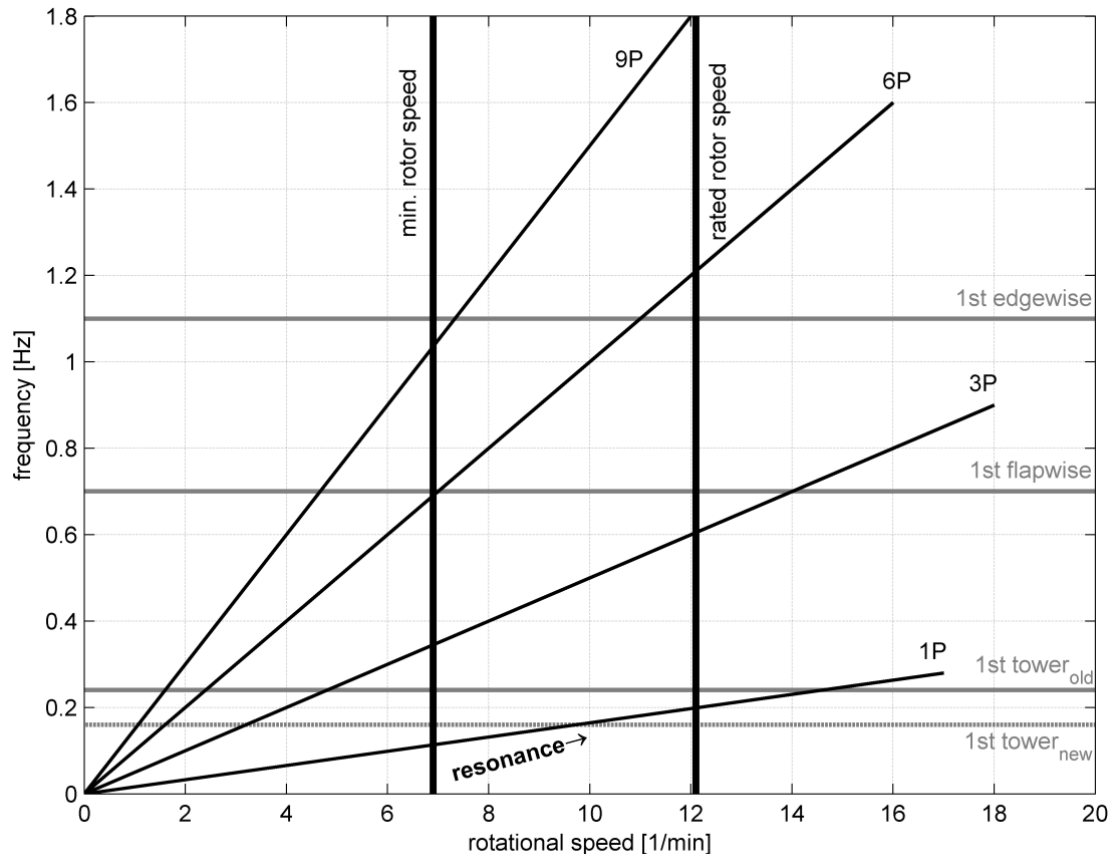
Figure 5.2: Campbell diagram for different support structure designs

The curvature shows that for a certain minimum speed, here at 670 rpm generator speed, the controller ramps up from point B to C in order to match the optimal power coefficient line, where the variable-speed controller then tracks the curvature for optimal operations. In the original controller this would be done until a certain point F is reached, where the rotor speed is kept constant and hence the optimal tip speed ratio is no longer held until the rated power is reached in point G. In point G the pitch controller takes over in order to maintain the rotational speed and torque by pitching the blades.
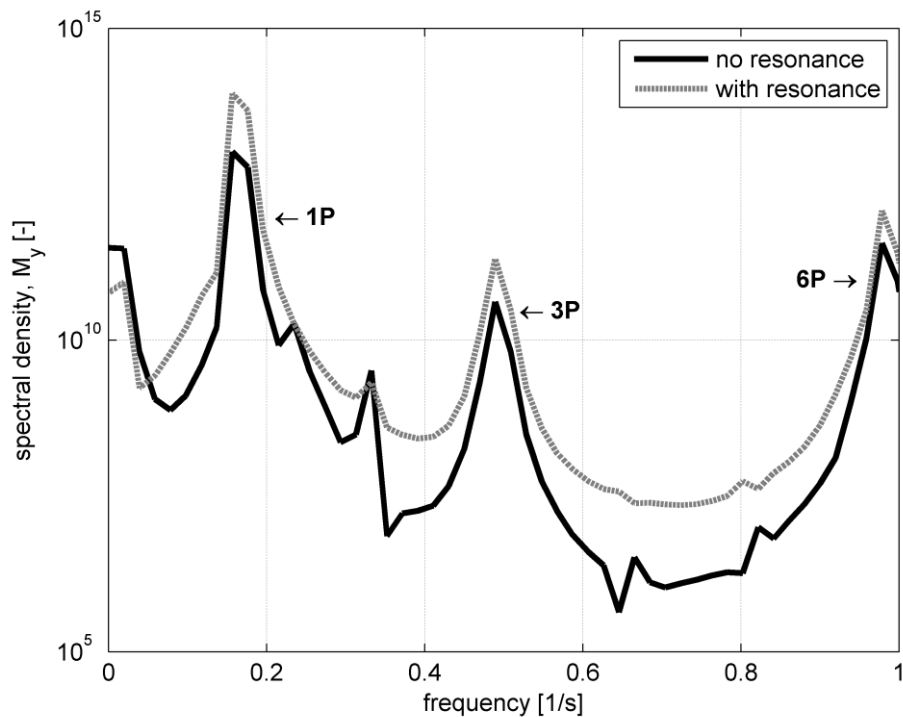
Figure 5.3: Spectral desity for the support structure fore-aft bending moment at mudline at V=8.7 m/s (here chosen to achieve turbine operations at the resonance frequency at 10 rpm)

In a resonance case within the variable speed region, as shown in Figure 5.4 again for a critical frequency at 10 rpm rotor speed or 970 rpm generator speed for the given turbine with a gear box ratio of 1:97, an exclusion zone for this speed can be included. In general, a safe exclusion range of +/- 10 % of the critical speed value is taken as standard in the industry in order to take uncertainties in design conditions into account. This zone is then centred around this 970 rpm generator speed value, which in the given example corresponds to the first support structure eigenfrequency being in resonance. Below and above this centred frequency, new operational ranges are included. Each region is bound by a certain rotational speed value. In the case where the rotational speed increases from a low value and tends to pass the resonance, here for example point C to point F, the lower bound of the rotational speed window will keep the rotational speed constant as soon as the bound is reached with the result of an increase in generator torque (here point D to D'). When the torque demand exceeds the value of point D' for a certain time the boundary point of the rotational speed is smoothly ramped down from D' to E'. Due to this the torque will follow and will be reduced by the controller respectively. The result is that a fast drive-through of the critical resonance frequency with a fixed rate is performed and thus no vibrations can build up.
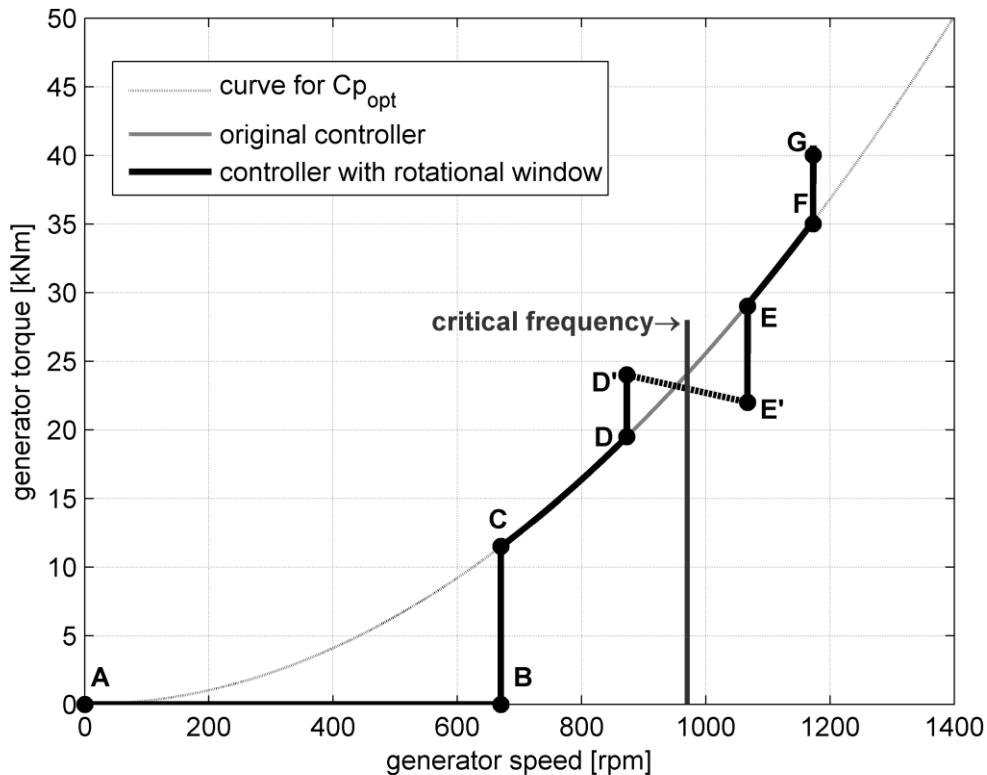
Figure 5.4: Turbine generator speed vs. torque curvature

The above described concept is mainly used for structures like monopiles which have resonances with system eigenfrequencies. But it can also be a solution for other structures and cases. Latest studies for jackets suggest that certain resonances of local braces might occur [35]. Here especially the lowest x-braces of the structure seem to be in resonance with some higher blade passing frequencies. As for the former described case, a rotational speed window could be an option to avoid this effect. However, the practical application is questionable, as it will be very difficult to determine these effects – both in simulations and especially offshore during operations.

5.2   Soft cut-out

The normal range of operation for a wind turbine is generally within a wind speed range of 3 to 25 m/s. In some rare cases the cut-out wind speed can be increased. Once the cut-out wind speed is exceeded and the turbine shuts down, a switch back to the power production mode is only possible with a hysteresis and at a lower wind speed. Onshore this concept seems reasonable. In contrast offshore this cut-out procedure might cause relatively high hydrodynamic excitation after the cut-out wind speed since no aerodynamic damping is present after a shut-down event and will return after the turbine is switched to operation again at a lower wind speed. Furthermore the intensity of wave heights increase for higher wind speeds, as seen in Figure 5.5. This adverse condition becomes even more critical because high waves will persist even when the wind has already calmed down due to the time lag between mean wind speed and the waves during a storm. Here the so-called soft (or extended) cut-out strategy (SCO) can be promising.

So far, the concept is mainly used to increase the energy yield and/or for grid stability reasons. However, one option to use this approach is to maintain a reduced power level beyond the original cut-out wind speed and use the aerodynamics to damp the wave responses. Here different strategies might be applied depending on the kind of maintained power output. As the major goal is to enhance aerodynamic damping rather than increase the power output, a reduced power level is proposed. This can be achieved by reducing the rotational speed of the generator by keeping the rated generator torque. This approach is illustrated in Figure 5.6. The chosen power level depends on several factors.
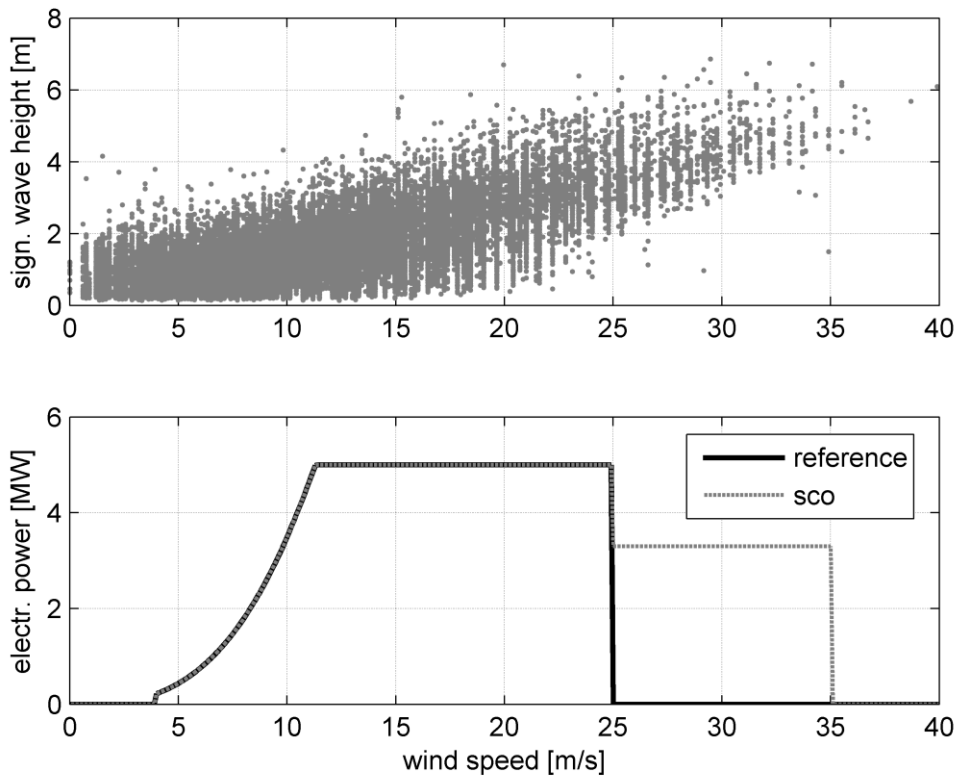
Figure 5.5: Extended cut-out wind speed versus wave heights

First of all, a reasonable amount of aerodynamic damping shall be produced, which generally requires a higher rotor speed. In doing so, the speed level has to be low enough in order not to overload other turbine components, such as blades or the drive-train. This is especially valid for extreme loads. Here the extreme operating gust (EOG) is driving the set point for the rotor speed of the soft cut-out, as at high wind speeds the gust intensity increases significantly and therefore also the importance of that load case. Thus, the concept has to ensure that extreme loads are not higher than in the former normal operational case, here illustrated with a cut-out at 25 m/s.
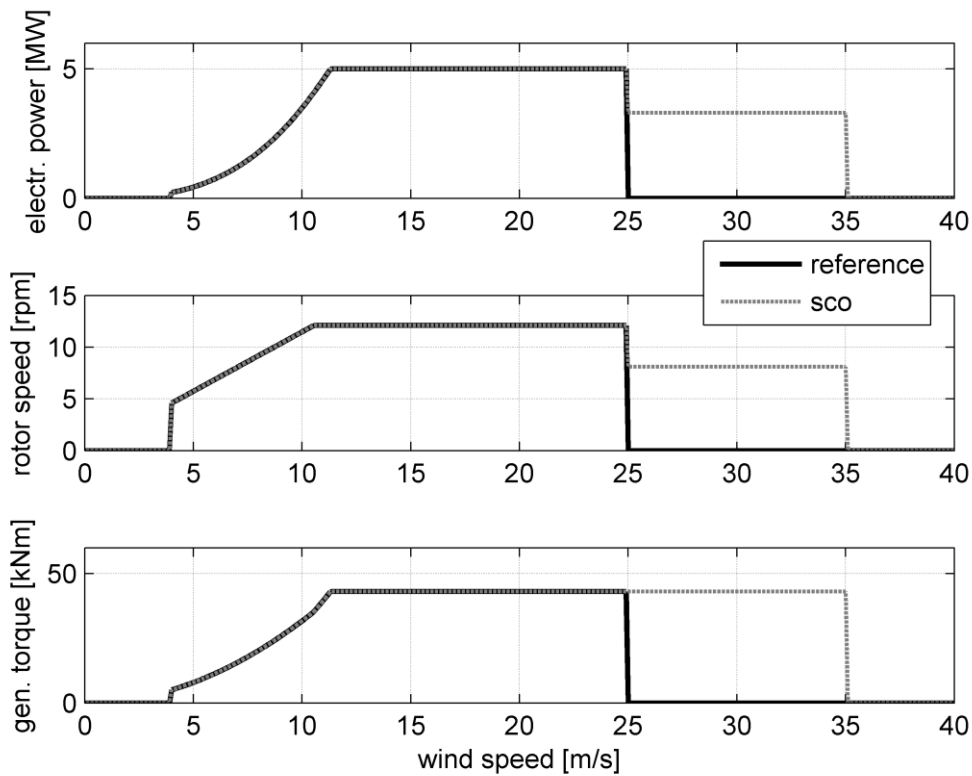
Figure 5.6: Concept of an extended cut-out wind speed

Based on studies [36] it can be concluded that a demanded generator speed level of 2/3 of the rated value and the corresponding pitch angle settings for ensuring this speed should be chosen for the soft cut-out regime. This value ensures a significant increase in damping and a safe operation in extreme cases. Figure 5.7 illustrates such an example, where for the reference 5 MW turbine on a monopile in 25 m deep water (see Appendix A) an EOG according to IEC 61400-1 [37] is simulated. The gust amplitudes are at 8.4 m/s for a mean wind speed of 25 m/s, and 11.2 m/s for 35 m/s respectively. The curvature shows that the extreme loads, here shown as the flapwise blade loads at the blade root and as support structure's overturning moment at mudline, are smaller for the soft cut-out case. This can be achieved by the reduced rotational speed level, which in such a case captures the gust with the rotor inertia and a slight increase in the rotor speed.
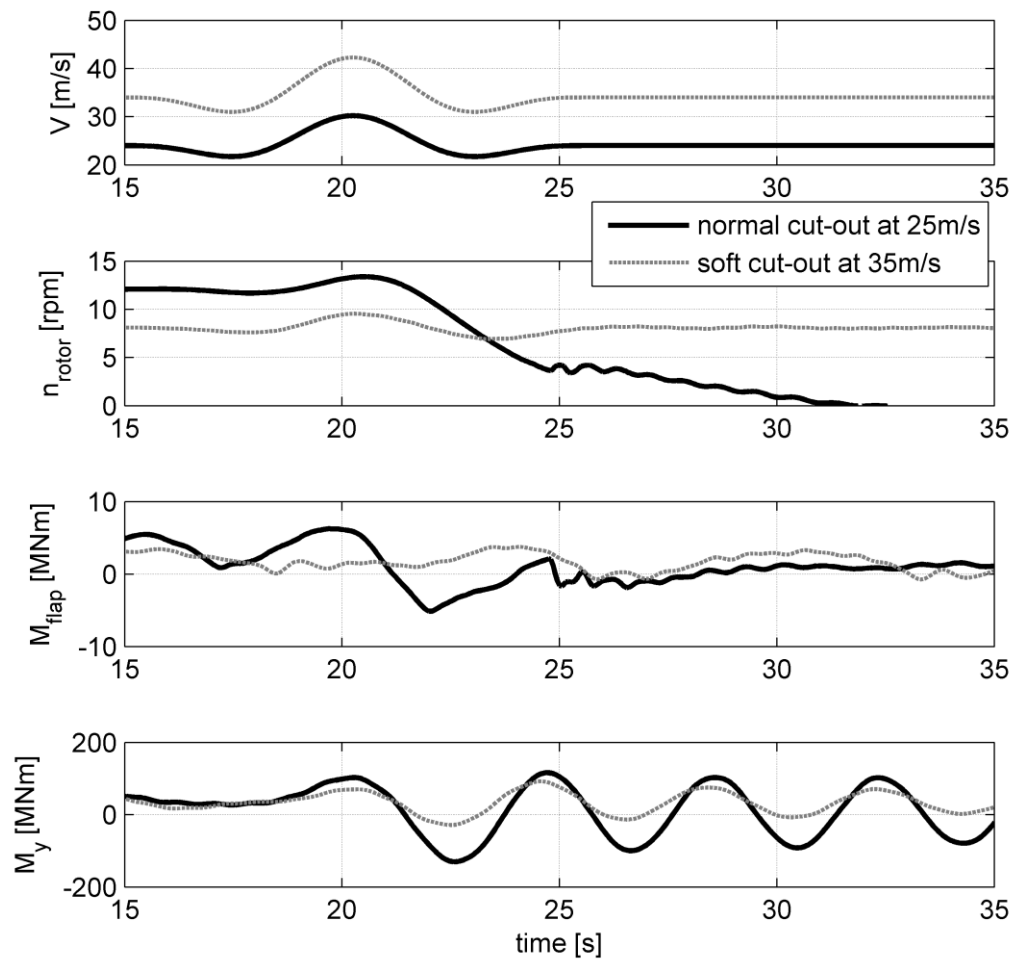
Figure 5.7: Detail of simulation results for an extreme operating gust at 25 m/s and at an extended cut-out of 35 m/s

Besides the lower load level, another important aspect of the soft cut-out concept can be identified in Figure 5.7. In the case for normal cut-out wind speed at the 25 m/s, the turbine shuts down due to an over speed trigger in the safety system. If such an event happens in a large offshore wind farm, the rapid loss of a whole wind farm power can cause significant problems in the grid and can lead to a breakdown of the electrical system. This happened for example in 2005 in Denmark [38], where a storm struck the whole part of Jutland and Funen over a broad front. It totally upset the production plan for wind power when during the afternoon it developed into a hurricane. Due to the safety equipment in the turbines, all turbines in the region went rapidly from full power production to a total standstill. As the gust and associated shut down was so enormous, many turbines enabled another safety device that required manual restart the next day. If the turbine would have been equipped with a soft cut-out device, this shutdown would probably not have happened, or at least would have happened in a more controlled and grid-friendlier manner.
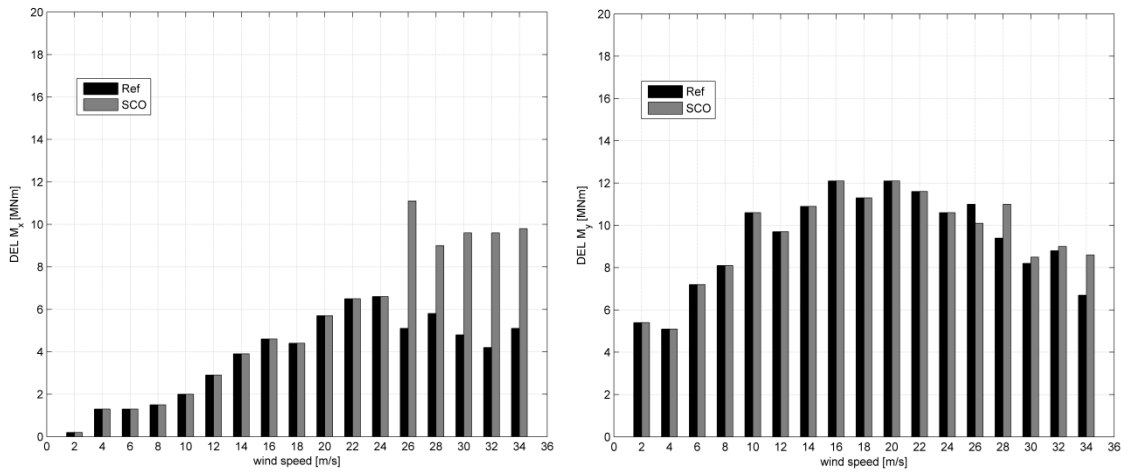
Figure 5.8: Non-lifetime weighted DELs (with N=2E+7) for the support structure moments (m=4) at mudline as comparison of the reference and the SCO-controlled case at the shallow water site

If the application of a soft cut-out is considered, it is important to validate its benefits according to the chosen offshore site, turbine type and support structure concept.

Structures with large water-piercing members, such as monopiles or tripods, have in general a higher portion of hydrodynamical loads. An increase in aerodynamic damping has in the most cases potential for overall load mitigation. For structures with smaller members, such as for jackets, the concept of a soft cut-out would not be beneficial, as the fatigue loads for such a structure are mainly governed by aerodynamic loads. Thus, an enlargement of the power production range would lead to more loadings from the aerodynamics and therefore a reduced lifetime of the structure.
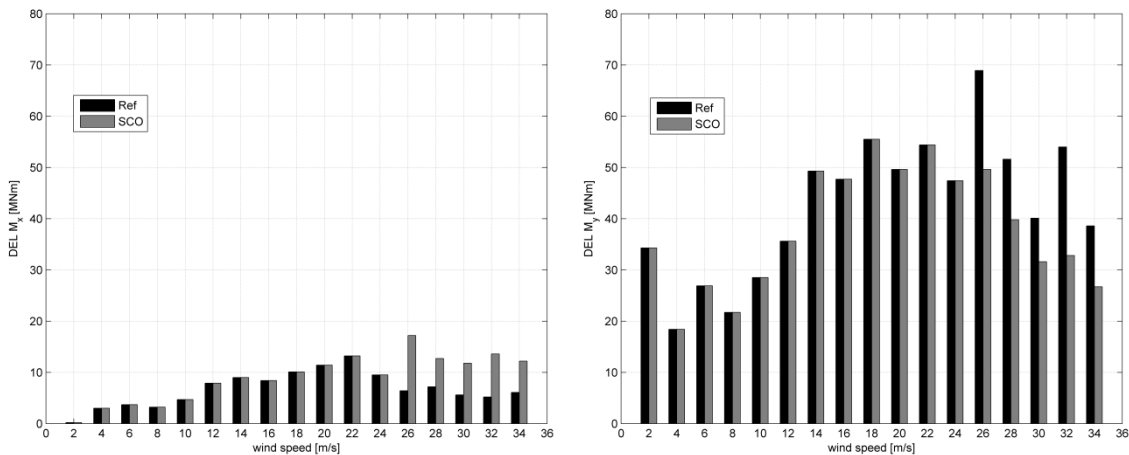
Figure 5.9: Non-lifetime weighted DELs (with N=2E+7) for the support structure moments (m=4) at mudline as comparison of the reference and the SCO-controlled case at the deep water site

But even for structures like monopiles, it has to be precisely checked if the concept is decreasing the overall fatigue loads or not. If a monopile is installed at a very shallow water site, like 0 to 10 m, the fatigue loading in the pile is in the most cases governed by the aerodynamic loads due to the lower energy in the waves. In such cases the soft cut-out would be counter-productive as for the jacket, because the main fatigue load driver, the aerodynamic loads, is increased by the larger power production range. Thus, the conclusion is that the concept can be

successful if the benefit from adding fore-aft damping to the wave response compensates for the additional production-induced aerodynamic loads. This is in general the case for sites with larger water depths, where the wave-induced fatigue loads are governing.

Table 5.1: Comparison of results between the reference and SCO-controlled case for two different offshore sites

	Loads as DEL [N=2E+7, m=4]			Change in energy yield and power fluctuations		Change in pitch rate
	Support structure at mudline					
	M_x	M_y	M_{xy}	AEP	P_{std}	$Pitch_{std}$
Reference Shallow site	13.01 MNm	28.09 MNm	26.38 MNm	25.6 GWh	0.15 MW	0.46 deg/s
Soft cut-out Shallow site	+ 66.0 %	+ 2.2 %	+ 7.6 %	+ 2.2 %	+ 3.3 %	+ 6.4 %
Reference Deep site	23.9 MNm	132.1 MNm	100.6 MNm	25.6 GWh	0.15 MW	0.46 deg/s
Soft cut-out Deep site	+ 33.4 %	- 11.5 %	- 2.7 %	+ 2.2 %	+ 3.1 %	+ 6.4 %

In the following, the soft cut-out concept is applied for two different sites, a shallow water site with 10 m water depth with an appropriate turbine and monopile design (see Appendix A) and at a deep water site with 25 m water depth and a respective design (both structural descriptions in Appendix A). The loads are expressed as damage equivalent loads (DEL) for a reference cycle number of N=2E07, a lifetime of 20 years and an inverse S-N-slope of m=4 for steel components and m=10 for composites. In the given cases, no misalignment between wind and waves are included, as the concept shall be evaluated for the damping of the fore-aft bending moment in the support structure, where it is designed for. Thus, the support structure fore-aft moments (M_y) are much larger than the corresponding side-to-side moments (M_x). Both moments are evaluated at mudline.

The Figures 5.8 and 5.9 show first of all that the sideways support structure loads are increased for the extended power range. This is due to the fact that this support structure mode is strongly coupled with the rotational-induced loads of the rotor and has furthermore a very low damping level by itself. The fatigue loads are significantly increased by 33 to 66 % (see also Table 5.1). However, the absolute change compared to the fore-aft load component is still very small.
For the fore-aft support structure loading, a difference between both sites can be seen. For the monopile at the shallow water site, the loading is increased, where it is decreased for the deep water site. This is due to the added loading to the system compared to the gained damping as explained before. For the monopile at the shallow water site, the added aerodynamic loading is higher than the gain in reduction of the hydrodynamic fatigue load component. Thus, the overall loading has increased. For the deep water site it is the opposite and here the concept works. This can also be concluded from Table 5.1, where for the shallow water site an increase of 7.6 % in the relative support structure moment M_{xy} is found and for the deep water site a reduction of 2.7 % in lifetime fatigue loading. Furthermore Table 5.1 shows a valuable secondary effect of the soft cut-out concept, which is an increase of the annual energy production (AEP) by over 2 % for the here considered cases by keeping a reasonable increase of power fluctuations.
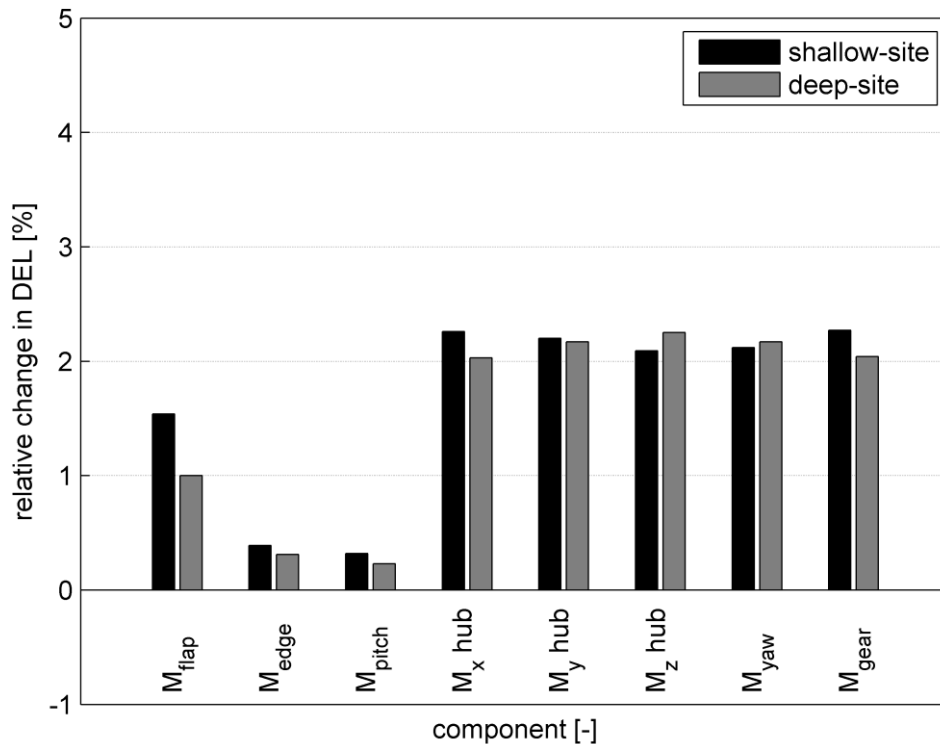
Figure 5.10: Relative change in component fatigue loading by applying SCO in comparison to the reference case

The concept has also some drawbacks. Due to the extended power production range, the RNA loads will be increased. As seen in Figure 5.10, the changes in fatigue loading for the main RNA components are in the order of up to 2 % for the nacelle components (hub, yaw bearing and gear box) and between 0.5 to 1.5 % for the blade.

The conclusion for using a soft cut-out controller in terms of load mitigation is that it works properly for sites with high amounts of hydrodynamic loadings. The shown case identified a possible load reduction potential of 2.7 % for the critical support structure moment. Other studies have shown that this mitigation potential can be even higher for sites with even more pronounced waves and larger monopiles [36].

5.3   LIDAR

The loading on offshore wind turbines is manifold and in particular most of the transient events occur very quickly. Therefore most of the control systems, both operational and dynamic, cannot react fast enough to mitigate these loads. Examples are transients like gusts or directional changes. A solution could be found if the upcoming transient event is detected before it reaches the turbine. Here remote sensing is currently discussed as a control solution. A common remote sensing device is the use of a so-called LIDAR system. A LIDAR (**LI**ght **D**etection **A**nd **R**anging) is an optical remote sensing device that measures the speed of aerosols by using the Doppler effect. Beside the common use of the LIDAR systems for wind speed measurements from the ground, the device can also be mounted on top of the nacelle or implemented in the spinner of the turbine as shown in Figure 5.11. Thus, the LIDAR can measure the incoming wind speed at different distances. The distance is very much dependent on the LIDAR system itself, but also the particles in the air and the scanning volume

Figure 5.11: Principle of a nacelle-mounted LIDAR (background Figure *Econcern*)

As the wind field can change its characteristics over time significantly due to turbulent influences, a scanning for different distances and maybe even volumes is necessary. Figure 5.12 illustrates possible so-called trajectories of the measuring laser. These have to be chosen dependent on the goal of the LIDAR system. If the device shall just be used for detections of gusts, a reduced trajectory might sufficient. But if effects like turbulence eddies shall be detected for later dynamic pitch control actions, a more detailed picture of the incoming wind field is necessary and thus a trajectory with more measurement points and details. This divides the usage of such a remote sensing device in terms of control. In general, the detected wind field information can be used for operational control and dynamic control.

Applications for operational control can be, for example, a more sophisticated yaw control. The wind vane on the nacelle used nowadays is not very accurate and creates errors in the wind direction estimate. Because the rotor is not well aligned with the wind direction, thus, power will be lost. A second option is to use the LIDAR as a safety device for transient event detection. In such a case, if a gust is detected in front of the turbine, the operational control can initiate a stop or a transition to a safe operational mode with reduced power and rotor speed in order to reduce the maximal loads on the turbine from the gust.
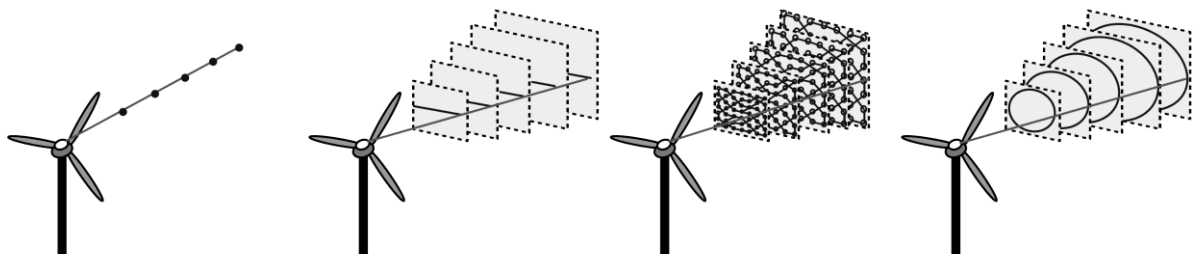
Figure 5.12: Different measurement trajectories using LIDAR [39]

In terms of the dynamic control, the LIDAR wind measurement can be included in the control loop. As from a control point of view wind speed is a disturbance to the system, knowledge of the disturbance can be included in the controller [39]. In such cases the pitch system can react on the incoming changes in the wind field. Such a device can be used for fatigue load reduction, if for example a collective or individual pitch controller is used to mitigate the loads. Here fatigue load reductions of more than 20 % are possible [40]. Of course such reductions still need to be verified by measurements. Furthermore in terms of transients, the LIDAR measurements could also be used to control the incoming gust rather than switch the turbine into a safety mode or even shut it down as for an operational control implementation. In such a case, the pitch system will be tuned to react as soon as the gust arrives at the rotor plane.

However, for all dynamic control concepts a LIDAR system is connected to additional costs in investment and maintenance, and therefore the trade-off is questionable compared to already available standard concepts like individual pitch control based on blade load measurements, which show a similar potential. Additionally the system has to operate reliably without errors, as an error in wind field detection can lead to even higher loads than in the case without LIDAR control.
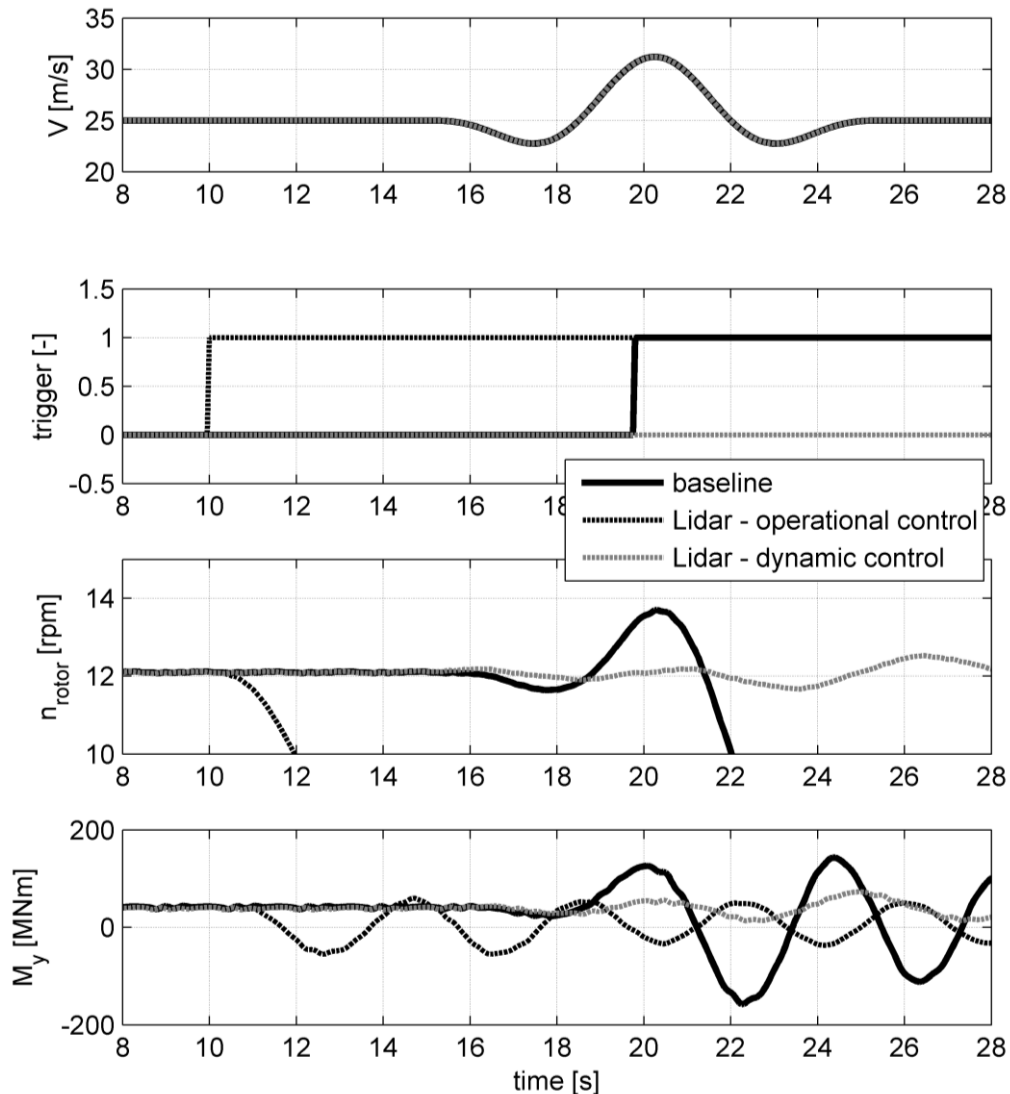
Figure 5.13: Detail of simulation results for an extreme operating gust at 25 m/s with and without LIDAR control

In the following paragraphs the benefit of using a LIDAR system for extreme gust control is shown. For the simulated case a 5 MW reference turbine model is used on a monopile in 25 m water depth (see Appendix A). The simulated cases are for an extreme operating gust with a return period of 50 years according to IEC [37]. The mean wind speed is set to 25m/s, which is the cut-out level. According to IEC and the used turbine design, the gust is introducing a wind speed change of 8.4 m/s. In the simulations, three different concepts are compared. In a first case, the turbine will experience the gust without any remote sensing device. Secondly, a LIDAR system is placed on the nacelle and is used as operational control device which can detect the wind gust and will initiate a stop of the turbine in order to avoid the maximal loading. In a third case, the LIDAR-detected wind speed change is included into a dynamic control loop and the gust is actively controlled. For the operational control case, a detection of the gust 1 rotor diameters in front of the turbine is assumed, which is a reasonable value for the current LIDAR systems. This results in a reaction time window of 5 seconds. This ensures as sufficient time window to shut down the turbine.

In the baseline case it can be seen in Figure 5.13 how the gust affects the turbine loads, here expressed as overturning moment of the support structure at mudline. Even if the turbine shuts down after the safety trigger of 10 % above rated rotor speed is reached (in Figure 5.13 illustrated as trigger value of 1), the loading is still high and the structural oscillations as well. In the operational control case this can be avoided as about 5 seconds before the gust reaches the rotor plane the safety trigger is set and a normal stop is initiated, as seen by the decreasing rotor speed due to the initiated stop event. The result is a much lower acceleration of the turbine through the gust. This can also be achieved if the LIDAR device is included in a dynamic control scheme. In this case no stop is necessary and the gust is controlled by the pitch system.

In conclusion, the usage of a remote sensing device can be a valuable solution for advanced operational control schemes. By knowing the incoming transient extreme event in a certain time frame before it arrives at the turbine, the turbine can change its operational characteristics in order to avoid any overloading. This reaction can either be a shut down, but also a switch into a safety mode like a reduced power level and thus lower rotor speed, which then for example catches the transient gust with the inertia of the rotor. The potential of this is also shown for the extended cut-out in Section 5.2. The advantage of an operation in a safety mode compared to a shutdown is of the course the retention in power operation and therefore a higher power output, but also the effect on the electrical grid, as every shut down of a wind farm imposes stability issues to the electrical system. Compared to dynamic control, for operational control purposes the LIDAR does not have to operate as accurately. Furthermore a LIDAR system on a neighbour turbine can be used as a redundant system in cases of failures. However, the usage of LIDAR for a broad band of transient extreme events like sudden wind directional changes is questionable, as the system can only measure in the line of sight.

The use of LIDAR devices for dynamic control concepts is still questionable in the near future, as the system has high investment costs and for dynamic control aspects it has to operate much more precisely and reliably. Especially in terms of costs the system has to compete with already available concepts like individual pitch control, which uses readily available components in the turbine. A further drawback of the current LIDAR devices is the lack of appropriate filter techniques, which enable a good knowledge of the small-scale turbulent wind field currently tested systems are able to detect only large-scale eddies in the turbulent wind field [39].

5.4 Passive structural control

In cases of non-availability and/or for very low or high wind speeds outside the operational range, active control concepts are useless due to the non-operation of the turbine. In such cases, but also for all the turbine's power production cases, a passive structural damper (PSD) device offers a possible solution. Such a concept is well-known throughout the engineering

industry, especially in civil engineering for applications in buildings and bridges, but recently also in wind turbines [41].

Figure 5.14 shows an example of a PSD integrated into a tower. The design also demonstrates further aspects to take into account, which are openings for transmitting an elevator, stairs and caballing. This can also influence possible sections in the tower where such devices can be included, as enough space is necessary.
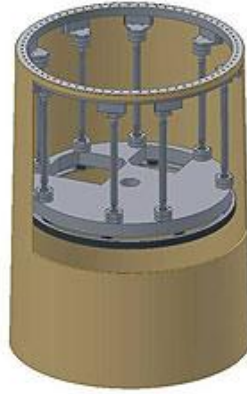
Figure 5.14: Example of a structural damper device implemented in a wind turbine tower [42]

In general, the stress acting on a structure in terms of long term stability is influenced by its eigenfrequency. When excited in the band of the eigenfrequency, the relative displacements of the structure are highest. According to the mode, different shapes of displacement are formed. Especially the first and second eigenfrequency have the highest energetic potential and therefore generate the most critical stresses for the structure. An appropriate level of damping, especially of these two modes, is consequently advised. The reduction of the mode displacement can be done by employing passive structural damping devices such as a mass damper.

Besides the effective reduction of tower base loads, the damping of oscillation and therefore accelerations in the nacelle can be a second positive aspect due to the integration of a mass damper. A reduced acceleration level actively preserves electrical components installed in the nacelle.
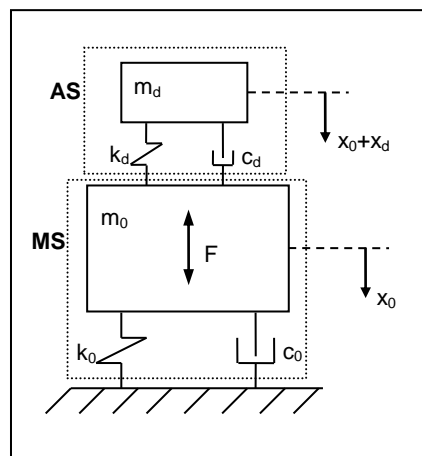
Figure 5.15: Two-mass oscillator system

A passive mass damper can schematically be described as an auxiliary mass m_d connected to a main structure m_o with a spring k_d and a viscous damper c_d. The damper is excited by the main

structure's frequency which causes a relative motion of the mass. This motion, which is intensified by resonance, reduces the main structures' deflection. Tuning the mass damper accurately enables as much energy as possible to be dissipated in the system. Still some oscillation of the main system will remain [43]. The schematic sketch of a single mass damper is illustrated Figure 5.15 showing the wind turbine as main system (*MS*) and the damper device as additionally system (*AS*).

For most of the applications in wind turbine towers, the mass damper is tuned to interact with the first eigenmode of the structure. The first eigenmode has the longest period, the highest amplitude of oscillation and so the highest energy. For this reason the first eigenmode causes in the most cases the highest stress in the structure. In comparison, the influence of the other modes such as the second one on the structure is generally marginal as their oscillation and their energy content is much smaller. By analysing the first eigenmodes, the maximum displacement is detected at the top of the tower. As the highest displacement correlates with a major change of kinetic energy, the mass damper is placed at this position. The same amount of kinetic energy will now move a larger mass, but over less distance, and therefore cause less stress in the structure.

The theory of passive structural damping is based on dissipating energy with a counter-acting additional system. The system characteristics of such a mass damper are the mass ratio μ, the natural frequency ω_0, and the damping ratio ζ_d.

A first design step can be undertaken by choosing a mass ratio of added mass to structural mass.

$$\mu = \frac{m_d}{m_0}$$

(5.1)

Here the mass m_0 relates to the modal mass of the mode to be damped. To achieve a satisfying damping result the usual applied mass ratio is according to [44] about 3 to 5 % of the modal mass. Nevertheless this value can be restricted by other aspects, where two limitations are most important in general. On the one hand, the added mass has to fit into the structural restrictions as increasing the overall mass of the system leads to increased structural stresses. On the other hand, a minimal mass ratio has to be guaranteed, as the deflection of the system is reciprocally proportional to the mass ratio. Thus, a small mass ratio results in large amplitudes of movement of the damper mass. Another aspect to be focused on concerning the mass ratio is the influence on the tolerance bandwidth. The higher the mass ratio, the more independent is the damping effect of small variation of the original structural eigenfrequency.

The damping factor of the mass damper correlates directly to the mass ratio.

$$\zeta_d = \sqrt{\frac{1}{2} \frac{\mu}{(1+\mu)}}$$

(5.2)

The classic damping value of Den Hartog [45] is defined with a factor of 3/8. But recently [44] it has been demonstrated that the factor 1/2 leads to better results. The later one is used for all following calculations.

The relation of damper frequency ω_d, structure frequency ω_0 and mass ratio μ is

$$\frac{\omega_d}{\omega_0} = \frac{1}{(1+\mu)}$$

<div align="right">(5.3)</div>

Installing the mass damper into the tower will change the tower characteristics and consequently the structures eigenfrequency. This is why the damper has to be configured to the first eigenfrequency of the entire system. The changed frequency can be calculated according to the following equation and has to be taken into account in further calculations.

$$\frac{\omega_d}{\omega_0} = \frac{1}{(1+\mu)} < 1$$

<div align="right">(5.4)</div>

The theoretical effect of a correct tuned PSD is the complete reduction of the 1st eigenfrequency resonance peak. In the idealized form with a single structural mass the usage of a single damper splits the original undamped mode into two modes with equal damping ratio [44].
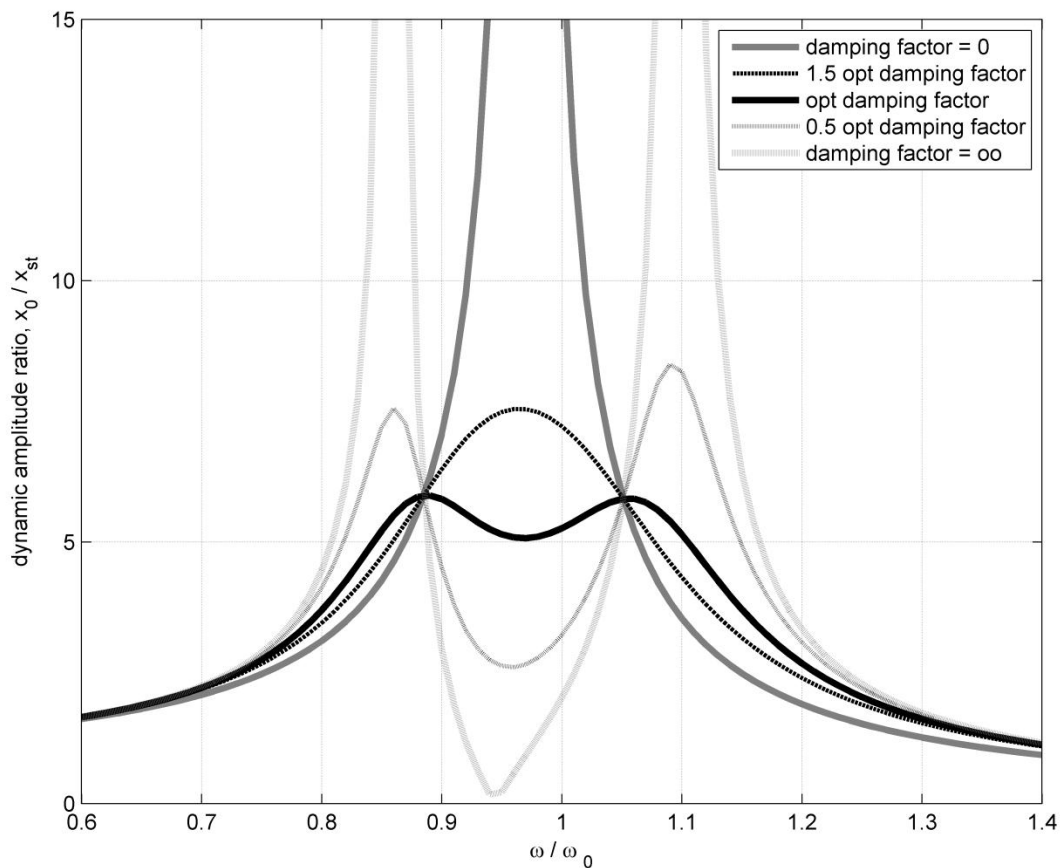
Figure 5.16: Exemplary amplitudes of the main system as a function of the exciter frequency relation

Figure 5.16 shows a plot of the amplification ratio against the forced frequency relation. The dynamic amplitude is defined as the system displacement, x_0, over the static vertical displacement due to the dead load of the structure, y_{st}. The forced frequency relation is the relation of the exciting frequency over the eigenfrequency of the main system. By choosing different damping ratios, the PSD will split the target original frequency in two new frequencies.

By choosing zero damping, the resonance occurs right at the undamped resonant frequency of the system. In the opposite case, infinite damping is used. If an optimal choice of the damping ratio is done, the curve is adjusted to pass with horizontal tangent through two points, which are independent of the damping value. Thus, the optimal tuned mass damper will split the original frequency into two new frequencies with damped peaks.

This effect has an important impact on the operating wind turbine system as, due to these two added amplification peaks, the exclusion zone where the turbine is not allowed to operate will be expanded. Depending on the design of the support structure and the turbine operational characteristics, some frequencies such as rotational dependent ones like *1P* or *3P* can be too close to support structure eigenfrequencies. In such a case either the support structure has to be re-designed in a softer or stiffer manner or the turbine must not operate in these exclusion zones. For a variable-speed turbine this can practically be done by introducing a so-called rotational speed window, as described in Section 5.1.
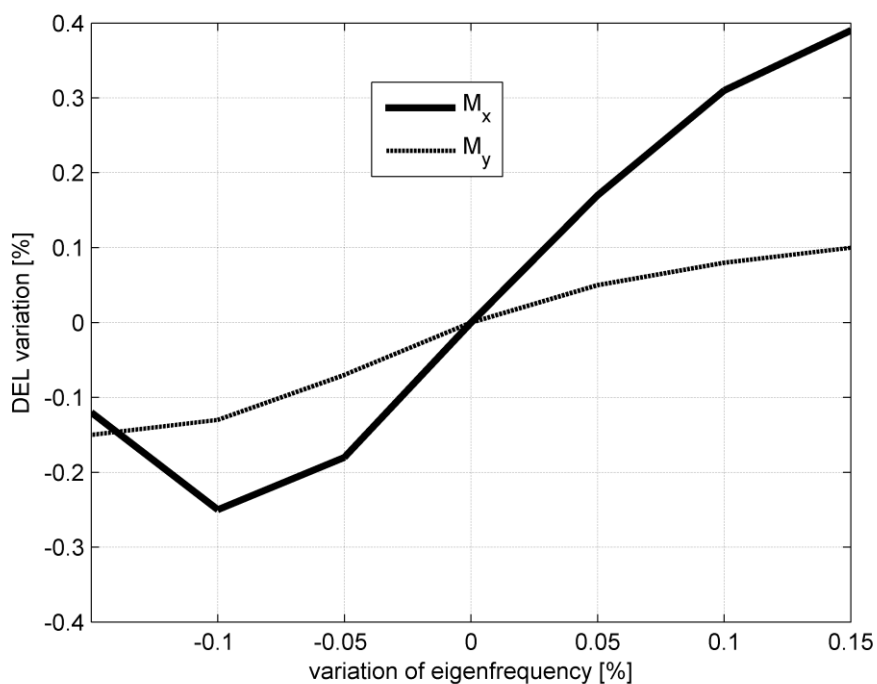
Figure 5.17: Influence of PSD and support structure eigenfrequency on lifetime fatigue loads

In the following, a PSD is applied at a reference site in 25 m deep water with a 5 MW offshore turbine design on a monopile (see Appendix A). In a first step, a sensitivity study for the damper design is performed. In theory the PSD eigenfrequency shall be aligned with the eigenfrequency of the support structure to be damped, here the first one at 0.274 Hz. In reality the support structure eigenfrequency can vary significantly after installation compared to the previously calculated value, for example due to differences in the soil conditions. In such case the PSD would be misaligned as its characteristics do not match with the actual structural conditions. The effect of misalignment between support structure and PSD eigenfrequency can be seen in Figure 5.17 for the applied reference case for a full fatigue calculation according to IEC [10]. The graphs illustrate the change in fatigue loading at mudline for the monopile for the fore-aft (M_y) and side-to-side (M_x) bending moment on the y-axis of the Figure. The x-axis illustrates the difference between the PSD and support structure eigenfrequency. The case for 0 % corresponds to the conditions in which the structural and PSD frequency is identical, the former

called optimal adjustment. This status also deals as reference in fatigue loading for the monopile.

For the curvature in Figure 5.17 where the damper frequency is lower than the support structure one, the loads on the monopile are decreased. Here, for example, a difference of -10 % in eigenfrequency results in over 15 to 20 % lower loads. After passing this frequency difference at -10 %, the loads reach a turning point. For the case with a higher damper frequency, the loads behave different and tend to rise. This is especially the case for the side-to-side moment which experiences a significant rise already for small variations of damper frequencies. As example for a 10 % difference the fore-aft fatigue loads increase by almost 10 %, the corresponding side-to-side loads even by 30 %.
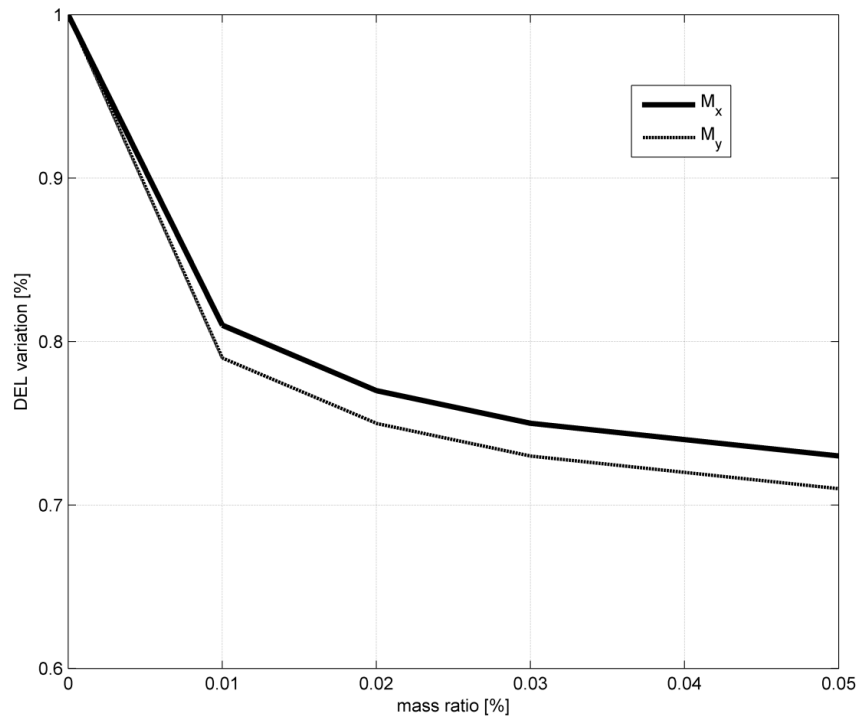
Figure 5.18: Fatigue load reduction by using a PSD with different mass ratios

The result of this sensitivity study opens up the questions why even higher damping values can be achieved if the damper is not placed in its theoretical optimal frequency. The reason is the optimal value is related to overall damping, not to actual frequency distributions of existing excitations. As during operation the exciting frequencies are different from the eigenfrequency of the structure, depending on actual load situations, the optimal frequency band for the PSD differs. The reason for better performance of the PSD in the demonstrated sensitivity study is related to the significant wave contribution to the overall fatigue loading. As the wave spectrum has its main energy below the first support structure eigenfrequency in the given soft-stiff monopile design, a PSD with a lower eigenfrequency will damp wave-induced loads and their connected excitations in the frequency spectrum in a better manner. This leads to a finally better performance of the PSD in the studied case.

Therefore just in theory if the main excitation frequency is always at the main structural eigenfrequency, any misalignment of damper and support structure eigenfrequency would lead to an increase of loads [46]. However, for some specific cases it might be more effective for the fatigue load reduction at the support structure to consider the frequency spectrum of exciting loads and then to adapt the damper eigenfrequency to it. Here the frequencies of occurrence

and loads at the various exiting forces have to be taken into account to achieve a maximum in load mitigation [16]. In general, the sensitivity study shows the importance of an accurate design of the PSD. Furthermore it identifies the importance of maintenance for such systems, as offshore the support structure eigenfrequency can change during lifetime. An example is a change in soil characteristics and thus stiffness, which may lead to a decrease of the overall support structure eigenfrequency over the offshore wind turbine lifetime. In such a case the PSD will have a higher eigenfrequency and the loading will be increased, as demonstrated in Figure 5.17.

In the following study the PSD will always be placed in its theoretical optimum at the target support structure eigenfrequency. According to the described procedure above, a mass ratio between PSD and modal mass of the system to be damped has to be chosen. As discussed before, a target value of 3 to 5 % is proposed in common literature. Figure 5.18 illustrates the decrease in fatigue loading for the considered monopile at mudline depending on different mass ratio for the fore-aft (M_y) and side-to-side (M_x) moments. The curvature clearly shows that the main effect can be achieved with a mass ratio of 1 %. For higher ratios the loading is decreased further but with the expense of a lower trade-off between extra mass and load reduction. Here fore-aft and side-to-side loads show a similar behaviour. Besides the effects in load reduction, the size of the damper is also an important parameter in order to choose a proper mass ratio. For the given design, the modal mass corresponding to the first support structure eigenfrequency is about 520 tons. Thus, if the optimal ratios of 3 to 5 % proposed in literature would be used, a damper mass of 15 to 26 tons would result. Such a structure will be difficult to place in the tower top of a turbine due to the space constraint but also the incorporation of the mass to the tower walls. Therefore a smaller mass has to be chosen. According to Figure 5.18, a mass ratio of 2 % leads already to reasonable reductions. Such a ratio would correspond to a damper mass of about 10 tons for the given case. Such a mass can fulfil the criteria for implementation by keeping a good damping potential and will define the following further damper characteristics for the given support structure design and its first eigenfrequency at 0.274 Hz.

Table 5.2: PSD settings for reference case

damper mass	10 tons
designed resonance frequency	0.274 Hz
damping factor	0.0972
damper position above MSL	82.76 m

This damper is then applied at the given 25 m reference site and effects on the fatigue loads at the support structure and the overall system are studied. The loads are expressed as damage equivalent loads (DEL) for a reference cycle number of N=2E07, a lifetime of 20 years and an inverse S-N-slope of m=4 for steel components and m=10 for composites. To show the effectiveness of the damper, the emphasis of the load mitigation concept is on the fore-aft support structure motion only. Thus the wind and wave directions are assumed to be co-directional and therefore the support structure fore-aft moments (M_y) are much larger than the corresponding side-to-side moments (M_x). Both moments are evaluated at mudline.
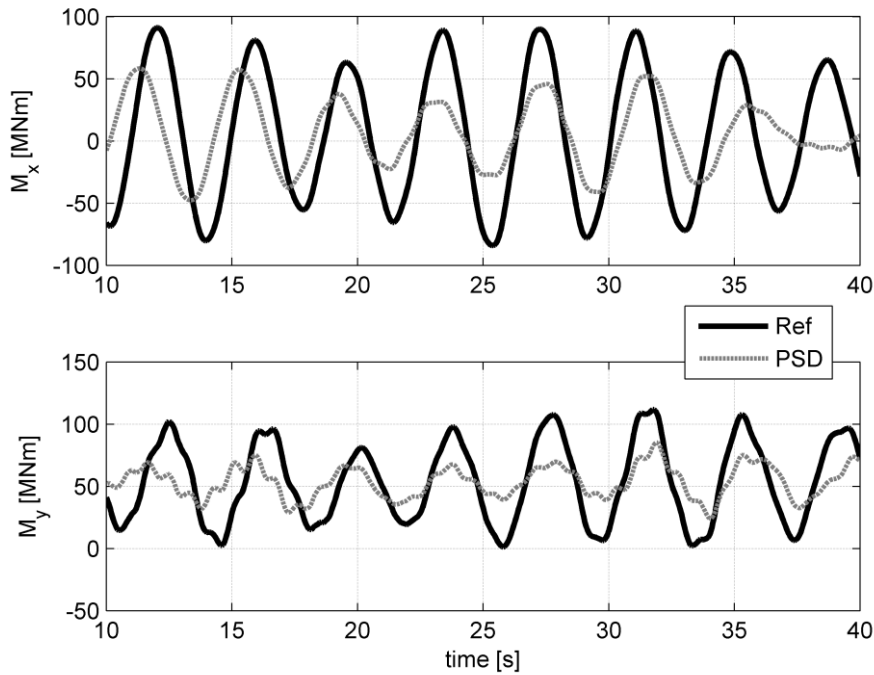
Figure 5.19: Detail of simulation results for a PSD versus a reference case for V=14 m/s

Figure 5.19 demonstrates the effectiveness of the former specified PSD at the reference site, showing the details for a specific load situation at a mean wind speed of V=14 m/s and a wind-wave-misalignment 60 degrees. It shows that both, fore-aft (M_y) and side-to-side (M_x), support structure bending moments at mudline are reduced significantly. This can also be seen in the values for lifetime-weighted fatigue loads. Table 5.3 summarizes the load reduction achieved by the PSD.

It can be seen that a good load reduction of the support structure is achieved by keeping other system quantities nearly unchanged. Different to active control concepts based on pitch or generator control, the PSD does not influence the power output and quality. As seen in Figure 5.20, the fatigue loads of the blades, the hub, yaw and drive-train are not much affected and even decreased in some cases.

Table 5.3: Load comparison between the reference and PSD for 100 % and 85 % availability

	Loads as DEL [N=2E+7, m=4]			Change in energy yield and power fluctuations		Change in pitch rate
	Support structure at mudline					
	M_x	M_y	M_{xy}	AEP	P_{std}	$Pitch_{std}$
Reference 100% avail.	23.9 MNm	132.1 MNm	100.6 MNm	23.6 GWh	0.15 MW	0.46 deg/s
PSD 100% avail.	-26.4 %	-15.7 %	-7.7 %	0 %	0 %	0 %
Reference 90% avail.	23.5 MNm	147.6 MNm	103.4 MNm	23.6 GWh	0.15 MW	0.46 deg/s
PSD 90% avail.	-26.4 %	-21.5 %	-11.0 %	0 %	0 %	0 %

Another aspect affecting the potential for a PSD is the turbine's availability. As Table 5.3 shows, a lower availability is increasing the relative mitigation potential of the PSD. This is contrary to active systems, which of course perform worse in such conditions due to the lower operational time range. This effect can also be seen in Figure 5.21 for different wind speeds. The graph shows the lifetime-weighted fatigue damage of the support structure at mudline for different wind speeds, here for an availability of 90 %. The bars per wind speed are divided in their damage contribution from power production and idling, where due to the reduced availability the relation is 90 % to 10 % respectively. First of all it illustrates again the importance of taking availability into account for offshore structures like monopiles in moderate and deep water, as for some cases the damage contribution from the non-available idling conditions contribute more in terms of overall damage than the corresponding power production case. This is due to the strong hydrodynamic loading at the given reference site, the large pile diameter of the monopile and of course due to the importance of the presence of aerodynamic damping depending on the operational mode. The Figure also shows the potential of the PSD in such conditions and here especially for the idling operations. It also identifies that the PSD reduces the loads at lower wind speeds more efficiently. According to the former presented sensitivity study, this is due to the effect that at lower wind speeds the wave periods of the sea states are lower and thus closer to the first support structure eigenfrequency. This also means that the wave-induced energy is closer to the frequency band of the PSD and therefore the damper is more effective.
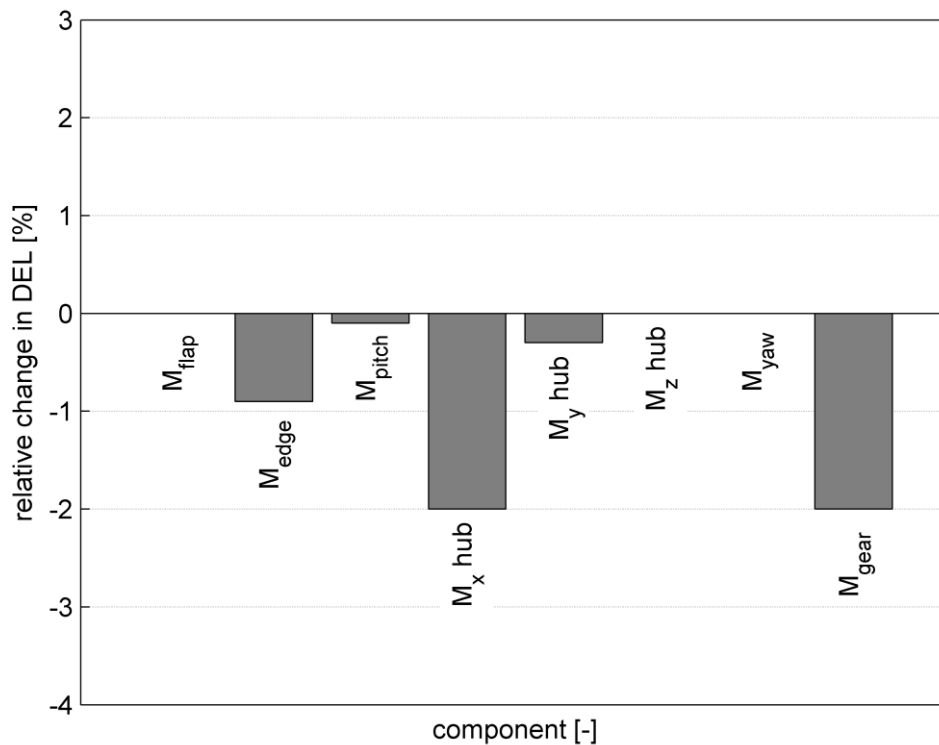
Figure 5.20: Relative change in component fatigue loading by applying PSD in comparison to the reference case

A final benefit of passive mass dampers is their applicability in all operational cases of the offshore wind turbines, as it is a fixed structural system independent of any external supply. This can be of special importance for some extreme load cases. For some monopiles, extreme sea states with, for example, a return period of 50 years can be critical. As in such conditions the turbine is non-operational due to the storm conditions, active control concepts cannot mitigate loads while a PSD is still operational in such conditions. In Figure 5.22, an example of a 50 year

sea state together with a constrained 50 year maximum wave is shown, which corresponds to the design load case 6.1 in the design guideline [10]. The simulations are performed for the same reference conditions as before for the fatigue study and by using the same PSD design. The plots show that the extreme wave, which in this case is over 15 m high, results in the maximum bending moment in the monopile, here shown at the mudline. If in such conditions would a PSD have been included, the extreme loads could have been reduced by over 15 %. Thus, a PSD can also be an important concept for such extreme conditions, which have an advantage compared to the active control concepts.
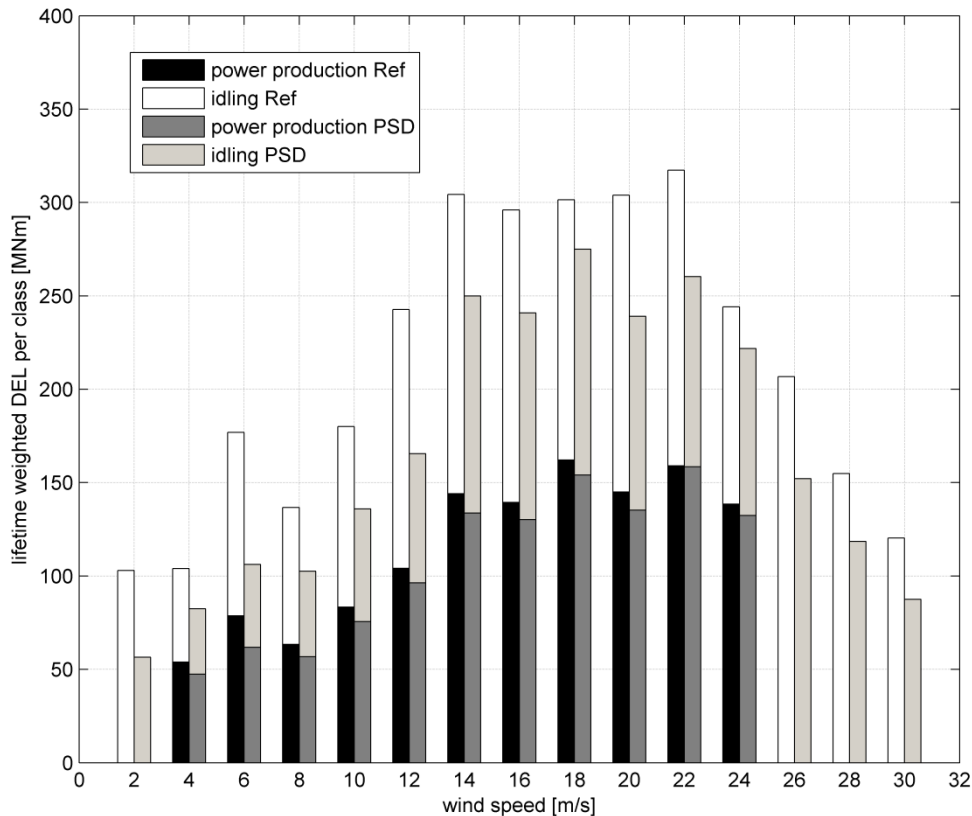
Figure 5.21: Distribution of support structure DEL of the overturning moment at mudline on wind speed classes for different availabilities

In conclusion it can be stated that a PSD is an effective system to reduce both fatigue and extreme loads on the support structures. In contrast to the active systems, such a passive device becomes even more effective for lower turbine availabilities. This might be important especially if the monopiles are to be installed in deeper waters by using controls rather than using the load mitigation systems to achieve a structural optimization at shallow offshore locations. In such cases where controls are used to enlarge the application range of monopiles to deeper water, extreme loads are becoming more and more important. Here in particular the extreme wave conditions during a storm with an idling rotor are important, as both the lever arm of the active loading is increased but also the maximum wave heights. This context might enable passive damping devices to become the better and more cost-effective solution compared to the active systems.

Another aspect for comparison to active system is the influence of the described PSD on other system quantities. The advantage of the PSD is that it is not imposing increased fatigue loads to the components like blades, hub or drive-train. Furthermore it is also not affecting the power output of the turbine. These are advantages with respect to active systems, which in most cases have their drawbacks in additional costs for the other system components. However, a PSD has

higher investment costs because of the damper itself, which erodes many of the advantages it has compared to the active systems.
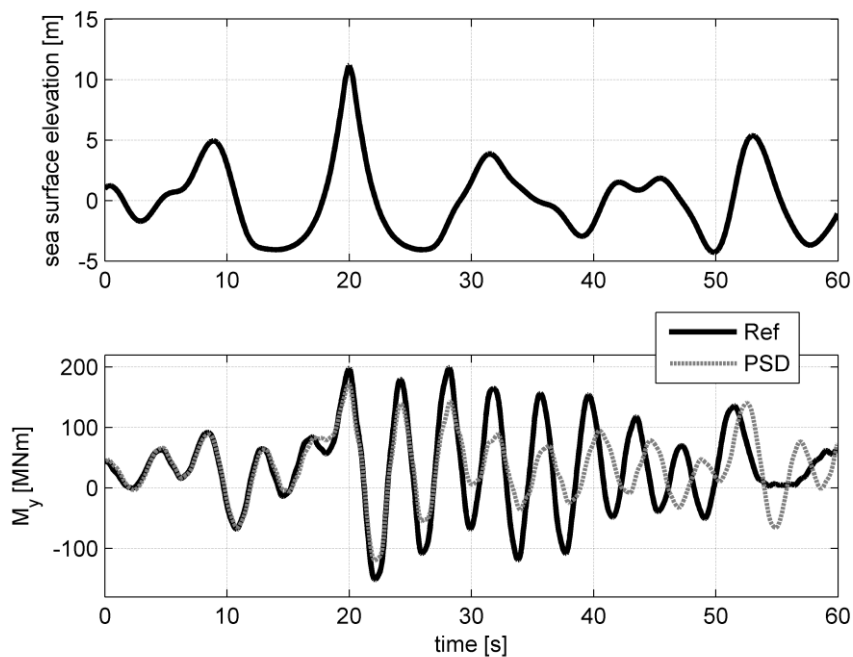
Figure 5.22: Detail of simulation results for an extreme sea state with and without PSD

Another drawback is the sheer size of such passive devices, as high masses have to be assembled in the weakest section of the tower, at the tower top with its thinnest wall sections. In the future more compact system might become available, which will withdraw this problem of space and size. A possible concept is described as semi-active damper configuration in Section 6.5.

6. Load mitigation concept analysis at dynamic control level

In the following Chapter, several concepts for load mitigation in the dynamic control level are introduced. These concepts use additional control loops and systems in order to reduce overall loading. The shown concepts just give an overview of possible options and could be extended.

6.1 Tower-feedback control

Aerodynamic damping is the main damping effect for modern wind turbines during operation. Both, aerodynamic and hydrodynamic loads are mitigated by this damping source mainly for flapwise blade and the nacelle fore-aft motion. Due to the major impact of the aerodynamic damping effect and since the effect is mainly caused by the aerodynamic conditions at the rotor blades and the tower top response of the support structure, active enhancement through the manipulation of the aerodynamic conditions via pitch control seems to be a powerful approach for the load mitigation. A possible approach to enhance this damping effect is the so-called tower-feedback control (TFC) concept.
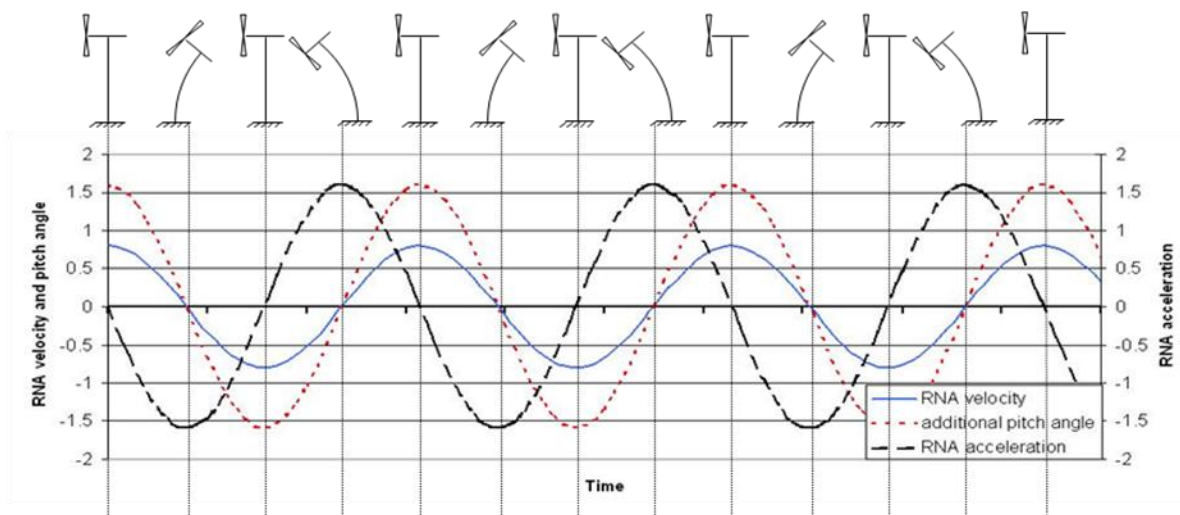
Figure 6.1: Principle of tower-feedback control

The strategy is based on an estimation of the RNA movement in terms of velocities. Both, the instantaneous velocity and an approximation of the change in the velocity within a short period of time can be derived from the acceleration by integration. The additional pitch angle denotes the pitch angle that is superimposed to the pitch angle provided by the regular controller. The required direction of the additional pitch angle depends on the direction of the RNA velocity. If the RNA has the same direction as the wind an increase of the pitch angle compared to the regular pitch angle as demanded by the regular controller is required. For the opposite direction of the RNA movement i.e. against the wind direction an increased thrust force is induced by an additional decrease of the pitch angle. In both cases an additional thrust force component, compared to the regular case without extra pitch, is induced, acting against the direction of the RNA movement. The additional pitch angle must change the sign as soon as the RNA movement changes the sign. An ideal correlation of the additional pitch angle and the RNA

velocity is shown in Figure 6.1. For convenience only a harmonic acceleration of the RNA is considered.

For the application in a real turbine, the controller uses measured nacelle acceleration as an additional input above rated wind speed. It works alongside the pitch controller by calculating an additional pitch rate demand. The pitch rate is derived from passing the acceleration signal through a lead compensator to achieve optimal damping of the 1st tower fore-aft mode. The stability margins of the original pitch-speed control loop are eroded by the addition of the tower-feedback controller. Therefore the gains on the pitch-speed proportional–integral controller (PI) are reduced slightly to allow the tower-feedback controller to operate. This has the negative effect of causing greater generator speed fluctuations which could require a more robust drive train.

$$a_0 = T + \tau_A \qquad b_1 = T - \tau_B$$
$$a_1 = T - \tau_A \qquad c_0 = T$$
$$b_0 = T + \tau_B \qquad c_1 = T$$

$$T = PitchStep$$
$$z^{-1} = Backward - shift \ operator$$
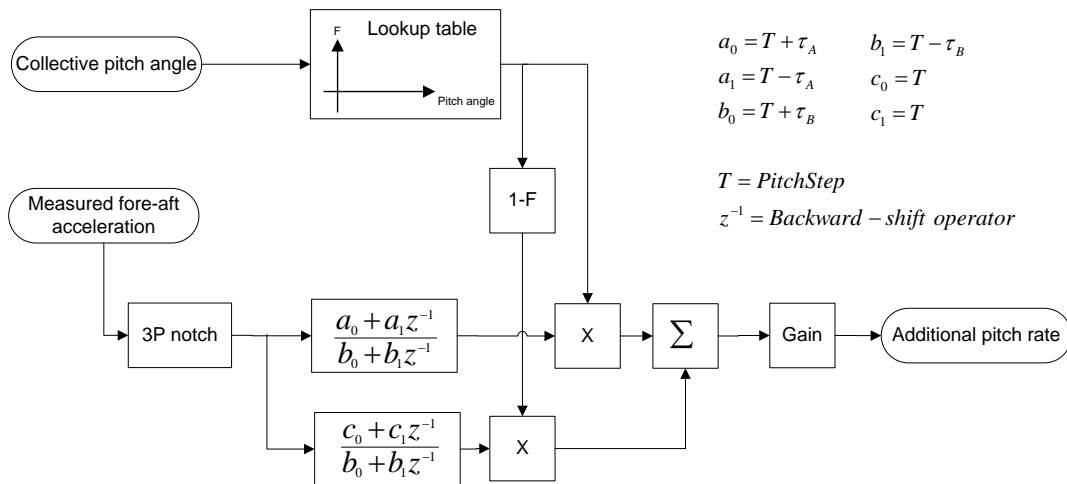
Figure 6.2: Tower-feedback controller block diagram

The dynamics of pitch-speed control loop vary considerably across the wind speed range. As the tower-feedback controller interacts strongly with the pitch-speed loop, it is important to ensure that the lead compensator is working optimally at all wind speeds. This has been achieved by tuning it separately at several wind speeds and using a gain schedule based on pitch angle to vary the compensator parameters appropriately.

The exact implementation is shown in block diagram form in Figure 6.2. The controller is implemented in discrete time, and represented in the diagram using the backward-shift operator. Many compensator parameters (gain, τ_A and τ_B) have to be investigated at each wind speed. In general it is found that good performance could be achieved by using just a single lookup table rather than one lookup table for each parameter. This approach simplifies the task of tuning and implementing the controller.
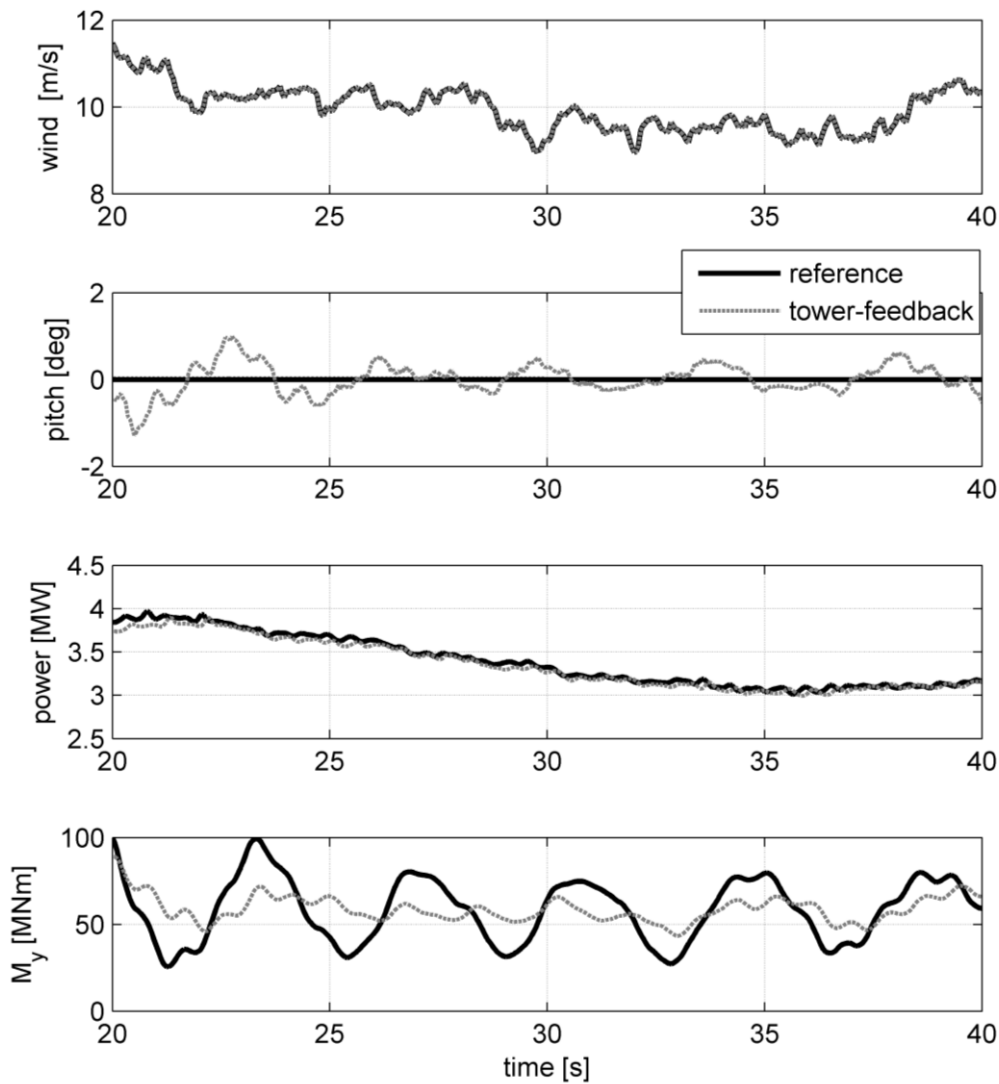
Figure 6.3: Detail of simulation results for a TFC versus a reference case for V=10 m/s

In Figure 6.3, an exemplary simulation of a TFC is shown. In this case the turbine is in its normal operations just below rated wind speed (here rated corresponds to 12 m/s). Therefore in the reference case the pitch system in still deactivated. If the TFC is enabled, the controller adds an additional pitch angle in order to enhance the effect of aerodynamic damping. The benefit can be seen in the lowest plot for the support structure overturning moment at mudline, where the case with the activated TFC reaches much lower load fluctuations and therefore also fatigue loads. The limit of the added pitch action is set by the quality of the power output, as here the fluctuations shall not become too high due to the added pitch actions. The plot for the power output illustrates the fine tuning of the controller, as nearly no changes in the power output can be seen.
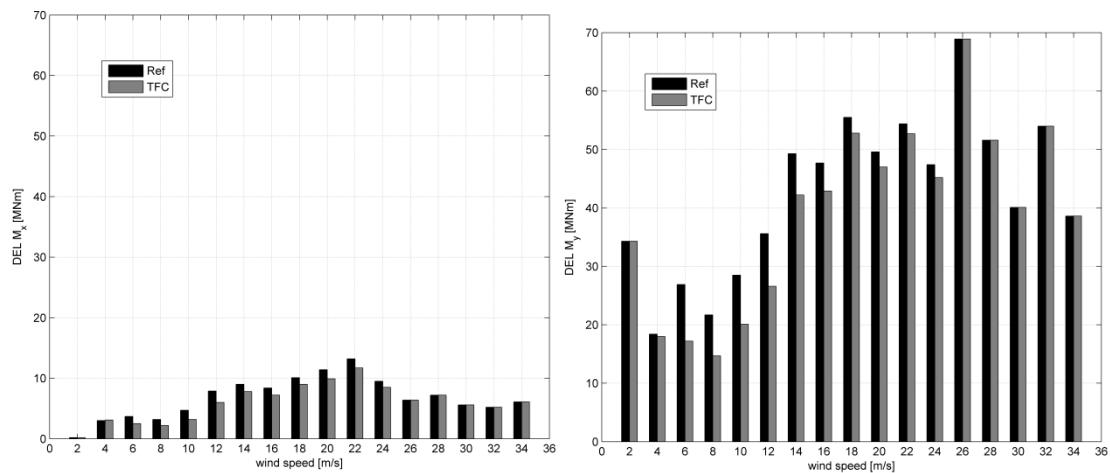
Figure 6.4: Non-lifetime weighted DELs (with N=2E+7) for the support structure moments (m=4) at mudline as comparison of the reference and the TFC-controlled case

In the following, the tower-feedback controller is applied for a reference case. Here a 5 MW turbine design on a monopile in 25 m deep water is considered (see Appendix A). The loads are expressed as damage equivalent loads (DEL) for a reference cycle number of N=2E07, a lifetime of 20 years and an inverse S-N-slope of m=4 for steel components and m=10 for composites. As the emphasis of the control concept is on the fore-aft support structure motion only, the wind and wave directions are assumed to be co-directional. Thus, the support structure fore-aft moments (M_y) are much larger than the corresponding side-to-side moments (M_x). Both moments are evaluated at mudline. Furthermore the focus will be on fatigue loads only.

For the support structure loads it can be seen in Figure 6.4 that the TFC reduces the fore-aft loading, M_y, well. The moment in the sideways direction, M_x, is also slightly reduced. This is due to the coupling in movement of the tubular structure in longitudinal and lateral direction, which generally moves on an oval path. If the main contributor to the movement, the fore-aft direction, is damped, this will also imply a damping to the sideways direction. The amount of damping is coupled with the thrust, meaning that the highest amount of damping can be achieved around rated wind speed, where the thrust is at its peak.

Table 6.1: Load comparison between the reference and TFC controlled case

	Loads as DEL [N=2E+7, m=4]			Change in energy yield and power fluctuations		Change in pitch rate
	Support structure at mudline					
	M_x	M_y	M_{xy}	AEP	P_{std}	$Pitch_{std}$
Reference	23.9 MNm	132.1 MNm	100.6 MNm	25.6 GWh	0.15 MW	0.46 deg/s
Tower-feedback	- 12.1 %	- 3.3 %	- 5.9 %	- 0.03 %	+ 1.3 %	+ 7.0 %

The results can also be discussed in terms of lifetime equivalent DEL, as listed in Table 6.1. The results show that the TFC can reduce the critical loading for the support structure by almost 6 %

by keeping the power output and quality nearly unchanged. Of course, higher damping values would have been possible with the penalty of losing more power and/or increasing the power fluctuations.
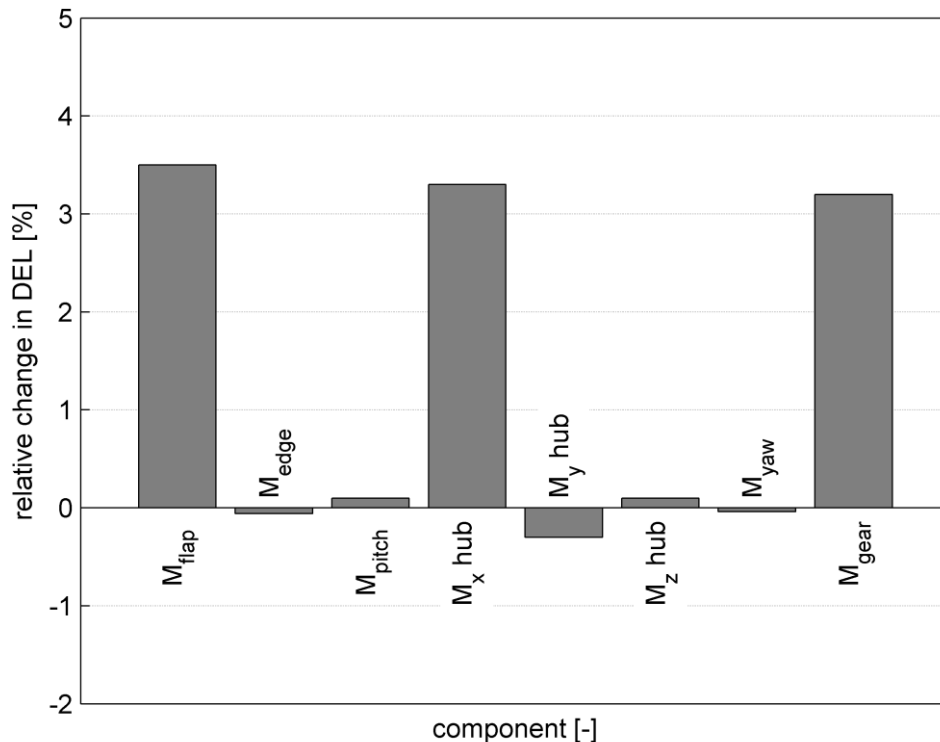
Figure 6.5: Relative change in component fatigue loading by applying TFC in comparison to the reference case

Still, the concept has also further effects on the system loading within the RNA. Figure 6.5 illustrates the change in fatigue loading for some main RNA components. It can be seen that especially the flapwise blade, the hub rolling (M_x hub) and the gear box loadings are increased by slightly over 3 %. The remaining components are nearly unaffected or even slightly unloaded.

The conclusion for using the proposed tower-feedback controller in terms of load mitigation is that it provides a good damping to hydrodynamically induced loadings while not overloading other system components too much. The potential of the TFC is somewhat restricted due to penalties for other system quantities, such as the power output and stability. For sites with very high hydrodynamic loadings and large piled structures, however, the achieved damping can be significantly higher than in the here discussed case, therefore making the TFC more attractive.

6.2 Active idling control

As already explained for the tower-feedback controller in Section 6.1, enhancement of aerodynamic damping is a crucial aspect to mitigate support structure loading and especially the fore-aft mode. As the tower-feedback controller is achieving this during turbine operations, there is also a concept available for non-operational cases using an active idling controller (AIC) [47].

In normal idling operations of a pitch controlled turbine the blades are pitched to feather (85 to 90 degrees) and are turning slowly or not at all. In order to enhance aerodynamic damping of

the rotor, the pitch angles can be reduced, which results in a higher rotational speed of the idling rotor. A small increase in idling rotor speed can already increase the effect of aerodynamic damping and can thus be used to aerodynamically damp the wave-induced loadings at the support structure.

In Figure 6.6, a detail of a simulation time series is shown for a 5 MW turbine design (see Appendix A) at mean wind speed of V=6 m/s. It shows that the former passive idling status with a feathered rotor at 90 degrees and almost 0 rpm rotor speed is changed by decreasing the pitch angle to approximately 25 degrees. The result is a higher idling rotor speed, here at almost 4 rpm. Due to this, the additional aerodynamic damping is used to damp the fore-aft loading of the support structure as shown in the bottom graph for the loading at mudline. Of course, this action will increase the sideways load component in the support structure due to the turning rotor. However, the load amplitudes of the side-to-side load component are much smaller than the corresponding fore-aft one. This shows the potential of this concept.
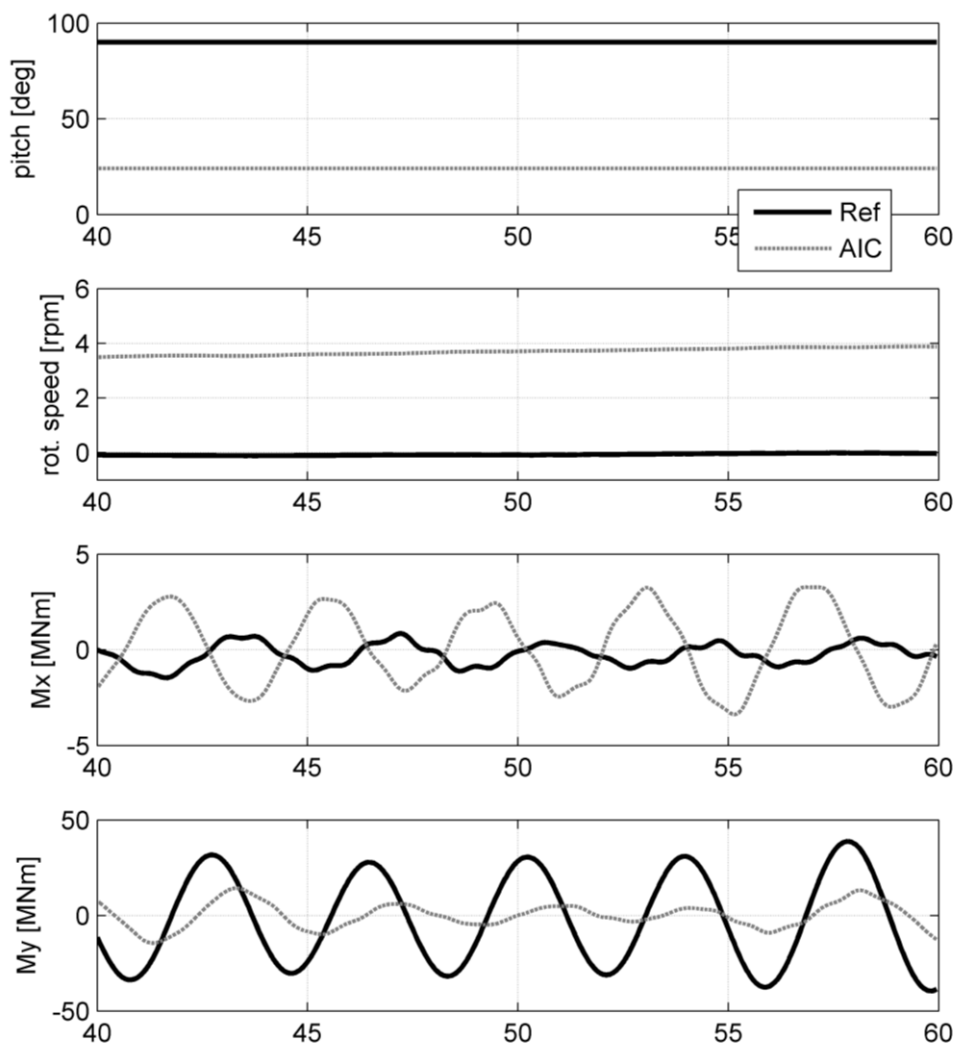
Figure 6.6: Detail of simulation results for an AIC versus a reference case for V=6 m/s

For safety reasons but also due to reasons of limiting other system loads, such as blade loads, the target rotor speed and the application range has to be limited. Due to extreme loads like an extreme operating gust or an extreme directional change, the upper limit should be set accordingly. A value slightly above rated wind speed seems to be reasonable, as beyond that

the transients are becoming too strong. A second set point for the concept is the target rotor speed, as this will be directly linked to additional loading of other system components and again to the safety system in terms of transients. In the following a potential study of three different rotor speed levels is evaluated – namely for 1 rpm, 3 rpm and 5 rpm.
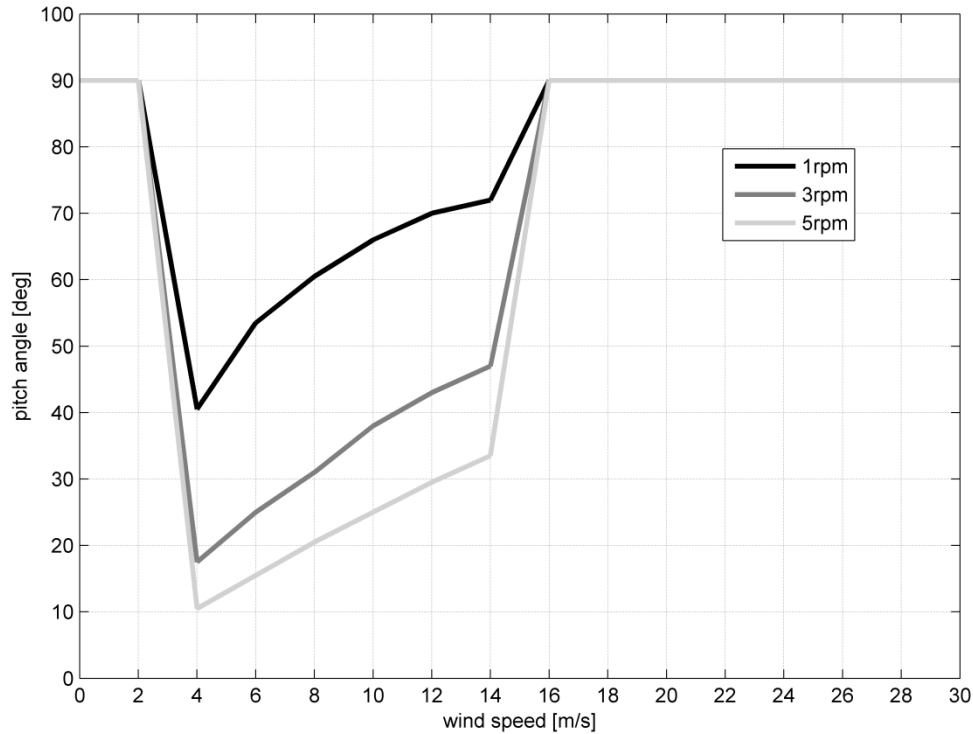
Figure 6.7: Pitch angles over wind speed for providing different idling rotor speeds

Figure 6.7 shows the necessary idling pitch angles for a 5 MW reference design (see Appendix A) in order to achieve the above mentioned three rotor speed levels. The Figure also shows that the concept is applied until a mean wind speed of V=14 m/s. This is as discussed just above rated wind speed, which is for the given turbine design at V=12 m/s. Figure 6.8 demonstrates the resulting fore-aft load reduction for the support structure at mudline for the three simulated idling rotor speed cases as relative change in fatigue loading. It clearly shows that a higher idling rotor speed is directly coupled to a higher provision of aerodynamic damping and thus a lower overall loading. Therefore an as high as possible rotor speed tend to be desirable. However, Figure 6.9 illustrates the corresponding change in blade fatigue loads, here for the in-plane (M_x) and out-of-plane (M_y) moments at the blade root. It shows that the in-plane load component experiences much higher loads up to 20 % above the reference case with normal idling operations. The out-of-plane blade moment is slightly decreased. Even if the changes seem to be dramatic for the in-plane moment, it has to be stated that in normal idling operations for such low wind speeds the blades experience very low loads.
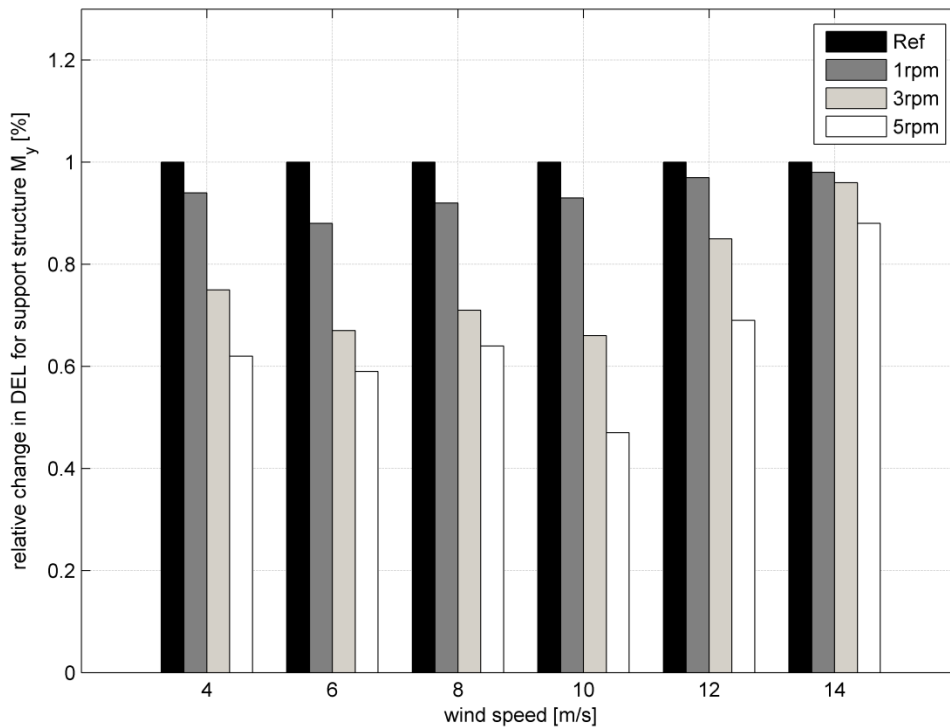
Figure 6.8: Relative fatigue load reduciton at the support structure by applying different idling rotor speeds

Thus, the AIC concept is not causing too high fatigue load changes, as also shown later in Figure 6.10. However, it is interesting to see that at a certain rotor speed the out-of-plane moments increase again. This is visible for nearly all wind speeds excect V=10 m/s. Furthermore the gain in load reduction between the concept with 3 rpm and 5 rpm for the target fore-aft support structure loading is also not that high. Therefore, as a conclusion, a rotor speed level of 3 rpm is set to be the limit for later implementations of the active idling control concept.
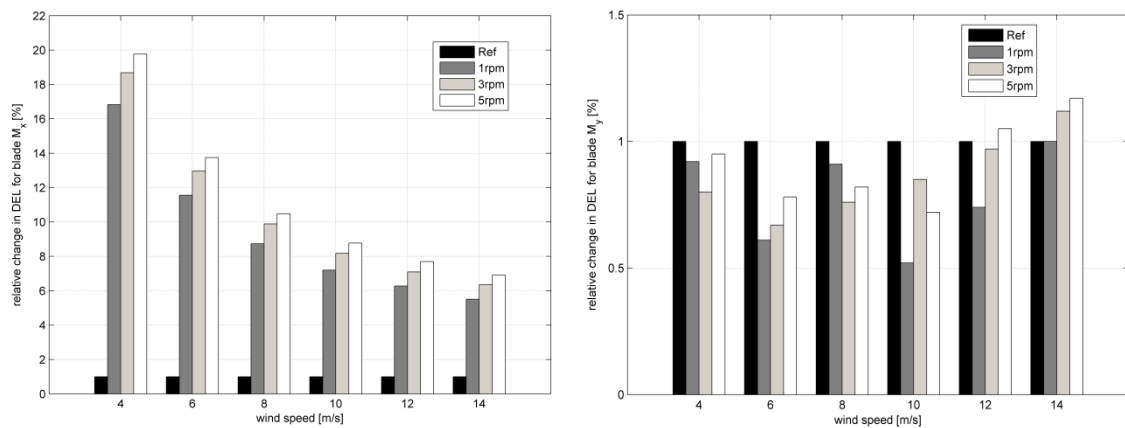
Figure 6.9: Relative change in fatigue loads (DEL) for the blades by applying different idling rotor speeds

In the following, the AIC is applied for a reference case. Here a 5 MW turbine design on a monopile in 25 m deep water is considered (see Appendix A). The loads are expressed as

damage equivalent loads (DEL) for a reference cycle number of N=2E07, a lifetime of 20 years and an inverse S-N-slope of m=4 for steel components and m=10 for composites. As the emphasis of the control concept is on the fore-aft support structure motion only, the wind and wave directions are assumed to be co-directional. Thus, the support structure fore-aft moments (M_y) are much larger than the corresponding side-to-side moments (M_x). Both moments are evaluated at mudline. Furthermore the focus will be on fatigue loads only.

Table 6.2: Load comparison between the reference and AIC controlled case

	Loads as DEL [N=2E+7, m=4]			Change in energy yield and power fluctuations		Change in pitch rate
	Support structure at mudline					
	M_x	M_y	M_{xy}	AEP	P_{std}	$Pitch_{std}$
Reference	23.5 MNm	147.6 MNm	103.4 MNm	23.0 GWh	0.15 MW	0.46 deg/s
Active idling controller	+ 1.3 %	-3.8 %	- 1.9 %	0 %	0 %	+ 3.5 %

For the support structure loads a decrease in the fore-aft moment can be seen and a slight increase for the side-to-side one as listed in Table 6.2. As mentioned before, the order of magnitude of both has to be kept in mind. In total a reduction of almost 2 % is found. This mitigation potential is possible without any significant expenses for other system quantities. As the controller is operating at no power, the power output and quality is of course unaffected. Therefore also loads in the RNA, namely hub, yaw and drive-train loads are not much affected as no counteracting generator torque is acting as seen in Figure 6.10. Just for the blade loads and the pitch system a slight increase is found.
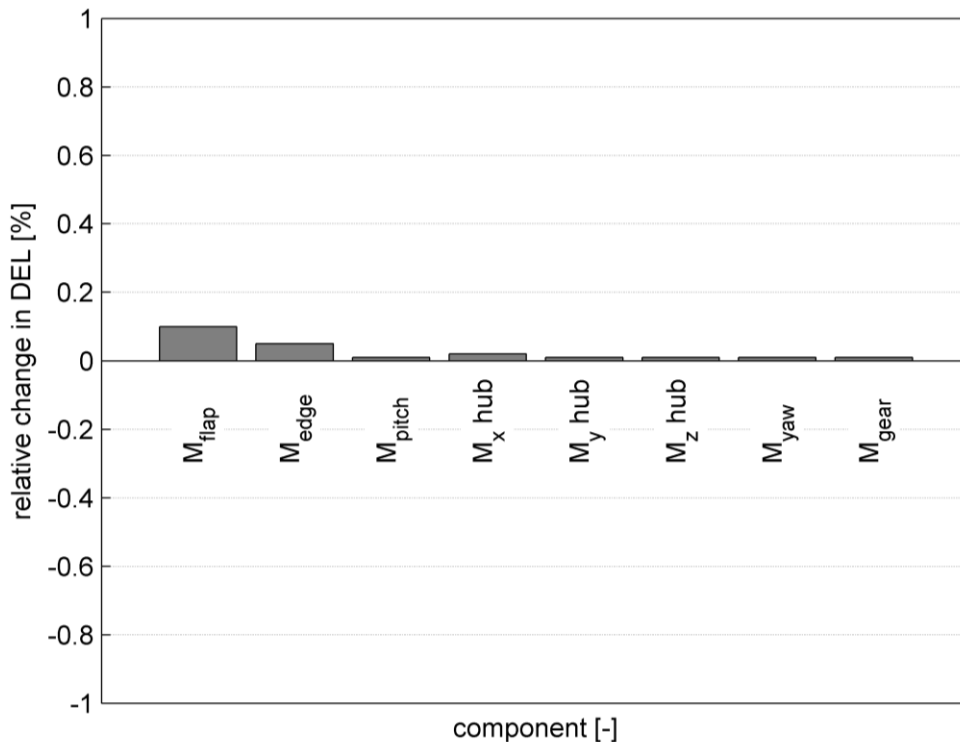
Figure 6.10: Relative change in component fatigue loading by applying AIC in comparison to the reference case

In conclusion it can be said that the active idling controller can provide additional damping to the support structure fore-aft mode without affecting other system components too much. Even if the potential in load mitigation seems to be low with a load reduction of approximately 2 %, the concept is a very good combination to active control concepts such as tower-feedback control. If the turbine is operating, the tower-feedback controller is active. In cases of non-availability of the turbine, the active idling controller can take over. However, if the reason for the non-availability is based on a failure in the turbine, it has to be seen if the active idling controller can still be operated. Thus, the load mitigation potential of the TFC of almost 6 % shown in Section 6.1 can be increased up to 8 % by using both control concepts in an integrated manner.

6.3 Active generator torque control

In Chapter 2, the importance of wind-wave-misalignment was explained. Due to this misalignment, support structures can experience a significant loading in the side-to-side direction. This is especially the case for structures with large water-piercing members, such as monopiles. It is possible to mitigate the increased lateral loadings with active damping algorithms in the turbine controller. One option is the usage of the so-called active generator torque controller (AGTC).
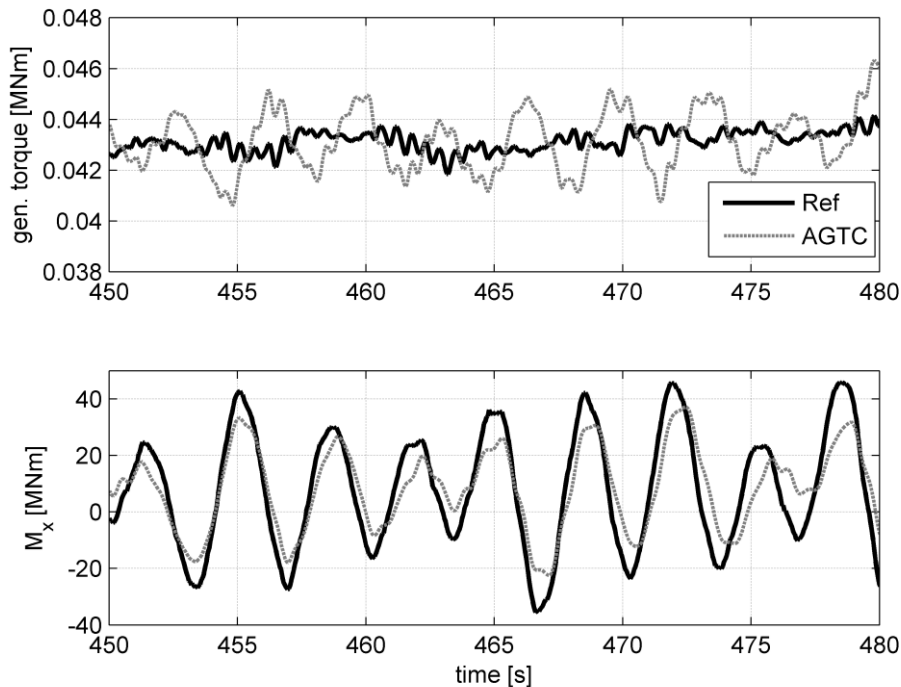
Figure 6.11: Detail of simulation results for an AGTC versus a reference case for V=24 m/s and 90 degrees misalignment

The AGTC uses the measured nacelle sideways acceleration input to vary the generator torque. It works in parallel to the torque-speed controller, with the tower side-to-side damping torque added to the output of the PI controller in the same way as the drive train damping torque. In the variable speed region, this torque modulation will affect the rotor speed, so impact on the energy capture occurs as there will be more variation around the optimal tip speed ratio. In the constant speed region the turbine is no longer operating at an optimal rotor speed, so extra variation should not affect energy capture. However the extra rotor speed variations will interact with the PI controllers (both pitch and torque). The gains have to be set at a level where the

tower side-to-side damping torque is only a few percent of rated torque, so that the effect on the PI controllers should be small. The electrical power will have greater variation, which affects the specification of the power electronics.

Effective damping is achieved when the control action leads to a force on the structure that couples with the mode of vibration that is to be damped, and acts in anti-phase with the modal velocity. The generator torque vary directly affects the torque applied by the shaft onto the gearbox. As the tower 1st side-to-side mode includes some rotation of the tower top, and so gearbox, the generator torque therefore directly couples with the relevant mode of vibration. The nacelle side-to-side acceleration is advanced in phase by 90 degrees relative to the tower top rotation. An integrator could be used to convert the side-to-side acceleration into a velocity; however, any non-zero mean in the measured acceleration signal would accumulate over time. Instead, a 1st order lag is used. Not only does this avoid the described problem with integrators, it also allows the lag to be fine-tuned. There are delays associated with the measurement of the acceleration, the communication to and from the programmable logic controller (PLC), the step time of the PLC, and the application of the torque by the power converter system. The time constant of the 1st order lag has to be chosen to provide optimal damping, taking all these delays into consideration.

Figure 6.11 illustrates the principle of the active generator torque controller. Here a detail of a simulation time series for a mean wind speed of V=24 m/s and a misalignment of 90 degrees is shown. The bottom graph shows the side-to-side bending moment at mudline for the reference case with and without activated AGTC. It can be seen that the vibrations are fairly damped by using the controller. The AGTC is achieving this at the expense of an additional generator damping torque as shown in the top graph of Figure 6.11. The effects can also be seen in the frequency domain. The right graph of Figure 6.12 illustrates the load reduction for the side-to-side bending moment at mudline. The plot demonstrates that the AGTC reduces well the 1st support structure eigenfrequency peak at 0.28 Hz. The additional generator torque amount can be seen in the left graph of Figure 6.12, where a clear frequency peak right at the support structure eigenfrequency can be identified. Moreover, the controller is introducing higher torque levels for almost the full frequency range.
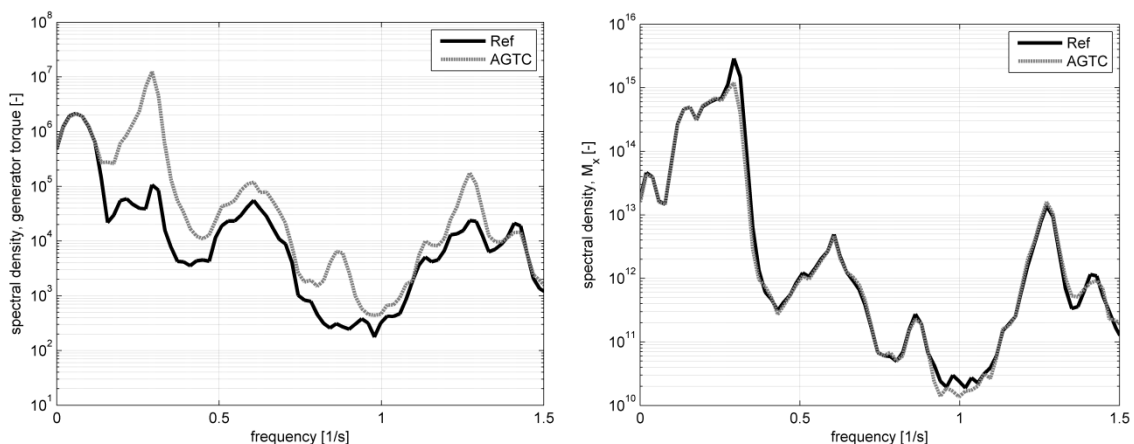
Figure 6.12: Spectral density of the generator torque and support structure side-to-side (M_x) moment at mudline

But this control concept is not always effective, especially with respect to different operational conditions where it can have significant effects on the loading of other system components. This is shown in Figure 6.13 for a reference case of a monopile in 25 m water depth (see Appendix A).
Here Figure 6.13 on the left side shows the side-to-side bending moment and on the right side the fore-aft bending moment of the support structure at mudline as DELs for different cases of

misalignment and different control strategies, where the wind is always coming from the North (here 0 degrees) and the waves are iterated respectively to create the misalignment. The DELs are shown as non-lifetime weighted distributions, which means that each wind-wave-misalignment case assumes a duration of 20 years by using the Weibull distributions of the given site as desribed in Sub-Section 8.1.1. For the side-to-side moment it can be seen that the AGTC is mitigating loads well. The controller is able to reduce the side-to-side loading significantly with an increase in damping towards the case of largest misalignment for the support structure, which are 90 degrees and 270 degrees respectively. The corresponding fore-aft moment is almost unchanged as can be seen in Figure 6.13, even if some minor increases can be identified for smaller misalignment cases.

To illustrate the effects for certain wind speeds, a specific misalignment is shown in more detail in Figure 6.14. Here the non-lifetime weighted DELs for the simulated wind bins are presented for the side-to-side (M_x) moment on the left side and the fore-aft (M_y) bending moment of the support structure at mudline on the right side. The shown case corresponds to a misalignment of 60 degrees – thus wind acting from 0 degree on the rotor and waves from 60 degrees respectively. The Figures demonstrate that the AGTC damps the critical side-to-side bending moment well for all wind speeds. Especially at lower wind speeds the concept is effective, which is important as for these conditions the probability of misalignments between wind and waves are the highest. Furthermore, the concept reduces the fore-aft bending moments, especially at high wind speeds. Just at partial loading the fore-aft moments are nearly unaffected and even slightly increased for some cases. This was also identified in Figure 6.13 for small misalignments. The reason is probably due to the fact that through the introduced varying torque and therefore also speed, the turbine is not operating in its optimal anymore and therefore the effect of aerodynamic damping is decreased.
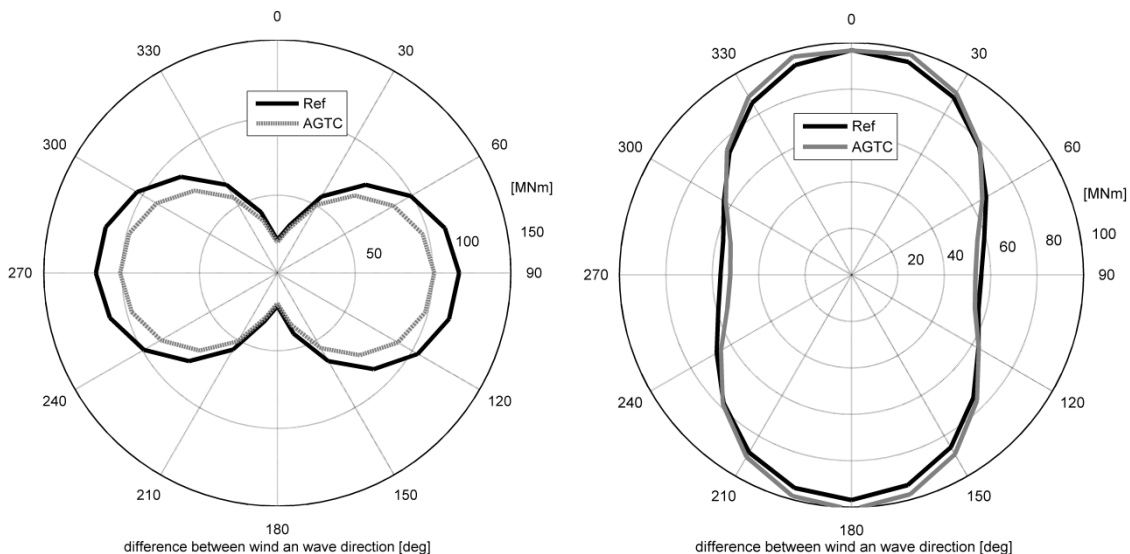
Figure 6.13: Polar distribution of non-lifetime weighted DEL for the support structure side-to-side (M_x) and fore-aft (M_y) moment at mud line as comparison of the reference to the controlled cases

In the following, the active generator torque controller is applied for a reference case to show its potential and effects on other system quantities. The concept is shown for a 5 MW offshore turbine design on a monopile in 25 m deep water . The loads are expressed as damage equivalent loads (DEL) for a reference cycle number of N=2E07, a lifetime of 20 years and am inverse S-N-slope of m=4 for steel components and m=10 for composites. The introduced misalignments are site-specific according to the evaluated measurement data at the given site as described later in Sub-Section 8.1.1. The focus of the study will be on fatigue loads only.
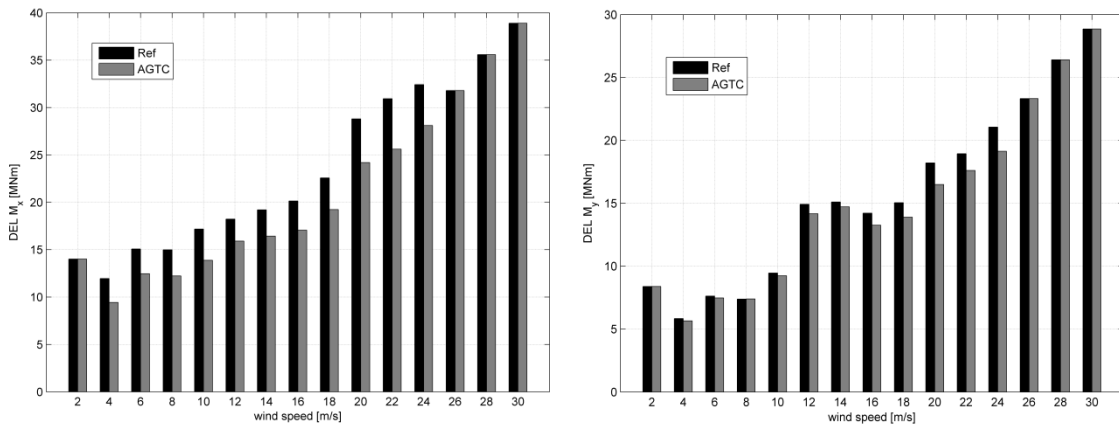
Figure 6.14: Non-lifetime weighted DELs (with N=2E+7) for the support structure moments (m=4) at mudline as comparison of the reference and the AGTC-controlled case

In Table 6.3, the results are listed as change in lifetime weighted DEL. It shows that the concept reduces well the M_x loading, which is mainly involving the side-to-side loading component, by keeping the M_y loading nearly unaffected. Here it has to be stated that the amount of damping for the side-to-side mode could have been larger, but with the penalty of overloading other components. Especially the power quality sets a certain limit, as otherwise the costs for the power electronics will become too high. The here shown value of almost 17 % increase of power fluctuations is probably already at the upper end of effectiveness.

Table 6.3: Load comparison between the reference and AGTC controlled case

	Loads as DEL [N=2E+7, m=4]			Change in energy yield and power fluctuations		Change in pitch rate
	Support structure at mudline					
	M_x	M_y	M_{xy}	AEP	P_{std}	Pitch$_{std}$
Reference	66.4 MNm	91.9 MNm	103.6 MNm	25.6 GWh	0.15 MW	0.46 deg/s
Controller	- 14.5 %	+ 0.8 %	- 8.1 %	- 0.07 %	+ 16.9 %	0 %

When the impacts on other components of the RNA are discussed, especially the change in drive-train load is important to consider, in Figure 6.15 it is expressed as change in gear box torque. For the shown case the loads in the gear box are increased by 2.5 %, which is acceptable. For the blades, the controller is not really affecting the fatigue loads. For the loads in the main bedplate, the controller is even decreasing loading. Especially the hub rolling moment (M_x hub) is decreased significantly.
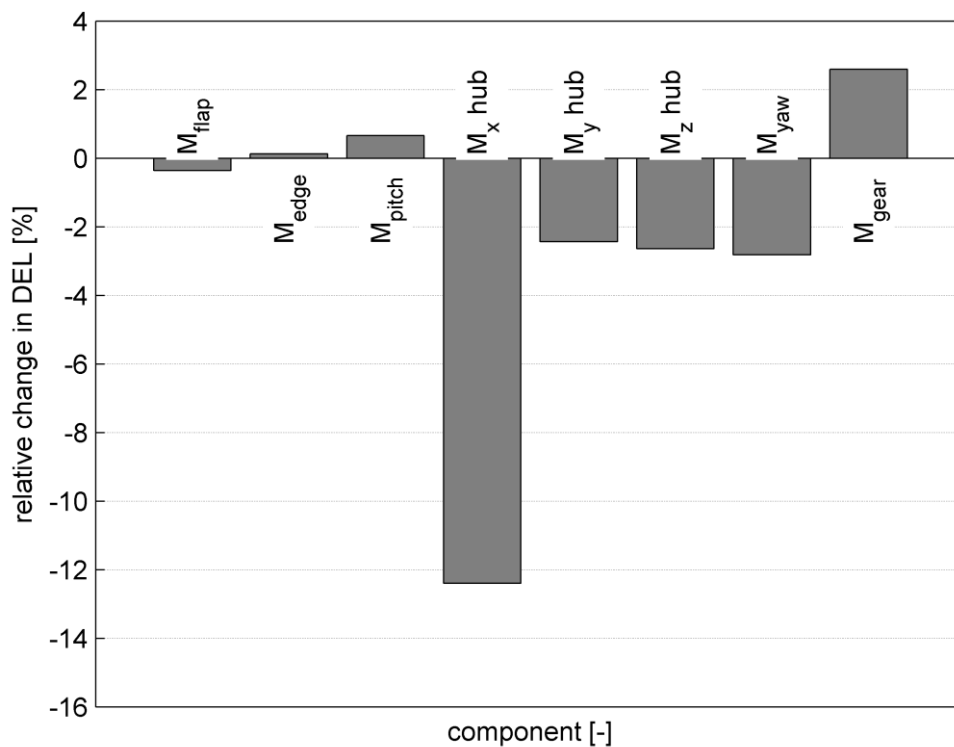
Figure 6.15: Relative change in component fatigue loading by applying AGTC in comparison to the reference case

In conclusion it can be stated that the concept of an active generator torque controller is able to mitigate the target side-to-side bending moments in the support structure to a significant extent. The concept works especially well in the partial loading region, where most of the misalignment occurs and where it causes most of the damage for the sideways support structure mode. Besides, it does not impose large additional loadings to other system quantities. Just the drive-train and the power electronics will experience higher loads and fluctuations.

6.4 Individual pitch control

The effect of wind- and wave-misalignment can have a significant effect on the fatigue loading for support structures like monopiles, as already explained in Chapter 2. Compared to the already presented concept for an active generator torque controller in Section 6.3, another control option is possible to damp the side-to-side support structure mode. Here individual pitch control (IPC) can be used.

As with the AGTC the measured nacelle acceleration input is used to damp the tower side-to-side motion. However, in this case the controller used the extra input to adjust the pitch position demand. The aerodynamic load on the blades that generates the driving moment on the hub also results in an edgewise shear force at the blade root. Normally these forces cancel each other out at the hub, with the net force only a function of the asymmetries like turbulence and wind shear. By issuing a pitch angle demand perturbation to each blade (in parallel to the collective pitch controller) it is possible to manipulate the blade root shear forces so that a component of the sideways force on the hub is actively controlled. The tower 1st side-to-side mode is more directly linked to side-to-side displacement than to tower top rotation, so in this sense the IPC can provide more efficient damping of the side-to-side mode than the AGTC.

In order to translate a collective pitch demand together with demanded sideways force from the controller into pitch angle demand for each blade, a reverse d-q axis transformation [21] is used. A force is only required in one direction (side-to-side), so the transformation takes only the mean pitch angle demand and a differential pitch angle demand in the vertical axis. This can be expressed in matrix format as

$$
\begin{pmatrix} \beta_1 \\ \beta_2 \\ \beta_3 \end{pmatrix} = \begin{pmatrix} 1 & \cos(\theta) \\ 1 & \cos(\theta + \dfrac{2 \cdot \pi}{3}) \\ 1 & \cos(\theta + \dfrac{4 \cdot \pi}{3}) \end{pmatrix} \cdot \begin{pmatrix} \beta_c \\ \beta_d \end{pmatrix}
$$

(6.1)

where β_1, β_2 and β_3 are the pitch angle demand for blade one, two and three respectively, β_c is the collective pitch angle demand and β_d is the differential pitch angle demand in the vertical axis.
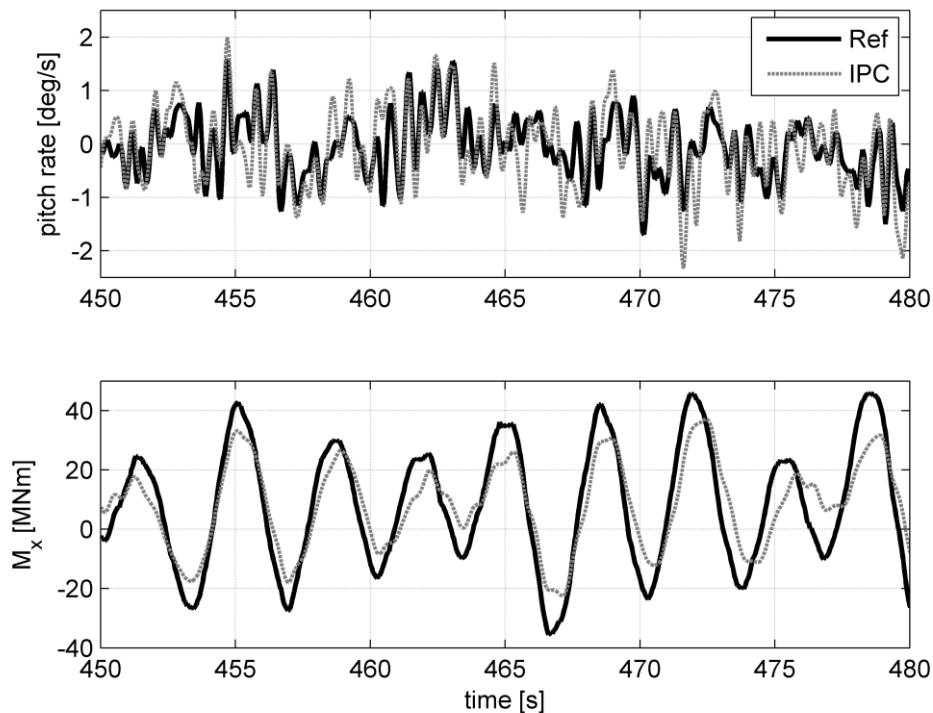
Figure 6.16: Detail of simulation results for an IPC versus a reference case for V=24 m/s and 90 degrees misalignment

Analogous to the AGTC, the phase of the measured nacelle acceleration is 90 degrees advanced in relation to a damping force. The measured nacelle acceleration is passed through a 1st order lag to achieve a phase lag without using an integrator. The pitch system is slower to respond than the power converter system, so more careful consideration needs to be given to compensating for the delays in the control loop. The final control algorithm design consisted of a lead compensator in series with the 1st order lag, and an azimuthal phase shift in the reverse d-q axis transformation. The azimuthal phase shift is defined by a time constant which is converted to a phase angle using an estimate of the rotor speed.
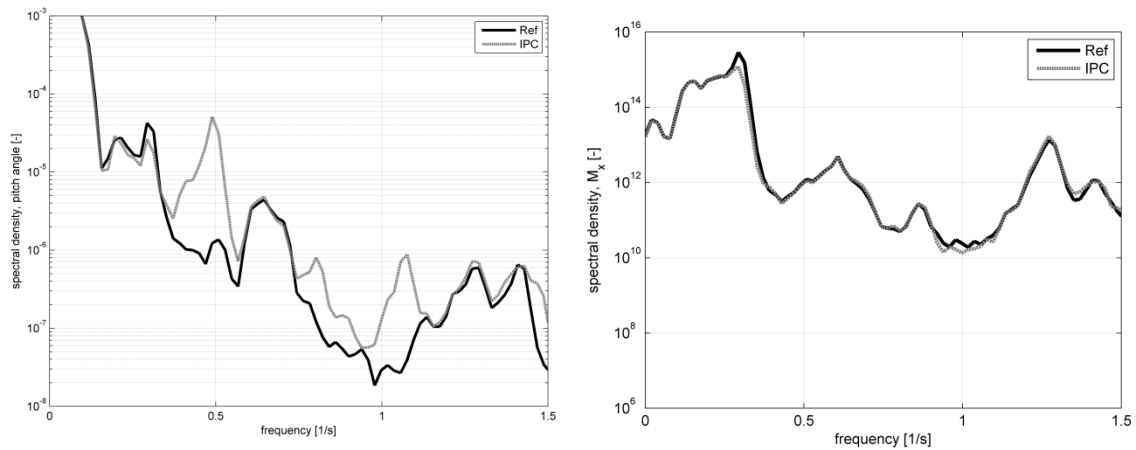
Figure 6.17: Spectral density of the pitch angle and support structure side-to-side (M_x) moment at mud line

The IPC relies on the fact that blade root in-plane shear force varies with the pitch angle. This is intuitively true at large pitch angles where the aerodynamic torque varies with pitch angle, but it is less clear when the blades are near fine pitch. The fine pitch angle should be where the aerodynamic torque is a maximum with respect to the pitch angle. In other words, a small change in pitch angle around fine pitch does not change the aerodynamic torque. This is significant because it is the same in-plane aerodynamic loads which are relied upon to cause variation in the in-plane blade root shear forces required for IPC. In practice it can be found that there is sufficient variation in the shear forces for IPC to work around fine pitch, but greater pitch angle variation is required. This is achieved by scheduling the gain of the IPC on the collective pitch angle.
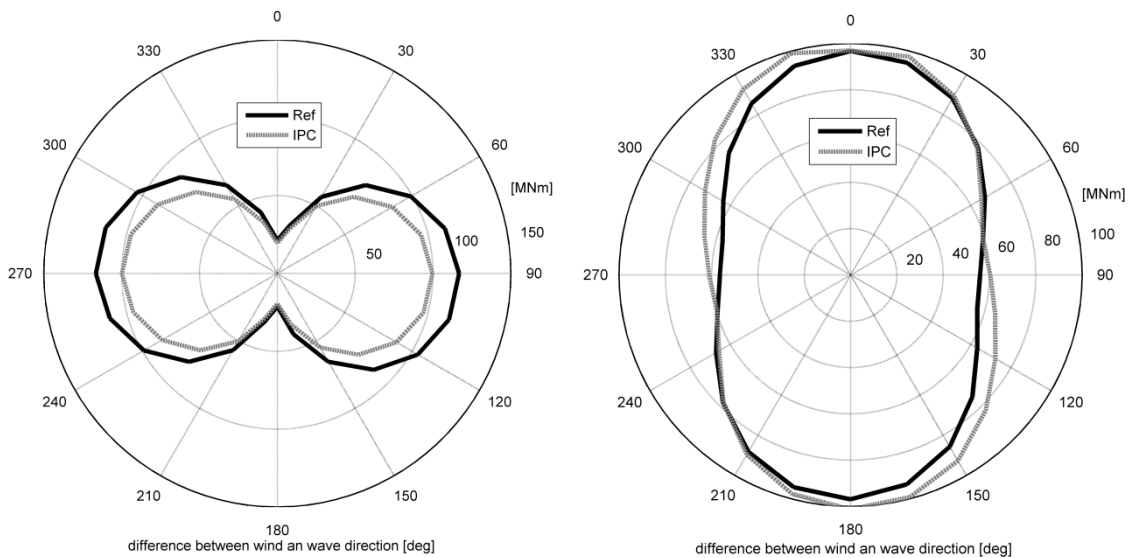
Figure 6.18: Polar distribution of non-lifetime weighted DEL for the support structure side-to-side (M_x) and fore-aft (M_y) moment at mud line as comparison of the reference to the controlled cases

In Figure 6.16 the principle of the IPC is shown for a detail of a simulation time series for a mean wind speed of V=24 m/s and a misalignment of 90 degrees. The bottom graph illustrates the side-to-side support structure moment at mudline for the reference case with and without

activated IPC. It shows that the vibrations are well damped by using the controller. The graph on top shows the corresponding pitch rate of the case where a clear additional pitch angle through the integration of the IPC can be seen. The effects can also be seen in the frequency-domain in Figure 6.17. The right graph shows the load reduction for the side-to-side bending moment at mudline, where a clear reduction of the 1st support structure eigenfrequency at 0.28 Hz is visible.

The additional pitch rate spectrum is shown in the left graph of Figure 6.17 and it presents the expected results. The constant loads on the turbine relate to pitching at the *1P* frequency. If the IPC is used to generate an oscillating load on the turbine, as here for the first support structure, the pitching frequency is altered. This is evident in the spectral peak in pitch activity found at the support structure eigenfrequency plus *1P*. This can be seen in the graph of Figure 6.17, as the peak occurs at 0.48 Hz, where 0.28 Hz is the support structure and 0.2 Hz the *1P* frequency for rated rotational speed.
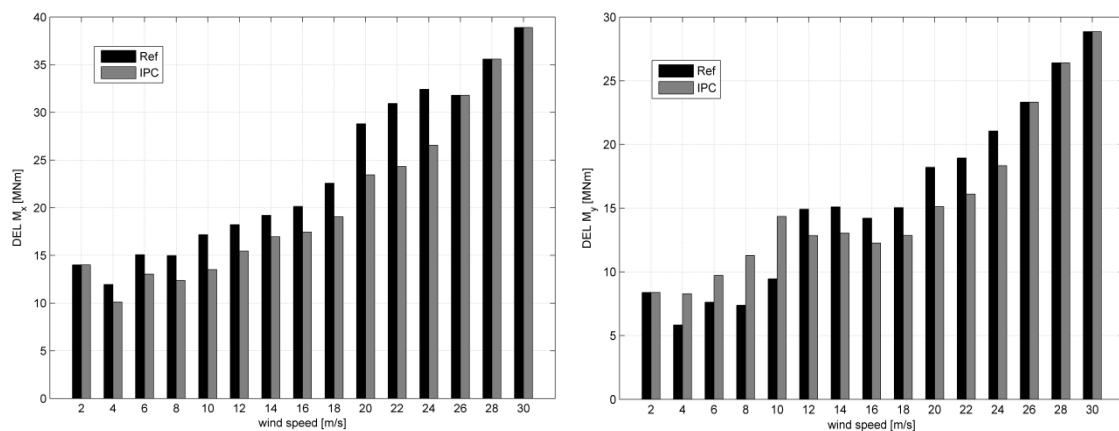
Figure 6.19: Non-lifetime weighted DELs (with N=2E+7) for the support structure moments (m=4) at mudline as comparison of the reference and the IPC-controlled case

As for the AGTC, the impact of the IPC can also be shown for different cases of misalignments, where it can be concluded that the IPC is not always effective. In Figure 6.18 a reference case of a monopile in 25 m water depth (see Appendix A) is shown. Here the Figure shows the side-to-side bending moment and the fore-aft bending moment of the support structure at mudline as DELs for different cases of misalignment and different control strategies, where the wind is always acting from North (here 0 degrees) and the waves are iterated respectively to create the misalignment. The DELs are shown as non-lifetime weighted distributions, which means that each wind-wave-misalignment case assumes a duration of 20 years by using the Weibull distributions of the given site as described in Sub-Section 8.1.1. For the side-to-side moment it can be seen that the IPC is mitigating loads well. The controller is able to reduce the side-to-side loading significantly with an increase in damping towards the cases of largest misalignment for the support structure, which are 90 degrees and 270 degrees respectively.

However, for the fore-aft case the loading at some specific misalignments is increased. It shows that the IPC leads to additional variations in thrust, which is probably due to variations in wind speed over the rotor area. If waves are acting on the structure from or into the downwards moving rotor direction, the IPC increases loading up to 10 %. Especially for misalignments of 315 degrees and 135 degrees, the increase is significant. To show the arising problem for the fore-aft moment by using IPC, a specific misalignment is shown in more detail. In Figure 6.19, the non-lifetime weighted DEL for the simulated wind bins is presented for the side-to-side (M_x) and fore-aft (M_y). The shown case corresponds to a misalignment of 60 degrees with wind

acting from 0 degree on the rotor and waves from 60 degrees respectively. First of all it is shown that the IPC is not as effective as the AGTC for lower wind speeds, where the turbine is still in its partial loading region. At the same time the IPC is increasing the fore-aft moment. In most of the simulations it is found that the IPC is not working effectively below full power. This reflects the reduced variation in aerodynamic torque with pitch angle as discussed before. Of course, the IPC could have been designed for not giving additional loading to the fore-aft moment, but with the expense of being less efficient for the target side-to-side load reduction.

Within this study, the IPC is compensating this loss in damping by having a better performance at full power in comparison to the AGTC. However, as large misalignments occur mainly for lower wind speeds, as illustrated in Chapter 2, this is a significant drawback of using IPC for this application.

Table 6.4: Load comparison between the reference and IPC controlled case

	Loads as DEL [N=2E+7, m=4]			Change in energy yield and power fluctuations		Change in pitch rate
	Support structure at mudline					
	M_x	M_y	M_{xy}	AEP	P_{std}	$Pitch_{std}$
Reference	66.4 MNm	91.9 MNm	103.6 MNm	25.6 GWh	0.15 MW	0.46 deg/s
Controller	- 14.6 %	+ 3.5 %	- 7.8 %	- 0.09 %	+ 0.1 %	+ 7.5 %

In the following, the IPC is applied for a reference case to show its potential and effects on other system quantities. The concept is shown for a 5 MW offshore turbine design on a monopile in 25 m deep water (see Appendix A). The loads are expressed as damage equivalent loads (DEL) for a reference cycle number of N=2E07, a lifetime of 20 years and an inverse S-N-slope of m=4 for steel components and m=10 for composites. The introduced misalignments are site-specific according to the evaluated measurement data at the given site as described in Sub-Section 8.1.1. The focus of the study will be on fatigue loads only.

Figure 6.20: Relative change in component fatigue loading by applying IPC in comparison to the reference case

In Table 6.4, the results are listed as change in lifetime weighted DEL. It shows that the concept reduces well the M_x loading, which mainly involves the side-to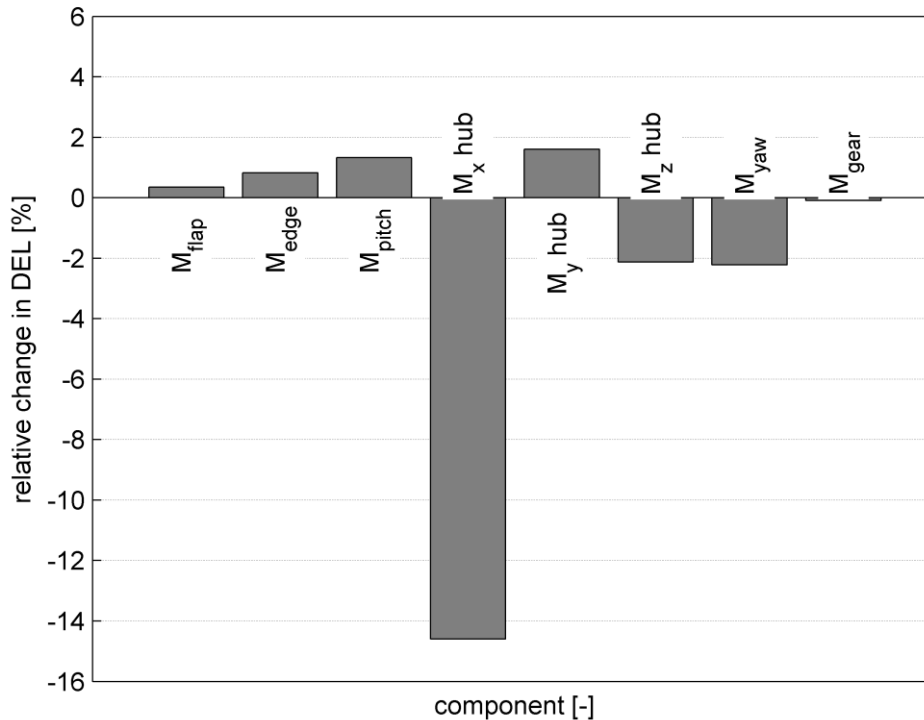-side load component. Here it has to be stated, as for the active generator torque controller, that the amount of damping for the side-to-side mode could have been larger, but with the penalty of overloading other components. Contrary to the M_x loading, the M_y load is increased by 3.5 %, which is due to the performance at low wind speeds. In contrast to the AGTC, the power level and quality is nearly unchanged. Another difference is the change in pitch rate, as the IPC introduces additional pitch actions. Here the standard deviation of the pitch rate is increased by 7.5 %. This value represents the increase in pitch activity above rated wind speed only, as below rated wind speed the system is active compared to the reference case and will therefore introduce an increase of several 100 %. The impact on other system loads is similar to the case using AGTC as shown in Figure 6.20. The hub and yaw loads are not significantly changed and for the hub rolling moment even decreased by over 14 %. As a difference to the AGTC, the IPC is not affecting the drive-train loads, but therefore the blade loads by introducing slightly lower fatigue lifetimes.

In conclusion, the individual pitch controller provides good damping to the side-to-side load component at the support structure. Compared to the AGTC the IPC has a lower performance at partial loading as a drawback. This leads to the conclusion that IPC is a beneficial concept for operations at rated wind and above. Considering system reliability, AGTC and IPC use standard control mechanisms (pitch and torque control), and both have the same input requirements (nacelle side-to-side acceleration signal). However, it is likely that additional pitch duty will lead to system failure than additional torque variations. Due to its operation at three different pitch angles, the IPC requires a more sophisticated safety system and extreme load checks. Here different concepts for such control algorithms are already available [48].

6.5   Semi-active structural control

With the increasing size of wind turbines and especially for offshore applications, dynamic loading of the support structures increases. These loads and the resulting vibrations can be reduced with the aid of damper devices. The use of dynamic vibration dampers is commonly used and known from the building industry, where the dampers are applied to work against vibrations from wind loads or earthquakes. In contrast to many applications for chimneys or tall buildings, wind turbines are soft structures, which experience large vibrations due to the high dynamic loadings.

Vibration damping devices can be classified according to their functional behaviour and their power supply requirements into active, semi-active and passive dampers.

Passive dampers, as already explained in Section 5.4, do not require any power supply, as their properties are based on priori design criteria and they do not change during the response of the structure. The concept of the passive damper is simply to change the structural stiffness and therefore the natural frequencies and the mode shapes.
Active damper devices need a power supply, as the controlled forces supplied by the power source are based on the actual response of the structure and the change in response of the structure. However, active damper systems have the disadvantage that for example in cases of a grid loss they are not able to operate anymore. Therefore a main advantage of structural damping devices is not valid anymore, that they are always operational, especially in cases of non-availability where high excitations from waves can be introduced to the support structure.
An intermediate solution is the usage of semi-active dampers, as they remain passive while the response amplitudes are small and they are triggered into action when the vibration exceeds a predefined threshold. Thus, a smaller power source is necessary, which might make this device more economical. Furthermore the system will turn into a passive device if the power supply is gone, and therefore it combines the advantages from active and passive damper systems.

A known solution for such a semi-active device is an oil damper, where the device consists of a heavy cylindrical steel pendulum which is clamped by a number of chains. The length of the chains defines the eigenfrequency of the pendulum, where the pendulum moves also in an oil bath to achieve a certain damping of the system. The damping depends on the oil amount and the viscosity, but also on the geometry of the pendulum and the gap between pendulum and bath bottom. Here the viscosity of the oil can be changed and therefore making the damper semi-active. However, such a system is problematic in terms of safety, weight and seize. The oil is seen as critical fluid if a leakage occurs. In terms of weight and seize, the pendulum concept will impose problems for the integration into the tower. This issue is also pointed out in Section 5.4 for the 10 tons heavy passive device studied in the shown reference case.

A solution is recently proposed [49], where a compact toggle-braced configuration using magneto-rheological dampers is used. It combines the advantages of viscous fluid dampers, like reaction out of phase to the system, with the advantages of active devices, like controllability. Furthermore it is compact and easier to implement into the tower.

Such a magneto-rheological fluid consists of ferrous particles, such as carbonyl iron, and a carrier medium which is in most of the cases silicon oil, hydrocarbon or water. As controlling field, not only a magnetic, but also an electric field is possible. However, the advantage of the magnetic field compared with the electric field is the higher dynamic yield strength and a greater insensitivity concerning the temperature range or variation and contamination of the fluid. Additionally, the minimum amount of fluid is two magnitudes smaller than the one for the electro-rheological fluid, so the devices are much smaller [50]. The change in the magnetic field takes place in the order of 10^{-3} to 10^{-4} seconds [51]. The damper can be controlled with a small power source of 50 W and 24 V for a reasonable time period of several hours. This enables a secure application in cases of a grid loss.

In an adequate numerical description, the dampers are mainly described with the Bouc-Wen model, which includes hysteretic behaviour [52]. It has to be adjusted to 14 values, which for example can be derived by measurement data of specific dampers [53]. The most practical way to model such a magneto-rheological damper is by using the Bingham mode [50]. The force of the damper can be calculated as

$$F_{MR} = f_s \cdot \text{sign}(\dot{u}_D) + C_0 \cdot \dot{u}_D$$

(6.2)

with f_S being the slip load, C_0 the damper coefficient and $\dot{u}_D$ the damper velocity.

Based on that, the dissipated energy can be determined by

$$D = f_S \cdot \text{sign}(\dot{u}_D) \cdot \dot{u}_D + \frac{1}{2} \cdot C_0 \cdot \dot{u}_D^2$$

(6.3)

Here, the possibility of magnifying the damper submitted velocity from the structure becomes important. The so-called magnification factor gives a relation between the structure displacement of the tower and the displacement transferred to the damper

$$f = \frac{u_D}{u}$$

(6.4)

with f being the magnification factor, u_D the damper displacement and u the structure displacement. By transforming this relation and deriving by a partial derivative of the magnification in the displacement with respect for small u values, the following relation is found

$$\dot{u}_D = f \cdot \dot{u} + \frac{df}{du} \cdot \dot{u} \cdot u$$

(6.5)

with $\dfrac{df}{du} = const$

(6.6)

If then the damper velocity is substituted with the structure's velocity multiplied with the magnification factor, a relation is found that describes the effectiveness of the system with the goal of achieving an as high as possible magnification factor.

$$D = f \cdot f_S \cdot sign(\dot{u}) \cdot \dot{u} + \frac{1}{2} \cdot f^2 \cdot C_0 \cdot \dot{u}^2$$

(6.7)

By differentiating to $\dot{u}$ the effective force added to the structure by the magneto-rheological damper can be found

$$\frac{\delta D}{\delta \dot{u}} = f \cdot f_S \cdot sign(\dot{u}) + C_0 \cdot f^2 \cdot \dot{u}$$

(6.8)

This identifies the same dependency of the added force to f^2 as if it is created out of the following formulas without friction

$$F_{horizontal} = f \cdot F_D$$

(6.9)

$$F_D = C_0 \cdot \dot{u}_D$$

(6.10)

$$F_{horizontal} = f^2 \cdot C_0 \cdot \dot{u}$$

(6.11)

The theoretical descriptions show the importance of a proper magnification factor in order to achieve good damping results. Besides, the integration of a damping system into a wind turbine tower is also challenging. The correct position for the damper has to be found in both height and horizontal distribution. Also, a supporting structure, which increases the dampers effectiveness, is advised (i.e. bracing). Compared to already known and used configurations in stiff buildings, the integration in a slender structure like a wind turbine seems to be easier, because of the higher deflections. As damping systems in general need deflection for the dissipation of energy, a higher movement of the tower is in the first approach helpful for an effective application [50].

The magnification factor has an important influence on the damper force (consequently damping ratio). The magnification factor is realized by a certain alignment of so-called damper braces. Several configurations for bracing systems have been studied in [50]. All of them use different geometrical alignments to reach high magnification factors. Typical values for magnification factors are between 2.5 and 3.5 for such configurations. Theoretically, magnification factors can reach values up to infinity [54]. These are not taken into account, as they do not fit to geometrical restrictions like tower diameter, maximal installation height or minimum installation angles. All magnification factors mentioned in the following consider a fixed installation height, where the installation height constitutes the distance between the upper and the lower connection of the damper assembly.

Three configurations are defined in more detail:

- Scissor-jack bracing
- Lower-toggle bracing
- Upper-toggle bracing

Scissor-jack bracing

The scissor-jack, originally developed by [54] for buildings and adjusted for wind turbines in [52], can reach values of magnification factor up to 2.2 to 2.8. The variation of the angles ψ and θ will increase the magnification factor as seen in Figure 6.21. A big advantage of the scissor-jack system is the ability to be installed even in tight space. Even then, the amplification factor can reach relatively high values, making it an interesting solution. Compared to other bracing systems, the geometry of a scissor–jack brace system is relatively complicated. Furthermore, it is difficult to achieve a high magnification factor and a reliable product, therefore this device is not considered for further investigations. The magnification factor of the scissor-jack geometry is defined as

$$f = \frac{\tan(\theta)}{\cos(\psi)}$$

(6.12)
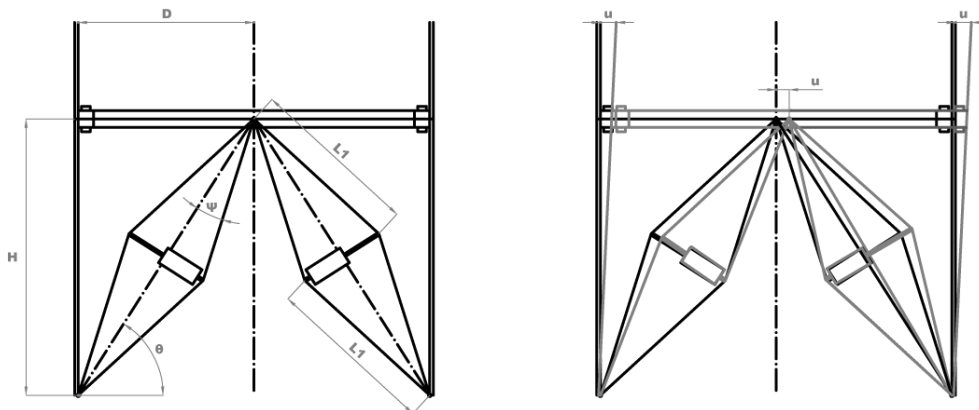
Figure 6.21: Scissor-jack bracing geometric alignment (left) and deformed (right) [55]

Lower-toggle bracing

The lower toggle bracing configuration as shown in Figure 6.22 depends on many different values and the limits, which are not only given by the stroke of the damper, some general constraints have to be listed. First of all, the angle θ_1 has to be smaller than the diagonal connection between the lower left boundary and the upper right boundary to ensure manoeuvrability. For every specific possible angle θ_1, it has to be ensured, that the brace is simply not longer than D. The last constraint is given by the maximal possible deflection in the horizontal plane. It has to be prohibited, that the braces snap through. The magnification factor of the lower-toggle bracing system is defined as

$$f = \frac{\sin(\theta_2) \cdot \sin(\theta_1 + \theta_3)}{\cos(\theta_1 + \theta_2)}$$

(6.13)
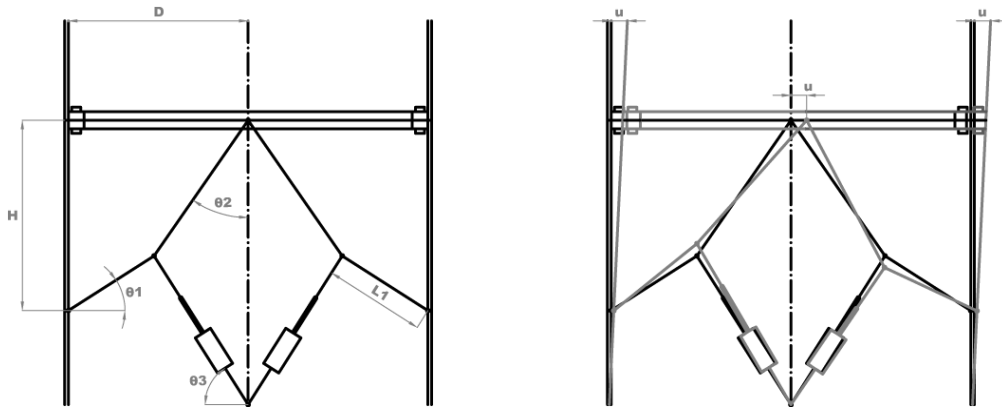
Figure 6.22: Lower-toggle bracing geometry alignment (left) and deformed (right) [55]

The lower-toggle configuration can achieve magnification factors up to 2.2 with the restrictions fixed for this example [54]. Compared to other systems, the lower-toggle assembly has big space requirements. Additionally, the magnification factor does not reach the highest values. Therefore, this geometrical alignment is not taken into account for further project steps.

Upper-toggle bracing
The upper-toggle bracing follows the same constraints as for the lower toggle bracing. Up to now, the upper-toggle bracing provides the highest possible magnification factor. Values are getting up to 3.2 [54]. As it can be seen in Figure 6.23, the magnification factor depends on the brace-length, the installation height H and the three angles.

$$f = \frac{\sin(\theta_2)}{\cos(\theta_1 + \theta_2)} + \cos(\theta_2)$$

(6.14)

The upper-toggle-bracing needs less space compared to the lower-toggle. Additionally, the magnification factor is very high.
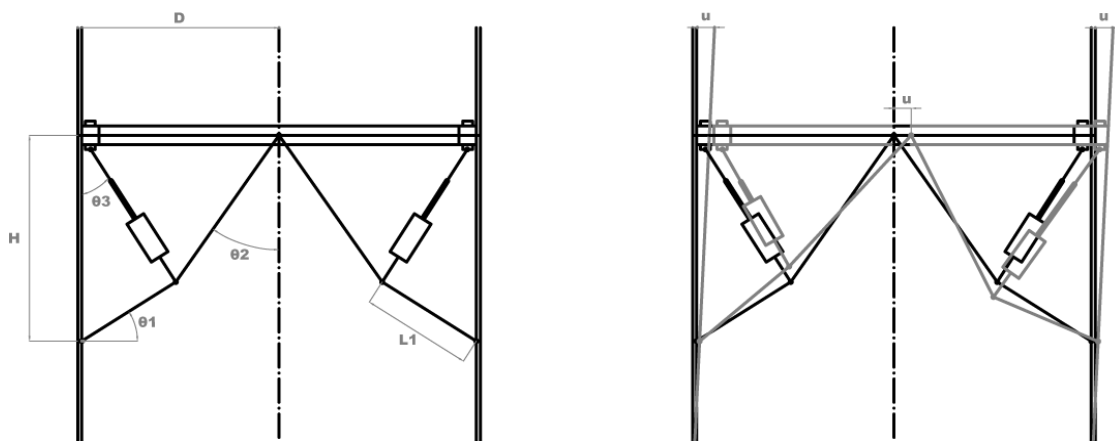
Figure 6.23: Upper-toggle bracing geometry alignment (left) and deformed (right) [55]

Based on the above described system configurations, the upper-toggle assembly seems to be the most suitable one. This is due to the fact that the upper toggle is more efficient in the energy

dissipation than the other configurations. On the other hand, integration and simulation of the upper bar toggle is more difficult than of the other configurations. The scissor jack can be assembled outside the tower and added afterwards, the lower toggle's damper does not need to be lifted. But for dissipation reasons, the decision is made to use the upper configuration as it is the most cost effective assuming the damper itself to be the most expensive part of the assembly. With the same amount of demanded damper force, a higher reduction can be observed with the toggle bracing configurations compared to the diagonal braces.
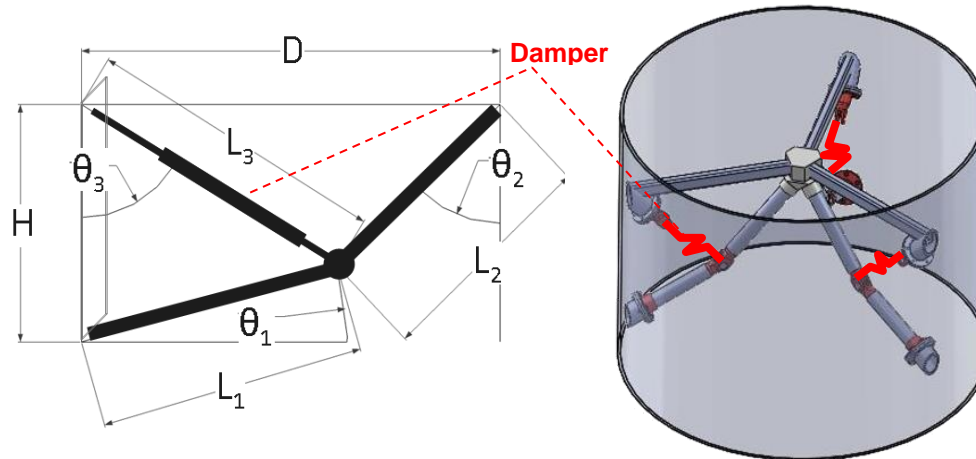
Figure 6.24: Upper toggle brace sketch and tower implementation [56]

In the following, the above described semi-active structural damper (SASD) system with an upper-toggle braced configuration is used to identify its effects in terms of load mitigation. The system is integrated into the ECO100, a 3 MW turbine design by Alstom-Wind (see Appendix A). The turbine is placed on a tubular steel tower with a hub height of 90 m. The damper is installed at tower top in order to supply maximum damping to the structure. The installation height is close to existing flanges, as there are already platforms installed, where the maintenance of the damper would be possible. Moreover, these sections are very stiff and can therefore provide an effective transmission of the damping forces into the tower.

The dampers themselves are installed in a 120 degrees shift relative to each other as seen in Figure 6.24. This ensures an operation for a wide range of frequencies. Furthermore it is assumed that the 120 degrees shift provides a symmetrical behaviour regarding stiffness added to the support structure and directional changes of the excitation. This also results in a resultant force which is more uniformly distributed among the dampers and can be smaller in magnitude and thus it enables thinner tower sections for supporting it.

As the semi-active system has to be controlled, the characteristics of the device are based on certain turbine sensors. The local tower acceleration signals are used to feed the new control loop, as depicted in Figure 6.25, providing a damper force demand as an output.
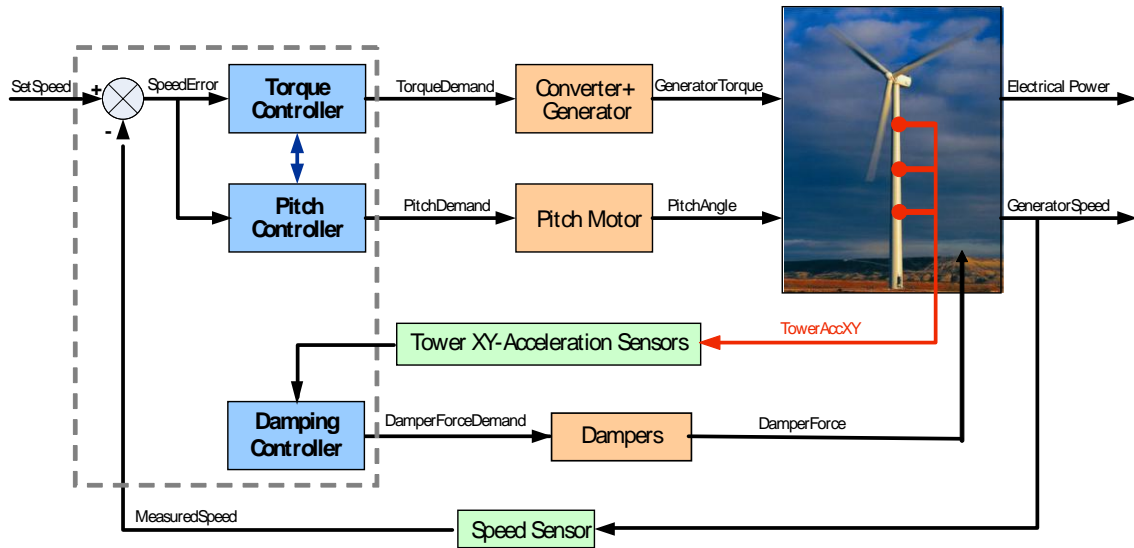
Figure 6.25: Wind turbine control System with tower damping loop [56]

The implemented damper configuration is designed to damp mainly the 1st support structure eigenfrequency due to its position at tower top. For the following load studies, the tower dampers are implemented and simulated using GH Bladed [57], with a specific add-on for this scope.

The semi-active device can, as discussed for the passive device in Section 5.4, be used for both extreme and fatigue load reduction, as it is always available independent of the turbine operational mode. Figure 6.26 illustrates the support structure bottom fore-aft bending moment of the studied Alstom turbine for a wind gust according to DLC1.6 of IEC [37]. In the plot the damper is used as semi-active and passive device, where the passive configuration means a disconnection of the active damper part, which results in a fixed damping frequency. The Figure shows how the oscillations after an extreme event are suppressed by both systems, and the total damping ratio is increased. The semi-active damper results in a better damping. Nevertheless, the effectiveness of the semi-active system is highly dependent on the used trigger and on turbulent conditions.

Beside the check for extreme loads, the semi-active device is also used for fatigue load reductions according to the IEC fatigue load cases [37]. In Table 6.5, the achieved reductions in fatigue loading and extreme loading are expressed for the support structure bottom bending moments. The fatigue loads are stated as reduction in damage for an inverse S-N-slope of m=4 for the steel tower. The extreme loads correspond to the former shown extreme gust load case.
It shows the potential of the damper with load reductions between 8 to 13 % for fatigue and 12 to 20 % for extremes. Here it has to be stated again that the studied turbine concept is an onshore configuration. In an offshore application with its much higher excitations from waves, the concept would probably show even better results in load mitigation.
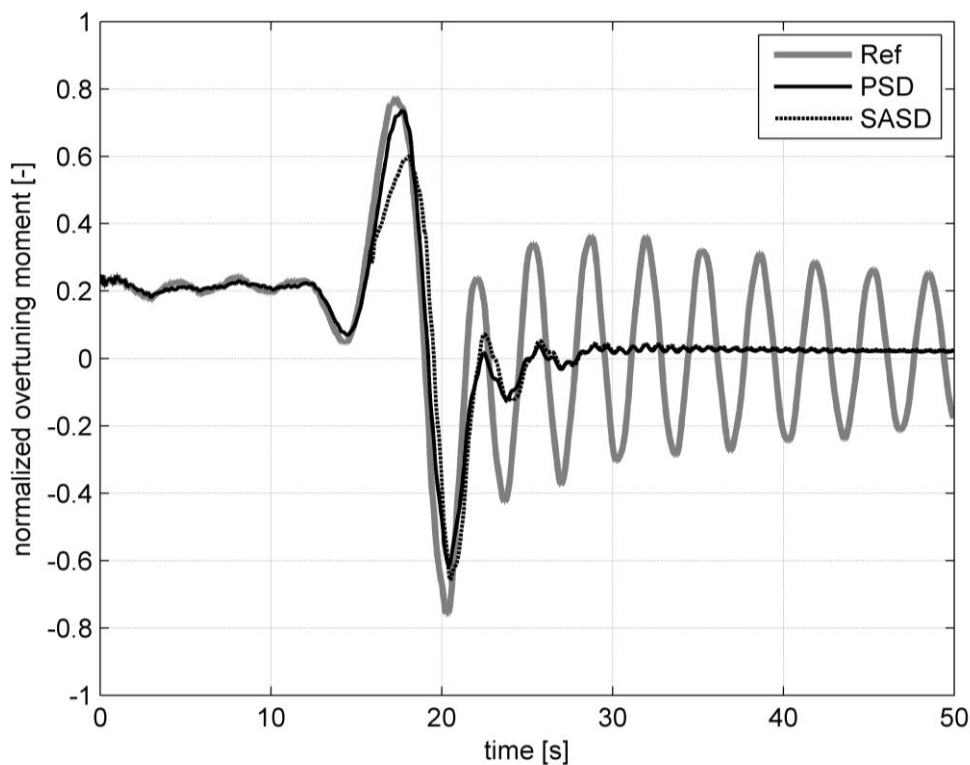
Figure 6.26: Tower base fore-aft moment response for an extreme gust as comparison of a semi-active and passive
damping system [56]

As for the passive damper system in Section 5.4, the semi-active damper is not introducing any additional loadings to system quantities like blades, hub or drive-train. Furthermore it is not affecting power output and quality. Therefore no additional costs occur in the turbine due to the damper implementation. However, the costs for the damping system have to be taken into account, which are including manufacturing, transportation and maintenance costs. Even though, special dampers are required for the application, which are able to bear the high number of cycles imposed by the wind turbine operations, a valuable decrease in the tower material still prevailed over the benefits.

Table 6.5: Load reductions by using SASD

| **Fatigue and Extreme Loads Reductions** | | |
| **Support structure at bottom** | | |
	M_x	M_y
Fatigue loads	- 7.6 %	- 13.0 %
Extreme loads	- 20.0 %	- 12.0 %

As an outlook, this system enables high potential for offshore applications as due to its semi-activity the damper can be tuned for different critical frequencies. This can be the case for certain wave conditions at low wind speeds, where the wave periods are in a lot of cases close to the structures eigenfrequency and therefore impose high damages.

7. Design methodologies

The design process for offshore wind turbines follows standardized sequences and is listed in the current guidelines [10]. The process is iterative and shall include all the sub-systems like RNA or the support structure in an integrated manner. This ensures that the interactions in loadings and the dynamics between each sub-system are incorporated. Although it is generally understood that an integrated design is preferable and beneficial in practice it is not always possible to perform integrated design for all the parts due to practical reasons, especially in the preliminary design stage [58].

The following Chapter will show that besides the conventional integrated design process, there is an adapted one including load mitigation to achieve a cost efficient design. For an optimal design of the offshore wind farm, the farm has to be considered as a whole including all sub-systems like turbine, support structure and grid connection. However, this work only focuses on the integrated design process of support structures and especially on monopiles, which are studied in details for the design demonstration. Different literature exists about fully-integrated offshore wind farm design process as for example in [5]. The proposed adapted design includes another loop in the process, which enables the implementation of load mitigation concepts in order to achieve an optimized design.

7.1 Conventional design process

Figure 7.1 shows the flow chart for a conventional offshore support structure design process for monopile structures. The process starts based on the given turbine parameters and site-specific environmental conditions, which are documented in the design basis. Based on these initial conditions an initial geometry is designed. This is usually done on the basis of experience and engineering judgements [59].
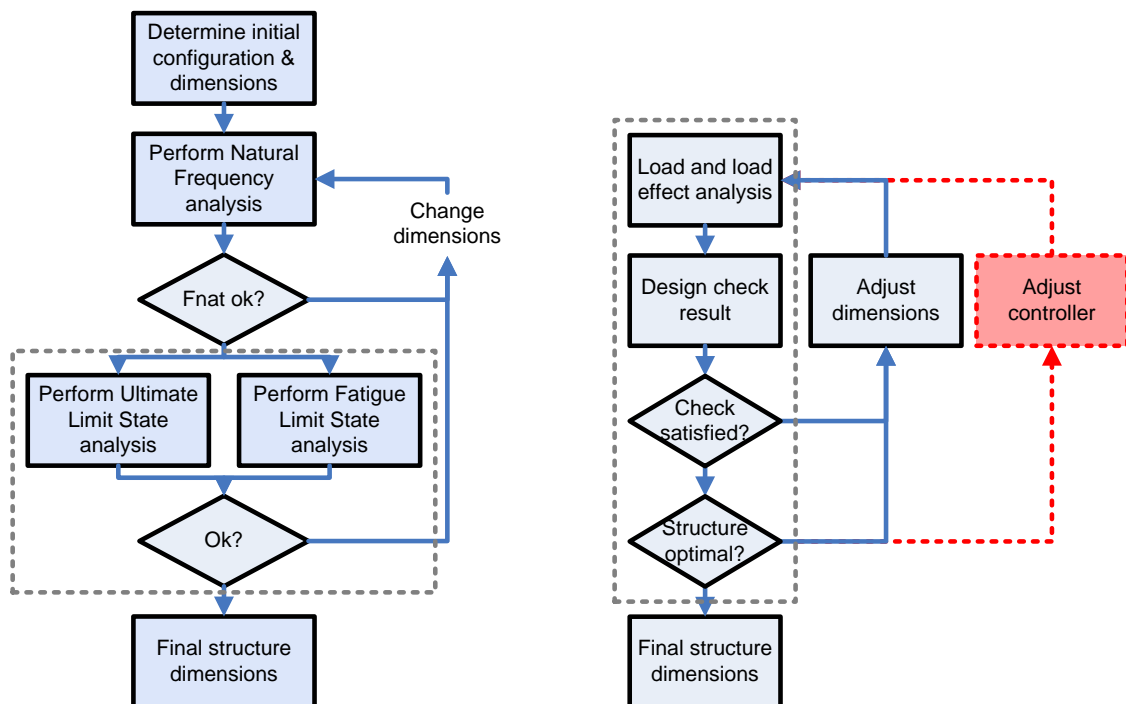
Figure 7.1: Conventional design process

The determination of initial conditions includes a first draft of the structure's dimensions in terms of diameter and wall thickness, but also grout connection and platform level.

The platform level is specified by the connection flange from the transition piece to the tower. It is defined by the highest wave elevation at the site and includes all tidal and storm surge water level variations. The platform level can be derived by

$$z_{platform} = LAT + \Delta z_{tide} + \Delta z_{surge} + \Delta z_{air} + \xi^{*}$$

(7.1)

with $z_{platform}$ as platform level, Δz_{tide} as tidal range, Δz_{surge} as storm surge, Δz_{air} as safety margin and ξ^{*} as highest wave elevation above still water level.

The highest wave elevation can be found by

$$\xi^{*} = \delta \cdot H_{D}$$

(7.2)

in which H_{D} is defined as design wave height and δ as wave elevation coefficient. These values can be determined based on the given site-specific environmental data and current standards [1] and are mainly dependent on the maximum wave height with a reoccurrence period of 50 years.

Finally the hub height can be calculated based on the found platform level, the rotor radius and a certain safety clearance between the service platform and the blade tip at the lowest rotor position as

$$z_{hub} = z_{platform} + \Delta z_{clearance} + 0.5 \cdot D_{rotor}$$

(7.3)

After the determination of the initial conditions, a natural frequency check is performed. Therefore the established geometrical dimensions are modeled in a structural analysis program in order to perform a frequency analysis. Here it has to be proofed that the support structure design matches the target frequency range. As stated in Section 3.1, this range is for most of the currently built monopile support structures in the soft-stiff design range between the *1P* and *3P* turbine rotational frequency band.

Based on this frequency range, the support structure dimensions are varied until a desired structural eigenfrequency is found. To achieve this, the diameter and the wall thickness of the pile are varied, where the diameter has the larger effect in the eigenfrequency of the structure. If no values are known for initial conditions, a starting ratio of 1:80 of the thickness to the diameter is common [60]. The decision on wall thickness and diameter has to take manufacturing and installation criteria into account as well as not each steel plate thickness is available and certain diameters cannot be installed with available installation tools. A solution could also be to include conical pile sections, for example at the top to decrease the hammer device diameter or the section at the water level in order to reduce the wave-excitations.

If the structure is defined for the target frequency range, certain preliminary extreme load calculations can be done with the aid of a structural analysis program. The reason for this preliminary load check is the determination of the pile penetration into the sea bed. The penetration-driving load cases are commonly extreme wind and wave cases, like the maximum rotor thrust from storm conditions or the maximum wave height in a certain design time range like 50 years. The derived maximum loads are then transferred to the pile and used to check the pile's axial and lateral stability, where for monopiles the lateral one is generally governing. In this check, the site-specific soil conditions have to be considered with appropriate modeling solutions like non-linear soil springs in the form of *p-y* curves [61]. The criteria for determining a

sufficient pile penetration are the horizontal displacement of the pile at mudline and at the pile toe. Here, based on practical experiences [60], the following criteria are used:

- Maximal horizontal displacement at mudline: 0.12 m
- Maximal horizontal displacement at pile toe: 0.02 m

After the penetration depth is determined, another frequency check is advised for finalizing the initial support structure design step.

As shown in Figure 7.1, the next step in the design process is the load analysis, which has to be performed with integrated simulations with a coupled RNA and support structure model.
Here the design check has to be done for the fatigue limit state (FLS) and ultimate limit state (ULS) analysis. On the right hand side of Figure 7.1 is an extended representation of the structural analysis procedure. In this Figure the limit state analysis is treated by performing a load and load effect analysis. For each of these analyses design checks are performed to check whether the structure meets the design criteria or not. If the structure fails the check the dimensions must be adjusted. If the check is satisfied it should be verified whether the structure is optimal, meaning that the mass of the structure cannot be reduced without violating one or more of the design criteria. If the structure is suboptimal, the dimensions of the structure should be adjusted. Each time the dimensions are changed the load and load effect analyses must be performed again followed by the design checks. This dimension adjustment can also be replaced by applying control changes to reduce the loading, which will be described in the later Section 7.2.

In the following, the fatigue and ultimate limit checks are described in more details.

Design load cases and checks for FLS
In the fatigue limit state analysis (FLS) the total damage incurred over the structure's design life is assessed by performing time domain simulations using integrated design tools. The fatigue load check shall represent all loads occurring in the lifetime of the offshore support structure, which is commonly 20 years. The design load cases to be considered are defined in the appropriate guidelines [10] and are based on the site-specific environmental conditions. The load cases shall take all operational and non-operational cases and installation and maintenance situations with their probabilities of occurrence into account. For monopile structures an evident source of fatigue damage might also come from pile driving, which is not considered here.

For fatigue loads, the wind and wave directionality but also turbine's availability can have a significant contribution as already discussed in Chapter 2. Therefore reasonable values for the availability and site-specific wind and wave directional distributions have to be included in the process.

Based on all performed load calculations, the structure's fatigue damage can be calculated. Therefore the structural loads are translated into local stresses by using a detailed FE structural model to determine the stress concentration factors and hot spots. When the local stress time histories are known, they can be characterised by, for example, the Rainflow counting method [62]. The stress history is then expressed in stress-ranges with the associated number of cycles. After the determination of stress ranges and their occurrences, the Palmgren-Miner rule [63] can be used to check if the structure survives the applied fatigue loads for the given lifetime.

The following equation illustrates the rule, in which the cumulative fatigue damage D_{fat}, for a constant stress magnitude, is defined by

$$D_{fat} = \sum_i \frac{n_i}{N_i}$$

(7.4)

where N_i is the maximum number of cycles the structure can endure with a stress range i and n_i is the number of actual occurring cycles with the stress range i. The rule states that the structural detail will fail due to fatigue if

$$D_{fat} > 1$$

(7.5)

If the cumulated damage is less than 1 than the structure will survive and the fatigue limit state analysis is finished.

Design load cases and checks for ULS
For the ultimate limit state analysis the loads are in general again obtained from integrated time-domain simulations. For some special cases, such as for ship impact analysis, specialized tools are necessary to account for the plastic deformation. As has been discussed for the fatigue analysis, appropriate design standards provide a list of extreme load events that need to be checked [10]. These cases include extreme environmental conditions like gusts, wind directional changes or extreme waves and currents, but also turbine failures like blades got stuck and are not able to pitch or emergency stops due to grid losses etc. Furthermore some exceptional cases like sea ice or ship collisions have to be checked if applicable. The load calculations additionally include the application of safety factors for the support structure sections. These are again defined in given guidelines [10] in order to take into account the uncertainties in the load calculations and material properties.

With the aid of the determined ultimate loads, several checks are done for the support structure to check if it fails under the applied loads. The following checks are necessary [59]:

- Yield stress check for the pile, the transition piece and the tower
- Global buckling check for the pile above the mudline, the transition piece and the tower
- Local buckling check for the pile above the mudline, the transition piece and the tower
- Foundation stability check to determine the required penetration depth

Yield stress check
In the yield check it is verified that the stress remains below the design yield stress to avoid plastic deformations in the structure. The check is performed by calculating the Von Mises stress at each node, taking the appropriate load safety factors into account and ascertaining that

$$\sigma_i \leq \frac{f_y}{\gamma_M}$$

(7.6)

where σ_I is the Von Mises stress at node i, f_y is the characteristics yield stress and γ_M is the material safety factor. The result is expressed as an utilisation ratio where the ratio between the Von Mises stress and the relation of the yield stress and the material safety factor should be less than 1.0 [1]. Further reductions of the design yield stresses at welded seams might be taken into account, depending on applied welding treatments and the type of welds as stated in the design guidelines.

Global buckling check
Under high compressive stress due to axial loading and bending, global buckling can occur. In the global buckling check it is verified that the overall stability of the structure is guaranteed. The global buckling check is carried out for each node according to [1] as

$$\frac{N_d}{\kappa \cdot N_p} + \frac{\beta_m \cdot M_d}{M_p} + \Delta n \leq 1$$

(7.7)

where N_d and M_d are the factored axial compression force and bending moment respectively, N_p and M_p are the plastic compression resistance and the plastic resistance moment, κ is a reduction factor for flexural buckling, β_m is a bending moment coefficient and Δn is calculated by

$$\Delta n = 0.25 \cdot \kappa \cdot \overline{\lambda}^2 \leq 0.1$$

(7.8)

in which $\overline{\lambda}$ is the reduced slenderness.

Local buckling check
Thin walled tubular sections may be susceptible to local shell buckling. Compressive axial loads and bending moments together with compressive hoop stresses due to external pressure can cause unstiffened sections to fail locally. There is sufficient resistance against local buckling if the following interaction equation is satisfied [1] as

$$\left(\frac{\sigma_x}{\sigma_{xu}}\right)^{1.25} + \left(\frac{\sigma}{\sigma_u}\right)^{1.25} \leq 1$$

(7.9)

In this equation σ_x and σ_φ are the acting axial compressive stress and circumferential stress due to external pressure respectively and σ_{xu} and $\sigma_{\varphi u}$ are the ultimate compressive and circumferential stresses respectively.

Foundation stability check
To ensure the overall stability of the structure, the deformation of the foundation must be within certain limits for the deflection and rotation at mudline. Also the stiffness of the foundation should be such that the natural frequency of the entire structure lies within the frequency range that allows safe operation of the wind turbine. The verification of the foundation stability is usually performed after the diameter of the foundation pile is chosen. Therefore, this verification mainly involves determining the required embedded length.
To this end a model of the pile foundation is subjected to the maximum loads at seabed, found from all performed load case simulations. Initially the embedded length of the foundation pile is selected sufficiently long. In a finite element model of the pile including p-y curves, non-linear spring elements representing the pile-soil interaction, the loads are applied to the model at the seabed level and the resulting deflections and rotations are found. If the deflections and rotations are within the limits the embedded length is reduced. If the limits are exceeded, the penetration depth is increased. The design penetration depth is defined as the smallest embedded length for which the limits are still satisfied.

As for the fatigue limit state analysis, the above described structural analysis procedure is iterated several times until a satisfying and economical design is achieved. If this is true, the

final support structure dimensions are found and the next steps like the fabrication, installation and logistic planning can start.

7.2 Integrated load mitigation methodology

In order to achieve an optimized support structure design, both aerodynamic and hydrodynamic loads and their associated dynamic responses should be reduced. This can be done by considering the RNA control and support structure in the design process. Hence, the RNA is considered as an active element to mitigate the loading on the support structure. Therefore the conventional design process of the support structure, as described in Section 7.1, has to be extended to integrate the impact of the control concepts on the design. This process is illustrated in Figure 7.2.

Figure 7.2: Adapted support structure design process

The proposed procedure assumes a given turbine and support structure concept. Of course, as described in Chapter 4, different turbine and support structure types can already be chosen in the design phase that consider a reduced load level and/or minimized levelized production costs.

As for the conventional design process in Section 7.1, the start of each design procedure is the determination of initial conditions and dimensions together with a natural frequency check (compare Figure 7.1). However, after this design stage the adapted design process differs from the conventional one.
The first step of the adapted support structure design process is to determine the dimensioning load cases for the support structure and the RNA. The goal of this step is to simulate the design load cases according to current guidelines [10] from a reduced set of load cases in the first

iteration of the design cycle prior to simulating the complete set of load cases. In general, the design can be fatigue or extreme load driven. In some cases or for some parts of the structure, it might also be a combination of both. Besides, the fatigue loading can be driven by the aerodynamic or hydrodynamic load components, depending on the turbine and support structure type and the given site.

According to these design-driving events, the RNA is used as active element in mitigating the design-driving loads on the support structure. The idea behind this is that depending on the turbine and control type, different control options are available for tackling different load events. In Chapters 5 and 6, different possible control concepts are described. The implemented load mitigation concept can be in the operational or dynamic control regime or in some cases a combination of both.

If, for example, a transient gust is a design-driver, a LIDAR device included in the operational control could lead to the required load mitigation and an optimized design. However, in most cases dynamic control will be the choice for load mitigation. Table 7.1 illustrates dynamic concepts and their impacts in the support structure but also the RNA loads. Furthermore, the Table shows that if a certain control concept requires a new check of extreme load cases due to the changed controller structure and behaviour.

Table 7.1: Qualitative fatigue load influences on system quantities by applying dynamic control concepts

	Energy yield	Power fluctuations	Support structure Fore-aft	Support structure Side-to-side	Blades	Hub	Yaw	Gearbox	Pitch drives	System costs	Additional ULS case check[1]
TFC^fa	→	→	↓	→	↗	↗	↗	↗	↗	→	
AIC^fa	→	→	↘	→	↗	↗	↗	↗	↗	→	●
IPC^ss	→	→	↗	↓	↗	↘	↘	→	↑	→	●
AGTC^ss	→	↑	→	↓	→	↓	↘	↗	→	→	
ASCO^fa, ss	↑	↗	↓	↗	↗	↗	↗	↗	↗	→	●
SAMD^fa, ss	→	→	↓	↓	→	→	→	→	→	↑	●

TFC – tower-feedback control , AIC – active idling control , IPC – individual pitch control , AGTC – active generator torque control , ASCO – soft cut-out including TFC and AGCT , SAMD – semi-active mass damper

fa – controller tuned to work for fore-aft support structure vibrations

ss – controller tuned to work for side-to-side support structure vibrations

[1] – application of this control device might impose new requirements for extreme load checks

For fatigue loads and here the fore-aft support structure loading, concepts like tower-feedback control (TFC), active idling control (AIC) or an active soft cut-out (ASCO) are promising, as they all focus on enhancing the effect of aerodynamic damping and thus achieve reductions in support structure fore-aft direction. Here the ASCO is a combination of the operational control concept of a soft cut-out with dynamic ones like TFC and AGTC. As Table 7.1 indicates, the implementation of an AIC will require a further check of extreme loads, as the turbine idles at

higher rotor speeds and reduced pitch angles. Therefore this control concept could be critical for some transient gust cases.

If the design-driving loads are excited in the sideways support structure direction, individual pitch control (IPC) and an active generator torque controller (AGTC) are reasonable concepts. The main difference between both is that IPC will impose some higher loadings in the fore-aft direction, which is not the case for the AGTC. Furthermore, IPC requires a further check of extreme cases and here especially transients and failure cases, as the turbine operates with three different pitch angles.

Finally, in addition to all the turbine control systems, a structural damper device (either passive or semi-active) can be a solution for the load mitigation. This concept has the benefit of mitigating both directions of the support structure movements equally. Of course, this can also be achieved by connecting different turbine control concepts like TFC and AGTC as an example.

If then the adapted control concept is chosen, another load check has to be performed. As mentioned, certain control concepts might create new load events to be design critical, hence the number of dimensioning load cases might increase. Thus, the last step of the support structure optimization process is a combination of the former determined dimensioning load cases and some additional controller-specific load cases. These cases are then evaluated until a sufficient optimization level is achieved. This optimized level also includes the check for possible increases of RNA loads, as most of the control concepts do impose some additional loading. For this reason the design including the adapted control concepts goes back to the full design process of the support structure, as described in Section 7.1, where the complete set of load cases are evaluated for the structural certification.

8.   Design demonstration

In this Chapter a design demonstration is shown in order to validate the described approach of an adapted support structure design process by including load mitigation concepts. The demonstration is shown for a reference turbine concept and site in the Dutch North Sea at 25 m water depth. Based on the site's load envelope, certain control concepts are chosen and implemented. Finally a trade-off evaluation is done, where the achieved savings in material are compared to additional loadings in the turbine.

8.1   Reference case

In this Section, the reference design for demonstration site is introduced. The Section describes the site conditions and the turbine configuration and shows the results of a reference support structure design.

8.1.1   Design location

The demonstration study is based on a location in the Dutch North Sea. The climate information is obtained from the wave and wind data published by *Rijkswaterstaat* for the location "K13" [64]. The site is also shown in Figure 8.1. The coordinates of K13 are 53°13'04" North and 3°13'13" East. The data are available as 3-hour average values for a period of 22 years (January 1979 - December 2000). A more detailed description of the site conditions can be found in the UpWind design basis [65]. Some major aspects are given in the following.
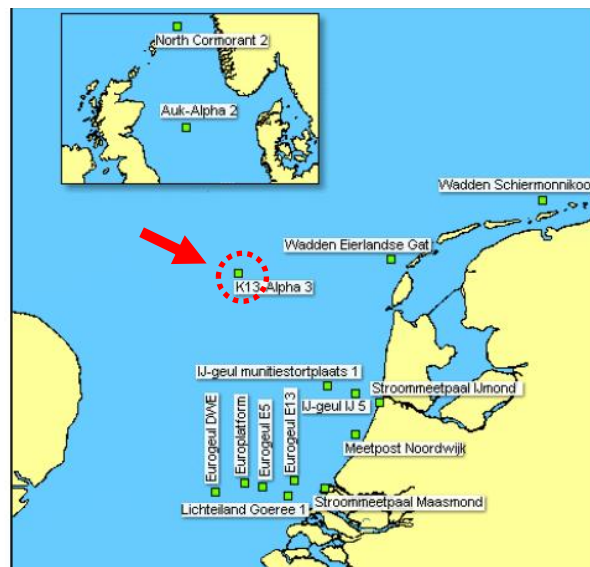
Figure 8.1: Locations for which Rijkswaterstaat measures wind and wave data [64]

For the wind conditions at K13, a mean wind speed of 10.1 m/s at 85 m height is found, fitting to a Weibull distribution it results in a scale parameter of A = 11.7 m/s and a shape parameter of k = 2.04.

For the turbulence intensity, different distributions are compared. As shown in Figure 8.2, the standard curves for IEC 61400-1 [37] and IEC 61400-3 [10] are shown for a reference turbulence intensity of 0.15. Besides, a distribution based on the assumptions of the Noordzeewind OWEZ project is shown [66], where again an IEC-3 distribution was assumed, but with a different reference intensity and with the wake effects taken into account. It is

commonly assumed that the IEC-1 curve is too conservative dn but the IEC-3 one probably too optimistic. For this reason the distribution from the Noordzeewind OWEZ project has been chosen as a good compromise, also because for its consideration of the wake effects.
The distribution can be described by the following relation (with I15 = 0.14 and a = 5)

$$I(U) = \frac{(15 + a \cdot U)}{(1 + a) \cdot U} \cdot I_{15}$$

(8.1)

Later in the design process for extreme load calculations, an extreme turbulence distribution has to be defined. Based on the normal turbulence model described in the expression above from the Noordzeewind OWEZ project, an extreme turbulence distribution has been calculated according to IEC 61400-3 [10]. The turbulence distribution is also shown in Figure 8.2.
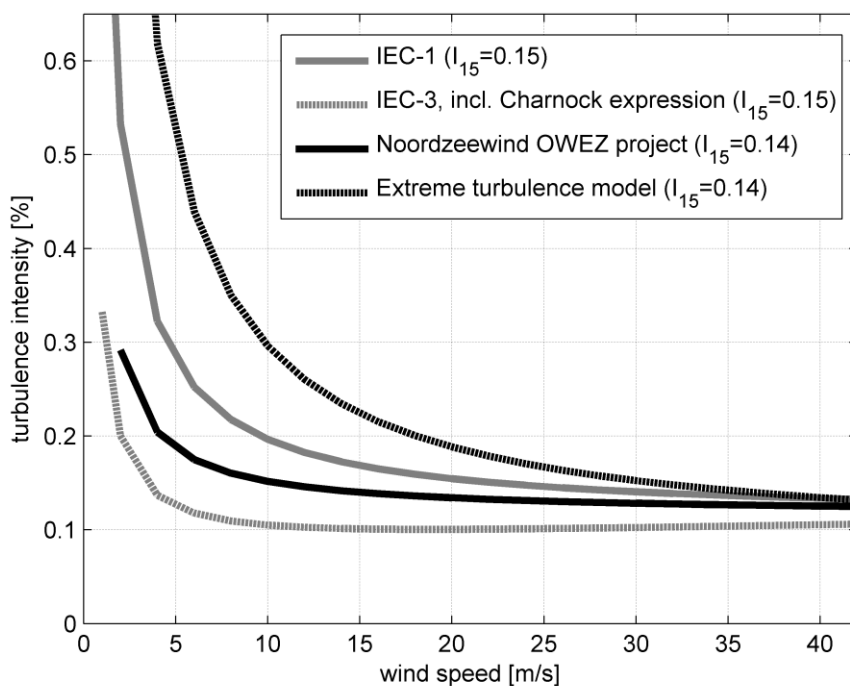
Figure 8.2: Considered turbulence intensities for the study

As the waves at K13 are quite low compared to others locations in Southern North Sea, adjustment to the date from the FINO1 met platform in the German North Sea is undertaken. The K13 platform is located in 30 m deep water while FINO1 is at about 23 m water depth. Even though the water depth at the Fino1 platform is lower than at K13, the wave heights are higher and present at harsher wave condition, like those to be expected in the German and UK part of the North Sea. Therefore the wave heights from Fino1 are correlated with the wave periods from K13 while a water depth of 25 m is assumed.

Based on the data from K13, the wind and wave data are lumped according to Kühn [5] in order to reduce the amount of load combinations. Here the data is first of all processed in a way which generates the wave scatter per mean wind speed bins in 2 m/s steps. Afterwards, for each wind speed bin a damage-equivalent sea state is derived. Table 8.1 shows the sea state parameters together with the previously presented distributions of wind speeds and turbulence intensities as well as the corresponding occurrence frequency.

Table 8.1: Lumped scatter diagram of the given offshore site

V	TI [%]		H_s	T_p	f
[m/s]	normal	extreme	[m]	[s]	[%]
2.0	29.2	99.3	1.10	5.40	0.0607
4.0	20.4	53.1	1.17	5.55	0.0891
6.0	17.5	37.1	1.25	5.60	0.1405
8.0	16.0	30.0	1.33	5.67	0.1392
10.0	15.2	25.4	1.75	5.71	0.1465
12.0	14.6	22.3	2.40	5.88	0.1427
14.0	14.2	20.1	2.80	6.07	0.0838
16.0	13.9	18.5	3.20	6.37	0.0832
18.0	13.6	17.2	3.70	6.71	0.0419
20.0	13.4	16.1	4.40	6.99	0.0348
22.0	13.3	15.3	5.10	7.40	0.0153
24.0	13.1	14.6	5.30	7.80	0.0097
26.0	12.0	14.0	5.80	8.14	0.0051
28.0	11.9	13.5	6.20	8.49	0.0020
30.0	11.8	13.1	6.30	8.86	0.0017

As for some support structure types and environmental conditions the effect of wind- and wave-misalignment can be important, a directional scatter of the measured wind and wave directions is necessary. Here the values shown are 10 minutes averaged wind speeds and significant wave heights with a stationary period of 3 hours. Figure 8.3 illustrates the site's wind and wave direction distribution. The graphs show a clear tendency to misalignment between the wind and waves, which will be an important issue for the later presented monopile design and control concept selection.
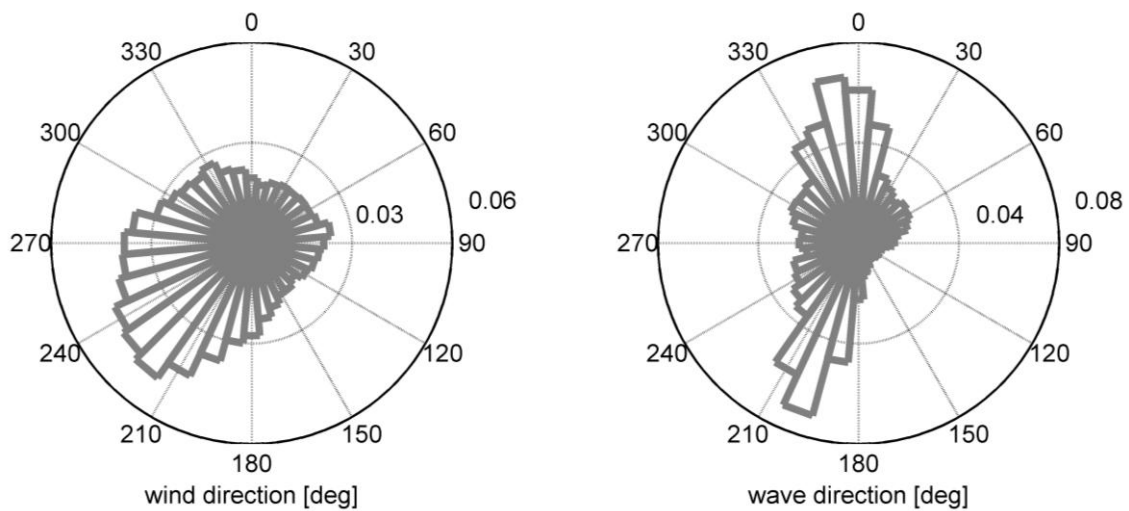
Figure 8.3: Directional distribution of wind (left) and waves (right) at the reference site

As for the studied site there are no soil measurements available, a distribution is assumed. For the given study, a set of hard soil layers are taken as shown in Table 8.2. The hard soil is seen as conservative. The soil parameters are given in terms of the effective soil unit weight γ', the angle of internal friction φ and the undrained shear strength C_u.

Table 8.2: Soil conditions for the reference site

Depths [m]	γ' [N/m³]	Φ [°]	C_u [Pa]
0-3	10000	38	-
3-5	10000	35	-
5-7	10000	38	-
7-10	10000	38	-
10-15	10000	42	-
15-50	10000	42.5	-

From the measured wind and wave data the extreme wind speeds and wave heights can be determined. The extreme conditions are determined as the maximum that occurs within a certain return period. The values are listed in Table 8.3.

Table 8.3: Extreme conditions according to IEC [10] at the reference site

$H_{s,50}$ [m]	8.24
$H_{max,50}$ [m]	15.33
$H_{red,50}$ [m]	9.06
$H_{,1}$ [m]	6.05
$H_{max,1}$ [m]	11.25
$H_{red,1}$ [m]	6.66
$V_{ref} = V_{50}$ [m/s]	42.73
V_1 [m/s]	32.74

8.1.2 Reference turbine

The main goal of the demonstration study is to show the effectiveness of including turbine controls in the design process of monopile support structures in order to stretch their applicability to larger water depths for nowadays turbine sizes. Therefore a currently standard 5 MW offshore wind turbine size is chosen. The turbine is an update of the well-known 5 MW NREL turbine [29]. The update is mainly due to the applied industry-standard power controller as described in the following Sub-Section and some minor changes in equivalent drive train shaft torsional spring and damping constants.

Table 8.4: Turbine characteristics

power output	5.0 MW
rotor configuration	upwind, three-bladed
controller-type	Pitch, variable-speed
rotor diameter	126 m
rated rotor speed	12.1 rpm
Cut-in and cut-out wind speed	3 m/s, 25 m/s
Rated wind speed	11.3 m/s
nacelle mass, incl. rotor	350 t

The turbine is a three-bladed, variable speed and pitch controlled design. Table 8.4 summarizes the main characteristics of the RNA design. As described in the following, the platform level is found at 14.8 m as described in Sub-Section 8.1.4. By using a tower of 68 m and a vertical offset in the nacelle of 2.4 m, the support structure design results finally in a hub height of 85.2 m above MSL. The monopile penetration depth is 24 m, which is low, but assumed stiff soil.
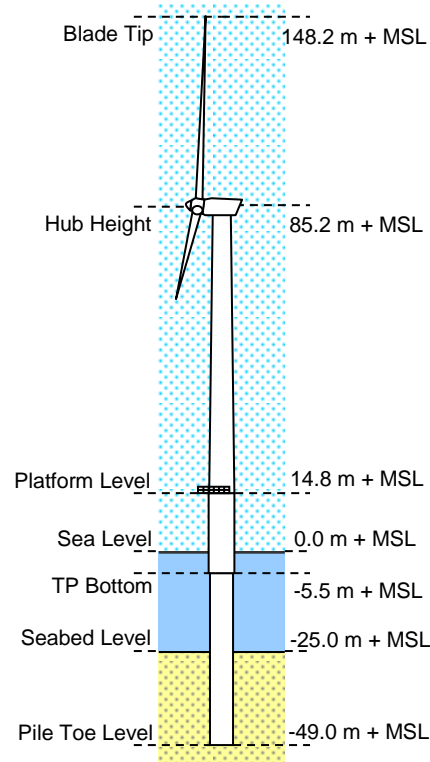
Figure 8.4: Schematic dimensions of the reference design for the given site

8.1.3   Reference controller

The UpWind baseline power controller is based on a design by Bossanyi [25]. The controller uses collective pitch to feather control above rated wind speed, and has a variable generator speed. The torque controller is capable of achieving any demanded torque (within limits) at the generator air gap with a short delay. The baseline controller takes measured generator speed as the controller input, and returns a demanded generator torque and a collective pitch angle demand.

During low wind speed, the generator torque control follows a quadratic torque-speed curve. This ensures that the rotor speed is optimal for energy capture. In moderate wind speed, when the rated rotor speed is reached, the generator torque demand is derived from the measured generator speed error using a proportional plus integral controller. When rated wind speed is reached, and the blades are pitched away from fine pitch angle, the torque is varied in inverse proportion to measured generator speed. This minimises power fluctuations.

In addition there is a drive train damping algorithm which adds small amplitude variation in torque demand which increases the damping of the drive train eigenmodes. The pitch controller is also a proportional plus integral (PI) controller on measured generator speed error. The proportional and integral gains are scheduled according to the pitch angle, as the aerodynamic torque is much more sensitive to pitch angle changes at higher pitch angle than around fine pitch. The pitch angle is held at fine pitch while the generator torque is below rated to keep the pitch and torque control loops decoupled.

8.1.4   Reference support structure

For a realistic monopile support structure design it is required to keep several practical limitations in mind. Requirements for manufacturing and installation may have significant influence on the final dimensions of the structure. The dimensions of various elements are dependent on the diameter of the foundation pile. Therefore the structure is parameterised, using the foundation pile diameter as a key parameter. This parameterisation leads to the support structure layout as shown in Figure 8.5. The tower geometry is not included in this Figure but is shown in Figure 8.7.
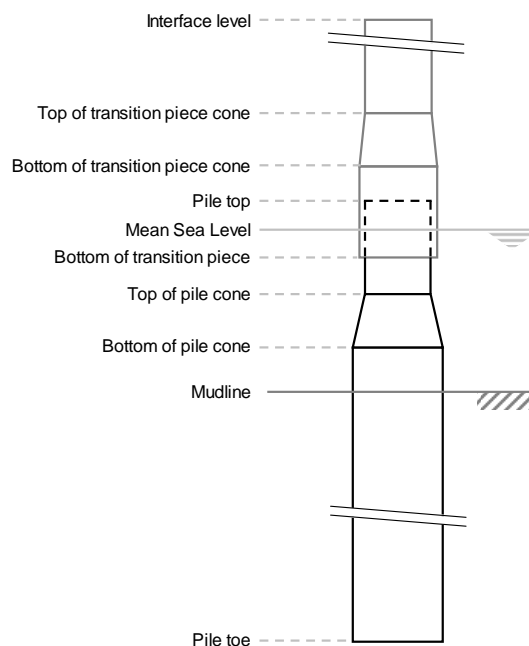
Figure 8.5: Overview of support structure geometry

The support structure consists of a foundation pile and a transition piece. The transition piece is mounted on top of the foundation pile and fixed using a grouted connection. The detailed assessment of the grout joint is not part of this work.

The interface or platform level is placed at the top of the transition piece. The determination of the height is based on equation 7.1 according to current standards [1]. Based on a 50 years maximum wave height of 15.33 m, a wave elevation coefficient of 0.65, a tidal range of 2.22 m, a value for storm surge of 2.13 m and an safety air gap of 1.5 m, the height is found at 14.8 m above MSL.

The pile top elevation is at 5.0 m above MSL so that it is above the splash zone at all times in order to facilitate installation. The diameter at the top of the foundation pile is fixed at 5.5 m as larger diameter piles cannot be driven due to the limited size of anvils currently in the market. A conical section tapers outward to a larger diameter. This allows the stiffness of the foundation to be controlled by the pile diameter, while respecting installation limitations.
The diameter of the transition piece has an outer diameter of 5.9 m at the lower end to accommodate the required wall thickness of the transition piece itself and a minimum grout thickness of 75 mm. The length of the overlap is 1.5 times the pile top outer diameter, with an additional length of 0.5 m to represent the grout skirt. With the overlap the bottom of the transition piece holding the sacrificial anodes is always submerged in water. A conical section reduces to an upper diameter of 5.6 m, matching the diameter at the tower bottom. The distance of this cone above the overlap is fixed at 1.5 m. This same value is adopted for the distance between the bottom of the transition piece and the pile cone.
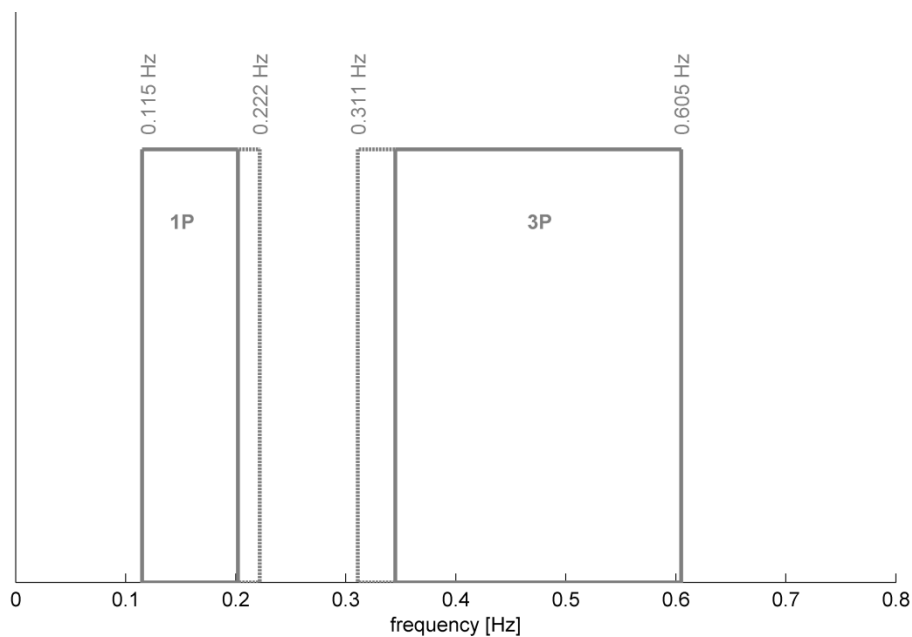
Figure 8.6: Allowable frequency range for the UpWind reference turbine

The presence of appurtenances on the support structure can attract significant hydrodynamic loading. Therefore the effect of the presence of the boat-landing and J-tube are taken into account by modifying the hydrodynamic coefficients. Additionally, equipment and additional non load-bearing elements are modelled as localised masses in the centreline of the structure.

The foundation is modelled using p-y curves to represent the lateral non-linear pile-soil interaction. The p-y curves have been modelled according to API [67]. Due to the large axial stiffness of the pile, the vertical displacements of the nodes below the mudline are considered

negligible for the purpose of this work. Therefore the pile is constrained in axial direction at each of these nodes. Also the torsional degree of freedom is constrained for the pile nodes. For the fatigue limit state analysis and the assessment of pile strength in the ultimate limit state analysis the material factor applied for the soil strength parameters is 1.0. For determining the pile penetration depth the design values of the soil strength parameters are reduced by applying a material factor of 1.35.

The occurrence of scour around the pile may significantly affect the dynamics of the support structure. A scour hole may develop up to a depth of 1.3 times the foundation pile diameter [68]. This will result in a smaller embedded pile length, leading to a softer foundation and in a larger unsupported structure length resulting in a softer structure. To avoid these effects it is assumed that scour protection is applied, thereby preventing a scour hole to develop.

For marine growth, a thickness of 100 mm according to the standards [69] is taking into account from sea bed up to the upper limit of the splash zone at 2.6 m. Corrosion is taken into account as half of the possible range in lifetime, which is 3 mm according to [69]. In the calculations, the pile is assumed to be fully flooded in order to take water-added mass effects into account.

The allowable range for the natural frequency of the given reference turbine design is shown in Figure 8.6. It shows the rotational frequency range of the rotor (*1P*) and the blade passing frequency range (*3P*). The support structure is to be designed with a fundamental frequency in the soft-stiff region, between the *1P* and *3P* ranges. A 10 % margin on the upper boundary of the *1P* range and on the lower boundary of the *3P* range is adopted to avoid excessive dynamic excitation in case of overspeed events, or due to dynamic amplification near the fundamental frequency. With the aforementioned limitations the allowable range for the fundamental frequency lies between 0.222 Hz and 0.311 Hz.

The natural frequency for the reference structure is evaluated assuming fatigue limit state conditions with water level at MSL. No seabed level variations or varying soil conditions are taken into account. The first bending mode in the fore-aft direction is at 0.277 Hz and the corresponding mode in the side-to-side direction is at 0.279 Hz. The second bending modes are at 1.290 and 1.369 Hz for the fore-aft and the side-to-side directions respectively. These frequencies are safely outside the blade passing frequency range.

To determine the stability of the pile in the sea bed, the following criteria have been set:

- The deflection of the pile at mudline is less than 0.1 m
- The rotation of the pile at mudline is less than 0.5°
- The ultimate lateral bearing capacity must be guaranteed when the characteristic soil strength parameters are reduced by a material factor 1.25 [69]

For the reference design the maximum overturning moment is 306 MNm and the corresponding base shear is 10 MN. Conservatively, these have been assumed to act in the same direction. The required minimum embedded length to withstand the ultimate loads is 24 m. It should be noted that the soil profile used for this reference design results in a stiff foundation. In practice, in most cases the foundation will be softer and pile lengths are usually longer.

In Figure 8.7, a sketch of the support structure dimensions is shown. For the reference structure the overall mass of the primary steel is 542 tons for the foundation pile and 147 tons for the transition piece. The baseline tower has a mass of 234 tons. The corresponding load envelope, on which the design is based, is described in the following Sub-Section.

Elevation	Wall Thickness			Diameter	Flange Mass	
82.76 m + MSL	20 mm			4.00 m	8.7 ton	
77.76 m + MSL	20 mm			4.12 m		
68.76 m + MSL	22 mm			4.33 m		
58.76 m + MSL	27 mm			4.56 m		tower
48.76 m + MSL	32 mm			4.80 m	3.6 ton	
36.76 m + MSL	36 mm			5.08 m		
26.76 m + MSL	40 mm			5.32 m		
14.76 m + MSL	60 mm			5.60 m	2.9 ton	
13.5 m + MSL	60 mm			5.60 m		
11.00 m + MSL	60 mm			5.60 m		
8.50 m + MSL	60 mm			5.60 m		
6.50 m + MSL	70 mm			5.90 m		transition piece
5.00 m + MSL	107 mm **			5.90 m		
2.60 m + MSL	107 mm **			5.90 m		
- 0.40 m + MSL	107 mm **			5.90 m		
- 3.40 m + MSL	70 mm			5.90 m		
- 3.90 m + MSL	65 mm			5.60 m		
- 5.40 m + MSL	65 mm			5.60 m		
- 11.40 m + MSL	65 mm			6.20 m		
- 13.00 + MSL	80 mm			6.20 m		
- 17.00 m + MSL	80 mm			6.20 m		
- 21.00 m + MSL	80 mm			6.20 m		pile
- 25.00 m + MSL	80 mm			6.20 m		
- 26.00 m + MSL	80 mm			6.20 m		
- 35.00 m + MSL	75 mm			6.20 m		
- 40.00 m + MSL	60 mm			6.20 m		
- 45.00 m + MSL	40 mm			6.20 m		
- 49.00 m + MSL				6.20 m		

** wall thickness includes transition piece, pile and grout thickness

Figure 8.7: Support structure dimensions

8.1.5 Load envelope

The load envelope of the reference support structure design illustrates the load level for both fatigue and ultimate loads according to the given site-specific environmental conditions. The load calculations are performed in the time-domain by using aero-elastic simulations using GH Bladed [57]. The simulations include three-component turbulent wind [70] and irregular waves as input.

Fatigue loads

In the fatigue load analysis, the considered design load cases (DLC) according to [10] are:

- DLC 1.2: Power production
- DLC 6.4: Idling before cut-in and beyond cut-out
- DLC 7.2: Idling in cases of non-availability

Further fatigue load cases, such as start and stop, are not considered as they do not significantly contribute to the overall fatigue loading of steel-type support structures. The details of the simulated DLCs can be found in Appendix B.

In the fatigue simulations for both operational and idling conditions, directionality and misalignment of wind and waves are taken into account. For co-aligned wind and waves the effect of aerodynamic damping can significantly reduce fatigue damage. Therefore the availability of the turbine is taken into account in the post-processing by assuming the turbine to be in operation for 90 % of the time. This availability value is supported by evaluations of the British Crown Estate that found an average availability for UK Offshore wind farms that amounts to 85 % until 2007 with a prospect increase to higher values for newer projects [71]. The importance of a high availability is based on the presence of aerodynamic damping during the operation of the turbine, which is able to damp hydrodynamic induced vibrations. Here a higher availability can lead, beside the comprehensible increase of revenue, to lower support structure fatigue damages for deep-water offshore sites.
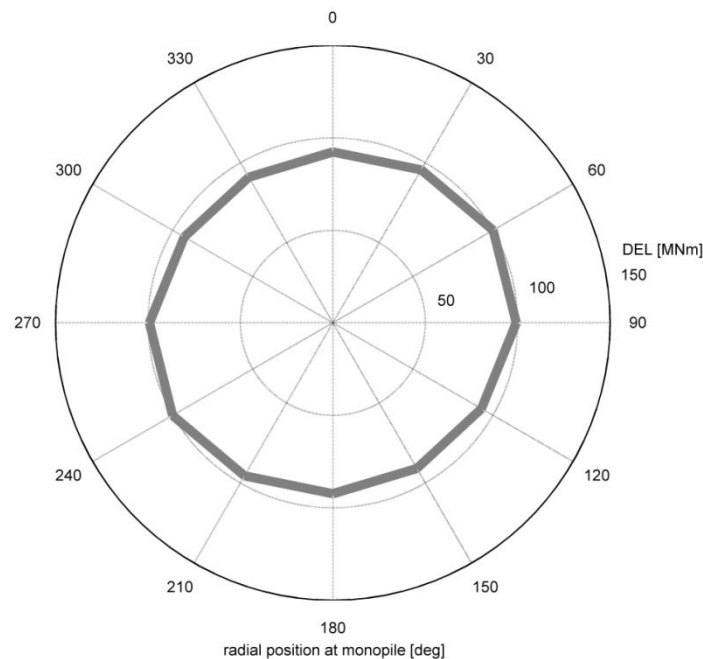

Figure 8.8: Angular lifetime DEL distribution at mudline

For all simulations, lumped sea states [5] are used in order to reduce the amount of simulations. Thus, for each wind speed bin just one wave condition representing the damage of all possible wave conditions for this wind speed is taken. The simulations take into account all possible site-specific wind and wave-misalignments. Here wind and waves are iterated in 30 degrees steps for 150 degrees around the monopile independently, which results in 36 different misalignment cases. The probabilities from the wind and wave distributions for resulting 180 degrees are mirrored to the direction from the opposite side. This simplification is valid for monopiles, as the side of the excitation is not that important but its direction. Afterwards the site-specific probabilities are divided among the 36 misalignments and a Rainflow count is performed to determine the corresponding stress cycles and the damage equivalent loads are determined. Based on this, the fatigue loads around the whole pile diameter can be evaluated. Figure 8.8 illustrates the lifetime equivalent fatigue loading at one pile section, here for the monopile at mudline with a reference cycle number of N = 2E07 and a Wöhler coefficient of m = 4 for steel. It can be seen that due to the site-specific loading, at 60 degrees pile diameter the radial section with the highest loading can be found.

Table 8.5: Fatigue DEL at mudline for the reference support structure design

Loads as DEL [N=2E+7, m=4]

| | **Support structure at mudline (-25 m)** | | |
	M_x	M_y	M_{xy_60deg}
Reference design	95 MNm	102 MNm	103 MNm

Table 8.5 shows the results in lifetime equivalent loading for the support structure at mudline. The Table illustrates the importance of the site-specific wind and wave-misalignment, as both moments (here M_x and M_y) are at a similar level. Furthermore, as discussed before and shown in Figure 8.9, the maximum fatigue loading is found at 60 degrees of the pile diameter. Therefore all later described fatigue limit state analysis will be based on this radial section of the support structure

For the fatigue limit state analysis (FLS) a conservative approach is chosen. This implies a check for fatigue loads for a set reference cycle number and Wöhler coefficient, here again N = 2E07 and m = 4. The resulting equivalent stresses are then checked against S-N-curves according to [1]. For the pile and transition piece a curve with a FAT class '90' is chosen, for the tower '80' respectively. Furthermore an additional partial material safety factor is applied on the stress ranges according to the part's ability for inspection and accessibility. Here the pile and transition piece is chosen to be non-fail-safe including no possibilities for monitoring and maintenance (safety factor of γ_M = 1.25), and the tower as fail-safe including possible monitoring and maintenance actions (safety factor of γ_M = 1.0).
For the fatigue analysis no effects of the presence of the secondary steel, such as boat-landing or J-tube, are taken into account. For the ultimate limit state analysis this is done by modifying the hydrodynamic coefficients. The reason for disregarding this for FLS is that the attachments of appurtenances effect the drag part of the Morrison's equation by several percent, where the inertia part is nearly unchanged. As for fatigue the inertia part is important which is nearly unchanged due to the appurtenances, the attachment of secondary steel is neglected for the fatigue analysis. However, even if the loading would have been slightly increased, Figure 8.8 shows that around the pile there is still some buffer in fatigue utilisation to attach these structures.
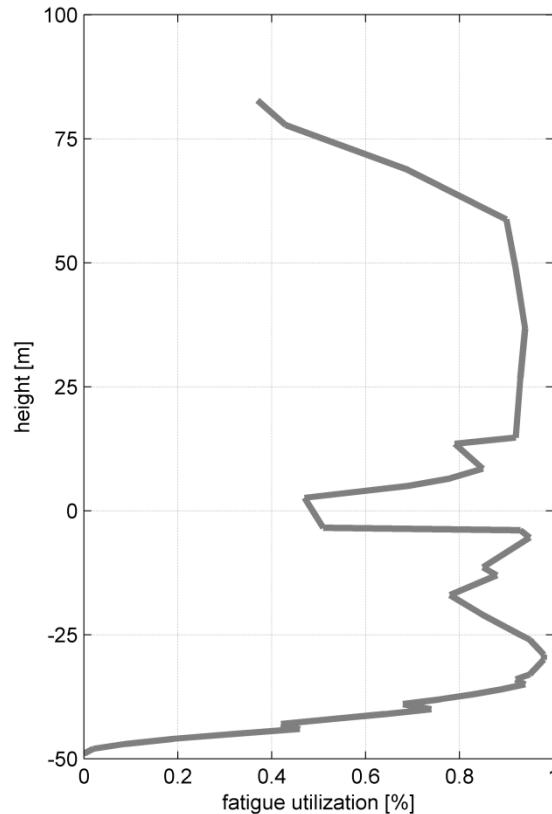
Figure 8.9: Fatigue utilization over support structure height

In Figure 8.9, the determined fatigue utilizations for a lifetime of 20 years taking the mentioned FAT classes and availability into account is shown for the whole support structure. The curvature shows that the lowest lifetime occurs below sea bed, exactly 5 m below mudline at -29 m. The rapid changes in utilizations are due to changes in wall thicknesses and diameters.

Ultimate loads
For the ultimate load analysis, the load cases are as for the fatigue loads calculated with GH Bladed. The considered DLCs according to [10] are:

- DLC 1.3: Power production loading with normal sea state and extreme turbulent wind
- DLC 2.1: Power production loading with occurrence of a fault, here a pitch runaway with all blades pitching to fine at a constant rate of 6 degrees/s
- DLC 2.3: Power production loading plus loss of electrical grid connection in combination with an extreme operating gust
- DLC 6.1a: Idling conditions at 50 years turbulent wind and an extreme sea state with 50 years maximum constrained wave
- DLC 6.2a: Idling conditions at 50 years turbulent wind and an extreme sea state with reduced 50 years maximum wave height together with loss of electrical network

These load cases do not cover the whole range of standard-relevant cases but the chosen ones are potentially seen to be the design-driver for offshore support structures. The details of the simulated DLCs can be found in Appendix B.

Table 8.6: Ultimate loads at mudline, platform and tower top level

		Load case	Mx (-25m)	My (-25m)	Mz (-25m)	Mx (14.8m)	My (14.8m)	Mz (14.8m)	Mx (77.8m)	My (77.8m)	Mz (77.8m)
			kNm	kNm	kNm	kNm	kNm	kNm	kNm	kNm	kNm
Mx (-25m)	Max	6.1ca_2_1_3	147,5	-122,5	1,6	65,8	-36,2	1,7	5,8	-4,3	1,6
Mx (-25m)	Min	6.1ac_1_1_3	-169,0	-149,0	-1,2	-67,4	-88,8	-1,1	-5,1	-15,0	-1,2
My (-25m)	Max	2.1d_3	0,3	306,0	0,8	3,5	158,4	0,8	4,9	12,9	0,7
My (-25m)	Min	2.1e_1	7,9	-251,8	-1,0	8,5	-138,8	-1,0	3,4	-13,6	-0,9
Mz (-25m)	Max	1.3eb_1	26,1	59,2	10,4	9,5	35,4	10,4	4,5	1,9	10,4
Mz (-25m)	Min	1.3eb_2	2,5	82,7	-11,6	2,9	37,6	-11,6	5,0	2,4	-11,6
Mx (14.8m)	Max	6.2d_1_2_3	138,7	10,8	2,9	82,8	5,8	2,9	7,0	-2,8	2,8
Mx (14.8m)	Min	6.1ac_2_1_2	-133,5	-65,3	-3,2	-78,6	-38,0	-3,2	-7,4	-6,3	-3,2
My (14.8m)	Max	2.1d_3	4,7	294,9	2,1	-0,4	164,1	2,1	5,4	12,9	1,9
My (14.8m)	Min	2.1e_1	8,5	-249,2	-1,2	6,7	-147,7	-1,2	4,0	-16,3	-1,2
Mz (14.8m)	Max	1.3eb_1	26,1	59,2	10,4	9,5	35,4	10,4	4,5	1,9	10,4
Mz (14.8m)	Min	1.3eb_2	2,5	82,7	-11,6	2,9	37,6	-11,6	5,0	2,4	-11,6
Mx (77.8m)	Max	2.1e_2	34,4	-64,6	-1,1	29,5	-26,6	-1,1	13,9	-3,6	-1,0
Mx (77.8m)	Min	6.1ac_1_1_3	-124,2	-176,5	-1,3	-76,7	-69,8	-1,4	-8,6	-7,8	-1,3
My (77.8m)	Max	6.1ab_1_1_2	-20,3	120,6	-2,0	-11,1	132,8	-2,0	-0,6	19,8	-2,0
My (77.8m)	Min	6.1ab_1_1_6	-52,2	-201,6	-1,6	-33,6	-113,5	-1,6	-3,5	-19,5	-1,6
Mz (77.8m)	Max	1.3eb_1	26,1	59,2	10,4	9,5	35,4	10,4	4,5	1,9	10.4
Mz (77.8m)	Min	1.3eb_2	2,5	82,7	-11,6	2,9	37,6	-11,6	5,0	2,4	- 11.5

Table 8.6 shows the gained maximum and minimum ultimate loading at the support structure, here including safety factors according to [10] and as listed in Appendix B. The loads are shown for three different heights – at mudline, platform level and at the tower top flange.

If the load components are studied in more detail, certain trends can be seen. For the torsion in the support structure, M_z, over the full height the extreme turbulent wind load case at normal power production (DLC 1.3) is decisive. Here the influence is mainly due to the high load fluctuations at the rotor and the connected torsional moments introduced over the rotor.
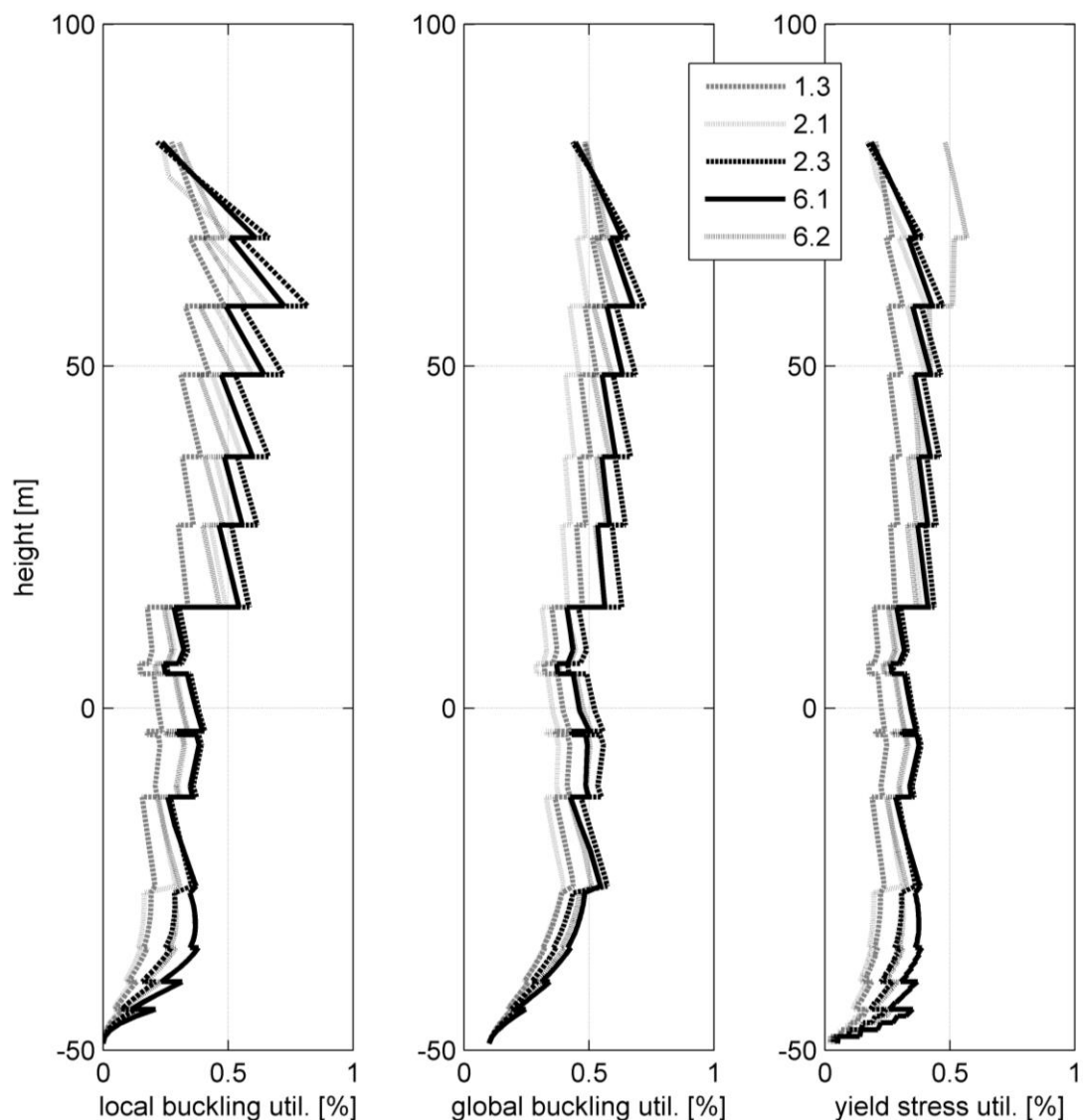
Figure 8.10: Ultimate utilizations over support structure height

For the support structure fore-aft moment, M_y, the overtuning moment resulting from a fault case (DLC 2.1) is giving the highest loading at mudline and platform level. In the given case (DLC 2.1d), all blades pitch into the wind at 20 m/s, which causes a high thrust peak before the turbine detects the fault and shuts down. For the tower top, the 50 years extreme turbulent wind during idling (DLC 6.1) is causing the highest loads.

For the side-to-side support structure load component, M_x, the 50 years extreme turbulent wind during idling (DLC 6.1) is causing the highest loads for all heights. Just at tower top, the side-to-side moment is equally loaded by DLC 6.1 and the pitch failure case at normal power production (DLC 2.1).

All the ultimate loads can then be used for the ultimate limit state analysis (ULS). Figure 8.10 shows the ultimate utilization for local and global buckling and yield stress. The utilizations are based on stresses taking the different loadings at each section and the corresponding load factors into account. The plots show that DLC 6.1 is the design-driver for the part of the

monopile and transition piece, where for the tower DLC2.3 becomes important. As for the fatigue utilization, the rapid changes in utilizations are due to changes in wall thicknesses and diameters. All utilizations are well below 0.6. Taking also the fatigue utilization into account, this leads to the conclusion that the support structure is fatigue load driven, as the fatigue utilization ratios are for almost all heights between 0.8 to 1.0.

8.2   Optimized design

In this Section, the adapted design process including load mitigation is applied for the reference design as introduced in Section 7.2. The Section is describing the choice of appropriate load mitigation concepts, the gained load reductions and the trade-off compared to the reference design.

8.2.1   Controller selection

As described in Section 7.2, the adapted design process starts with a setup of an initial geometry. This geometry is the one described in Section 8.1 as reference design for a monopile in 25 m deep water. In order to make a choice for appropriate load mitigation concepts, the next step is to determine the design-driving load cases.
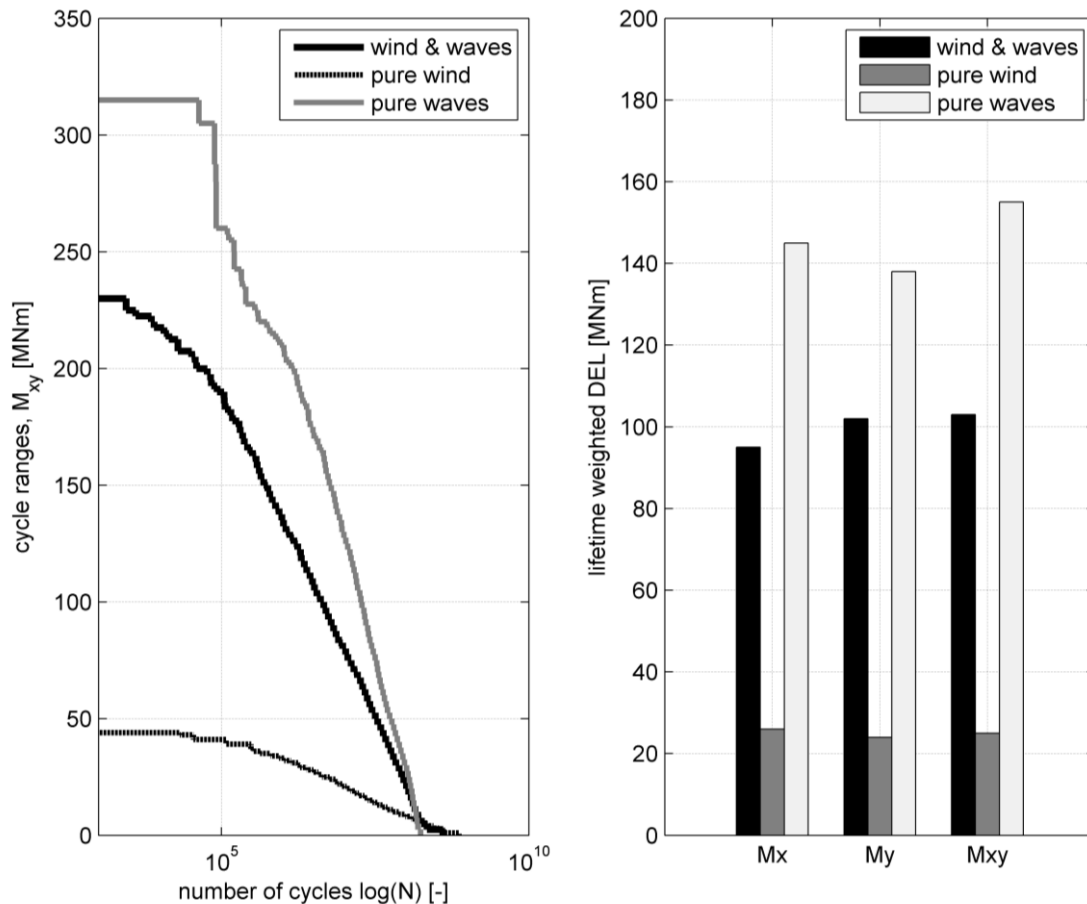

Figure 8.11: Cumulative Rainflow counting and damage equivalent load ranges for the resulting maximum moment at mudline (left) and lifetime weighted damage equivalent loads (DEL) for three moments at mudline (right) for the reference support structure

In Sub-Section 8.1.5 it is shown that the monopile at the given site is fatigue load rather than ultimate load driven (compare Figure 8.9 and Figure 8.10). This leads to the conclusion that the load mitigation concepts to be chosen have to aim at a fatigue load reduction. Still, different sources can contribute to fatigue loading, which have to be evaluated carefully. Figure 8.11 illustrates the amount of lifetime equivalent fatigue loading at the reference support structure for moments at mudline with a reference cycle number of N = 2E07 and a Wöhler coefficient of m = 4. The loads take all fatigue design load cases into account as explained in Sub-Section 8.1.5.

Three cases are compared. In case one, aerodynamic and hydrodynamic loading is acting on the turbine simultaneously as requested by the standards and as discussed in Sub-Section 8.1.5. For case two, only aerodynamic loads are acting in a calm sea, where in the third case it is vice versa with no wind (and here also no aerodynamic damping) and acting full sea states.

The plot on the left in Figure 8.11 shows the cumulative Rainflow counting and damage equivalent load ranges of the moment at mudline for the pile position with the highest fatigue loading, here the radial position at 60 degrees. The plot reveals the relative contribution of the aerodynamic and hydrodynamic loads, as it clearly identifies the strong impact of wave-induced loads compared to pure wind loading. This can also be seen in the right plot of Figure 8.11, where damage equivalent loads are compared for three moments at mudline and again the three loading cases. The curvatures and bars illustrate clearly that the site's fatigue loading is hydrodynamic driven. Thus, concepts for enhancing the effect of aerodynamic damping would be reasonable. According to the studied concepts in Chapter 5 and 6 and the overview Table 7.1 in Section 7.2, the following concepts are available and chosen:

- Tower-feedback controller (see Section 6.1)
- Active idling control (see Section 6.2)
- Soft cut-out (see Section 5.2)

Beside the shown strong hydrodynamic impact, the right plot in Figure 8.11 and the angular load distribution around the pile in Figure 8.8 of Sub-Section 8.1.5 point out another important fatigue load contributor. Both Figures identify a comparable high loading of the side-to-side and fore-aft support structure load direction. This effect results from the strong misalignment between wind and waves at the given site (as seen in Figure 8.3).

Figure 8.12: Lifetime weighted damage equivalent (DEL) loads for the side-to-side moment (M_x) on the left hand side and for the fore-aft moment (M_y) at the right hand side at mudline under aligned conditions

Therefore a further load mitigation concept for reducing these sideways loadings is advised. Again, according to the studied concepts in Chapter 6 and the overview Table 7.1 in Section 7.2, an active generator torque or an individual pitch controller are proper concepts. Since most

of the larger misalignments at the given site occur at low wind speeds and here the individual pitch controller does not operate effectively, the following concept is chosen:

- Active generator torque controller (see Section 6.3)

In the following, all four concepts are used in an integrated manner. This means that over the normal power production range (3 to 25 m/s) the tower feedback and active generator torque controller are activated with the goal of adding additional damping to the support structure modes while keeping the power as stable as possible. Besides, the soft cut-out is used for the extended power range (25 to 31 m/s) together with again the tower-feedback and active generator torque control with the goal of maximum damping to the structure modes. The soft cut-out is operated at 2/3 of rated rotor speed, which has shown reasonable results in former studies as described in Section 5.2. For a limited range of idling cases (here 0 to 15 m/s), an active idling controller is active with a limit of a rotor speed of 3 rpm, i.e. 25 % of rated speed, in order to not increase blades loads too much.
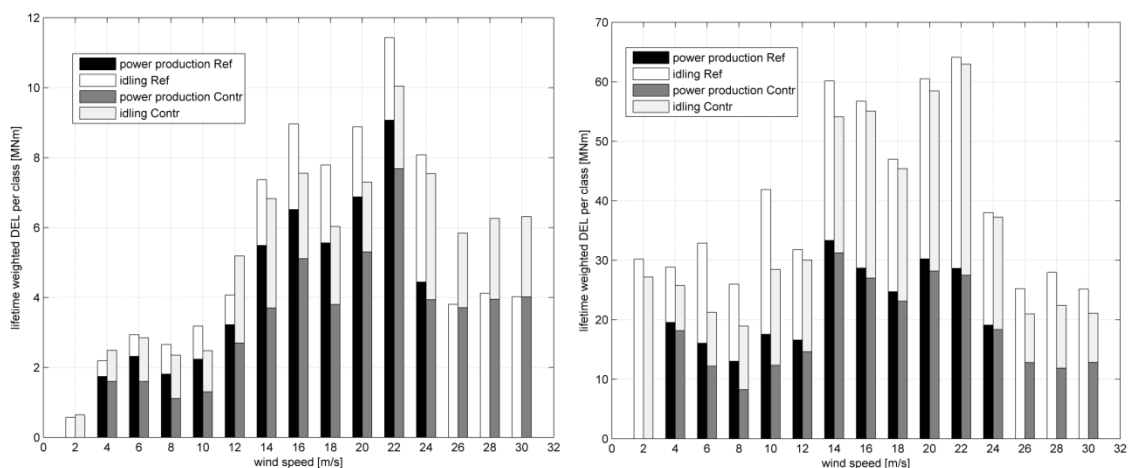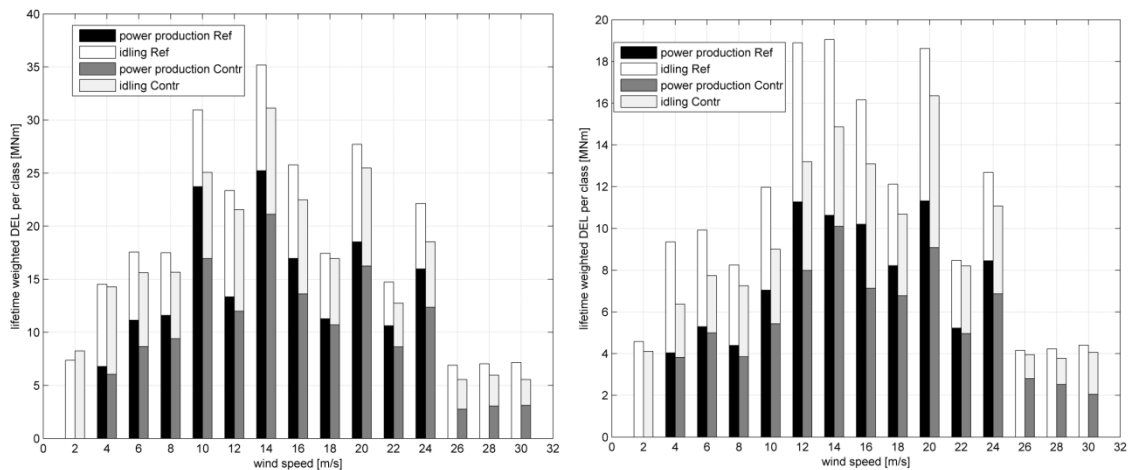

Figure 8.13: Lifetime weighted damage equivalent (DEL) loads for the side-to-side moment (M_x) on the left hand side and for the fore-aft moment (My) at the right hand side at mudline under misaligned conditions

Before the concepts are used for load mitigation and design optimizations, they have to be tested at the reference design in order to see their effects and to evaluate if they are tuned correctly. The test is performed for two different cases. The first one (Figure 8.12) shows the conditions with wind and waves acting both from North (0 degrees). The bars describe the lifetime weighted damage equivalent loads per wind class for power production (DLC 1.2) and idling (DLC 6.4 and 7.2) for the reference case without additional control for load mitigation and with the implemented concepts. In the second case (Figure 8.13), the corresponding one is shown for misaligned conditions with wind again acting from 0 degrees and waves from 60 degrees. In both cases the moments, here shown at mudline, can clearly be detected as side-to-side (M_x) and fore-aft (M_y) one, as the wind is always acting perpendicular to the rotor area.

The tower-feedback controller works well for all wind speeds and reduces the target fore-.aft moments during power production. This is especially true for the non-misaligned cases and here especially for the partial loading region. The side-to-side loading during power production is also well reduced for all wind speeds by the applied active generator torque controller. Especially the contributions at partial loading have to be mentioned, as this is the benefit of the concept compared to the not chosen individual pitch controller.

The active idling controller reduces reasonably the fore-aft idling loads at the target wind speed classes of 2 to 14 m/s. As this concept introduces a higher idling rotor speed, some increases in idling side-to-side loads can be seen, but still in a reasonable order of magnitude compared to the ones at the fore-aft direction. Finally beyond the former cut-out the soft cut-out concept is active and reduces both side-to-side and fore-aft loads. This is first of all true for the fore-aft load component, as the soft cut-out concept together with the implied tower-feedback controller enhances the effect of aerodynamic damping. In the non-misaligned cases, the extended power production range imposes through its additional rotor speed an increase in side-to-side loading, which alleviates the benefits of the active generator torque controller implied during the extended power range. However, for the misaligned cases, the main side-to-side load contribution is introduced by the waves, which results in an overall lower side-to-.side loading through the effectiveness of the active generator torque controller.

The investigated load cases show that the chosen and applied load mitigation concepts reduce the target load phenomena significantly. Therefore the controller setup is used in the further scope of the adapted design process.

8.2.2 Load evaluation

In the following, the effects of the applied additional control concepts on fatigue and ultimate loads are discussed. The effects are compared to the load levels for the reference design as described in Sub-Section 8.1.5.

Fatigue loads

The new features described above have been tested in dynamic simulations using GH Bladed with three-component turbulent wind and irregular wave trains as input, both in all site-specific directions. Table 8.7 summarizes the results as changes in lifetime weighted equivalent fatigue loads for the support structure and as change in power and pitch actions. The loads are here illustrated as damage equivalent loads referring to a lifetime of 20 years and an equivalent load cycle number of $N = 2E07$. The coordinates for the support structures, here M_x, M_y and M_{xy}, are fixed in space. As misalignments and different incoming wind and wave directions were simulated, the moments cannot clearly be evaluated as fore-aft or side-to-side modes.

Table 8.7: Comparison of results between the reference and the controlled case

	Loads as DEL [N=2E+7, m=4]			Change in energy yield and power fluctuations		Change in pitch rate
	Support structure at mudline (-25 m)					
	M_x	M_y	M_{xy_60deg}	AEP	P_{std}	$Pitch_{std}$
Reference case	95 MNm	102 MNm	103 MNm	23.0 GWh	0.15 MW	6.6 deg/s
Applied controller	-14.3 %	-14.9 %	-12.7 %	+ 1.6 %	+ 19.0 %	+ 6.4 %

The results show that the controller strategy reduces the dominant support structure moments at mudline and at the pile section with the highest loading (here at 60 degrees) up to 13 %. Furthermore, a gain in energy yield can be achieved, which is a result of the extended production range from former 25 m/s to 31 m/s cut-out wind speed.
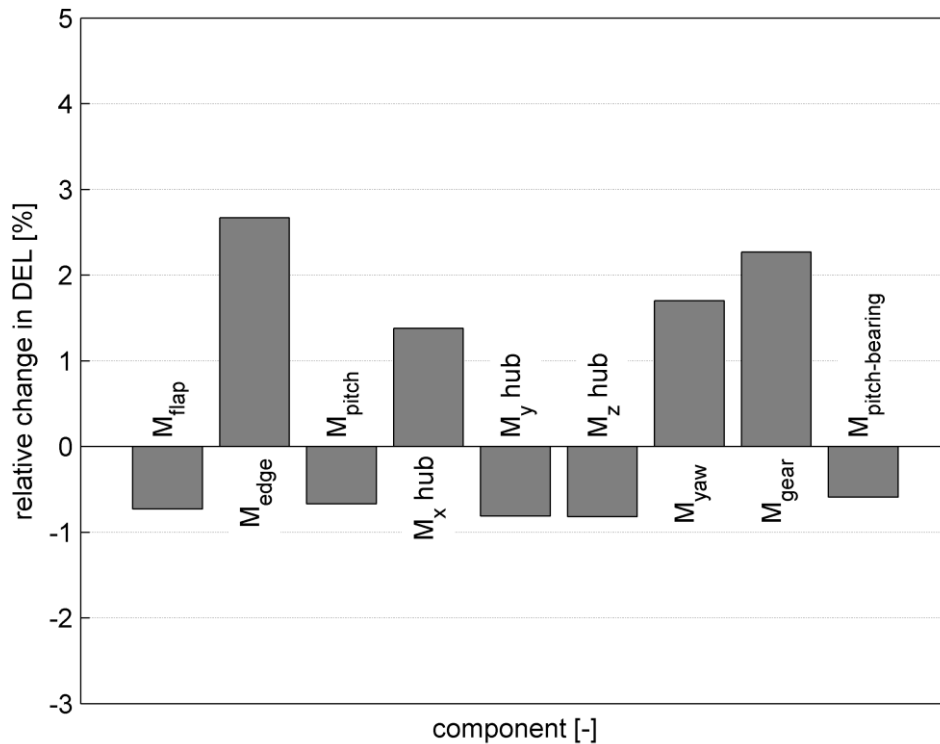
Figure 8.14: Relative change in component fatigue loading by applying adapted controller in comparison to the reference case

However, the controller concepts also introduce additional loading to the system. The usage of the tower-feedback controller introduces an additional pitch action of about 6 % higher pitch rate, where mainly the active generator torque controller is reasoning the increase in power fluctuations. In addition to the reductions in loading, further components of the turbine have to be evaluated to judge the applied concept. In Figure 8.14, the change in lifetime equivalent fatigue loading for different components is shown. The change is stated as difference to the reference conditions in Section 8.1.

Table 8.8: Comparison of blade fatigue loads between the controlled case and an IEC class *Ia* case

Blade root loads as DEL [N=2E+7, m=10]

	M_{edge}	M_{flap}	M_{pitch}
Design	9.7 MNm	6.7 MNm	0.2 MNm
IEC Class *Ia*	10.2 MNm	7.4 MNm	0.2 MNm

It can be seen that the blade loads, here expressed as flapwise, edgewise and pitch moments, are not significantly changed. Just the flapwise bending moment is increased by 2.5 %, which is mainly due to the extended cut-out and partly due to the tower-feedback controller. The blade edgewise and pitch fatigue loads are even decreased. For the hub and nacelle loads, an increase in the hub rolling moment (M_x) is related to an increase in gear box torque. Both increases are caused by the change in torque from the rotor (due to the tower-feedback controller) and the generator (due to the active generator torque controller), which can be in some cases counterproductive in terms of mechanical losses. Still, the increases of 2 to 3 % are

still in an acceptable range. For the two other hub components (hub M_y and hub M_z), the loads are even slightly reduced. Finally, the loading of the yaw system is also increased by about 2 %, which is mainly introduced by the change in pitch through the TFC.

It is clear that an implementation of such additional control concepts will impose new loadings in the turbine. In reality wind turbines are designed and certified for certain classes according to standards [37]. For the given turbine design and its offshore applications a wind class *Ia* is reasonable. Table 8.8 shows a comparison of the achieved blade fatigue loads from the discussed study and the corresponding loads according to class *Ia* conditions for the same turbine. The Table illustrates that even through the application of the additional control concepts the fatigue load levels at the blades are still well below the standard-relevant wind class loads. Of course, this is not justifying the design, but it shows that the achieved loads are not out of scope and still within reasonable limits. Additionally, it is not known if the RNA components are fatigue or ultimate load driven, what means that a fatigue check can become irrelevant anyway, if it turns out that extreme events are design-driving.

Ultimate loads

As the support structure is fatigue load driven, a main emphasis of the ultimate load analysis is to check if the RNA loads are changed due to the applied controller concepts. As indicated in Table 7.1 in Section 7.2, especially the extended power range through the soft cut-out imposes new ultimate load checks. This is especially true for certain transient load events such as gusts and certain failure modes, which can lead to increased ultimate loads when occurring at higher wind speeds.

Table 8.9 lists three of the simulated ultimate load cases, which are affected by the extended power range, and shows the maximum loads for three blade moments as indicators. It shows that the ultimate loads of the extended power range at 30 m/s are not larger than the ones at the former cut-out wind speed at 24 m/s. The reason is that the soft cut-out operates at a reduced rotor speed (i.e. 2/3 of rated speed), which compensates high variations in turbulence (DLC 1.3), failure modes (DLC 2.1) or gusts (DLC 2.3) compared to the case at rated rotor speed at 24 m/s. This was already mentioned in Section 5.2. Just the ultimate loads for the edgewise blade moment during extreme turbulence (DLC 1.3) shows a slight increase. The reason here is that the rotor speed during soft cut-out is reduced but not as strict limited as for the rated rotor speed range. Therefore the wind load peaks induced from strong turbulence affect the rotor speed variations more intensively and thus the edgewise blade loading. But still the increase is marginal.

Table 8.9: Comparison of ultimate loads for a normal cut-out wind speed at 24 m/s and the extended power range at 30 m/s through a soft cut-out control concept

		Blade root loads as DEL [N=2E+7, m=10]		
		M_{edge}	M_{flap}	M_{pitch}
DLC 1.3	Reference at 24 m/s	9.1 MNm	9.9 MNm	0.2 MNm
	Soft cut-out at 30 m/s	9.3 MNm	7.9 MNm	0.2 MNm
DLC 2.1	Reference at 24 m/s	7.1 MNm	13.8 MNm	11.5 MNm
	Soft cut-out at 30 m/s	7.0 MNm	11.5 MNm	0.1 MNm
DLC 2.3	Reference at 24 m/s	5.1 MNm	12.5 MNm	0.3 MNm
	Soft cut-out at 30 m/s	4.4 MNm	4.9 MNm	0.1 MNm

The achieved load reductions can now be used to optimize the design of the support structure in terms of mass reductions, as explained in the following.

8.2.3 Design optimization and evaluation

After the implementation and analysis of the new control concepts, the achieved load reductions are used to re-design the given support structure. The optimization is based on the principles described in Section 7.2. Several monopile optimization iterations have determined that the wall thickness of the structure can be reduced by 3 to 6 mm, which leads to a change in eigenfrequency from 0.277 Hz to 0.268 Hz. The weight of the structure can be reduced by about 85 tons of steel in total, which leads to a saving of 9 % in structure weight. This means that not the full savings in loading can be transferred to savings in wall thickness, as the lower eigenfrequency imposes again higher hydrodynamic excitations. In addition, the non-linear behaviour of stresses and the relation to the diameter-thickness-ratio for steel structures plays a role that not all load reductions can directly be transferred to material savings. Figure 8.15 shows the wall thickness and diameter of the optimized support structure together with the geometry of the reference structure. The diameter remains unchanged, but a substantial reduction of the wall thickness has been made overall. The large wall thickness around MSL is due to the fact that both the pile wall thickness and the transition piece wall thickness are included at these elevations.
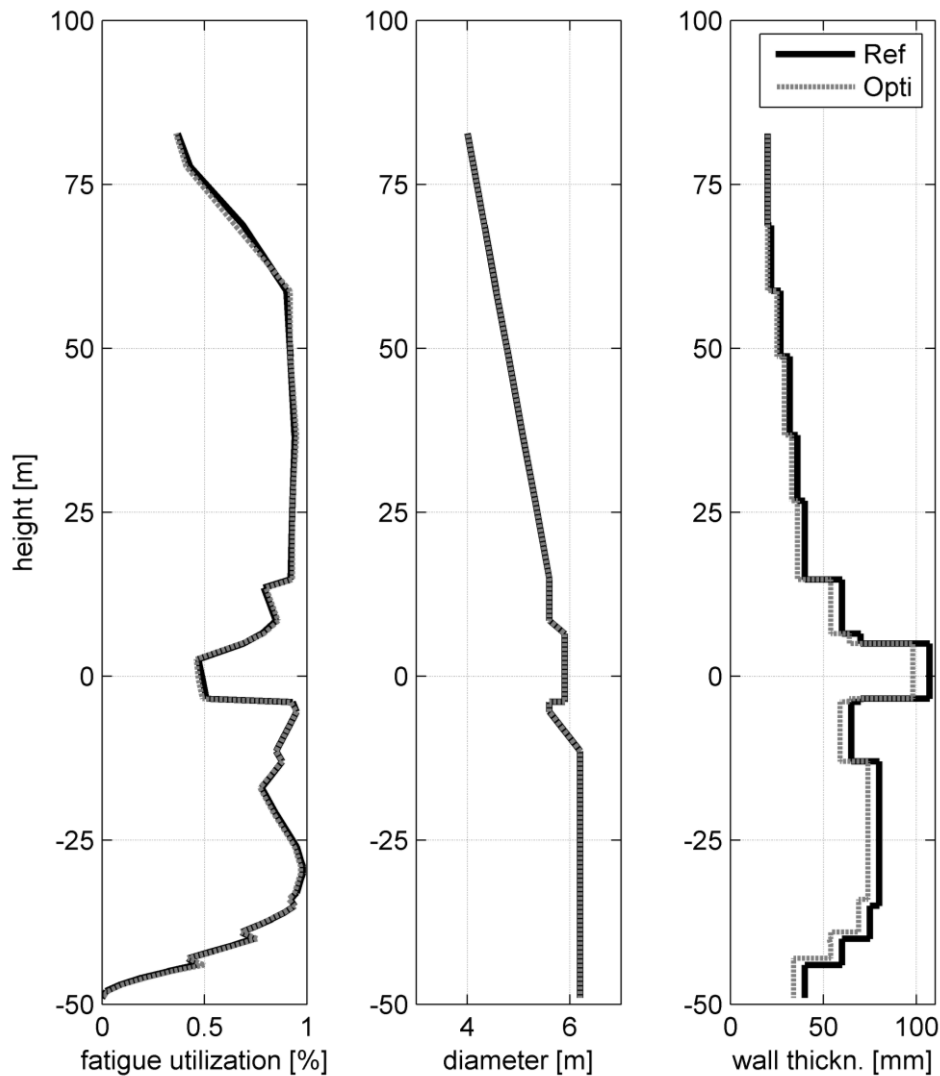
Figure 8.15: Support structure dimensions (left and centre) and fatigue strength utilisation (right) for both the reference structure and the optimised structure along the support structure height

From Figure 8.15 it becomes clear that the wall thicknesses at the support structure are iterated as long as comparable fatigue utilizations are achieved to maintain comparability between the designs. For the ultimate loads, the utilizations are slightly changed as illustrated exemplarily in Figure 8.16 for DLC 6.1. This means that the support structure is still fatigue load driven after the optimization. For the optimized structure the maximum base shear found from the ULS analysis is 10 MN and the overturning moment is 316 MNm. The required minimum embedded pile length remains unchanged at 24 m. Further ultimate utilization plots for the remaining load cases can be found in Appendix C.
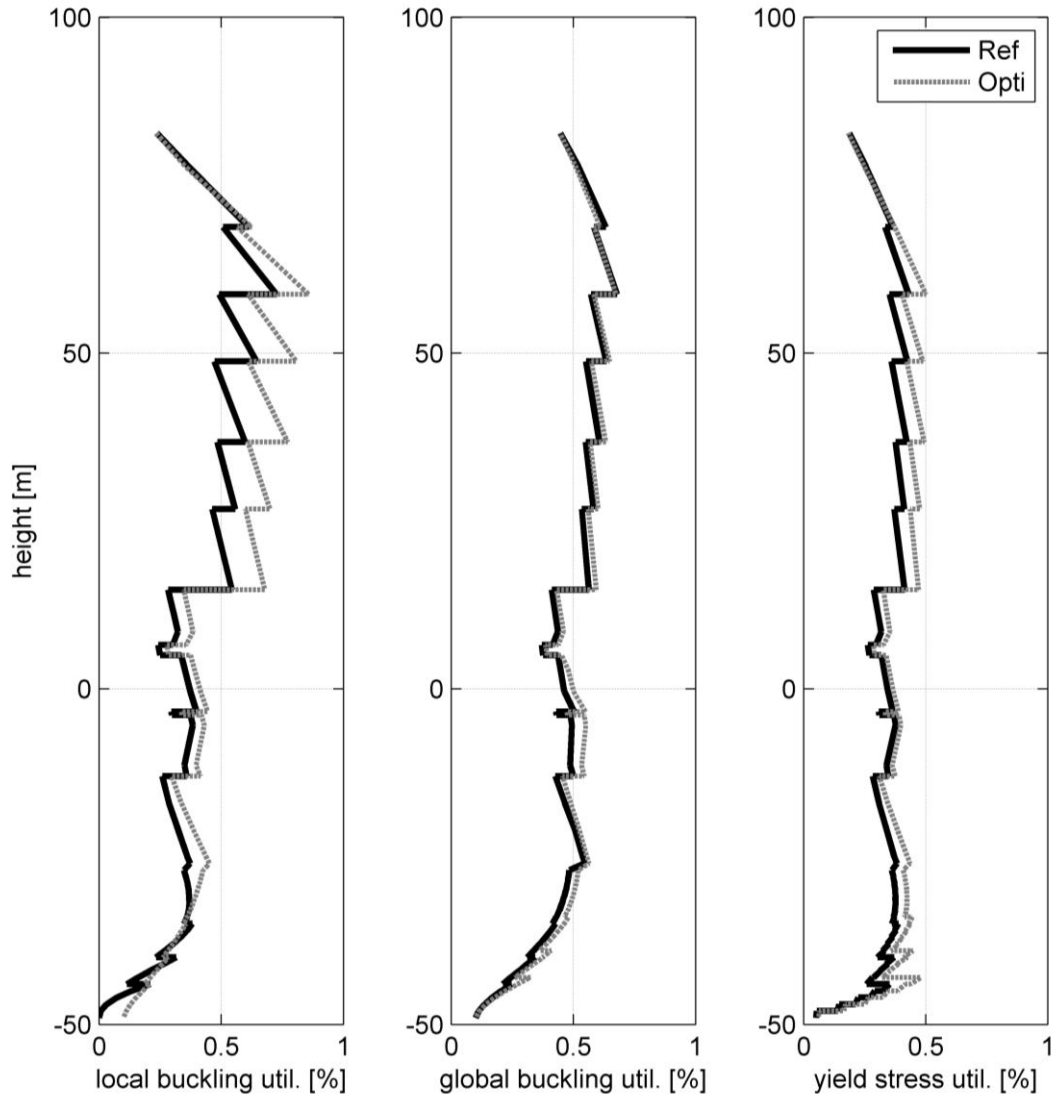
Figure 8.16: Ultimate utilizations over support structure height for DLC 6.1 as comparison between the reference and the optimized support structure design

Additionally to the pre-discussed load distributions, it is also important to take the gains of using the control system into account. Table 8.10 shows the gains in steel savings and energy yield. Due to the applied control system, about 85 tons of steel can be saved in the support structure. Of course, these savings in steel cannot directly be transferred to a reduction in cost of energy,

as therefore the cost contribution of the support structure to the overall turbine costs have to be known. But the additional 1.6 % in energy yield can be directly allocated and will lead, with its 7 GWh higher extra energy yield over an assumed project lifetime of 20 years, to an equivalent reduction in costs of energy.

Even if no final trade-off in terms of costs can be given, the relative changes demonstrate already that the applied system seems to be beneficial. As none of the control systems need an additional component, just some parts of the RNA might have to be designed more robustly. However, as it is not known if the RNA components are fatigue or ultimate load driven, the discussions in Sub-Section 8.2.2 show that through the application of the control concepts there is no overloading of components compared to the reference design and/or the standard-relevant design wind classes. On the other side the gains in material savings for the support structure and energy yield are high.

Table 8.10: Optimization results of adapted control concepts

Optimization gains

	Reference case	Optimized case	Degree of optimization	
			absolute	relative
Support structure mass	922.7 tons	837.9 tons	84.9 tons	- 9.2 %
Energy yield over 20yrs	459.4 GWh	466.6 GWh	7.2 GWh	+ 1.6 %

9.   Conclusions and recommendations

The mitigation of aerodynamic and hydrodynamic loads is essential for future developments of offshore wind turbines. In this report the prospects and effects of different levels of load mitigation are discussed. This includes different concepts in the design level, such as two-bladed turbines or truss-tower designs but also in the operational control level by for example using LIDAR technology or a soft cut-out. Finally concepts in the dynamic control level are applied, where active or semi-active controls such as tower-feedback or structural dampers are used. For each concept the advantages and disadvantages are shown and recommendations for specific applications are given. This means that the choice of an effective load mitigation concept very much relies on the given site condition, but also support structure and turbine type.

The core part of the work in Task 4.1 was to define an adapted integrated design process for offshore support structures by including the above mentioned load mitigation concepts. The process was described and applied for a demonstration study. The performed study considers a standard 5 MW turbine design on a monopile support structure in 25 m water depth, currently considered to be the approximate depth limit for a 5 MW wind turbine. A reference design of the support structure is made following a conventional design approach and using data from measurements at a site in the Dutch sector of the North Sea. The focus is on the reduction of the dominant hydrodynamic loads on the support structure. The implemented load mitigation concept leads to significant reductions in loading, allowing considerable material savings and therefore a more cost-effective structural design. Undesired side effects, such as increased wear of turbine components, are unlikely as other system loadings and characteristics remain within an acceptable range. Even if some of the rotor-nacelle-assembly loads are slightly increased by the applied controller, the increases are low and probably still within the margins of the type-class fatigue loads. Furthermore, a significant increase in energy yield could be obtained by applying an extended cut-out range. It has to be stated that for the demonstration study a very stiff soil distribution was chosen. A common soft soil profile would significantly increase the load mitigation benefit. This concludes that the achieved load reductions could have been even higher for softer soil types. Of course, to give a final trade-off for the proposed concept, further investigations have to be performed. An example is an analysis of the safety system and how it will be affected by the new control mechanisms.

In general, the study showed that offshore-specific controls can be effective in reducing hydrodynamic-induced loading, a conclusion which was demonstrated for monopile support structures. Here the degree of mitigation is very much dependent on the importance of hydrodynamic loading with respect to the overall fatigue. But the reference study has shown that a fine-tuned controller system can provide sufficient damping to the system in order to reduce hydrodynamically induced vibrations without significantly increasing the loading on other components. In the given example the load reduction was used to optimize the structure in terms of cost. But the application of such control concepts could also extend the application range for monopiles to deeper sites, as this concept will probably still be competitive against other more complex structures, such as jackets or tripods.

In future, where turbines are getting larger and heavier and the planned sites deeper, the need for such load mitigation concepts will increase in order to achieve cost effective designs. In conclusion, the work of Task 4.1 on different load mitigation concepts and the adapted integrated design process will therefore become even more important for future large wind turbines, in particular offshore. Larger turbines have higher tower top masses and that is why the water-piercing members of their support structures will increase in diameter to provide sufficient stiffness. Moreover, this increase in size will intensify hydrodynamic loading and thus requires more sophisticated control concepts to reduce such loading. Additionally for larger turbines, different design concepts might be implemented, such as two-bladed turbines in a

downwind configuration and on full truss towers. Such concepts will impose new requirements in controls and here Task 4.1 offers a range of possible solutions.

10. References

[1] Germanischer Lloyd, "Rules and regulations - guideline for the certification of offshore wind turbines," Germanischer Lloyd, Hamburg, Germany, 2005.

[2] M Kühn et al., "Opti-OWECS Final Report Vol. 2 - Methods assisting the design of offshore wind energy conversion systems," Project Report, Delft University of Technology , Delft, The Netherlands, 1997.

[3] W Pierson and L Moskowitz, "Proposed spectral form for fully developed wind seas based on similarity theory of Kitaigorodskii," Journal of Geophysical Research, 1964.

[4] K Hasselmann, "Measurements of wind and wave growth and swell decay during the JONSWAP project," Deutsches Hydrographisches Zeitung, Hamburg, Germany, 1973.

[5] M Kühn, "Dynamics and design optimisation of offshore wind energy conversion systems," PhD Thesis, Delft University of Technology, Delft, The Netherlands, 2001.

[6] J Morison, M O'Brien, J Johnson, and S Schaaf, "The force exerted by surface waves on piles," Petroleum Transactions (AIME), 1950.

[7] G Batchelor, "An introduction to fluid dynamics," Cambridge, UK, 1973.

[8] R McCamy and R Fuchs, "Wave forces on piles: a diffraction theory," in *Tech. Memo No. 69, U.S. Army Corps of Engrs,* 1954.

[9] NJ Tarp-Johansen et al., "Comparing sources of damping of cross-wind motion," in *European Offshore Wind (EOW)*, Stockholm, Sweden, 2009.

[10] IEC 61400-3, "Wind turbines - part 3: design requirements for offshore wind turbines," International Electrotechnical Commission, Geneva, Switzerland, 2009.

[11] Burbo Banks. (2010) Dong Energy, http://www.dongenergy.com/burbo.

[12] M Rodenhausen, "Soil response of offshore wind turbines," Master Thesis, Universität Stuttgart, Stuttgart, Germany, 2010.

[13] B Schmidt, "Aerodynamic damping of offshore wind turbines," Master Thesis, Universität Darmstadt, Darmstadt, Germany, 2008.

[14] K Kaiser, "Luftkraftverursachte Steifigkeits- und Dämpfungsmatrizen von Windturbinen und ihr Einfluß auf das Stabilitätsverhalten," VDI Fortschrittsberichte, Reihe 11, Nr. 294, Düsseldorf, Germany, 2000.

[15] G Genta, "Vibration of structures and machines," Springer, Turin, Italy, 1998.

[16] R Bittkau, "Concept study for using active turbine controls vs. structural control systems for load mitigation for offshore wind turbines using monopile support structures," Project Thesis, Universität Stuttgart, Stuttgart, Germany, 2010.

[17] W de Vries, "Assessment of bottom-mounted support structure types with conventional design stiffness and installation techniques for typical deep water sites," Delft, The Netherlands, 2007.

[18] M Steinle, "Design of a two bladed 10MW offshore wind turbine," Master Thesis, Universität Stuttgart, Stuttgart, Germany, 2009.

[19] R Gasch and J Twele, "Windkraftanlagen," Teubner Verlag, Wiesbaden, Germany, 2005.

[20] S Engström, "Arguments for large two-bladed wind turbines," Nordic Windpower, Taby, Sweden, 2007.

[21] E Bossanyi, "Individual blade pitch control for load reduction," in *Wind Energy Journal*, 2005.

[22] J Cotrell, "The mechanical design, analysis and testing of a two-bladed wind turbine hub," National Renewable Energy Laboratory, Golden, Co, USA, 2002.

[23] R Nielsen. (2009) Website of danish wind power industry, http://www.windpower.org.

[24] H Long, T Fischer, and G Moe, "Design methodology and optimization of lattice towers for

bottom-fixed offshore wind turbines in the ultimate limit state," Journal of Offshore Mechanics and Arctic Engineering , 2011.

[25] E Bossanyi and D Witcher, "A state-of-the-art controller for the UpWind reference wind turbine," in *European Wind Energy Conference (EWEC)*, Marseille, France, 2009.

[26] H Carstens, "Lower costs by individual design of foundation structure," in *European Wind Energy Conference (EWEC)*, Milan, Italy, 2007.

[27] T Fischer and M Kühn, "Site sensitive support structure and machine design for offshore wind farms," in *European Wind Energy Conference (EWEC)*, Marseille, France, 2009.

[28] R Rivas, J Clausen, K Hansen, and L Jensen, "Solving the turbine positioning problem for large offshore wind farms by simulated annealing," in *Wind Engineering*, 2009.

[29] J Jonkman, S Butterfield, W Musial, and G Scott, "Definition of a 5-MW reference wind turbine for offshore system development (NREL/TP-500-38060)," National Renewable Energy Laboratory, Golden, Co, USA, 2006.

[30] J King, "Deliverable D7: EU-TOPFARM - A comparison of the developed models with existing methods employed to estimate wind turbine fatigue loads within a wind farm for large offshore and simple terrain sites," in *TOPFARM project*, Brsitol, UK, 2011.

[31] B Schmidt, J King, G Larsen, and T Larsen, "Load validation and comparison versus certification approaches of the Risoe dynamic wake meandering model implementation in GH Bladed," in *European Wind Energy Event (EWEA)*, Brussels, Belgium, 2011.

[32] T Buhl and G Larsen, "Wind farm topology optimization including costs associated with structural loading," in *Science of Making Torque from Wind Conference*, Heraklion, Greece, 2010.

[33] G van Bussel and MB Zaaijer, "DOWEC concepts study - reliability, availability and maintenance aspects," in *European Wind Energy Conference (EWEC)*, Copenhagen, Denmark, 2001.

[34] B Bulder et al., "The ICORASS feasability study," Petten, The Netherlands, 2007.

[35] C Böker, "Load simulation and local dynamics of support structured for offshore wind turbines," PhD Thesis, Universität Hannover, Hannover, Germany, 2009.

[36] T Fischer, P Rainey, E Bossanyi, and M Kühn, "Optimization of a monopile support structure using offshore-specific wind turbine controls," in *European Offshore Wind (EOW)*, Stockholm, Sweden, 2009.

[37] IEC 61400-1, "Wind turbines - part 1: Design requirements," International Electrotechnical Commission, Geneva, Switzerland, 2005.

[38] P Andersen, ""When the storm increased, the turbines switched off"," Eltra Press, Copenhagen, Denmark, 2005.

[39] D Schlipf et al., "Testing of frozen turbulence hypothesis for wind turbine applications with a scanning lidar system," in *International Society of Acoustic Remote Sensing of the Atmosphere and Oceans (ISARS)*, Paris, France, 2010.

[40] D Schlipf, T Fischer, C Carcangiu, M Rossetti, and E Bossanyi, "Load analysis of look-ahead collective pitch control using LIDAR," in *Deutsche Windenergiekonferenz (DEWEK)*, Bremen, Germany, 2010.

[41] M Lackner and M Rotea, "Passive Structural Control of Offshore Wind Turbines," in *Wind Energy*, 2010.

[42] F Mitsch and KH Hanus, "Schwingungstechnik in Windkraftanlagen," Hannover, Germany, 2004.

[43] W Popko, "Load analysis and mitigation of an offshore wind turbine with jacket support structure," Copenhagen, Denmark, 2010.

[44] S Krenk and J Hoegsberg, "Design of multiple tuned mass dampers on flexible structures," in *Nordic Seminar on Computational Mechanics* , Lund Institute of Technology, 2006.

[45] J Den Hartog, "Mechanical vibrations," New York, USA, 1934.

[46] K Argyriadis and N Hille, "Determination of fatigue loading on wind turbine with oil damping device," in *European Wind Energy Conference (EWEC)*, London, UK, 2004.

[47] B Kuhnle, "Aerodynamic damping in offshore wind turbines by means of pitch control while idling," Stuttgart, Germany, 2011.

[48] B Savini and E Bossanyi, "Supervisory control logic design for individual pitch control," in *Eurpean Wind Energy Conference (EWEC)*, Warsaw, Poland, 2010.

[49] A Rodriguez T et al., "Enhancement of wind turbine structural damping by using passive, active and semi-active structural control devices for tower load reduction," in *Deutsche Windenergiekonferenz (DEWEK)*, Bremen, Germany, 2010.

[50] B Kuhnle, "Design optimization of the Alstom ECO 100 3 MW wind turbine," Project Thesis, Universität Stuttgart, Stuttgart, Germany, 2010.

[51] L Chen and CH Hansen, "Active vibration control of a magnetotheological sandwich beam," in *Acoustics Conference*, Busselton, Australia, 2005.

[52] A Rodriguez T, *Wind turbine structural damping ratio augmentation hybrid device (Patent - EP 09167385.5)*. Barcelona, Spain, 2010.

[53] WH Liao and CY Lai , "Harmonic analysis of a magnetorheological damper for vibration control ," in *Journal of Smart Materials and Structures*, 2002.

[54] M Constantinou, P Tsopelas, W Hammel, and N Sigaher, "Toggle-brace-damper seismic energy dissipation systems," in *Journal of Structural Engineering*, 2011.

[55] S Chu, T Soong, and A Reinhorn, "Active, hybrid and semi-active structural control," New York, USA, 2005.

[56] A Rodriguez T et al., "Wind turbine structural damping control for tower load reduction," in *Conference on Structural Dynamics, Models and Measurements in Aerospace Engineering (IMAC)*, Jacksonville, USA, 2011.

[57] E Bossanyi, "GH Bladed User Manual," GL-Garrad Hassan, Bristol, UK, 2010.

[58] J van der Tempel, "Design of support structures for offshore wind turbines," PhD Thesis, Technical University of Delft, Delft, The Netherlands, 2006.

[59] T Fischer et al., "Offshore support structure optimization by means of integrated design and controls," in *to be published in Wind Energy Journal*, 2011.

[60] W de Vries and J van der Tempel, "Quick monopile design," in *European Offshore Wind (EOW)*, Berlin, 2007.

[61] R Salgado, "The engineering of foundations," Boston, USA, 2006.

[62] S Downing and D Socie, "Simple rainflow counting algorithms," International Journal of Fatigue, 1982.

[63] M Miner, "Cumulative damage in fatigue," Journal of Applied Mechanics , 1945.

[64] Rijkswaterstaat. (2009) Ministerie van Verkeer en Waterstaat: Monitoring van de Waterstaatkundige Toestand des Lands (MWTL), www.golfklimaat.nl.

[65] T Fischer, W de Vries, and B Schmidt, "Design Basis - Upwind Project," Project Report, Universität Stuttgart, Stuttgart, Germany, 2010.

[66] Noordzeewind. (2010) http://www.noordzeewind.nl/.

[67] API, "Recommended practice for planning, design and constructingfixed offshore platforms," American Petroleum Institute, Washington, USA, 2000.

[68] B Sumer and J Fredsoe, "The mechanics of scour in the marine environment," World Scientific Publishing, Singapore, 2002.

[69] DNV-OS-J101, "Design of offshore wind turbine structures," Det Norske Veritas, Hoevik, Norway, 2007.

[70] J Kaimal, J Wyngaard, Y Izumi, and O Cote, "Spectral characteristics of surface-layer turbulence," Meteorologic Sociaty , 1972.

[71] D Gilli, "Im Kampf gegen Stillstandszeiten," Erneuerbare Energien 10/2009, Sun Media

Verlag, Hannover, Germany, 2009.

[72] M Rodriguez, "Analysis of structural damping," Master Thesis, Lulea University of Technology, Lulea, Sweden, 2006.

11. Appendix

Appendix A – Data of the reference designs

Table A.1: Turbine data

	UpWind 5 MW	**Alstom ECO 100**
Rated power	5.0 MW	3.0 MW
Wind speed range	3 – 25 m/s	3 – 25 m/s
Rated wind speed	11.3 m/s	8.5 m/s
Rotor diameter	126 m	100.8 m
Rotor concept	3-bladed, upwind, active yaw	3-bladed, upwind, active yaw
Tilt angle	5 degrees	6 degrees
Rotor speed range	6.9 – 12.1 rpm	7.9 – 14.3 rpm
Gearbox	Planetary	Planetary
Control concept	Variable-speed, pitch-controlled	Variable-speed, pitch-controlled
Generator	Double-feed induction	Double-feed induction
Nacelle mass (incl. rotor)	350 tons	170 tons

Table A.2: Data of monopile support structures

Monopile[1] in 10 m MSL	**Monopile in 25 m MSL**
Monopile: ø5.5 m x 60 mm[2] x 35 m	Monopile: ø6.2 m x 80 mm[2] x 54 m
Penetration depth: 20 m	Penetration depth: 24 m
Tower: 68 m length with $ø_{base}$ 5.6 m x 40 mm and $Ø_{top}$ 4.0 m x 20 mm	Tower: 68 m length with $ø_{base}$ 5.6 m x 40 mm and $Ø_{top}$ 4.0 m x 20 mm
1st eigenfrequency: 0.281 Hz	1st eigenfrequency: 0.277 Hz

[1] - Exemplary design without any checks for fatigue and extreme lifetime
[2] - Wall thickness at sea bed (varies along the pile)

Table A.3: Data of multi-member support structures

Truss[1] in 35 m MSL	Jacket in 50 m MSL
3-leg structure, bottom / top width 20 m / 4 m	4-leg structure, bottom / top width 12 m / 8 m
Penetration depth: None (rigid foundation)	Penetration depth: 48 m (piles with ø2.1 m x 65 mm)
Leg size: ø0.89m x 35 mm	Leg size: ø2.1 m x 60 mm (bottom), ø1.2 m x 35 mm (top)
Brace size: ø0.36 m x 14 mm	Brace size: ø0.8 m x 20 mm
1st eigenfrequency: 0.31 Hz	Tower: 64 m length with $\varnothing_{base}$ 6.0 m x 34 mm and $\varnothing_{top}$ 4.0 m x 22 mm
	1st eigenfrequency: 0.31 Hz

[1] - Exemplary design without any checks for fatigue and extreme lifetime

Appendix B – IEC 61400-3 Design Load Cases

DLC 1.2 – FATIGUE	
Operating conditions	Power production
Wind conditions	Normal turbulence model (NTM)
Sea conditions	Normal sea state (NSS), no currents, MSL + 10% of tidal range
Partial safety factor	1.0

Description of simulations:

Filename	Mean wind speed [m/s]	Longit. turbulence intensity [%]	Sig. wave height [m]	Peak spectral period [s]	Time [hrs/year]	Wind-wave-misalignment [deg]
1.2a_x_y	4	20.4	1.17	5.55	See design basis [65]	0° – 150° (30° sectors)
1.2b_x_y	6	17.5	1.25	5.6		
1.2c_x_y	8	16.0	1.33	5.67		
1.2d_x_y	10	15.2	1.75	5.71		
1.2e_x_y	12	14.6	2.4	5.88		
1.2f_x_y	14	14.2	2.8	6.07		
1.2g_x_y	16	13.9	3.2	6.37		
1.2h_x_y	18	13.6	3.7	6.71		
1.2i_x_y	20	13.4	4.4	6.99		
1.2j_x_y	22	13.3	5.1	7.4		
1.2k_x_y	24	13.1	5.3	7.8		
Comments	3D, 3-component Kaimal turbulent wind field (2 minutes sample) 6 different wind speed (and wave) seeds for each wind speed bin - The first 18 runs are with a yaw error of +8 deg, the last 18 with -8deg per wind bin - The 6 seeds are 6 times re-used for each wind speed bin - x = 1-6 according to wind direction (0-150deg in 30deg steps) - y = 1-6 according to wave direction (0-150deg in 30deg steps) - log. vertical shear with ground roughness length of 0.002m - NTM is site specific - NSS with irregular waves defined using Jonswap spectrum (peakness = 1.0) - tidal range is equal to HAT – LAT, 10% = 0.22m					

DLC 6.4 – FATIGUE

Operating conditions	Idling
Wind conditions	Normal turbulence model (NTM)
Sea conditions	Normal sea state (NSS), no currents, MSL + 10% of tidal range
Partial safety factor	1.0

Description of simulations:

Filename	Mean wind speed [m/s]	Longit. turbulence intensity [%]	Sig. wave height [m]	Peak spectral period [s]	Time [hrs/year]	Wind-wave-misalignment [deg]
6.4a_x_y	2	29.2	1.1	5.4	See design basis [65]	0° – 150° (30° sectors)
6.4m_x_y	26	12.0	5.8	8.14		
6.4n_x_y	28	11.9	6.2	8.49		
6.4o_x_y	30	11.8	6.3	8.86		
Comments	• 3D, 3-component Kaimal turbulent wind field (2 minutes sample) • 6 different wind speed (and wave) seeds for each wind speed bin • The first 18 runs are with a yaw error of +8 deg, the last 18 with -8deg per wind bin • The 6 seeds are 6 times re-used for each wind speed bin • x = 1-6 according to wind direction (0-150deg in 30deg steps) • y = 1-6 according to wave direction (0-150deg in 30deg steps) • log. vertical shear with ground roughness length of 0.002m • NTM is site specific • NSS with irregular waves defined using Jonswap spectrum (peakness = 1.0) • tidal range is equal to HAT – LAT, 10% = 0.22m					

DLC 7.2 – FATIGUE	
Operating conditions	Idling after fault
Wind conditions	Normal turbulence model (NTM)
Sea conditions	Normal sea state (NSS), no currents, MSL + 10% of tidal range
Partial safety factor	1.0

Description of simulations:

Filename	Mean wind speed [m/s]	Longit. turbulence intensity [%]	Sig. wave height [m]	Peak spectral period [s]	Time [hrs/year]	Wind-wave-misalignment [deg]
7.2a_x_y	2	29.2	1.1	5.4		
7.2b_x_y	4	20.4	1.17	5.55		
7.2c_x_y	6	17.5	1.25	5.6		
7.2d_x_y	8	16.0	1.33	5.67		
7.2e_x_y	10	15.2	1.75	5.71		
7.2f_x_y	12	14.6	2.4	5.88		
7.2g_x_y	14	14.2	2.8	6.07	See design basis [65]	0° – 150° (30° sectors)
7.2h_x_y	16	13.9	3.2	6.37		
7.2i_x_y	18	13.6	3.7	6.71		
7.2j_x_y	20	13.4	4.4	6.99		
7.2k_x_y	22	13.3	5.1	7.4		
7.2l_x_y	24	13.1	5.3	7.8		
7.2m_x_y	26	12.0	5.8	8.14		
7.2n_x_y	28	11.9	6.2	8.49		
7.2o_x_y	30	11.8	6.3	8.86		

Comments	3D, 3-component Kaimal turbulent wind field (2 minutes sample) 6 different wind speed (and wave) seeds for each wind speed bin - The first 18 runs are with a yaw error of +8 deg, the last 18 with -8deg per wind bin - The 6 seeds are 6 times re-used for each wind speed bin - x = 1-6 according to wind direction (0-150deg in 30deg steps) - y = 1-6 according to wave direction (0-150deg in 30deg steps) - log. vertical shear with ground roughness length of 0.002m - NTM is site specific - NSS with irregular waves defined using Jonswap spectrum (peakness = 1.0) - tidal range is equal to HAT – LAT, 10% = 0.22m

DLC 1.3 – ULTIMATE

Operating conditions	Power production
Wind conditions	Extreme turbulence model (ETM) , $V_{in} < V_{hub} < V_{out}$
Sea conditions	Normal sea state (NSS), normal current model (NCM), MSL
Partial safety factor	Normal (1.35)

Description of simulations:

Filename	Mean wind speed [m/s]	Longit. turbulence intensity [%]	Sig. wave height [m]	Peak spectral period [s]	Surface Currents [m/s]	Yaw error [deg]
1.3aa_1-6	V_{rated} - 2 (10.0)	25.4	1.75	5.71	1.2	- 8°
1.3ab_1-6						0°
1.3ac_1-6						+ 8°
1.3ba_1-6	V_{rated} (12.0)	22.3	2.4	5.88	1.2	- 8°
1.3bb_1-6						0°
1.3bc_1-6						+ 8°
1.3ca_1-6	V_{rated} + 2 (14.0)	20.1	2.8	6.07	1.2	- 8°
1.3cb_1-6						0°
1.3cc_1-6						+ 8°
1.3da_1-6	V_{out} - 4 (20.0)	16.1	4.4	6.99	1.2	- 8°
1.3db_1-6						0°
1.3dc_1-6						+ 8°
1.3ea_1-6	V_{out} (24.0)	14.6	5.3	7.8	1.2	- 8°
1.3eb_1-6						0°
1.3ec_1-6						+ 8°

Comments	• 3D, 3-component Kaimal turbulent wind field (10 minutes sample) • 6 bin-combinations for each wind speed bin • log. vertical shear with ground roughness length of 0.002m • ETM is site specific • NSS with irregular waves defined using Jonswap spectrum (peakness = 3.3) • NCM using near-surface current, decreasing linearly to the sea bed • extreme loads for each load case group (e.g. 1.3aa) are calculated as the mean of the maxima from each of the six seeds

DLC 2.1 – ULTIMATE

Operating conditions	Power production plus occurrence of fault
Wind conditions	Normal turbulence model (NTM), $V_{in} < V_{hub} < V_{out}$
Sea conditions	Normal sea state (NSS), normal current model (NCM), MSL
Partial safety factor	Normal (1.35)

Description of simulations:

Filename	Mean Wind speed [m/s]	Longit. turbulence intensity [%]	Sig. wave height [m]	Peak spectral period [s]	Fault
2.1aa _1-6	V_{rated} - 2 (10.0)	15.2	1.75	5.71	a
2.1ba _1-6	V_{rated} (12.0)	14.6	2.4	5.88	a
2.1ca _1-6	V_{rated} + 2 (14.0)	14.2	2.8	6.07	a
2.1da _1-6	V_{out} - 4 (20.0)	13.4	4.4	6.99	a
2.1ea _1-6	V_{out} (24.0)	13.1	5.3	7.8	a
Comments	3D, 3-component Kaimal turbulent wind field (1 minutes sample) 6 bin-combinations for each wind speed bin - fault occurs 10s into simulation - log. vertical shear with ground roughness length of 0.002m - NTM is site specific - NSS with irregular waves defined using Jonswap spectrum (peakn. = 3.3) - NCM using near-surface current, decreasing linearly to the sea bed - faults: a) Pitch runaway. All blades pitches towards fine at -8°/s b) no other failures considered in this study - extreme loads for each load case group (e.g. 2.1aa) are calculated as the mean of the maxima from each of the six seeds				

DLC2.3 – ULTIMATE	
Operating conditions	Power production plus loss of electrical grid connection
Wind conditions	Extreme operating gust (EOG)
Sea conditions	Normal wave height (NWH), normal current model (NCM), MSL
Partial safety factor	Abnormal (1.1)

Description of simulations:

Filename	Mean wind speed [m/s]	EOG gust [m/s]	Wave height [m]	Wave period [s]	Yaw error [deg]
2.3aa_x					- 8°
2.3ab_ x	10.0	3.86	1.75	5.36	0°
2.3ac_ x					+ 8°
2.3ba_ x					- 8°
2.3bb_ x	12.0	4.45	2.4	6.28	0°
2.3bc_ x					+ 8°
2.3ca_ x					- 8°
2.3cb_ x	14.0	5.05	2.8	6.79	0°
2.3cc_ x					+ 8°
2.3da_ x					- 8°
2.3db_x	20.0	6.80	4.4	8.51	0°
2.3dc_ x					+ 8°
2.3ea_ x					- 8°
2.3eb_ x	24.0	7.98	5.3	9.34	0°
2.3ec_ x					+ 8°

Comments	- steady wind with transient gust (gust period 10.5s) - one minute simulations, gust occurs 15s + grid loss phasing into simulation - log. vertical shear with ground roughness length of 0.002m - gust magnitude for EOG calculated from formula in section 6.3.2.2 of [31] - grid loss phasing (indexed x=1-4) - beginning of gust - lowest wind speed right before gust - point of highest acceleration during gust - gust peak - NWH modelled with regular waves using stream function model - NCM using near-surface current, decreasing linearly to the sea bed

DLC 6.1a – ULTIMATE	
Operating conditions	Idling
Wind conditions	Extreme wind model (EWM) ,(turbulent), ($V_{hub} = V_{50}$)
Sea conditions	Extreme sea state model (ESS) with $H_s = H_{s,50}$, extreme current model (NCM), EWLR
Partial safety factor	Normal (1.35)

Description of simulations:

Filename	Mean wind speed [m/s]	Longit. turbulence intensity [%]	Sig. wave height [m]	Peak spectral period [s]	Yaw error [deg]	Wi-Wa-misalignment [deg]
6.1aa_x_y_1-6						-30°
6.1ab_x_y_1-6					-8°	0°
6.1ac_x_y_1-6						30°
6.1ba_x_y_1-6						-30°
6.1bb_x_y_1-6	V_{50} (42.73)	11.0	$H_{s,50}$ (8.24)	$T_{p,50}$ (11.97)	0°	0°
6.1bc_x_y_1-6						30°
6.1ca_x_y_1-6						-30°
6.1cb_x_y_1-6					8°	0°
6.1cc_x_y_1-6						30°

Comments	3D, 3-component Kaimal turbulent wind field (10 minutes sample) 6 bin-combinations for each wind speed bin - log. vertical shear with ground roughness length of 0.002m - turbulence intensity for EWM set to 11% as specified in section 6.3.2.1 of [31] - ESS with irregular waves defined using Jonswap spectrum (peakness = 3.3) - ECM using near-surface current, decreasing linearly to the sea bed - EWLR: variation from LSWL to HSWL (indexed x=1-2) - constrained extreme non-linear wave included in irregular wave history corresponding to extreme wave height required in dlc6.1b,c. Hence dlc6.1b,c can be omitted. - constrained wave height = Hs,50max = 15.33m - constr. wave period = T=13.88s and T=17.88s (indexed y=1-2) - time for constrained wave crest: 100s - extreme loads for each load case group (e.g. 6.1aa_x_y) are calculated as the mean of the maxima from each of the six seeds

DLC 6.2a – ULTIMATE	
Operating conditions	Idling with loss of electrical network (up to 6 hrs before storm occurs)
Wind conditions	Extreme wind model (EWM) ,(turbulent), ($V_{hub} = V_{50}$)
Sea conditions	Extreme sea state model (ESS) with $H_s = H_{s,50}$, extreme current model (NCM), EWLR
Partial safety factor	Abnormal (1.1)

Description of simulations:

| Filename	Mean wind speed [m/s]	Longit. turbulence intensity [%]	Sig. wave height [m]	Peak spectral period [s]	Yaw error [deg]
6.2a_x_y_1-6					0°
6.2b_x_y_1-6					30°
6.2c_x_y_1-6					60°
6.2d_x_y_1-6	V_{ref} (42.73)	11.0	$H_{s,50}$ (8.24)	$T_{p,50}$ (11.97)	90°
6.2e_x_y_1-6					120°
6.2f_x_y_1-6					150°
6.2g_x_y_1-6					180°
Comments	3D, 3-component Kaimal turbulent wind field (10 minutes sample) 6 bin-combinations for each wind speed bin - log. vertical shear with ground roughness length of 0.002m - turbulence intensity for EWM set to 11% as specified in section 6.3.2.1 of [37] - ESS with irregular waves defined using Jonswap spectrum (peakness = 3.3) - ECM using near-surface current, decreasing linearly to the sea bed - EWLR: variation from LSWL to HSWL (indexed x=1-2) - constrained extreme non-linear wave included in irregular wave history corresponding to extreme wave height required in dlc6.2b. Hence dlc6.2b can be omitted. - constrained wave height = Hred,50 = 1.1 Hs,50 = 9.06m - constr. wave period = T=10.67s and T=13.74s (indexed y=1-2) - time for constrained wave crest: 100s - extreme loads for each load case group (e.g. 6.2a_x_y) are calculated as the mean of the maxima from each of the six seeds				

Appendix C – Ultimate utilization plots (reference vs. optimized design)
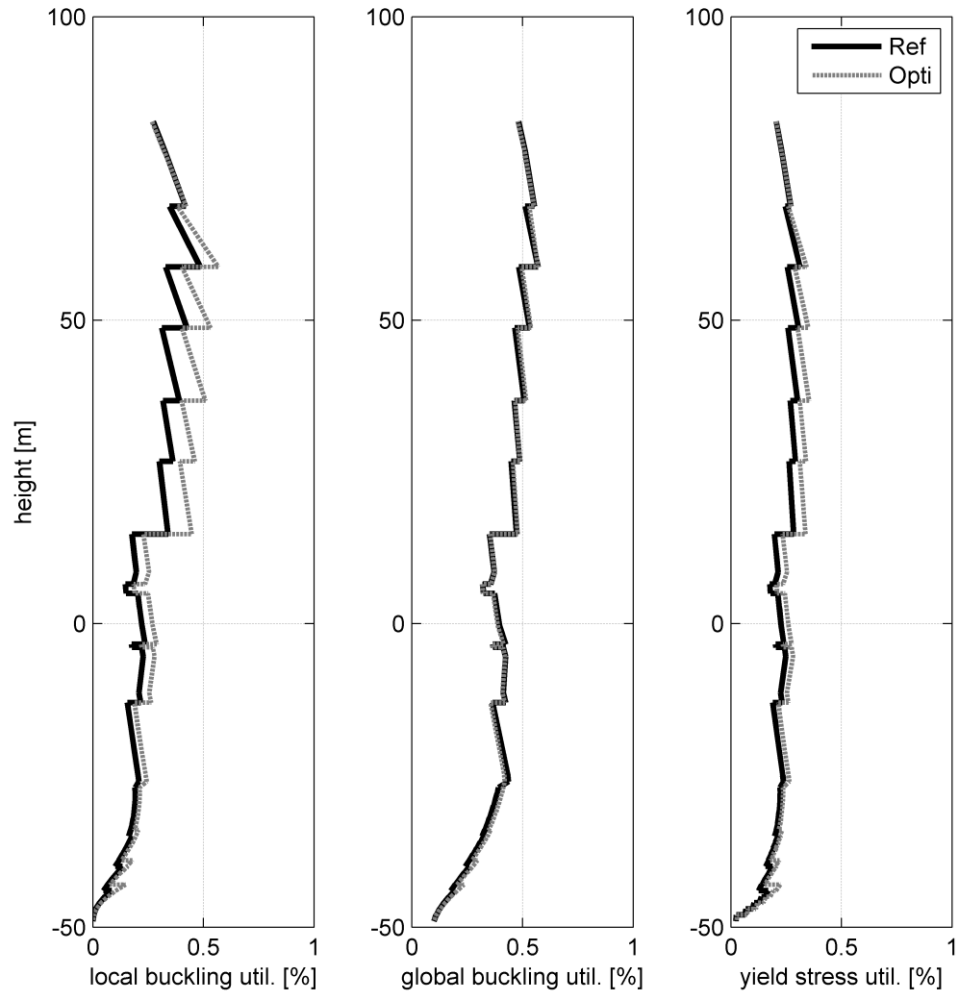
Figure C.1: Ultimate utilizations over support structure height for DLC 1.3 as comparison between the reference and the optimized support structure design
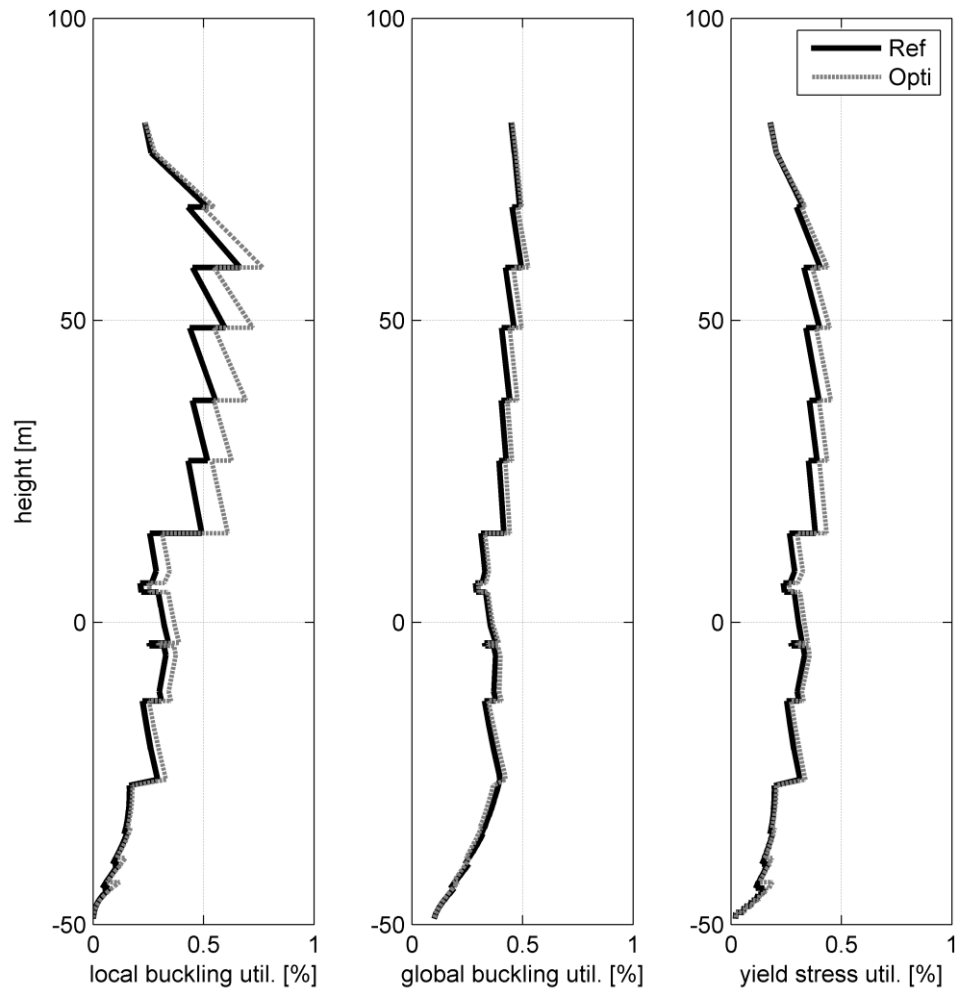
Figure C.2: Ultimate utilizations over support structure height for DLC 2.1 as comparison between the reference and the optimized support structure design
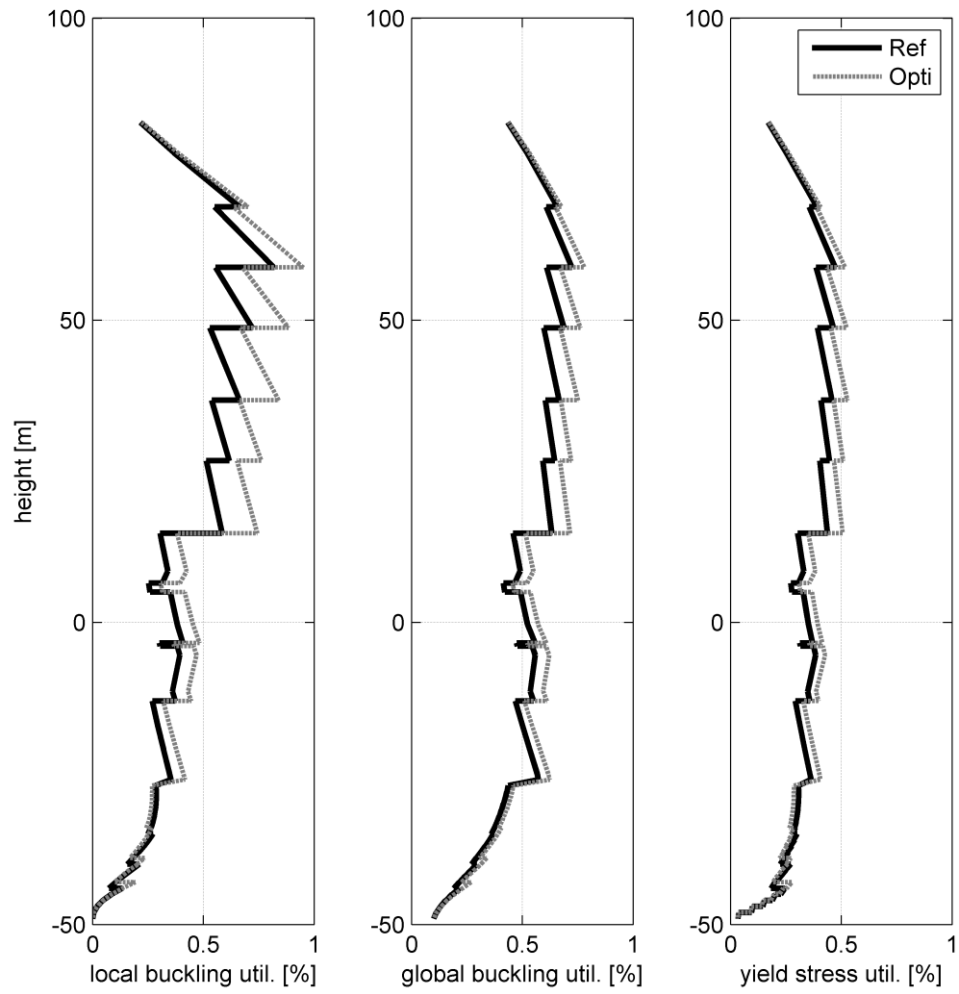
Figure C.3: Ultimate utilizations over support structure height for DLC 2.3 as comparison between the reference and the optimized support structure design
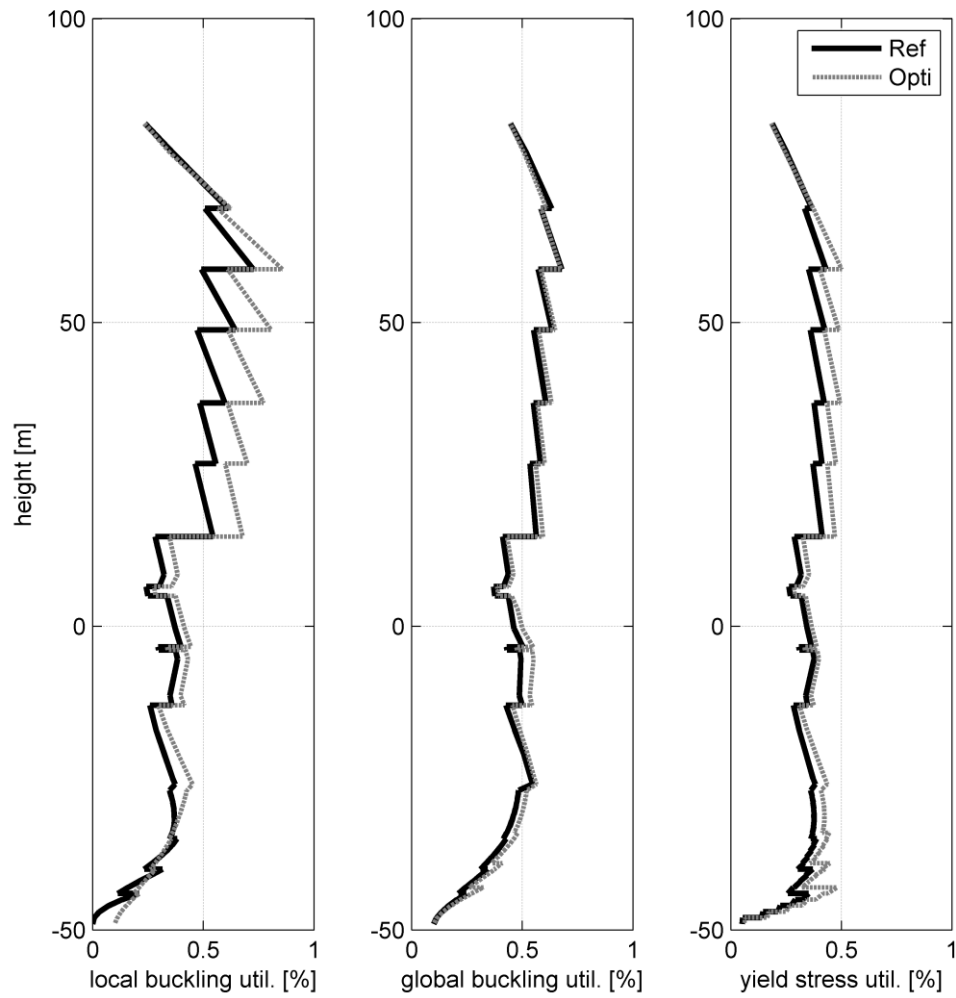
Figure C.4: Ultimate utilizations over support structure height for DLC 6.1 as comparison between the reference and the optimized support structure design
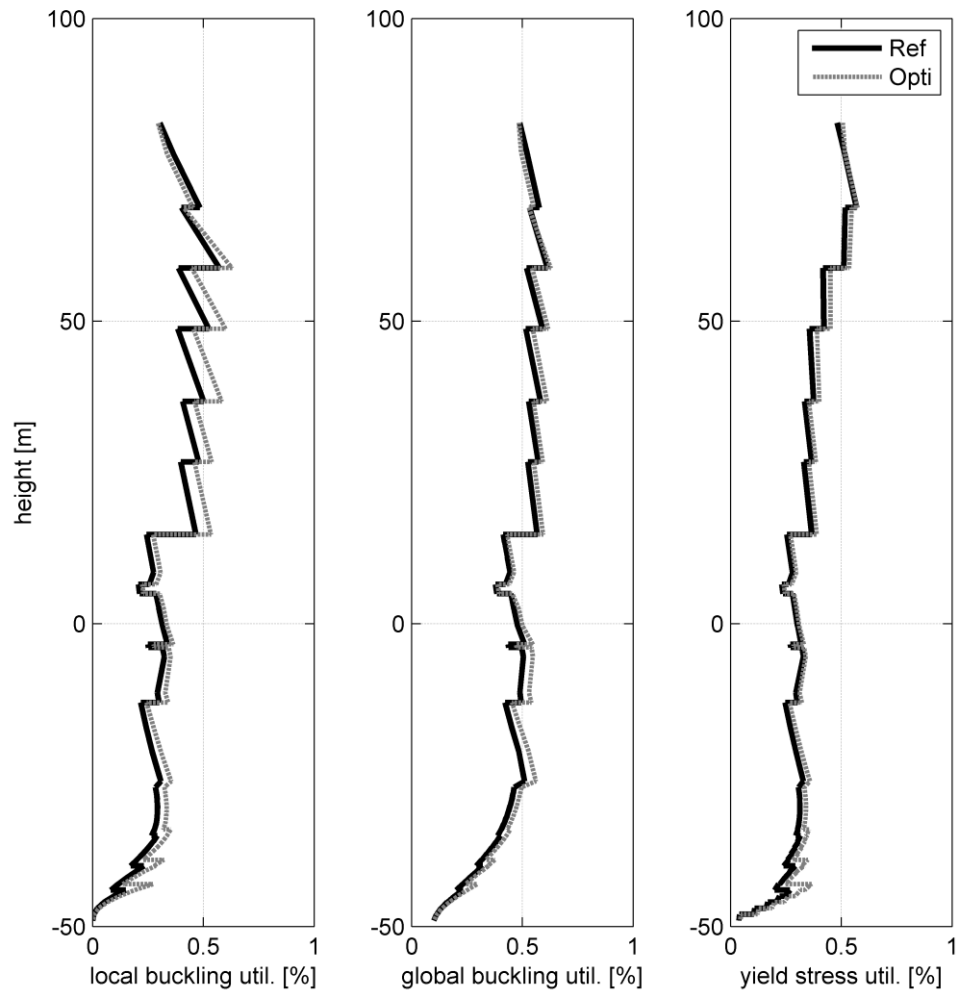
Figure C.5: Ultimate utilizations over support structure height for DLC 6.2 as comparison between the reference and the optimized support structure design